Ecosystem Responses to Abrupt Climatic and Environmental Change in Southern Siberia during the Late Quaternary

Thesis submitted for the degree of Doctor of Philosophy

UCL

Poppy Rebekah Harding

I, Poppy Rebekah Harding confirm that the work presented in this thesis is my own. Where information has been derived from other sources, I confirm that this has been indicated in the thesis.

Poppy Harding

Acknowledgements

This Ph.D. project could not have come to competition without the contributions from many other people, some of whom I would like to acknowledge here. First and foremost, I thank my primary supervisor, Anson Mackay for his time, advice and ideas, which have been invaluable throughout the project. I also thank Jonathan Holmes for his additional perspective throughout the project. I am also incredibly thankful for my collaborators at the Academy of Sciences, Irkutsk, who have contributed their knowledge and data towards this Ph.D. I particularly thank Sasha, for his assistance with fieldwork planning and for providing essential context about Baunt and Elena for her provision of additional data and her warm hospitality during my time in Irkutsk. Additionally, to Svetlana for her help with isotopes and all the sampling preparations for diatom isotopes at Baunt. I additionally thank the fieldwork team for their essential role in collecting the samples from Baunt. I am also grateful to Professor Melanie Leng (BGS/Nottingham), who's assistance with isotopes has been essential. A further essential team for this project are the UCL Geography laboratory staff, who's help and advice have been gratefully received, and to the post-grad microscope room members, for all the fun and advice. Thank you to my family for all their support, and particularly my dad for keeping the ginger one fit, while I haven't had the time, and to grandma for her life lessons. To Kita, my 'typing' companion, and of course to Simon, for his encouragement, support and ability to pick me up and put me back on the horse whenever I've wanted to quit. Through all the highs and lows of the past 4 years, I couldn't have imagined going through it with anyone but you. And a final thanks to all the Baunt diatoms, particularly *pant* and *gran* who summarise my life for the past four years.

This thesis could not have been undertaken without funding from a NERC London DTP studentship, alongside additional support provided by the Quaternary Research Association, the UCL Mead Travel Fund and The NERC BGS Stable Isotope Facility (IP-1725-0517 and IP-1678-1116).

Abstract

The Late Quaternary documents climatic changes over a number of timescales. These are well studied in many regions, including Northern Europe, but much less so in some critical areas. One such region is continental southern Siberia, which is highly sensitive to modern climate changes. Palaeoenvironmental reconstructions are essential to provide context for these changes, and to examine regional sensitivity to climate forcing, however studies in Siberia are limited and good records of the last 30 ka BP, an important period for studying climatic changes, are rare. This thesis reconstructs the palaeoenvironment of Lake Baunt (55°11'15" N, 113°01'45" E), a site situated at the southern limits of Siberian permafrost, over the Late Quaternary (~30-6 ka BP). The reconstruction is based on a high-resolution diatom study from a record with excellent preservation, combined with organic geochemistry, and $\delta^{18}O_{diatom}/\delta^{13}C_{diatom}$, for the LGIT and Early Holocene, and supporting data, integrated through Bayesian age modelling. Baunt records the LGM, Heinrich events 1 and 2, the Lateglacial Interstadial, Younger Dryas, and Holocene fluctuations, shown through changes in ecosystem productivity, carbon cycling and hydrology. This highlights Baunt's sensitivity to extrinsic climate forcing. Internal forcing's have also been important factors, with local glacier melt influencing the record. Comparisons to regional and key Northern Hemisphere sites, along with climate models, has added to the understanding of the expression of these events in Southern Siberia. In particular, this work has shown that there is a complex response to Heinrich events, and also confirms suggestions of a link between AMOC and Siberian climate in the Early Holocene. This work highlights the sensitivity of southern Siberia to past climatic forcing and shows the need for more work in both this lake, and other sites within the region, to further understanding of how palaeoclimatic change influences regions remote from oceanic influences.

Impact Statement

This Ph.D. makes important contributions to our understanding of past environments in central Asia in general and southern Siberia in particular. Data within this region has previously been quite limited, due to (i) focus of previous studies being mainly made on one lake (Baikal) and (ii) difficultly of extracting natural archives that span the past 30,000 years, (iii) logistical issues of reaching suitable sites in this remote region. However, research is urgently required to understand the potential impacts of abrupt climate change in this climatically sensitive region.

Benefits inside academia:

New knowledge of importance for the scientific community includes the increased understanding of the impact of abrupt climatic change on hydrology, carbon dynamics and ecosystems. The work highlights southern Siberia's sensitivity to extrinsic climate shifts and intrinsic forcing's through glacier melt. This highlights the importance of teleconnections between climate systems driving climatic and environmental shifts. The ecosystem changes documented across the past ~30,000 years in this thesis highlight the rapid ability of lacustrine ecosystems to respond to change.

The data provided within this Ph.D. are ideal for testing models of climatic change, and particularly for testing models of fluctuations associated with the Siberian High; such variations are now within the ability of the modelling community to assess using full GCM simulations during full glacial, interglacial and intermediate (D/O) conditions (Vettoretti and Peltier 2018). Currently models of future climate change in this region require testing and validation in these climate scenarios, and therefore it is essential that palaeoenvironmental research is available to provide the information needed for data/model inter-comparisons. This will therefore allow improvement of models, which can be included in government policies to address modern climate change. Presentation of this research at international workshops (below) has shown this potential to relevant climate modellers and data generated in this project will form part of future inter-comparison exercises

The data provided in the project are currently being drafted for publication to allow the results to be accessed by the wider scientific field, while it is also being used to test upcoming software, including the INTIMATE Integrating tool. It has been presented at several national (Quaternary Research Association Post-graduate symposium 2015, 2017, Perspectives on Environmental Change 2016, Quaternary Research Association Annual discussion meeting, 2016) and international (European Geosciences Union, 2017, International Diatom Symposium 2018, INTIMATE EGU Galileo 2018) conferences.

Benefits outside academia:

The work from this Ph.D. have also already been used for many public outreach events, allowing the public to understand more about past environmental changes. Events including the Quaternary Research Association (QRA) Public Outreach day (January 2016) and Science Outreach days (2014, 2016) have utilised the work from the Ph.D. to raise awareness. Specific talks have been presented to smaller interested public groups including the Harrow and Wealdstone Geological Society. The publications produced from this Ph.D. will contribute to the growing knowledge of ecosystem responses to abrupt climatic change, which are essential to inform policy concerning ecosystem management.

Contents

List of Figures

List of Tables

Notes on Terminology:

- All dates within this thesis are reported as calendar years before present (BP), following the convention that present is fixed at 1950AD, abbreviated to ka BP unless otherwise stated. Dates have been abbreviated to age/per thousand years - ka. For example: 30 ka BP is equal to thirty thousand years before 1950AD.
- Where radiocarbon dates have been calibrated by this author they have been calibrated using IntCal13 (Reimer *et al.*, 2013).
- Ma is the abbreviation used for Million years. Ka BP is used as the abbreviation for thousands of years BP. Unless otherwise specified all dates are reported to ka BP. Greenland Ice core years that have been originally defined as ice core years before the year 2000 (b2k) have been converted to ka BP where appropriate.
- When comparing to Greenland ice core records these are either based on the Greenland Ice Core 2005 Chronology (GICC05) and compared, where appropriate, to the Greenland event stratigraphy, following the recommendations of the INTegration of Ice-core, MArine, and Terrestrial records group (Lowe *et al.* 2008, Blockley *et al.* 2012, Rasmussen *et al.* 2014). The Greenland event stratigraphy is split into Greenland Stadial (GS) and Greenland Interstadials (GI) and these are used within the discussion when the relationship between Baunt and the North Atlantic realm is being considered. Comparisons to the GISP2 record are based on (Mayewski *et al.*, 2004) using the Meese/Sowers timescale (Meese *et al.*, 1994).
- When discussion follows climatic oscillations that are recorded in terrestrial records, more general terms found commonly in the literature are used (e.g. Younger Dryas (YD)), with the caveat that these are a shorthand and are often not well defined regionally. The Last Glacial Maximum (LGM), is taken here to present the broad period of time of maximum cooling late in the last glacial. The Heinrich events 1 and 2 are mainly defined as a pulses of Ice Rafted Debris (IRD) from the Laurentide Ice Sheet in North Atlantic marine archives (Broecker *et al.*, 1992), but the relevance for this study is that they are also used

commonly as terms to describe time periods where a number of records in ice core, marine and terrestrial realms are thought to be related to these iceberg discharge events (Peck *et al.*, 2007). Thus, in this study, Heinrich 1 or 2 is used to as a term to discuss the wider event, and its possible expression, rather than the specific marine phenomenon. The Bølling-Allerød (BA) and Younger Dryas (YD) are used here as shorthand for the warm Interstadial episode following Heinrich 1 and the Younger Dryas the final cooling event before the onset of the current Holocene Interglacial. Both the Bølling-Allerød and Younger Dryas were terms originally proposed by Mangerud *et al.* 1974 as a stratigraphic subdivision specifically for Scandinavia. In many regions, including Siberia, this has become adopted as a local terminology but because local end regional expressions of climate change can be very different and can be temporally time transgressive (Lowe and Hoek 2001) this should, at best, only be taken as a shorthand for the approximate time period. In this thesis this strategy is adopted and a detailed discussion of how, or if, these events are seen within Lake Baunt, and the wider region is a key part of the interpretation of this thesis.

1 Introduction and Literature Review

1.1 Introduction

This thesis examines lacustrine sediments from Lake Baunt, southern Siberia, over the Late Quaternary period (~30 ka BP), to assess the impact of abrupt climatic changes on southern Siberian ecosystems. The Late Quaternary period is well known for its substantial climatic variability, which operate across a range of timescales. While many studies have considered the impact of abrupt events on ecosystems, there is limited research in remote regions, including southern Siberia. This is problematic as southern Siberia, the most continental region in the world (Chytrý *et al.*, 2007; Huhne and Slingo, 2011), not only provides a key locality to study these changes far from oceanic influences, where many abrupt events are driven, but the region is also undergoing rapid climatic warming, with greater wintertime warming occurring than anywhere else globally (Huhne and Slingo, 2011). Modern day warming is already driving important changes the region, and it is essential therefore to study how the region has responded to past rapid climatic shifts to provide context for a region dominated by vulnerable carbon pools (Bloom *et al.*, 2010). Modelling of future climate change in Siberia is uncertain (Swann *et al.*, 2018) yet it is also one of the regions of the world where direct comparison between climate models and data have been hampered by the limited number of palaeoenvironmental studies (Zhang *et al.*, 2017a). The environmental reconstructions from Lake Baunt are initially considered against regional records, to examine variations in responses to known climatic forcing, and to explore the factors causing discrepancies in the expression of these events. Additionally, the Baunt record is, therefore, considered against key global sites, which provide evidence for potential planetary-wide changes in oceanic-atmospheric interactions. This is in order to explore their influence on the Siberian High pressure cell (Tubi and Dayan, 2013) and ultimately their role in driving and propagating climatic and environmental change in this region.

1.2 The Quaternary Period

The Quaternary is the most recent period of Earth's history, starting 2.58 million years ago (Ma), and continuing until the present day (Gibbard and Head, 2009). The period is made up of two epochs, the Pleistocene and the Holocene, with ongoing debate surrounding a potential further division to include the Anthropocene (Walker *et al.*, 2012; Zalasiewicz *et al.*, 2011, 2008). It is characterised by major oscillations in climate (Lisiecki and Raymo, 2005), beginning with the onset of Northern Hemisphere glaciations at the start of the Quaternary, with an intensification of amplitude of these events occurring after the Mid-Pleistocene Revolution (MPR) ~1Ma, which is coupled with a change in the periodicity of the dominant signal (Imbrie *et al.*, 1993).

The climatic oscillations within the Quaternary cover a range of timescales and are driven by many different forcings. They include: (a) changes linked to alterations in the earth's orbit (see section 1.3.1), due to changes in eccentricity, obliquity and precession, which are implicated in climate changes through causing variations in the amount and distribution of solar radiation received; (b) sub-Milankovitch millennial scale events, which include Heinrich Events, Dansgaard-Oeschger events and Bond cycles; and (c) events occurring over centuries to decades, which are driven by internal feedback mechanisms, alongside external solar activity and volcanic forcing (Bond, 1997; Cole-Dai *et al.*, 2013; Engels and van Geel, 2012).

It is essential to understand the detail of these changes in different regions to improve fundamental frameworks for studying the interaction between the different aspects of climate, environmental and ecological systems. This can provide a test bed for model simulations, as well as evidence of natural climate variability, which provides essential context for modern and future climatic changes (Maslin *et al.*, 2001).

1.3 Mechanisms of Quaternary Climate Change

1.3.1 Orbital Forcing

Orbital forcing is well established as the principal driver of Quaternary glacial-interglacial cycles. Orbital variations are thought to be linked to alterations in the astronomical relationship between the earth, moon, planets and sun, which cause changes in the amount, seasonality and geographical distribution of solar radiation (insolation) on the earth (Imbrie *et al.*, 1993). The three main cycles are eccentricity, obliquity and precession of the equinoxes, which generally operate on a 100 ka, 41 ka and 21 ka cycle, respectively (Hays *et al.*, 1976), with the model for the impact of these cycles on the earth's climate being developed through the work of J. Croll and elaborated by M. Milankovitch (Lowe & Walker 2015). Orbital eccentricity is where the earth's orbit changes from a circular orbit to an elliptical shaped orbit an back, over a period of 95-135 ka and also over a ~400 ka cycle, although it is generally known as an 100 ka cycle (Imbrie *et al.*, 1993), as the 400 ka eccentricity cycle is not manifested climatically. Eccentricity alters the total amount of insolation received due to variations in the distance between the earth and the sun, although the variability in the amount of radiation received is relatively minor, it magnifies seasonal variability between summer and winter at different points in the cycle. Obliquity variations are changes in the axial tilt of the earth between 21°39' to 24°36' and back over a 41 ka timescale (Hays *et al.*, 1976). This triggers changes in the radiation received on the earth's surface, and has a particularly strong effect on high latitudes (Hays *et al.*, 1976). Precession of the equinoxes is driven by two cycles, axial precession, which is induced by the gravitational pull of the sun and moon, causing the earth to 'wobble' on its axis, and precession of the ellipse, which is the rotation of the elliptical shape of the Earth's orbit (Kingston 2005). This causes gradual changes which move the seasons around the sun, resulting in variations in which season occurs while closest to the sun (perihelion) or furthest from the sun (aphelion). This operates on a 23 and 19 ka cycle (Hays *et al.*, 1976), with the Northern Hemisphere currently experiencing perihelion during the winter, while aphelion occurs during the summer. The last period that the Northern Hemisphere experienced perihelion during the summer was ~10.5 ka BP ago. The

variations caused by precession of the equinoxes also alter the distribution of heat across different latitudes, however it is considered to be more dominant at low to middle latitudes (Hays *et al.*, 1976). Additionally, this cycle influences seasonality, for example, when spring and autumn occur during aphelion and perihelion in the different hemispheres, there is least seasonality globally, while if summer and winter occur at perihelion and aphelion seasonality is much greater, and this can cause asymmetry between climate in the two hemispheres (Merlis *et al.*, 2013; Müller *et al.*, 2013).

Orbital parameter changes combine to alter the global insolation budget, and they are seen within astronomical theory to cause changes in global temperatures, and this, in turn, influences ice sheet growth (Hays *et al.*, 1976). These changes are thought to be of paramount importance at 65°N (figure 1.1), as this is where insolation has the most influence on the behaviour of large Northern Hemisphere ice sheets, as these have the largest potential to grow during glaciations as they are not constrained by large water bodies, unlike Antarctica (Ganopolski *et al.*, 2016; Hays *et al.*, 1976).

Although orbital forcing is widely considered as the driver of glacial-interglacial cycles, there are several issues with the theory as developed by Milankovitch and later authors. Some of these complexities include the fact that temperature records do not just follow insolation changes, as other forcing factors are superimposed on these glacial interglacial changes (see later sections) e.g. sub-Milanktovitch and decadal and centennial scale forcings, while others may be linked to additional factors not considered in traditional astronomical theory. For example, one issue is that astronomical theory did not originally consider changes in the inclination of the Earth's orbit relative to the sun, and this has been argued to influence the 100 kyr cycle (Kawamura *et al.*, 2007). Other work has supported Milankovitch's theory, with support from Antarctic Ice cores showing that for the previous 4 terminations, Northern Hemisphere summer insolation has triggered the deglaciations, with Antarctic climate changes lagging these changes by a few millennia (Kawamura *et al.*, 2007). Therefore, it can be concluded that although the basic theory of orbital forcing is understood there are still many complexities to be considered, and these

are hindered by issues around chronological control and limitations in records available that cover glacial-interglacial timescales.

Figure 1.1: Shows the orbital parameters **(A)** eccentricity **(B)** precession index plotted on an inverted vertical axis **(C)** obliquity, **(D)** June insolation at 65°N **(E)** $\delta^{18}O$ stack from LR04 (Lisiecki & Raymo, 2005), **(F)** atmospheric CO_2 from Antarctic Ice Cores, **(G)** atmospheric CH_4 in Antarctic EDC ice core, **(H)** δD from EDC ice core. Marine isotope stages and substages to corresponding interglacials are shown, with dashed lines showing current 21st June insolation level for 65°N north. Figure taken from Tzedakis *et al.,* (2012; page 138).

1.3.1.1.1 Evidence of Orbital Forcing

The evidence of orbital forcing triggering change are documented in marine (Lisiecki and Raymo, 2005), ice (EPICA, 2004), and terrestrial archives (Zhu *et al.*, 2007). Marine records, in particular, have provided the most substantial long term underpinning of orbital theory since the initial observations that variations in benthic $\delta^{18}O$ records from deep marine cores were correlated with the pattern of high latitude Northern Hemisphere insolation (Broecker and van Donk, 1970; Shackleton *et al.*, 1983). Robust stacks of multiple marine Sea Surface Temperature records and $\delta^{18}O$ archives, such as the SPECMAP record (Imbrie *et al.*, 1993; Martinson *et al.*, 1987), have been matched to the combined insolation signal to produce long proxy records of temperature and ice volume. These suggest that the majority of the variability in the benthic record is explained by ice sheet response to orbital forcing although with a range of internal feedback mechanisms producing significant non-linear responses (Imbrie *et al.*, 1993; Ruddiman, 2006a; Shackleton and Opdyke, 1973).

One limitation of these stacking exercises is the relative difficulty in directly dating benthic marine cores, meaning the chronologies are largely based on the 'tuning' of the main peaks in the isotope signal with the insolation record (see Raymo 1997). This has led to attempts to test the chronology of the SPECMAP model by utilising sea level indicators. As the long term records within the SPECMAP stack record changes in global ice volume they can be effectively seen as sea level indicators, as ice volume is the predominant controlling factor in absolute global sea level. While some attempts to test the timing of specific elements of the SPECMAP chronology have suggested that there are problems of timing, as mentioned above (Henderson and Slowey, 2000), long term validation of the SPECMAP timscale over several glacial cycles suggests that overall the orbital chronology is broadly robust (Thompson and Goldstein, 2006), at least for the last two full glacial cycles, although it is fair to say that until recently (below), few independent chronological tie points are available beyond this point. A global stack of 57 benthic $\delta^{18}O$ records for the last 5.3 Ma is now available (see figure 1.2), based on orbital tuning and averaging of sedimentation rates across the record

(Lisiecki and Raymo, 2005); the LR04 stack is now used widely as the default global correlation archive for long term records covering glacial to interglacial cycles.

Figure 1.2: The upper 3.5Ma $\delta^{18}O$ record from the LR04 benthic stack constructed by the graphic correlation of 57 globally distributed records, taken from Lisiecki and Raymo, (2005; page 6).

Long ice core and terrestrial sequences provide useful additional climatic information on glacial to interglacial timescales, alongside marine records. The Antarctic ice cores Vostok (Petit *et al.*, 1999, 1997) and EPICA Dome C (EPICA, 2004), provide records of isotopic and greenhouse gas variations through successive glacial to interglacial cycles, with Vostok covering 420 ka and EPICA Dome C covering 740 ka. Greenland ice cores supplement the Antarctic records by providing a record of changes over the last interglacial-glacial period (Rasmussen *et al.*, 2014a).

Terrestrial archives covering multiple glacial cycles are more limited, however they include long records of vegetation change in Europe (Camuera *et al.*, 2019; Litt *et al.*, 2014; Pross *et al.*, 2015; Tzedakis, 1993; Tzedakis *et al.*, 2009, 2006), long European and Asian Loess accumulation records (e.g. Zhu *et al.,* 2007), and lacustrine records of ancient lakes such as Baikal (Williams *et al.*,

1997). Of particular relevance for this study are long archives of environmental response to climate forcing over the last glacial cycle from Siberia and Asia, including Lake Baikal, and the U-Series dated isotopic records from Chinese stalagmites (e.g. Cheng *et al.,* 2016; Wang *et al.*, 2001). The latter is important as it is an independently dated record of monsoon variability that suggests that, along with abrupt changes, the Asian Monsoon system is significantly influenced by mid latitude (~30˚N) precession (see figure 1.3) (Yuan *et al.*, 2004). For example, the 640 ka Chinese speleothem record of Cheng *et al.,* (2016) highlights that the precession cycle plays a role with the 100 ka ice volume cycle and in the pacing of millennial scale events. These factors may also be critical for pressure systems such as the Siberian High, which is known to influence the East Asian Monsoon in modern studies (Wu and Wang, 2002).

Figure 1.3: Taken from Wang *et al.,* (2001: page 2346) showing the $\delta^{18}O$ of Hulu Cave stalagmites, shown green, red and purple against Greenland Ice (blue) and solar insolation at 33°N (black) (averaged over June, July and August). Abrupt Heinrich events and the Younger Dryas are also shown. The $\delta^{18}O$ scales are reversed for Hulu (increasing down) as compared with Greenland (increasing up).

1.3.1.2 Complexities

1.3.1.2.1 The 41 ka world

One of the issues that has been apparent in understanding the nature of orbital forcing on glacial to interglacial cycles relates to the dominance of the obliquity cycle for the early Pleistocene. If, as in the Milankovitch model, summer

insolation in the Northern Hemisphere high latitudes is seen as the key driver of glacial to interglacial cycles then it has been argued that the precession cycle could be the most likely driver of orbital forcing, assuming that insolation at the Northern Hemisphere summer solstice (insolation intensity) is the critical factor. Variations in summer solstice insolation are dominated by precession, but this is at odds with the fact that in the early Pleistocene the 41 ka obliquity cycle is dominant. However, Huybers (2006) pointed out that because summer duration and insolation intensity are anti-correlated, a more appropriate measure of orbital forcing is the insolation integrated over the duration of the summer. This value can be approximated by examining air temperatures in the higher latitudes (40 to 70 degrees) and a cut off for positive degree days of 275 W/m^2, and this can then be used to estimate the sum of the insolation on days where this threshold is crossed (Huybers, 2006). Doing so allows the calculation of effective summer energy, which can be calculated for 65˚N over the Quaternary. Variance in summer energy above 275 W/m^2 is dominated by obliquity changes, which can explain the 41 ka cycles in ice volume in the early Pleistocene (Huybers, 2006). Alternatively, the 'caloric summer half-year insolation' may be a more appropriate insolation metric because it has equal contributions of precession and obliquity near 65°N. Using this measure suggests that the 41 ka glacial–interglacial cycle arises because every second insolation peak is boosted by high obliquity, which provides sufficient energy to cross a deglaciation threshold (Tzedakis et al., 2017).

1.3.1.2.2 The 100 ka world

Improvements in the generation of absolute chronologies of glacial to interglacial cycles by U-Th disequilibrium dating of Chinese speleothem records have contributed to the debate over the timing and drivers of the proposed 100ka world (Cheng *et al.*, 2016). This suggests that there is not a clear 100k cycle, at least in the last 640,000 years, but rather the inception of interglacials occurs over timescales of ~115,000 to 93,000 years and these appear to be triggered after either 4 or 5 precession cycles. One issue with understanding the pattern and potential forcing of cycles of interglacials are the criteria used to define them. These have traditionally been defined as a time period that is as warm or warmer than the Holocene. However, a more

recent definition is the absence of substantial Northern Hemisphere ice outside Greenland (Past Interglacials working group of PAGES *et al.*, 2016), which suggests that the idea of the 100 ka glacial-interglacial cycle for the last 800,000 years is an oversimplification. By examining global ice volume recorded in the best available long term archive, the LR04 stack (Lisiecki and Raymo, 2005), they note that in the last 800,000 years some MIS sub stages classified as interstadials have similar marine benthic oxygen isotope values as their associated interglacial phases. In this scheme, substages MIS 7a-c and MIS 15a were classified as interglacials in addition to the traditional integlacials of MIS 7e and 15e. Thus, there are more interglacials within the last 800,000 years than would be accounted for if the 100 ka cycle was the only driver of a successful initiation of an interglacial. This effectively means that there is a more complex pattern of forcing behind interglacial inception and this has led Tzedakis *et al.*, (2017) to develop a model based on the effective energy of an insolation peak, which is a combination of the caloric half year summer insolation value, and the time since the previous interglacial. The latter component is a function to recognise that the build-up of ice over time will generate inherent instabilities and reduce the caloric energy threshold for a successful interglacial. Thus, the current interglacial was successfully initiated partly due to insolation forcing but also because MIS3 did not cross the threshold for deglaciation, thereby lengthening the time since the previous interglacial and allowing the effective energy of MIS1 to cross the threshold of a successful initiation of an interglacial.

1.3.1.2.3 The Mid-Pleistocene-Transition

One of the most difficult to understand events in the Quaternary climate history has been that of the Mid-Pleistocene Transition (MPT; also known as the Mid-Pleistocene revolution (MPR)), which occurred between 650 ka – 1 .25 Ma years ago and is documented by a change in dominance from low amplitude high frequency ~41 ka ice volume changes, to higher amplitude lower frequency ~100 ka ice volume changes (Clark and Pollard, 1998; Imbrie *et al.*, 1993; Maslin *et al.*, 2001) (see figure 1.2). As there is no change in the astronomical forcing over this interval, the causes of this transition are complex.

Several theories have been suggested to have triggered this transition, and many of these include the need for internal natural climate system changes in response to long term cooling, potentially linked to lowering atmospheric pCO_2 (e.g. Tziperman and Gildor, 2003). In the Tziperman and Gildor (2003) theory, the MPT is triggered as general cooling as a result of lowering CO_2 and this allows extensive sea ice cover, which activates their 'sea ice switch' (SIS) mechanism (Tziperman and Gildor, 2003).This mechanism is thought to be driven by the influence of sea ice on atmospheric energy balance and air-sea fluxes, allowing a switch in the climate system. Other studies have suggested that the large ice sheets emerged in relation to atmospheric CO_2 and CH_4 concentrations, either with CO_2 driving ice volume (Imbrie et al., 1992) or ice sheets controlling CO_2. Ruddiman (2006a, 2006b) propose a hypothesis based around both an insolation forced component of ice volume and amplification of the signal by a complex series of ice sheet and CO_2 feedback mechanisms. These include ice sheet influences on ocean circulation, ocean stratification, and strengthening of the Asian winter monsoon. In this model, these drivers continue to operate either side of the MPT. However, reduced ice ablation, as a result of long term cooling, and the influence this had on ice sheet mass balance, allowed ice sheets to be sustained during weaker insolation maxima, that in the 41 ka world would have resulted in a termination. One theory for this increased ice volume can be explained by the regolith hypothesis. This was based on the observation that ice sheets before the MPT covered a similar land area as those after the MPT, but as total global ice volume was smaller, these ice sheets must have been thinner, leading to the development of the regolith hypotheses. This theory suggests the MPT could have been triggered by ice sheet dynamic changes driving a switch from large thin ice sheets in the 41 ka world, to thicker ice sheets with dominant changes over an ~100 ka time period after the MPR (Clark *et al.*, 2006; Clark and Pollard, 1998). Ice sheet dynamic changes are proposed to be caused by a shift from a soft bedded to a mixed bedded ice sheet (increased hard bedded areas), which is driven by progressive erosion of the regolith and exposure of the un-weathered crystalline bedrock (Clark *et al.*, 2006; Clark and Pollard, 1998). The changes at the base of the ice sheet allow alterations in the thickness of the ice, with soft beds allowing movement through a combination

of internal ice deformation, basal sliding and subglacial sediment deformation, while movement by deformation occurs more readily on hard beds and allows the build-up of thicker ice sheets (Clark *et al.*, 2006; Clark and Pollard, 1998). Interestingly, a combination of both reduced CO_2 and the removal of the regolith produce realistic models of Quaternary glaciation, as indicated by a comparison of modelled and observed benthic $\delta^{18}O$ in transient simulations of the CLIMBER-2 model (Willeit *et al.*, 2019). Although it should be noted that this is a model of intermediate complexity with course spatial resolution and a number of simplifications and assumptions. These processes can account for the required reductions in sea level, documented after the MPT, with increased transfer of organic matter to DIC in oceans being driven by exposure of increased continental shelf and slope deposit, and this accounts for an observed shift in deep sea $\delta^{13}C$ values (Clark *et al.*, 2006). Alternatively, it has been proposed that a gradual rise in the deglaciation threshold from 1.55 to 0.61 Ma led to an increase in the frequency of skipped insolation peaks after 1 Ma, with longer glacials allowing the accumulation of larger ice sheets (Tzedakis *et al.*, 2017). Global cooling, perhaps driven by a decreasing atmospheric CO_2 concentrations, may have been responsible for the rise in the deglaciation threshold.

1.3.1.2.4 Late Quaternary Orbital Forcing Records in Siberia

The framework of orbital forcing for the Late Pleistocene and Holocene are well established, with key records and chronologies underpinning the theory. For the time period considered by this PhD project (back to ~30 ka BP) summer insolation data for mid and high latitudes are available (Berger *et al.*, 1999; Berger and Loutre, 1991), providing a clear baseline of the orbital forces operating over the considered timescale. These insolation data have already been considered against proxy records from Lake Baikal, where it appears that diatom productivity is influenced by changes in the Earth's orbit (Colman *et al.*, 1995; Khursevich *et al.*, 2001; Mackay, 2007; Prokopenko *et al.*, 2001; Williams *et al.*, 1997), suggesting that the Siberian High is influenced by variation's in insolation, in addition to being influenced by more abrupt events.

1.3.2 Solar Activity

An additional external forcing factor that operates at more abrupt timescales are variations in solar activity. Further to events occurring on millennial timescales, climate is influenced by several shorter-term events on centennial to decadal scales. This includes the influence of sunspots. Sunspot activity varies on many cycles, although the 11-yr Schwabe cycle is the most prominent in recent records. Additionally, sunspot numbers, and by extension solar activity, are known to fluctuate on longer timescales and this has been argued to be a driver of climatic instability, particularly in the Holocene (e.g. van der Plicht *et al.,* 2004). For example, correlations between cooling, particularly across the Northern Hemisphere, have been observed between reductions in temperature of ~1˚C and a range of proxies for reduced solar activity. These include the Dalton and Maunder minima (17^{th}-19^{th} century) in sunspot activity (Mursula *et al.*, 2001) and changes in cosmogenic nuclide production being coincident with the reductions in temperature in some parts of the Northern Hemisphere, including Greenland, the North Atlantic, Northwest Europe and across the Northern Hemisphere continents as far East as China (e.g. van Geel *et al.,* 1996; Mann *et al.,* 2009).

Beyond the period of recorded sunspot activity, cosmogenic nuclides carbon-14 (^{14}C) and beryllium-10 (^{10}Be) (Ogurtsov, 2005; van Geel *et al.*, 1999) have been measured in annually resolved archives such as ice cores and tree rings and used to reconstruct solar activity. These cosmogenic nuclides are produced through cosmic ray bombardment of the upper atmosphere, which is weakened during periods of high solar activity, through interaction with the solar wind. The mechanisms of the impact of solar activity are debated, particularly as the reduction in solar energy to the upper atmosphere during solar minima is relatively small. As little as ~1 W/m^2 is reconstructed for the Little Ice Age (LIA) solar minima (Kopp *et al.*, 2016), and thus feedback mechanisms have been proposed as a means of propagating the energy reduction into a more widespread impact on climate. These include changes in cloud cover and coupling between stratospheric heating and tropospheric weather patterns, alongside changes in stratigraphic ozone (Engels and van Geel, 2012). In particular, instrumental data suggests that the position of the

North Atlantic Oscillation is deflected south during solar minima inducing cool conditions in the North Atlantic region (Gray *et al.*, 2010). The impact of grand solar minima similar to the LIA on future climate, at least across the Northern Hemisphere continents and North Atlantic, may be an important modulating factor on future human induced warming (Lockwood *et al.*, 2010). Recent work has also suggested that the link between solar activity and NAO may also influence sea ice cover, which is part of the internal feedback drivers discussed below (Sha *et al.*, 2016). Solar forcing has also been implicated as a driver behind some of the larger amplitude changes observed earlier in the Holocene, including the 2.8 ka BP event seen across the North Atlantic region (Martin-Puertas *et al.*, 2012).

1.3.3 Internal forcing factors

Orbital and solar activity forcing control the total amount of solar radiation, the distribution of that radiation and differential heating of the atmosphere. There are, however, significant internal feedback mechanisms, ocean circulation, albedo effects, and volcanic activity that can induce climate changes superimposed on long term climate forcing. Alongside these changes, it has been demonstrated by key archives, such as ice cores, that Quaternary climatic changes can occur much more abruptly and over much shorter timespans, overlain over orbital changes. These changes are characterised by rapid transitions between different conditions, as the climate system is moved into a new state through crossing a threshold (Alley *et al.*, 2003). High resolution records suggest that large temperature shifts can occur within decades (Anderson, 1997), but the reorganisation of the atmospheric system that accompany them can both be annual (Steffensen *et al.*, 2008) and regionally time transgressive (Lane *et al.*, 2013; Rach *et al.*, 2014). The dominant proposed mechanisms driving these changes, across a range of studies, are shifts in ocean circulation patterns. These are suggested to be driven by the interaction of ice sheets, sea ice and oceans (Broecker, 1994; Vettoretti *et al.*, 2018; WAIS Divide Project Members *et al.*, 2015).The detail of these interactions are not, however, fully understood and how they drive key episodes of change within the Last Glacial cycle and the Holocene are debated. Thus, these forcing factors are reviewed with relevance to the key

climatic events prevalent in the literature, where there is the potential for wide scale climatic impacts of relevance for Siberia during the past 30 ka.

1.3.4 Dansgaard-Oescheger cycles, Heinrich events and Bond cycles

Millennial scale or 'abrupt' events include Dansgaard-Oescheger (D-O) cycles, rapid shifts between stadial and interstadial conditions (Hicock *et al.*, 1999) and Heinrich events, which are recorded by high levels of ice-rafted-debris in the North Atlantic known as Heinrich layers (Bond *et al.,* 1993, Prokopenko 2001, Hemming 2004). These two types of events are linked, with several rapid D-O cycles being bundled together, getting successively cooler and forming a saw toothed shaped cooling cycle (figure 1.4), culminating in a Heinrich event (see below), after which there is rapid warming (Bond *et al.*, 1993). These packages of climate change, noted in both marine and ice core records, make up Pleistocene Bond cycles (Bond *et al.*, 1993).

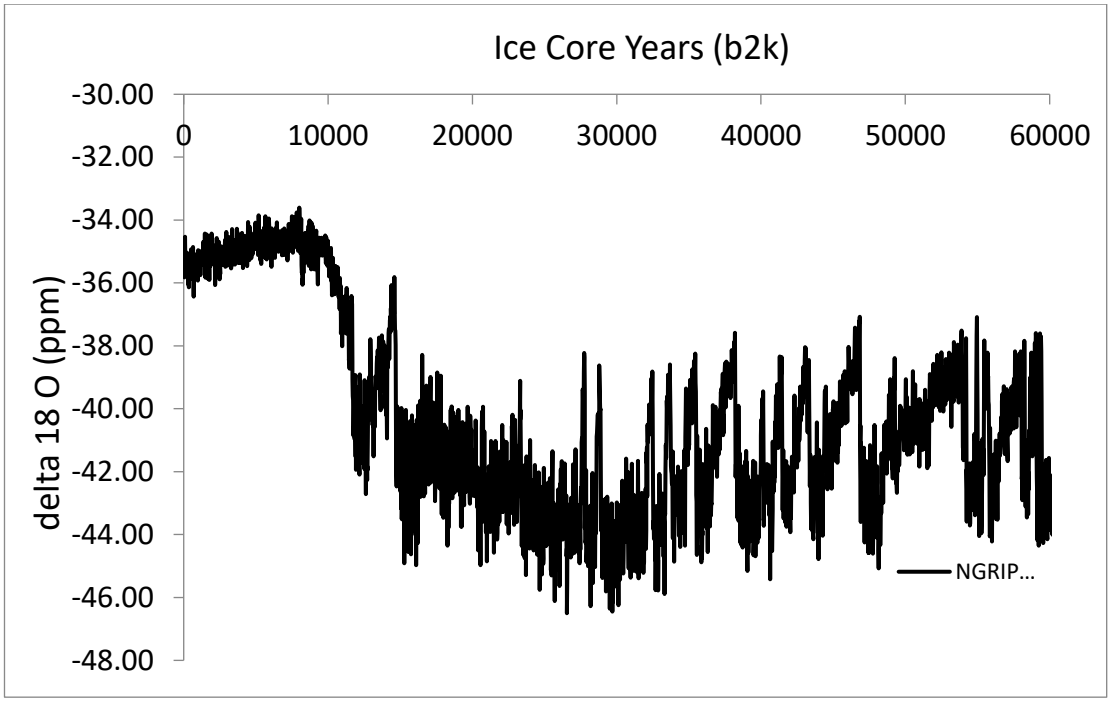

Figure 1.4: The NGRIP Greenland Ice Core record of abrupt climate change over the last 60 ka in Ice Core Years before 2000 (Rasmussen *et al.*, 2014a). The record shows key features of the climate system including the saw tooth pattern of climate change, especially during MIS 3 (~29-60 ka BP) and Last Glacial to Interglacial transition (18-8 ka BP). The Last Glacial Maximum ~25 ka BP and Heinrich event 1 cooling ~17 ka BP are also visible in the record.

D-O cycles are seen throughout the last glaciation as rapid shifts between warmer interstadial periods and colder stadials, on a millennial timescale. The

cycles were first recognised in Greenland ice cores (Dansgaard *et al.*, 1993, 1982), and cause large amplitude climate changes with suggestions of a 5°C temperature shift between the two phases (Bond *et al.*, 1993). The warming at the start of a D-O cycle is considered to be the more abrupt, while cooling is more gradual (Rasmussen *et al.*, 1997), creating an asymmetrical shape (Bond *et al.*, 1993). The initial causes of the D-O cycles are debated, with some linking it to two solar cycles operating on a 210 year and 81 year cycle, which synchronise on changes in the North Atlantic every ~1470 years (Dansgaard *et al.*, 1993). Other suggested mechanisms include freshwater forcing (Bigg *et al.*, 2011), with interstadial modes starting abruptly as the Polar front migrates northwards, while the gradual cooling corresponds to the southward spread of polar waters and southward movement of the polar front (Rasmussen *et al.*, 1997). Over several cycles significant quantities of ice are able to accumulate on the North American Ice sheet (Bigg *et al.*, 2011). The cycles have also been discussed as being linked to changes in Atlantic Meridional Overturning Circulation (AMOC), and, thus, variability in oceanic heat transport to the North Atlantic, though ocean-ice and meltwater interaction are also known to be significant (e.g. Petersen *et al.,* 2013).

The pacing of D-O cycles has been thought to indicate that these events may continue into interglacial periods, where they are known as Bond events (Bond, 1997; Wanner and Butikofer, 2008). During the Holocene, these cold episodes have left IRD peaks, which are suggested to be driven by a cycle centring on ~1470±532 years (Bond, 1997). During these periods it is thought that ice bearing waters sourced north of Iceland reach equivalent latitudes to Britain, accompanied by atmospheric shifts around Greenland, which suggests coupling between ocean and atmospheric systems (Bond, 1997). The occurrence of these abrupt events through the interglacial Holocene period is supportive of the cyclic D-O cycles during the Late Pleistocene not being driven by internal ice sheet instability, but by climate cycles (Bond, 1997). Some studies have suggested these cycles are driven by variations in solar output, showing correspondence between production rates of cosmogenic nuclides carbon-14 (^{14}C) and beryllium-10 (^{10}Be) and proxies of drift ice (Bond *et al.*, 2001). Models have supported the theory that these

changes may be driving abrupt climate changes during the Holocene, with periods of reduced solar irradiance causing atmospheric cooling in high northern latitudes, which in turn drives a southward shift of the northern subtropical jet and a decrease in northern Hadley circulation (Bond *et al.*, 2001). These changes may lead to increases in North Atlantic drift ice, ocean surface cooling and cooling of the atmosphere above Greenland, and additionally these events may have, at points, been amplified by reduced North Atlantic THC, particularly if the events are accompanied by increased sea ice in the Nordic seas (Bond *et al.*, 2001). Other studies have argued that Holocene Bond events are not real, and that climatic events seen through the Holocene are the result of different forcings, with early Holocene events linked to meltwater pulses, while later events are driven by a range of factors, including changes to ocean circulation in the North Atlantic, sunspot activity and volcanic eruptions (Wanner *et al.*, 2011; Wanner and Butikofer, 2008).

D-O events are coupled in an antiphase relationship with Antarctic climate oscillations through the bipolar seesaw (Stocker and Johnsen, 2003; Wunsch, 2003) and it may be that this global teleconnection is the driver behind both signals. Mechanisms that have been proposed as drivers of the interhemispheric system include changes in oceanic heat distributions, and potentially an atmospheric driver through shifts in the inter-tropical-convergence-zone (ITCZ; Cvijanovic *et al.,* 2013), the latter also suggesting that tropical precipitation regimes are influenced by climate forcing from high latitudes in both hemispheres.

Recent high resolution coupling of the Greenland GICC05 record and the West Antarctic Ice Sheet (WAIS) using CH_4 synchronisation (WAIS Divide Project Members *et al.*, 2015) indicates an even more complex relationship between high latitude climate change between the two hemispheres that also suggests an ocean heat transfer as the most likely driving mechanism for abrupt change in both regions. During the cold and warm oscillations of the Greenland D-O cycles the Antarctic record lags Greenland in cycles of warming or cooling, following the bi-polar relationship. At turnover points, Greenland warming leads Antarctic cooling by 218 ± 92 years across multiple D-O cycles along with a similar 208 ± 96 years lag as Antarctic cooling follows Greenland

warming (WAIS Divide Project Members *et al.*, 2015). Lags on the scale of hundreds of years suggest the coupling mechanism is likely to be driven through ocean current heat distribution, as an atmospheric mechanism would be likely to be much faster. It also suggests, however, that the interhemispheric coupling is a key part of the driver behind abrupt change in the two regions as the lag time is consistent in both Greenland warming and cooling.

Two recent papers have attempted to add additional light onto this issue by running full coupled General Circulation Model simulations of D-O cycles (Peltier and Vettoretti, 2014; Vettoretti *et al.*, 2018). These models are the type used for future climate prediction and are computationally expensive, thus, a transient simulation of the earth system over several thousand years is rare. The model is run in Glacial/Interglacial and intermediate conditions. During the latter set of conditions D-O cycles and the bipolar seesaw are simulated. The key driver appears to be sea ice formation in the Arctic ocean periodically trapping and releasing heat and driving thermohaline variability. The simulated D-O cycles and the thermohaline oscillation do not require freshwater forcing from ice sheets, unlike other models simulating abrupt change in this period.

Another key feature of glacial climates are Heinrich stadials. These cold periods correspond to periods where Heinrich events (H1, H2 etc.) occurred, leaving large fluxes of IRD with a component from the Laurentide Ice sheet found in North Atlantic deep sea sediments (Bond *et al.*, 1993). First documented by Heinrich in 1988, Heinrich events themselves are thought of as incredibly rapid, with IRD being deposited across the North Atlantic (Heinrich, 1988; Hemming, 2004). Heinrich stadials tend to last slightly longer than normal D-O cycle stadials, and in many cases individual Heinrich events create varying responses. Despite this, Heinrich events do not stand out more prominently that other D-O stadials in the Greenland ice core stratigraphy (Hemming, 2004) (Figure 1.3 and 1.4). The IRD material that forms Heinrich layers is thought to have been sourced from a limited region, which indicate the major iceberg source was from the Hudson Strait outlet of the Laurentide ice sheet (Hemming, 2004). This is supported by petrographic and isotopic provenance indicators (Hesse and Khodabakhsh, 2016), alongside the thinning of detrital layers, which is significant between the Labrador sea and

the European end of the 46°N iceberg route (Broecker, 1994). However H3 and H6 are suggested to have a wider spread of provenances, with a stronger influence of European sources (Hemming, 2004). IRD that makes up Heinrich layers is generally characterised as having high levels of detrital carbonates and low foraminifera content, due to lower productivity and dilution by rapid deposition of sediments (Broecker, 1994; Hesse and Khodabakhsh, 2016). Utilising the information available about the source regions of IRD can assist in understanding the mechanisms that drive the events.

Originally Heinrich events were initially thought to appear on a periodicity of 11,000 ±1000 years; a half period of the precession cycle (Heinrich, 1988). Heinrich (1988) indicated this was due to periods of high and low summer insolation; the former due to meltwater discharge from ice sheets into polar seas, which enhanced sea ice growth in winter, while the latter caused continental ice growth and iceberg carving, reducing surface water salinity. Heinrich (1988) proposed that these changes would both drive polar waters southwards. Since Heinrich's proposals, the triggers have been debated, and it has been noted that between 70-10.5 ka BP, Heinrich event cycles are seen to occur every ~7.2ka ± 2.4ka (Sarnthein *et al.*, 2001), and they are followed by abrupt warming (Bond *et al.*, 1993). Heinrich events have been proposed to be driven by interaction between ocean circulation in the North Atlantic, iceberg discharge and meltwater pulse events, and the waxing and waning of high latitude Northern Hemisphere ice sheets. These interactions are suggested to drive two stages of North Atlantic thermohaline circulation (THC), with an 'on' mode where the Atlantic conveyor brings warm tropical waters, supplying heat to the North Atlantic (as observed at present), and an 'off' setting where freshwater input into the North Atlantic shuts off the thermohaline driver of North Atlantic THC, allowing significant ice sheet growth, and ultimately iceberg discharge and cold North Atlantic conditions (Alley, 2007). Heinrich stadials are thought to be induced by changes in winds, including the westerlies which cause propagation of cold conditions across the Northern Hemisphere high latitudes (Guillevic *et al.*, 2014; Hemming, 2004), while changes correlated in the tropics are thought to be linked to stronger

trade winds; stronger winter monsoons are also thought to propagate the changes (Hemming, 2004).

Various mechanisms have been proposed as driving the interactions that lead to the on/off phase in THC. These include the binge-purge hypotheses suggested by MacAyeal (1993), which involves the Laurentide ice sheet building 'binge' phase, where the ice is cold-based and builds mass, followed by 'purge' phase where a thick ice sheet is wet-based with basal sliding causing iceberg carving, which inputs freshwater into the North Atlantic from the Hudson Strait (MacAyeal, 1993). The purge phase is thought to be bought about by a combination of geothermal heat, advection of heat from the upper surface of the ice and internal friction at the base of the ice, which act to destabilise the ice sheet causing basal sliding (Hemming, 2004). The freshwater input this causes reduces the strength of the North Atlantic THC due to reduced salinity, which in turn promotes further ice sheet growth (MacAyeal, 1993). Eventual thinning of the ice sheet due to iceberg calving leads to periodic failure of the Laurentide ice sheet (MacAyeal, 1993).

The major issue with this proposed mechanism links to additional data from glacial advances, which suggest that glaciers advance almost simultaneously, within radiocarbon uncertainties, and for this to occur the Heinrich events cannot be triggered by internal instabilities within the Laurentide ice sheet (Broecker *et al.*, 1992; Broecker, 1994). Alternatively external climatic forcing has been implicated, with temperature changes allowing advances in both glaciers around the globe and iceberg discharge to be on a relatively similar timescale (Broecker *et al.*, 1992), however the issue with global temperature as a driver is that ice sheets can take tens of thousands of years to respond (Broecker, 1994). Precursor events to Heinrich events have been proposed, with suggestions that the same driver may be pushing all the ice sheets to operate on the same frequency, however the smaller ice sheets may reach collapse more rapidly than the larger ones, producing earlier precursors (Kaspi *et al.*, 2004). These again suggest that a forcing is required to drive the different ice sheets to respond on the same timescale, and it has been proposed that large amplitude atmospheric temperature changes have been

driven by sea ice through sea ice albedo and insulating feedbacks rather than large amplitude changes to the THC (Kaspi *et al.*, 2004).

A further mechanism for Heinrich events was outlined by Johnson and Lauritzen (1995) who suggested Heinrich events were caused by repetitive massive floods or jökulhlaups. These are suggested to cause significant freshwater to be almost instantaneously added to the North Atlantic, from the mouth of Hudson Bay as ice dams failed (Johnson and Lauritzen, 1995). Evidence that supports this theory comes from the York canyons on Meta Incognita Peninsula in the Hudson Strait, which acted as spillways, and additionally from a submarine braided sand plain which is thought to have received sediments from sheet flow turbidity currents from the Hudson Strait slope (Hesse and Khodabakhsh, 2016). The main issue with this theory is that it assumes that it is feasible for a lake to occupy Hudson Bay during the time of Heinrich events, and although this may have been possible during some periods, it does not appear feasible for this to have existed during the Last Glacial Maximum (LGM), around Heinrich 2 (onset ~ 24.1-24.4 ka BP) (Bigg *et al.*, 2011; Hemming, 2004). Additionally the sedimentary evidence from the region has suggested that this scenario is unlikely (Hesse and Khodabakhsh, 2016).

Catastrophic ice sheet collapse has also been suggested as a mechanism for Heinrich events. First described by C. Hulbe (1997, 2004), this theory suggests that Hudson Strait ice streams flowed into the Labrador Sea from an ice dome in Hudson Bay (Hulbe, 1997). This caused formation of an ice shelf which catastrophically collapsed causing release of icebergs and thus a Heinrich event. This model was not originally strongly supported (Hemming, 2004), and was later revised by C. Hulbe and others, to suggest that the ice shelf fringed the Laurentide ice sheet margin, with Heinrich events occurring following explosive disintegration (Hulbe *et al.*, 2004). More recently simple models have been used to support this theory, with studies suggesting that climate cooling allows ice shelves to grow, which in turn impedes ice stream discharge (Hulbe, 2010). Studies have then suggested that following this build up, basin wide subsurface warming occurred in the North Atlantic prior to a Heinrich event, as a result of a weak AMOC, and this increases the rate of ice shelf

mass loss, producing an ice-stream surge and a Heinrich event (Hulbe, 2010; Marcott *et al.*, 2011). This has been supported over recent years by evidence provided following the breakup of the Larsen B ice shelf (Hesse and Khodabakhsh, 2016; Marcott *et al.*, 2011; Rignot *et al.*, 2004), where Antarctic peninsula glacier flow accelerated significantly (between three and eightfold increases), following removal of the ice shelf, while glaciers situated further south, including the Leppard and Flank glaciers, which remained buttressed by the remains of the ice shelf, did not undergo acceleration (Rignot *et al.*, 2004). Theories surrounding this have existed for some time, with ice shelf acceleration being accompanied by the ice being stretched and thinned, and this allows increased iceberg calving, reducing buttressing, allowing faster flows (Rignot *et al.*, 2004).

In some proposed mechanisms D-O cycles are seen to drive Heinrich events. For example, meltwaters from Iceland and Greenland could reduce North Atlantic Deep Water (NADW) formation, and through the bipolar seesaw, the Southern Hemisphere warms, which in turn drives melting of sea ice or the Antarctic ice sheets, reducing formation of Antarctic Bottom Water (AABW). This causes warming of the Northern Hemisphere, and therefore triggers the next D-O cycle. It is proposed that eventually these cycles cause enough sea level rise to undercut the Laurentide ice sheet (Maslin *et al.*, 2001), triggering release of icebergs into the North Atlantic, causing a Heinrich event, which will trigger significant alternations in the salinity and temperature and cause widespread cooling, thus producing a Heinrich stadial.

Clearly the mechanisms concerning D-O cycles and Heinrich events and stadials are highly complex, and thus further studies are required to assist in resolving this. The events are linked, and it has been suggested that it takes a number of D-O cycles to build enough ice up to cause a Heinrich event (Hemming, 2004). The rapid warming following a Heinrich event has often been linked to feedback systems, with rapid sea ice melting allowing the atmosphere to warm allowing strong albedo-insulating feedbacks to occur (Kaspi *et al.*, 2004). This has also been suggested as a driver for the rapid warming phases of D-O cycles (Kaspi *et al.*, 2004). The variations in source

materials between H3 and H6 compared to H1, H2, H4 and H5 may indicate that the mechanisms of Heinrich events may vary.

Understanding these abrupt climatic oscillations is essential as they provide an analogue for studying unstable climate conditions (Ilyashuk *et al.*, 2009) in general. This allows modellers to be better informed and, therefore, improve their predictions of the future, through testing the ability of different models to encapsulate the rapidity and magnitude of change in past unstable climates. Models are currently limited in their ability to reconstruct known past climatic occurrences accurately (Alley, 2004; Roche *et al.*, 2014), and even the latest models focus largely on testing outputs based on the Polar ice core records (Peltier and Vettoretti, 2014). For a much fuller understanding of the climate system, and a more comprehensive test of model predictions spatially, it is essential that palaeo studies provide good baseline palaeoclimatic reconstructions across different regions to provide an accurate template for testing these models (Rasmussen *et al.*, 2014b). Currently the responses to these events is limited in some regions and mechanisms for amplification of the events in some localities are poorly understood (Zhang *et al.*, 2017b), meaning further study of these abrupt events and their impacts are required. One such region is southern Siberia, where understanding of the response of the Siberian High to these abrupt events is limited.

1.3.5 Centennial to Annual Scale Changes

Additionally to sunspots, volcanic eruptions can have an influence on the climate on a seasonal to decadal timescale (Anchukaitis *et al.*, 2010; Sigl *et al.*, 2015), although quantifying the effects are limited by several inconsistencies (Sigl *et al.*, 2015). Climatic variability resulting from volcanic eruptions is due to the influx of sulphate aerosols and dust into the stratosphere, which increases backscatter of solar radiation, reducing the solar radiation at the earth's surface and therefore causing cooling at regional to global scales (Sigl *et al.*, 2015). This can continue for the entire period that the sulphate aerosols are present in the atmosphere, which is usually 1-3 years in the stratosphere (Sigl *et al.*, 2015). Examples of climatic change caused by volcanic eruptions include the impact of the long term 1783-1784

Laki eruption where lower temperatures were experienced for 3 years following the eruption (Schmidt *et al.,* 2012). However, despite the increased albedo effect of the atmosphere after an eruption, there is also potential warming, due to non-uniform back reflection of radiation which can cause stratospheric warming (Kravitz and Robock, 2011), and this may also explain the very warm summer in 1783 following the onset of the Laki eruption in June (Schmidt *et al.,* 2012), although this is followed by two winters of cooling suggesting the full complexities of these feedbacks are not yet fully understood.

The season during which an eruption occurs may also influence the severity of the eruption on climate, with late spring to early summer being considered the time of year when a volcanic eruption can have the greatest effect on climate, preventing early summer warming, while from August through the winter months in the Northern Hemisphere, the effect of an eruption of the same magnitude is said to be less (Kravitz and Robock, 2011). The effects of volcanic cooling have been shown by reduced tree growth (Churakova *et al.,* 2014) and have been suggested to cause civilisation collapses, for example by triggering widespread famine which caused population declines across the Mediterranean as a result of the Justinian Plague (Sigl *et al.*, 2015), although linking this as a causal mechanism is problematic. The greatest impact in terms of climate has been proposed from the larger tropical eruptions as there is the greatest chance for a global distribution of the atmospheric particulates, although complex responses have been observed in relation to regional as opposed to global cooling and in particular winter warming in the Northern Hemisphere, despite annual average global cooling (Robock and Mao, 1992)

1.3.6 Human Induced Change

During the late Pleistocene to early Holocene there is the first evidence of the impact of *Homo sapiens* on the landscape and on climate. The onset of humans triggering climatic change is debated, with most suggesting that humans began altering the climate, as industrialisation over the past ~200 years started to increase atmospheric greenhouse gases (GHGs). Other hypotheses of humanity's influence on climate include Ruddiman's Early

Anthropogenic Hypothesis, where humans began altering climate through deforestation from c. 8 ka BP, and rice irrigation c. 5 ka BP, and this is suggested to have caused natural decreases in carbon dioxide and methane to be reversed (Crucifix *et al.*, 2005; Ruddiman, 2017, 2005). Although the early anthropogenic hypothesis has been criticised (Broecker and Stocker, 2006), the modern influence of humans on climate is clear. This has led to debate as to whether humanity has entered a new geological epoch, known as the Anthropocene (Lewis and Maslin, 2015). The use of the term is being increasingly utilised, however defining the Anthropocene is problematic, as epochs are formally classified using a Global Stratotype Section and Point (GSSP) or a date agreed by a committee, known as a Global Standard Stratigraphic Age (GSSA), and it is difficult to define this for the Anthropocene due to the time transgressive nature of events such as the industrial revolution (Lewis and Maslin, 2015). Particular dates that fit this criteria and have therefore, been considered to define the start of the Anthropocene include the 1610 Orbis spike dip in CO_2, which is considered as it gives a historical context, or the 1963 atomic weapons testing peak seen in ^{14}C (Lewis and Maslin, 2015). Despite the debate surrounding the definition of the Anthropocene epoch, it is clear that humans influence on the climate system is now accepted, with significant impacts being documented globally. Humans have caused atmospheric levels of CO_2 to reach levels not seen for over ~800,000 years, if not over several million years, and numerous studies are now documenting climatic warming trends during the 19th and 20th centuries detected in a range of settings from the oceans to cryosphere (Vaughan *et al.,* 2013), which indicate that greenhouse gas emissions are generating a significantly greater proportion of radiative forcing than solar activity (Engels and van Geel, 2012; IPCC, 2013).

1.4 The Expression and Understanding of Change

1.4.1 Late Marine Isotope Stage 3 and Early Marine Isotope Stage 2

MIS3 is a period of known climatic instability, starting ~57 ka cal BP (Lisiecki and Raymo, 2005) and this period is broadly assigned to the Middle Pleniglacial (Tzedakis *et al.*, 2013). Following the instability of MIS3, the earlier climatic conditions of MIS2 are characterised by low Northern Hemisphere

insolation and prolonged cooling, centred around the Last Glacial Maximum (LGM), resulting in significant ice advance and lowered CO_2 (Adkins, 2013). However, the transition between these two periods is often hard to define, with the transition placed as early as ~29 ka BP in marine settings based on the benthic $\delta^{18}O$ (Lisiecki and Raymo, 2005), while in terrestrial settings it has been placed as late as ~24 ka BP (Tzedakis *et al.*, 2013). This discrepancy in timing is due to different expression of changes and because of the occurrence of HE2 at ~25 ka BP, as this event is often considered to show instability that is more characteristic of MIS3, rather than MIS2. Therefore, this thesis will consider the period ~29-24 ka BP as a transitional period between MIS3 and MIS2, with the period from ~24 ka BP being considered as MIS2 and the Late Pleniglacial.

During MIS2, the Greenland ice cores document the coldest conditions and high dust content, at ~24 ka, the time period that broadly coincides with HE2, which occurs as orbitally forced insolation remains low (Alley *et al.*, 2010). Alongside this, terrestrial records document cold and arid conditions with reduced sea levels, while palaeoenvironmental records often suggest vegetation shifts, including herb dominance seen in the East China sea cores as a result of open vegetation growing on the exposed continental shelf (Xu *et al.*, 2009). Overlain over this general cooling trend, are several abrupt changes recognised within the Greenland ice cores and a variety of North Hemisphere palaeoclimatic records (Lowe *et al.,* 2008, Buizert, *et al.,* 2015), including short warming events, Greenland interstadials 2, 3 and 4 (GI-2.2, GI-2.1, GI-3 and GI-4) (Lowe *et al.*, 2008; Rasmussen *et al.*, 2014a), which last only a few hundred years (Rasmussen *et al.*, 2014a), along with two periods of significant cooling, Heinrich events 1 and 2 (Hemming, 2004) (discussed below).

Several of these MIS2 changes have been well studied in Greenland ice cores, which provide a continuous record with excellent resolution and chronological control (Rasmussen *et al.*, 2014b; Steffensen *et al.*, 2008), with different ice core locations showing striking similarities, and synchrony shown at transitions. However, it is known that specific factors also affect individual records, such as NGRIP being more influenced by Pacific precipitation compared to summit cores GRIP and GISP2 (Seierstad *et al.*, 2014). Abrupt

millennial scale D-O events in Greenland, are documented by an abrupt 10°C warming over central Greenland, which is followed by gradual cooling and then more rapid cooling, and eventually a slight warming occurs and the cycle repeats (Alley *et al.*, 2010). These abrupt events have been defined as Greenland Interstadial (GI) and Greenland Stadial (GS) events, which have been numbered according to the INTegrating Ice-core, MArine, and TErrestrial records group (INTIMATE), although in some instances these individual stadial or interstadials have been subdivided further, and is shown through additional lettering (Rasmussen *et al.*, 2014a). These rapid events have comparatives across the globe including from Chinese speleothem records (Wang *et al.*, 2001), where changes in monsoon strength are broadly similar in timing to stadial-interstadial transitions in Greenland, and also generally in line with overall long term orbital forcing (Wang *et al.*, 2001). Additionally, in Europe, records as far south as the Mediterranean (e.g. Monticchio, Tenaghi Phillipon) suggest ecosystems were being influenced by the same forcing factors recorded in Greenland (Müller *et al.*, 2011), while in central Asia evidence for some of the key transitions that occur during MIS3/2 have been reported as responses in both biological and sedimentological variability from Lake Baikal (e.g. Swann *et al.,* 2005).

1.4.1.1 Heinrich Event 2

Heinrich event 2 (HE2) (~25ka BP) (Peck *et al.*, 2007; Wang *et al.*, 2001; Zorzi *et al.*, 2015) is one of the most well documented events during the transitional period from the Middle to the Late Pleniglacial (Tzedakis *et al.*, 2013), with widespread evidence of iceberg discharge shown in ice-rafted debris layers found across the North Atlantic (Hemming, 2004). Corresponding stadial event responses are also seen across the Northern Hemisphere and have been expressed in many palaeoenvironmental archives, documented by increased aridity, lowered temperatures and vegetation shifts in several areas including central Asia, at sites including Lake Baikal (Mackay, 2007), and in Northern Europe (Cascalheira, 2013). At Hulu cave HE2 is expressed as a weakening of the summer monsoon, followed by strengthening synchronous with GI-2 in Greenland (Wang *et al.*, 2001). A weakening of global monsoons at this time has been suggested by comparison of speleothem and other archives

including tropical south America and marine cores from the Arabian sea (Medina-Elizalde *et al.*, 2017). In some localities the climatic and environmental shifts are said to have promoted technological, social and economic changes, such as in Iberia were it has been suggested to have caused development of the proto-Solutrean lithic complex (Schmidt *et al.,* 2012, Cascalheira 2013).

1.4.1.2 Heinrich Event 1 and the Mystery Interval

The expressions of Heinrich event and stadial 1 (HE1), which occurs between ~18.5-15 ka BP (Penaud *et al.*, 2010) are also widespread. As with HE2, HE1 is also documented by significant IRD being deposited in the North Atlantic (Broecker *et al.*, 1992; Heinrich, 1988; Hemming, 2004; Vidal *et al.*, 1997), and a corresponding stadial period is expressed in many different archives and proxies including: (a) widespread ice sheets across the Northern Hemisphere (Steffensen *et al.*, 2008), including re-advance of the British-Irish Ice Sheet immediately following Heinrich 1 (McCabe *et al.*, 2007); (b) vegetation shifts across Europe and as far south as the Mediterranean, such as those shown in pollen concentration changes off the Moroccan coast, where increased *Pinus* suggests extreme wind strengthening (Penaud *et al.*, 2010). The widespread nature of this event is documented through changes in monsoon strength, including the south American monsoon system, which is strengthened during Heinrich stadials (Stríkis *et al.*, 2015), while the East Asian Monsoon is suggested to have undergone changes due to HE1, with the highest mean $\delta^{18}O$ values of -5.8% being observed in Chinese stalagmites from Jiuxian cave, between 16.6-15.2 ka BP due to decreases in the summer monsoon in central China (Cai *et al.*, 2010). Similar changes are also observed in other Chinese speleothem records, such as at Hulu and Sanbao caves and these changes are thought to be due to southward retreat of the East Asian Summer monsoon as cold air masses develop fully over Siberia as a result of a strong Siberian High (Cai *et al.*, 2010). Several records have shown a twofold structure as a response to Heinrich Stadial 1, including in lake sediments in New Mexico, where it is documented by the Big Dry between 17.5-16.1 ka BP and the Big Wet between ~16.1-14.6 ka BP (Allen and Anderson, 2000; Stríkis *et al.*, 2015), which is accompanied by a weakening of the East Asian

monsoon at ~16.1 ka BP (Stríkis *et al.*, 2015), and in speleothems in Brazil where two wet events occur between 17.7-16.8 ka BP and 16.0-14.8 ka BP, which has no exact Northern Hemisphere equivalent (Novello *et al.*, 2017).

The mystery interval of MIS2 is then, perhaps, one of the least understood periods of change in the Late Quaternary Period. It encompasses the period ~17.5-14.5 ka BP, and is documented by contradicting evidence for climate in the period (Denton *et al.,* 2006). This evidence includes widespread HE1 iceberg discharge, cold sea-surface temperatures, shutdown of AMOC (Williams *et al.*, 2012), and accompanying cold conditions in North-western Europe, Greenland, the Mediterranean Sea and North Atlantic ocean, alongside an intertropical-convergence-zone (ITCZ) southward shift and weakened Asian summer monsoons. However, ice retreat is documented in East Greenland, Northern Europe and North America (Williams *et al.*, 2012), alongside temperate mountain glacier retreat in the European Alps, and in the Southern Hemisphere, including in New Zealand (Denton *et al.,* 2006).

One suggested theory to explain how these events occurred during the same period relies on the impact of HE1, with icebergs reducing North Atlantic salinity, causing AMOC shutdown. The spread of sea ice that this shutdown triggers allows the cold conditions seen to be generated, and pushes the ITCZ south, while increased Asian snow cover reduces summer warming and, therefore, reduces summer monsoon strength (Denton *et al.,* 2006). A further consequence of the AMOC shutdown is ocean circulation reorganisation through the bipolar seesaw, and this has been used to explain the reduced sea ice fringe around Antarctica and Antarctic warming alongside CO_2 increases, which may be linked to glacier retreat (Denton *et al.,* 2006). Ice sheet and glacier retreat in the Northern Hemisphere has been thought to suggest that the stadial period's summers are relatively warm, as indicated by beetles in Northern Europe (Atkinson *et al.*, 1987). One particular complexity of this theory, and the mystery interval as a whole, is why HE1 has been able to cause this widespread variety of responses, unlike earlier Heinrich events. (Denton *et al.,* 2006). Further work is required to understand the complex interplay of factors that are clearly operating in this period.

1.4.1.3 The Last-Glacial-Interglacial-Transition (LGIT)

The Last-Glacial-Interglacial-Transition (LGIT) is one of the most intensively studied time periods for considering abrupt climatic changes. This is because it is the most recent natural period of large magnitude abrupt climatic changes (Blockley *et al.*, 2004; Lane *et al.*, 2012), which make the time period a natural laboratory (Walker *et al.*, 2003). Changes during the LGIT include a rapid warming or interstadial period, which starts at ~14.7 ka BP (Alley *et al.*, 2010) and lasts for ~1800 years, followed by an abrupt stadial period between ~12.9-11.7 ka BP (Rasmussen *et al.*, 2014a). Although some of the mechanisms driving changes seen across this period are clearly understood , drivers behind some events, including the Younger Dryas, are subject to greater debate (Bakke *et al.*, 2009), although there is general agreement these relate, in part, to shifts in Atlantic Meridional Overturning circulation(AMOC) (Lane *et al.*, 2013). AMOC shifts are thought to be induced by freshwater inputs from the Laurentide and Scandinavian ice melt altering the salinity and temperature of the North Atlantic (Bond, 1997). These are thought to have induced large scale reorganisations in ocean circulation and the atmosphere (Bakke *et al.*, 2009), but their impact is spatially variable, and it is, thus, essential to understanding how they propagate across different regions (Coope *et al.*, 1998).

While the precise detail of how these events are expressed in many regions is still uncertain, a number of independently dated records clearly show similar patterns of long term and abrupt climate change throughout the LGIT. Abrupt warming such as that seen in Greenland Interstadial 1 (GI-1) (~14.7- 12.9 ka BP) are documented in terrestrial and marine records across Europe and Asia, particularly around the North Atlantic seaboard (e.g. Brooks *et al.,* 2012; Walker *et al.,* 2003), continental Europe (e.g. van Raden *et al.,* 2013) and as far east as Japan (Kossler *et al.*, 2011). Asian speleothems have highlighted similar features to Greenland during this period (Wang *et al.*, 2001). In many regions the warm interstadial period during the LGIT has been referred to as the Bølling-Allerød, which is part of the nomenclature originally found in Denmark but has subsequently been used in other contexts (Rasmussen *et al.*, 2014a). Records in Europe often show clear differences between the earlier part of the interstadial period, which makes up the Bølling (~14.7-14.0

ka b2k) and the latter Allerød period (~14.0-12.9 ka b2k) (Rasmussen *et al.*, 2006). Reconstructed temperature records made using chironomids from Lago di Origio (South Switzerland) show a 2.5-3.2°C increase at the onset of the Bølling, with a gradual increase afterwards, and this is also seen in other sites including at Lac Lautrey (Eastern France), where the Bølling period has been reconstructed with a temperature range of 14-16.5°C, while the Allerød range is 16.5-17.0°C (Heiri and Millet, 2005). At other sites, including Ammersee, south Germany, ostracod based $\delta^{18}O$ climate reconstructions suggest a much more stable interstadial (von Grafenstein *et al.*, 1999), although the differences could be related to the different proxy. Contrastingly the stable isotope record from Greenland is thought to document a gradual decline (Rasmussen *et al.*, 2006), and thus regional discrepancies appear to exist and require further study. It is possible that specific factors mean discrepancies are seen between different proxies, with chironomid records potentially showing summer trends (Samartin *et al.*, 2012), so this must be considered when comparing different proxies.

High resolution data provided by Greenland Ice cores has suggested further structure exists within this interstadial period, with 5 substages (a-e) being defined, in which stages GI-1b and GI-1d are cold periods and GI-1a,c,e are warmer periods (Rasmussen *et al.*, 2006; Rasmussen *et al.*, 2014a). GI-1e is thought of as a warm stage corresponding to the warm period of the Bølling, while stages GI-1a,b,c,d all correspond to the Allerød (Rasmussen *et al.*, 2006). Terrestrial sites have also suggested that there may be centennial scale climate oscillations through the interstadial, with Lac Lautrey documenting 2 cooling episodes of 1.5-2°C during the Allerød, with the suggestion that the first may be a response to the Gerzensee oscillation, which was first described in the Swiss lake Gerzensee (Eicher & Siegenthaler, 1976), and it is thought to correlate with GI-1b. Despite documenting two cooling periods, it is thought that Lac Lautrey does not show a response to GI-1d (Heiri and Millet, 2005). Three centennial scale climate oscillations are documented in Abernethy Forest, Scotland, which document cooling episodes, thought to occur synchronously with Greenland's, GI-1d, GI-1c and GI-1b, however, Loch Ashik in Scotland only documents a response to GI-1d where it cools by ~3.8°C

(Brooks *et al.*, 2012). The variations in specific responses to these cooling events indicates that local factors may be influencing a sites response, and further work is required to improve understanding. Despite this, studies looking at such abrupt events are often hindered by chronological issues, as large uncertainties can make determining the timing of these events difficult, while very high resolution analyses are required to capture evidence of such rapid changes.

The stadial period shown during the LGIT (12.9-11.4 ka BP) in Greenland (GS-1) is also suggested to have comparatives across the globe. In Scotland, a stadial period known as the Loch Lomond is documented as a time of ice re-advance (MacLeod *et al.*, 2011; Sugden, 2017), while in Europe a cold stadial known as the Younger Dryas, is also a period of environmental changes. However, the timing and the amplitude of these events vary in different localities, with some ice sheets and glaciers experiencing their maximum extents towards the end of the stadial while others reach them much earlier (Mangerud *et al.,* 2010; MacLeod *et al.*, 2011). Being first described by J. Mangerud in Scandinavia (Mangerud *et al.*, 1987), the Younger Dryas has become used as a global term for the late-glacial stadial period, and has been described from many localities including Jaraguá Cave (Brazil), where it is suggested to be drier during the period corresponding to the Younger Dryas, due to a colder Northern Hemisphere causing the ITCZ to be displaced south, which in turn increases moisture influx in South America and reduced the Northern Hemisphere monsoons (Novello *et al.*, 2017). Further propagation of this stadial is found in several Chinese speleothem records, such as those found in Hulu, Sanbao, and Dongge Cave that show major shifts in their $\delta^{18}O$ signals, which appear synchronous (within errors) with changes documented in Greenland (Wang *et al.,* 2001; Dykoski *et al.,* 2005; Liu *et al.,* 2014).

Despite synchronicity being suggested for the timing of the shifts seen during the LGIT at several sites, Antarctic temperatures do not follow this trend, with the warm GI-1 stage in Greenland occurring at the same time as the cold Antarctic Cold Reversal (ACR), while the cooling shown in GS-1 occurs as Antarctica undergoes warming (WAIS Divide Project Members *et al.*, 2015).

This is thought to be due to the bipolar see-saw as discussed previously (WAIS Divide Project Members *et al.*, 2015).

Responses to these events propagate to different localities through shifts in atmospheric circulation patterns, possibly as a response to initial changes in ocean circulation (Lane *et al.*, 2013). Studies are now starting to demonstrate greater details in the propagation of these abrupt events, such as their time-transgressive nature, which has been documented between Meerfelder Maar and Kråkenes, where warming is delayed at sites situated further north in Europe due to the gradual retreat in the polar front (Lane *et al.*, 2013). Further high resolution studies, with precise and accurate chronologies, are required to allow deeper understanding of the time-transgressive nature of these events, and additionally to further knowledge in areas where studies are more limited, including Siberia, where expression of these abrupt events are poorly understood and constrained. Of the few detailed records that exist from Lake Baikal, mean annual temperatures and precipitation were lower during the Younger Dryas in southern Siberia (Tarasov *et al.*, 2007), leading to a reduction on summer river flow into the lake (Mackay *et al.,* 2011).

1.4.2 Marine Isotope Stage 1 – The Holocene

The current interglacial period, the Holocene has long been viewed as more climatically stable than the last glacial period (Dansgaard *et al.*, 1993; deMenocal and Bond, 1997), however over the past few decades, it has now become clearer that climate during the Holocene is more complex than previously thought. One of the best overviews for Holocene climate is provided by the Global Temperature Stack produced by Marcott *et al.,* (2013). This temperature stack is based on 73 globally distributed records covering the last ~11.3 ka BP, and it documents a general trend of Early Holocene warming between 10-5 ka BP, which is followed by a decline in temperatures of ~0.7°C in the Mid to Late Holocene (Marcott *et al.*, 2013). Regional variations are documented by records that have been incorporated in the stack, with the Northern Hemisphere 30-90°N region documenting more cooling than the region 30°N to 30°S, and this is suggested to be linked to a greater role of summer insolation across these latitudes and additionally due to feedbacks

with vegetation and snow-ice albedo (Marcott *et al.*, 2013). This demonstrated that regional variations are clearly documented through the Holocene due to specific locational features, although currently the stack is not fully resolved for periods shorter than 2000 years, and, therefore, it is not yet able to document more rapid climatic changes (Marcott *et al.*, 2013).

Overlain over these general trends recorded in the Marcott *et al.,* (2013) temperature stack, the Early to Mid Holocene (from ~11.7-6 ka BP) undergoes several periods of climatic instability, although magnitudes of these shifts are more muted compared to the LGIT. The period features several key climatic excursions, including the Pre-Boreal Oscillation (PBO), the 9.3 ka and 8.2 ka BP events, the latter two being clearly documented in the Greenland Ice cores (Lowe *et al.*, 2008). These excursions have also been recorded in numerous marine and terrestrial archives, particularly in North Atlantic sea-board records (Hoek and Bos, 2007) and in continental Europe (e.g. Heiri *et al.,* 2004). The forcing factors behind early and mid-Holocene climate changes are also debated with some authors suggesting Holocene climate change is controlled by Holocene Bond cycles (Bond, 1997). This model has been augmented by the hypotheses that the major early Holocene THC events are triggered by catastrophic meltwater pulses driven by glacial lake outburst floods (Barber *et al.*, 1999; Rohling and Pälike, 2005) as the Laurentide ice sheet retreated (Teller *et al.*, 2002). Lake Agassiz outburst floods have been proposed as a driver for both the PBO and 8.2 event alongside Greenland stadial 1, with releases of 9300 km^3 for the PBO and 163000 km^3 for the 8.2 BP event (Teller *et al.*, 2002). The significant quantity of water available for the 8.2 ka BP event is suggested to be due to a merge between Lake Agassiz and Lake Ojibway, which lay along the Laurentide Ice Sheet margin, and it is possible that this large quantity of water caused this event to be particularly prominent in archives across the Northern Hemisphere (e.g. Wagner et al., 2002; Cheng et al., 2009). In comparison the PBO is much more subtly recorded in some proxy records (Björck *et al.*, 1997), although this is regionally variable, with some areas demonstrating shifts in climate as large as the 8.2 BP event (Blockley *et al.*, 2018). Debate exists as to whether the freshwater triggering the PBO may actually have been sourced through Baltic Ice Lake drainage (Teller *et al.*,

2002), and the positioning of the freshwater source's outflow is said to have influenced the magnitude of the events. The PBO is suggested to be smaller in magnitude than the cooling linked to the Younger Dryas, due to the outflow being in a north-west direction into the Arctic ocean, rather than east into the North Atlantic (Teller *et al.*, 2002). It is also thought that the THC may have been less sensitive by this time as the Gulf of Mexico was no longer receiving meltwater and thus there was less preconditioning to change by the time of the PBO. The timing of the PBO is thought to be comparative to a cooling event found in the Greenland Ice cores, known as the 11.4 ka BP event (Rasmussen *et al.*, 2014a), however dating of the PBO has long been considered problematic due to the event's short duration and an atmospheric radiocarbon plateau occurring at the time of the event, which limits the precision of dating (Björck *et al.*, 1997). Additionally, the Greenland NGRIP ice core suggested there are two events occurring in close succession at 11.4 ka and 11.1 ka BP, although there is only one event documented in GRIP (Rasmussen *et al.*, 2007). Terrestrial sites including Star Carr, England, have also suggested two abrupt climate events occur during this period, coincident with the events seen in NGRIP (Blockley *et al.*, 2018) and, therefore, there is significant complexity in the climate over this interval, and potentially, site specific factors are critical for how well they are recorded. Propagation of these events, like those seen during the Late Pleistocene are also seen further afield, including in $\delta^{18}O$ records from Chinese speleothems where they punctuate the record, suggesting declined East Asian summer monsoon intensity during these abrupt episodes, and several of these shifts can be correlated within errors, to the Greenland Ice cores and to the Lake Agassiz outburst (Dykosko *et al.*, 2005).

Mid to Late Holocene climate change in the pre-industrial period is generally muted by contrast to earlier records, due to different forcing mechanisms after deglaciation of the last glacial ice sheets had completed. However, there is now well documented evidence for abrupt warming and cooling episodes of a few degrees in temperature. The 4.2 ka event documented by Bond (1997), is linked to aridity across parts of western Asia (e.g. de Menocal 2001), with environmental effects and impacts on populations seen as far east as China

(Liu and Feng, 2012; Wenxiang and Tungsheng, 2004), however the drivers of this event are not certain (Wanner *et al.*, 2014). The late Holocene event dated at c. 2.8 ka BP may have been caused by an abrupt deep reduction in solar activity, often called a Grand Solar Minimum. This led to a decline in North Atlantic surface water temperatures (Andersson *et al.*, 2003) and weaker AMOC (Hall *et al.*, 2004). The cool 2.8 ka BP event is thought to have impacted past populations as far east as Siberia (van Geel *et al.*, 2004).

The Medieval Warm Period (MWP) (or Medieval Climatic Anomaly (MCA)) (Stine, 1994) followed by cooling through the Little Ice Age (LIA) are some of the best documented of the more recent Holocene events, which is suggested to have been the most recent cool phase of a Holocene Bond cycle (Wanner and Butikofer, 2008). LIA temperatures are thought to have declined by 1-2°C, at least in the Northern Hemisphere. This has been documented in high resolution temperature archives including, tree rings, lake records and speleothems (Blyakharchuk *et al.*, 2017; Goosse *et al.*, 2006; Paulsen *et al.*, 2003; Pfister and Brázdil, 2006; Reid, 1997). The driving mechanisms behind the LIA, and other Holocene climate variability are debated, as both solar activity (Cole-Dai *et al.*, 2013; Engels and van Geel, 2012; Reid, 1997) and volcanic forcing have been suggested (Cole-Dai *et al.*, 2013).

Human influence on climate and environments, have been well documented through recent centuries and decades (Cubasch *et al.*, 2013; IPCC, 2013; Vaughan *et al.*, 2013). Many studies are now highlighting environmental responses to these changes, which include significant ice loss (Hanna *et al.*, 2008), and warming lake waters, (O'Reilly *et al.,* 2015) including a 2°C increase between 1977-2003 in Lake Baikal, the largest freshwater lake in the world (Izmest'eva *et al.,* 2016). These changes have resulted in many secondary effects such as permafrost melt (Gordov and Vaganov, 2010), increased forest fires (Soja *et al.*, 2007), biome shifts and degradation (Gordov and Vaganov, 2010). Depletions in carbon and nitrogen ratios have been documented since the 19th century as emissions have increased from fossil fuels and fertiliser production (Dean *et al.*, 2014), and the global nitrogen cycle has been significantly affected by the introduction of the Haber-Bosch process in 1909 (Howarth, 2008). Despite being well documented, individual impacts

from humans vary in different regions, with some areas appearing more sensitive than others. Additionally, in some cases the onset of these changes is registered at different times and occurs at different rates. Therefore, further work is required to understand these modern changes, and palaeoenvironmental studies are necessary to provide context for human induced changes.

1.5 Siberia

Modern Day Siberia is one of the most continental regions in the world (Chytrý *et al.*, 2007; Huhne and Slingo, 2011), occupying an area of 13.1 million km^2, between the Arctic Ocean to its southern border with Mongolia and China and north-central Kazakhstan, and east from the Ural mountains to the Pacific Ocean (see figures 1.5 and 1.6). This region includes a variety of ecosystems, with the forest-steppe ecotone being very sensitive to climatic alterations (Mackay *et al.*, 2017). The continentality of the region provides a key opportunity to study palaeoenvironments, away from areas heavily influenced by oceanic forcing. Additionally, the region is currently undergoing rapid warming at twice the global average rate and this is causing Siberia to undergo many alterations (Tchebakova *et al.*, 2009; Törnqvist *et al.*, 2014), and climate model predictions for this region are uncertain (Swann *et al.*, 2018).

1.5.1 Modern Day Climate: The Siberian High

Siberia's climate is strongly seasonal being dominated by the Siberia High during winter months. This Siberian High is a semi-permanent anti-cyclone, which builds from August and dissipates by April. The system has extreme central core pressures exceeding 1030 kPa (Tubi and Dayan, 2013), and brings the densest, coldest air-masses found in the Northern Hemisphere, which trigger continental-scale cold conditions across Siberia, and additionally Mongolia, Eastern China and Korea (Park *et al.*, 2014). Regions which are situated in the core of the anticyclone, particularly northern Mongolia and the Baikal region of Russia, achieve lows of -40°C as a result of continuous radiative cooling (Tubi and Dayan, 2013) (see figure 1.5).

During the summer the Siberian High dissipates, and in the absence of the blocking high, westerly winds from the North Atlantic enter the region, bringing

moisture into the continent, causing a summer season peak in precipitation levels, although precipitation levels decline moving east (Huhne and Slingo, 2011). Additionally, summer temperatures are relatively high, allowing warm advection over the region (Tubi and Dayan, 2013).

The Siberian High interacts with surrounding synoptic systems, particularly the Icelandic low to the north-west and the Aleutian low to the east (see figure 1.5). The pressure gradients between the Aleutian low and the Siberian High generate the strong horizontal pressure gradient required to drive the monsoonal northerlies, which are characteristic of the East Asian winter monsoon (Tubi and Dayan, 2013). As a result of this, the Siberian High and the East Asian monsoon are closely linked, with a strong East Asian Summer Monsoon occurring after a weak Siberian High, while a strong East Asian Winter Monsoon occurs alongside a strong Siberian High, as a result of the larger pressure differences (Tubi and Dayan, 2013). During periods of strength the Siberian High also moves southward and intensifies (Park *et al.*, 2014; Tubi and Dayan, 2013). A strong Siberian High is also associated with a negative phase of the Arctic Oscillation, driven by reduced westerly zonal winds in the mid-latitudes and strong polar highs (Tubi and Dayan, 2013), while Northern Hemisphere Ice sheets are also implicated in Siberian High strengthening (Löfverström *et al.*, 2014).

The strength of the Siberian High therefore has a significant control over the region's climate. Recent anthropogenic warming has influenced the Siberian High, triggering changes in its strength (Jeong *et al.*, 2011), and these current patterns suggest changes in Siberian High strength over the late Quaternary are possible, with some proxy records, including the K^+ record from GISP2 (Mayewski *et al.*, 2004), suggesting changes in strength have occurred during this period.

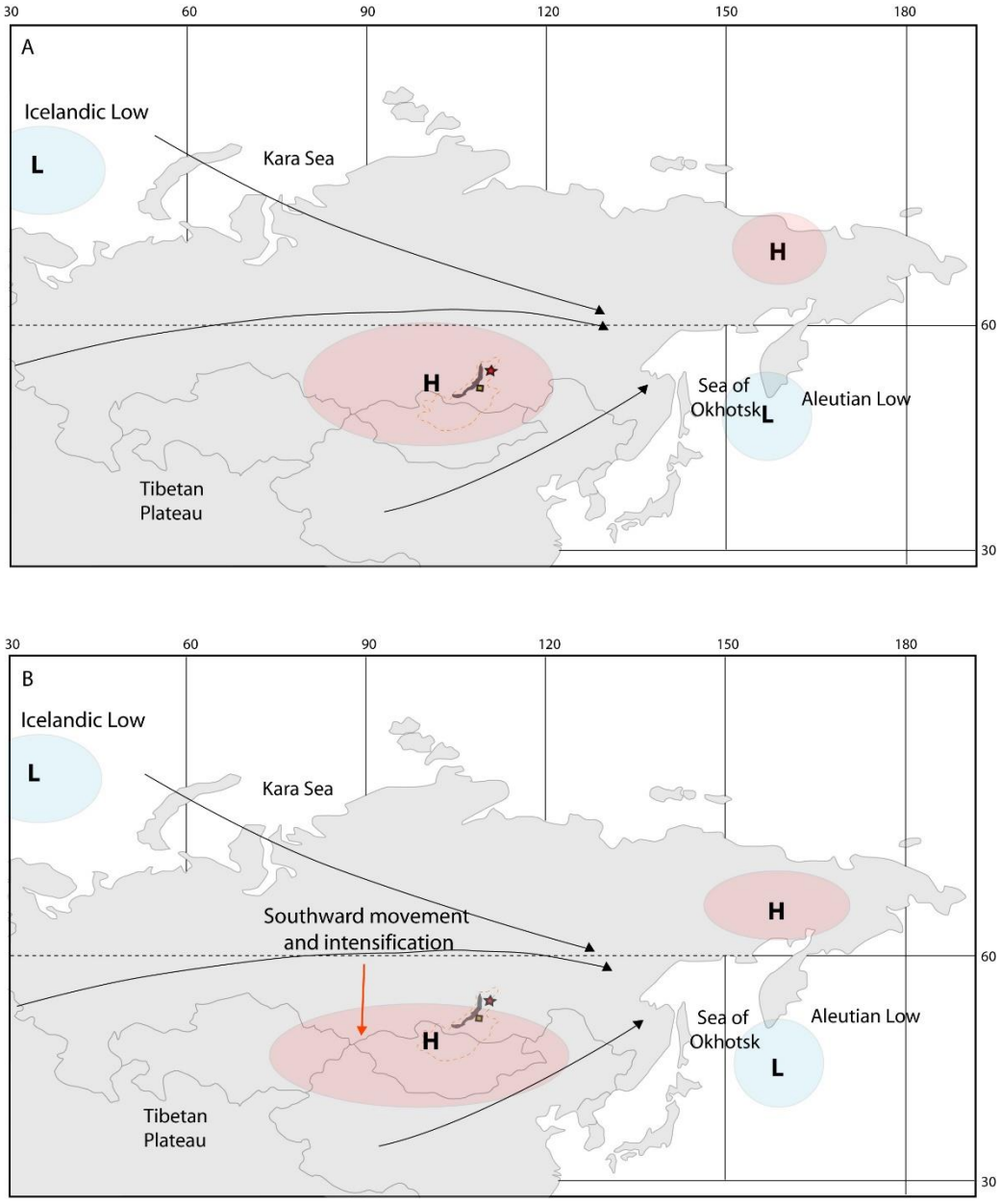

Figure 1.5: Schematic of the Siberian High and surrounding atmospheric systems (Aleutian and Icelandic Low) during periods of **(A)** weak Siberian High and **(B)** strong Siberian High. Red arrow highlights southward movement. Black arrows highlight dominant wind directions.

1.5.2 Modern Climate Alterations

Studying the Siberian region is of paramount importance for future climate prediction due to the warming that is occurring in the region, which is most intense in Eastern Siberia (Fedotov *et al.*, 2012), and during the wintertime when the warming seen is greater than that documented anywhere else in the world (Huhne and Slingo 2011). Siberia is known to be particularly sensitive to climatic changes, and it's continental position provides a rare opportunity to

study climatic changes (both modern and past) away from oceanic influences, which is important given that its remoteness from the oceans makes extrapolation from the Pacific or Atlantic unsuitable (Oberhansli and Mackay, 2005) and that much of Northern Hemisphere climate dynamics are understood from marine sediments or terrestrial sites with close proximity to these regions (e.g. Northern Europe). However, the impacts of these climate changes in continental regions is critical for understanding feedback mechanisms, for example methane release (Bloom *et al.*, 2010).

The effects of global warming in the region are already being felt, with a 2°C warming being documented in the surface waters of Lake Baikal between 1977-2003 (Izmest'eva *et al.*, 2016), which is a significant increase, particularly in respect to the average summer water temperature being only 5°C. These alterations are accompanied by shifts in the lake ecological community structure and stratification, with Lake Baikal already documenting declining ice cover (Todd and Mackay, 2003) and a strengthening of the thermal gradient in the upper 50 meters of the water column, causing alterations in the spatial distribution of species, and thus altering the overlaps between grazers and phytoplankton, therefore, triggering changes in diet (Hampton *et al.*, 2014). Warming is accompanied by changes in vegetation patterns, including redistribution of wetlands, tundra, steppe and boreal forests, (Gordov and Vaganov, 2010), which in turn affect catchment processes. Catchment process alterations have increased the dissolved organic carbon (DOC) and nutrient input to rivers and lakes in the northern boreal watersheds (Izmest'eva *et al.*, 2016), affecting biological productivity and aquatic communities in these environments (Mackay *et al.*, 2012).

Changes in permafrost distribution have also been documented as a result of warming climates, with boundaries moving northward (Gordov and Vaganov, 2010). As permafrost contains one of the largest organic carbon pools globally, warming has the potential to release significant amounts of carbon to the atmosphere this century, through microbial degradation (Schuur *et al.*, 2008; Vonk *et al.*, 2012). Permafrost is predicted by models to retreat north and eastward, causing changes to the regional hydrology and geomorphology (Tchebakova *et al.*, 2009). This issue is particularly affecting regions of

sporadic isolated permafrost, where degradation is ongoing as a result of global warming, direct human influence and wildfires (Vonk *et al.*, 2012). Alterations in wildfire frequency and season length have also been seen to increase as a result of atmospheric warming (Gordov and Vaganov, 2010; Soja *et al.*, 2007), leading to significantly higher levels of wildfires in Siberia across the 2015 season (NASA Earth Observatory, 2015), resulting in several deaths and significant damage (Agence France-Presse, 2015). Increased ignition, season length and total burned area have significant affects, triggering vegetation shifts, particularly in montane regions, such as the Transbaikal region, while the size of Siberia means these wildfires and their effects have the potential to influence climate feedbacks, particularly through alterations with carbon storage in the productive steppe ecosystems, and alterations in albedo (Soja *et al.*, 2007).

Variation is also being documented in the Siberian High as a result of climatic changes, particularly linked to alterations in the intensity of atmospheric systems. Recent studies have demonstrated significant weakening of the Siberian High during the 1970-1980's, reaching an unprecedented low during the 1990's (Jeong *et al.*, 2011), which has been attributed to global warming. However, despite this, the last two decades have seen a recovery in Siberian High strength. This is thought to result from alleviated surface warming and decreased atmospheric stability, linked to Eurasian snow cover triggering recovery (Jeong *et al.*, 2011), although further work is required to understand the complexities of the Siberian High responses to global warming.

Therefore, it is clear that the current situation in Siberia requires further work to understand the forcings that have triggered this region to warm faster than the remainder of the world (Tingley and Huybers, 2013), and palaeo-reconstructions are required to understand the region's past responses to abrupt climatic changes to provide valuable context for these alterations.

1.5.3 Palaeoenvironmental and Palaeoclimatic Context for Studies of hominin distribution and faunal turnover

Not only is understanding of Siberia essential in the context of future climate change, but palaeoenvironmental studies are also important in the

environmental and climatic context of the region for understanding human evolution, dispersal and occupation. Siberia holds several key sites for human evolution and dispersal, the most notable being Denisova cave, where a pharynx and teeth have been identified as Denisovans (Brown *et al.*, 2016; Gibbons, 2015; Reich *et al.*, 2011, 2010). These were found alongside *Homo neanderthalensis* teeth and Upper Palaeolithic technology including microblades and body ornaments, and additionally Middle Palaeolithic Levallois technology (Reich *et al.*, 2010). Neanderthal fossils from this site are dated to 80-140 ka cal BP, while Denisovans are thought to be present from ~110 ka cal BP, and potentially as far back as ~170 ka cal BP (Gibbons, 2015), while the youngest specimens are dated to between 52-76 ka cal BP (Douka *et al.*, 2019). Denisova cave has also provided genetic evidence of interbreeding between the two species, with the 'Denisova 11' specimen being the daughter of a Neanderthal mother and a Denisovan father (Slon *et al.*, 2018). The find of a first generation offspring has suggested that mixing between the Denisovans and Neanderthals was common when they co-existed (Slon *et al.*, 2018). Additionally to Denisova Cave, other finds in the Altai Mountains have also documented the presence and eastward spread of *Homo neanderthalensis*, which are found alongside Mousterian lithics (Krause *et al.*, 2007), although there is debate as to whether teeth found at sites in the Altai Mountains dating to 34,750±750 years BP are Neanderthals or whether they are from modern humans with *Homo erectus* traits (Krause *et al.*, 2007).

After the transition from the Middle to Upper Palaeolithic the region was occupied by anatomically modern humans, but there is variability in human occupation due to climate change. For example, during the Younger Dryas there is a general agreement that the modern human population persisted despite lowered numbers in southern Siberia (Buvit and Terry, 2011; Vasil'ev, 2011), although there are issues with sparse evidence and chronological controls (Vasil'ev, 2011). It appears subsistence activities occurred through hunting practices being diversified, with sites including Elenev Cave demonstrating increased bird procurement, while groups around Lake Baikal significantly increased their use of fish and riverine resources (Buvit and Terry, 2011; Vasil'ev, 2011).

Modern Humans have been present in Siberia throughout the Holocene, with presence in the Baikal region at Sagan-Zaba cave on Ol'khon Island documented at ~9 ka BP, while petroglyphs from the nearby white cliffs are known from 4 ka BP (Mackay *et al.,* 2013). During the late Holocene pastoralists are also known to have occupied the region, although it appears their impact on the ecosystem is limited (Mackay *et al.,* 2013), although climatic impacts on their occupation of the region are discussed above.

Siberia is also a key region for understanding the existence and demise of several megafauna species, including giant deer and woolly mammoth. The demise of giant deer *Megaloceros giganteus* Blumenbach, is placed at 7.7 ka BP in western Siberia, a much later date than other sites (Stuart *et al.*, 2004). *M. giganteus* is known to have covered a mid-latitude range from the east of Lake Baikal through to Ireland during the Late-Pleistocene (presence in Transbaikalia at ~42 ^{14}C yrs BP), although there is a lack of records from 20-12.5 ^{14}C years BP (Stuart *et al.*, 2004), and therefore understanding the region's palaeoenvironments during this time provides essential context to improve understanding on the drivers of extinction, which are debated. Woolly mammoths *Mammuthus primigenius* Blumenbach, follow a similar story to giant deer, with a once widespread distribution across much of Europe and Asia during MIS3 and then a more restricted distribution during the LGM. *M. primigenius* reappearance is however, much more rapid than that of the giant deer, which highlights the individual species requirements (Lister and Stuart, 2008).

Siberia is, thus, a key region to improve scientific understanding of the complex histories of hominin and faunal species. High resolution understanding of the palaeoenvironmental and palaeoclimatic background to these processes are essential, providing vital context for these events.

1.5.4 Previous Studies in Southern Siberia

Despite Siberia being less well studied than other regions, particularly due to the logistical issues of working in this region (Biskaborn *et al.*, 2012), palaeoenvironmental and palaeoclimatic studies are growing in number. Currently, southern Siberian studies are dominated by those from Lake Baikal,

although more records are appearing from other sites (e.g. Bezrukova 2012, Kostrova *et al.,* 2013). Here key studies from sites in Siberia are discussed, the locations of, which are shown on figure 1.6.

Figure 1.6: Simple Map of Siberia showing approximate locations of sites discussed in this section (1.4).

1.5.4.1 Long Term Records

Globally, the availability of terrestrial records of long term climatic changes are rare, with some of the major archives being discussed in section 1.3.6. The Siberian region however holds the key archives from Lake Baikal, the world's oldest lake, which formed over 20 Ma ago as a result of tectonic activity (Murakami *et al.*, 2012). The site has been analysed across the Quaternary period and beyond for palaeoenvironmental, palaeolimnological and palaeoclimatic studies. Due to the long continuous nature of Lake Baikal sediments, biogenic silica records have been able to provide a climatic record

back to the Pliocene (Williams *et al.*, 1997). This long record highlights the clear cyclicity of Quaternary climatic changes with the periodicities of 19, 21, 41 and 100 ka (Colman *et al.*, 1995; Mackay, 2007; Williams *et al.*, 1997), and has allowed the substage structure of interglacials to be considered (Prokopenko, 2001). These records have demonstrated rapid alterations between arid cold glacial and stadial periods and moist interglacials and interstadials (Murakami *et al.*, 2012). Key features include shifts between steppe and forest-steppe during glacial periods, and coniferous taiga during the current and previous interglacial (BDP Members 2005). Lake Baikal records have, additionally, highlighted the almost continuous deposition of diatoms between MIS15a to MIS11 (580-380 ka BP; Prokopenko *et al.,* 2002). This record highlights glacial clays with IRD at periods when glaciers have descended into the lake, although the period between MIS12-MIS14 does not contain these IRD layers, suggesting restricted glaciations during this period (Prokopenko *et al.*, 2002). Work on MIS11 (427-362 ka BP) has demonstrated the importance of understanding the hydrology of the region when interpreting changes in the isotopic composition of lakewaters, with high isotopic values during MIS11.3 indicating a dominance of hydrological inputs from rivers flowing into the south and central basins of Lake Baikal, particularly the influence of the Selenga river (Mackay *et al.*, 2008). Despite the dominant influence of river hydrology the records also document an abrupt cooling event at 390 ka BP that appears to be coincident with iceberg discharge in the North Atlantic, with declining diatom oxygen isotopes suggesting hydrological changes to increased northern river input, due to increased winter precipitation and snow melt (Mackay *et al.*, 2008).

1.5.4.2 The Last Interglacial (MIS5e) in Siberia (Kazantsevo Interglacial)

Studies of the last interglacial from Lake Baikal have suggested strong teleconnections between central Asia and the North Atlantic region, potentially through the westerlies (Mackay *et al.* 2013). The interglacial record from Lake Baikal have also demonstrated millennial scale events found in European and marine sediments, including a mid-Eemian cooling which is seen in marine and terrestrial realms (Prokopenko *et al.*, 2001)

1.5.4.3 Last Glacial Part 1 – MIS 5 & 4 (Ermakovo Glaciation)

Records through MIS5 and MIS4 are sparse in Siberia, however evidence from Lake Baikal has demonstrated that the sub-stage of MIS5d produced an abrupt and intense regional glaciation as a result of extreme insolation minima (Prokopenko *et al.*, 2001). This glaciation is shown in records of biogenic silica, ice rafted debris and clay mineral composition, and is thought to be similar to the glaciation of MIS7d (Prokopenko *et al.*, 2001). Glacier development during MIS5d is thought to have occurred as a result of the strengthening of interior westerlies, bringing increased precipitation during the insolation minimum. It is thought that this has enhanced the transition from MIS5e to MIS5d, causing a wet and cold interior continent (Murakami *et al.*, 2012).

1.5.4.4 Last Glacial Part 2 – MIS 3 – (Karginsky Period)

During the last glacial several further occurrences of climatic changes have been documented from Lake Baikal including Heinrich stadials 2-5 which are found during the Karginsky Interstadial, thought coincident with MIS3 (Mackay, 2007). A high resolution record from core BDP-93-2 demonstrates these rapid events, with abrupt declines documented in fossil diatom assemblages, and layers enriched with terrestrial organic carbon, indicating episodes of cooling known as Kuzmin events. These have possible correlations to North Atlantic Heinrich events (Prokopenko, 2001), however in some cases it is thought that responses in Baikal are to longer term Bond cycles, rather than just the abrupt Heinrich stadials (Prokopenko, 2001). Abrupt events through MIS3 in Lake Baikal are considered to be complex due to location and proxy specific factors, which means some areas record responses to abrupt climatic changes, while changes are more muted in other areas. For example, C/N ratios from core CON01-603-5 across the periods associated with Heinrich events 5 and 4 do not show evidence of terrestrial soil input, which is often seen during Kuzmin events, and thought to be a response to Heinrich event driven precipitation changes (Swann *et al.*, 2005). However, this absence may be linked to the site being situated away from significant riverine input, compared to sites in the Buguldeika saddle, which receive considerable input from the Selenga river (Swann *et al.*, 2005), highlighting how site specific factors can complicate

understanding of ecological responses to abrupt climate changes. Evidence from Lake Kotokel, close to Lake Baikal, between 47-30 ka BP also records an unstable climate, with periods of warmer and wetter climates marked by increases in taiga, which are considered to be broadly synchronous with hemispheric temperature and precipitation changes in Greenland ice cores and Chinese stalagmites (Bezrukova *et al.*, 2010).

1.5.4.5 Last Glacial Part 3 – MIS 2 and the Last Glacial Maximum (Sartanian Glaciation)

Studies covering the Sartanian Glaciation, which is considered equivalent to the last glacial maximum (LGM), in Lake Baikal have demonstrated an ecological collapse during this period with the lake being almost uninhabited, without accumulation of planktonic and benthic diatoms, sponge spicules and chrysophyte cysts in lake sediments (Karabanov *et al.*, 2004). This is considered to result from decreased nutrient loading from the watershed, low water and ice transparency, particularly due to inputs of fine dense clays from glacial outwash, and lowered surface water temperature inducing ecosystem stress (Karabanov *et al.*, 2004). This is however an oversimplification, as other studies have highlighted that the lack of diatoms in Lake Baikal's sediments may be due to the influence of dissolution, rather than an ecosystem collapse (Mackay, 2007). Despite this, other studies have shown that pollen accumulation during this period is low, having declined from a landscape dominated by *Artemisia* and Asteraceae just prior to the LGM, with only a sparse herbaceous vegetation recorded during the LGM (Shichi *et al.*, 2013), suggesting the region had limited productivity at the height of the glacial maximum. Throughout MIS2 precipitation to the region and soil moisture was very low, as North Atlantic moisture is blocked by orographic blocking trade winds, associated with the growth of the Fennoscandian ice sheet (Murakami *et al.*, 2012), and these conditions are also documented by Lake Kotokel, where the driest and coolest conditions, with a steppe dominated landscape are recorded between 30-24 ka BP (Bezrukova *et al.*, 2010). During this period Lake Kotokel is significantly reduced in size and diatoms are absence from the sediments (Bezrukova, 2012), which has also been considered to represent an ecological collapse in this smaller lake, although as discussed above for

Baikal, other issues, including dissolution could be affecting the record. In Kotokel this period is followed by warming between 24-22 ka BP and then a shorter period of colder conditions until 17 ka BP, where there is a marked increase in tree and shrub pollen and a reappearance of diatoms in the lake sediments (Bezrukova, 2012). A warming close to the end of the LGM is also highlighted in Lake Baikal through successional vegetation shifts (Demske *et al.*, 2005).

1.5.4.6 Last Glacial Part 4 – The Last-Glacial-to-Interglacial-Transition (LGIT)

Cores from Lake Baikal have been extensively studied during the LGIT, with several cores recording a Bølling-Allerød period, with initial warming documented between 14.8-14.3 ka BP, while a brief cooling thought coincident with the Younger Dryas in Europe is also seen in many proxies (Demske *et al.*, 2005; Mackay *et al.*, 2011). Diatom abundances during the LGIT are thought to lag behind the GISP2 delta $\delta^{18}O$ temperature record by ~1ka, however, this is not thought to be the case during the more pronounced Younger Dryas record that is found in some Baikal cores (Prokopenko *et al.*, 1999). The Younger Dryas signal in Baikal has been considered to be linked to a watershed influence where fine grained material is in-washed, reducing light transmission and thus reducing the photic zone, limiting diatom production (Prokopenko *et al.*, 2001). Pollen records from Lake Baikal indicate an expanding riparian area during the Bølling interstadial, with elevated soil moisture, while *Alnus* shrubs become dominant during the Allerød, suggesting cooler but more humid conditions (Shichi *et al.*, 2013). The nature of the Younger Dryas in Lake Baikal is more complex, as despite being widely recorded in some records, in others, such as those from Academician ridge and in north-eastern coastal mire sediments, it is not seen in the pollen record (Shichi *et al.*, 2013), indicating a regional variation in response to this event, and highlighting different proxies responses. Evidence suggests that the strong Younger Dryas signal is found in areas influenced by the Selenga River, which is due to the dryness on the upper Selenga basin (Shichi *et al.*, 2013), while regions of Lake Baikal that are not influenced by the Selenga are not as impacted by this event, thus creating regional discrepancies.

Studies from Lake Kotokel have indicated that the period from 14.7 ka BP are warmest and wettest with increased forest cover between 14.5-14.0 ka BP, which is considered to correspond to the Allerød interstadial. The palynological evidence at Kotokel also shows unambiguous evidence of a cooling between 12.7-11.6 ka BP, which shows close synchronicity to GS-1 in NGRIP (Bezrukova, 2012). Vegetation records around Baikal and Kotokel are thought to have changed drastically and simultaneously throughout this period, although across the Baikal region the composition of taxa is considered to vary considerably between north-eastern and south-western regions, due to the large region covered by Lake Baikal (Shichi *et al.*, 2013).

The lateglacial oscillations are seen in several other sites, including from shallow lakes at the western side of the Lower Lena river where enhanced minerogenic pyrite suggests a cold episode between ~12.7-11.6 ka BP (Biskaborn *et al.*, 2012), and at Lake Grusha, where warming at 14.3 ka BP is followed by cooling between 13.3-11.9 ka BP, as demonstrated by reduced organic matter (Westover *et al.*, 2006). This has been considered to be a Younger Dryas event, although there are large age uncertainties within the record. Sysy-Kyuele demonstrates a muted transition from the Younger Dryas (~12.7-11.6 ka BP) to the Holocene with only a slightly warmer temperature indicated by diatom productivity changes, potentially suggesting a more localised response to larger scale drivers (Biskaborn *et al.*, 2012).

Despite clear evidence for a period of warming following the LGM followed by a cold episode, potentially synchronous with GS1, there are clearly several differences between records, potentially as a result of individual site sensitivity, and variations in the particular proxy, for example, where an event is shown in oxygen isotopes on diatoms but not in pollen, as is the case in some Lake Baikal records (Shichi *et al.*, 2013). Additionally, although in several cases these changes are thought to be synchronous with events seen in Greenland ice cores, there are apparent chronological issues, particularly due to large dating uncertainties that limit the ability to demonstrate synchrony in every case.

1.5.4.7 The Holocene

Palaeoclimatic studies in Siberia generally agree on the occurrence of warmer and wetter conditions during the early Holocene (Bezrukova, 2012; Westover *et al.*, 2006). At Lake Kotokel these are thought to persist until ~7ka BP (Bezrukova *et al.*, 2010), while lakes around the Lower Lena River, and others including Lake Grusha, Lake Lama and Horton Nur show discrepancies with when they document a shift warmer climates at the start of the Holocene. At Lake Grusha warming occurs at 10.4 ka BP, accompanied by increased humidity and forest development (Westover *et al.*, 2006), while shallow lakes in the Lower reaches of the Lena river indicate warmer climates from 9.1-5.7 ka BP (Biskaborn *et al.*, 2012). Horton-Nur's pollen and diatom records document alterations from a lake dominated by low concentrations of planktonic *Cyclotella* species before 11.5 ka BP, to a more productive lake system after 10.7 ka BP with more diverse and abundant taxa (Rudaya *et al.*, 2009). These discrepancies, suggest localised environmental factors affect the speed of response, although chronological uncertainties make understanding if this warming was regionally synchronous or time-transgressive difficult to determine (Colman *et al.*, 1996; Lowe and Walker, 2000).

Despite slight discrepancies in the start of warming across the region, most records indicate a Holocene Climatic Optimum warmth between 9-6.5 ka BP (Bezrukova *et al.*, 2011). Sites in the North Pre-Baikal region, where Atlantic and Arctic air masses meet place this climatic optimum between 9.0-6.8 ka BP, while at Lake Lama the thermal maximum sits between 8-6.5 ka BP (Kumke *et al.*, 2004), close to the timing of 8.2-6.5 ka BP seen at Lake Grusha (Westover *et al.*, 2006).

One key period of climatic change during the Holocene is seen to be the 8.2ka BP event, the expression of which is debated in Siberia. Morley *et al.,* (2005) have considered the propagation of North Atlantic driven changes in Baikal, however there is uncertainty whether there is a clear signal relating to the 8.2 ka BP event due to dating precision, although other early Holocene alterations such as the Pre-Boreal oscillation have been identified, while others including

the 9.2 ka BP event are not shown clearly in Lake Baikal records (Mackay *et al.*, 2011). This issue also occurs from the Okunaika cores from the North Pre-Baikal region (see figure 1.6), where there is no clear response to the 8.2 ka BP event, although a decline in arboreal pollen between 7-8 ka BP, with dominance of *Betula nana* and mesophytic herbs, which could be considered to reflect this event. This change is difficult to confidently tie to the 8.2 ka BP event, as this change occurs across a large time period, while the 8.2 ka BP event is rapid, and this shift could be a response to longer term trends.

After the insolation maximum, steady deterioration of climate is documented at several sites, including Lake Baikal (Mackay *et al.*, 2011), Lake Grusha (Westover *et al.*, 2006) and Lake Lama, where significant alterations in the diatom composition are seen. Lake Lama, however, also records a warmer period between 4-2.8 ka BP (Kumke *et al.*, 2004). This warmer period is also seen at Lake Sysy-Kyuele between ~5.7-2.8 ka BP (Biskaborn *et al.*, 2012), suggesting regional discrepancies in responses to the same driver. The period between 5.8-1.7 ka BP at Lake Kotokel includes several abrupt attenuations between warm and cold conditions, with an optimal warm and wet period around ~4 ka BP, which are also seen in Lake Baikal and Lake Hovsogul (Fedotov *et al.*, 2012).

Abrupt Late Holocene environmental changes are also seen at Lake Beloye, where the lake's conditions alter from eutrophic to oligotrophic at ~3.4 ka BP. This is potentially due to climatic shifts from a warmer and wetter regime, pre 3.4 ka BP, to cooler conditions, which cause basal freezing of the shallow lake and thus trigger deposition of carbonates, adjusting the environmental parameters of the lake (Krivonogov *et al.*, 2012). There is, however, debate concerning whether these alterations are due to regional climatic factors or localised hydro-geochemical and geological changes. Records from Lake Shira between the Rivers Ob and Yenisei have demonstrated changes over the past 2.5 ka years are due to large scale atmospheric circulation processes affecting the regional water balance. These are shown through changes in the *Artemisia*/Chenopodiaceae ratio, which indicate decadal alterations in vegetation cover (Hildebrandt *et al.*, 2015). These are thought to relate to strengthening and attenuation of the Indian Summer Monsoon and

temperature variability in the North Atlantic, documented by changes in the IRD record, whereby a warmer North Atlantic has higher evaporation, allowing moisture to be bought further into continents (Hildebrandt *et al.*, 2015). High turnover rates are also seen at Lake Khall, Ol'khon Island between 2.75-2.48 ka BP, where alterations to a drier more continental climate are observed, coincident with IRD in the North Atlantic and an attenuated East Asian summer monsoon (Mackay *et al.,* 2013). The last 1.5 ka BP at Lake Kotokel show a slight cooling in chironomid and diatom records between 1.5-1 ka BP, however this event is not detected in the palynological record (Fedotov *et al.*, 2012), while Lake Khall demonstrates warming between 1.9-0.7 ka BP (Mackay *et al.,* 2013), demonstrating regional discrepancies between the east and west of Lake Baikal.

The Little Ice Age and Medieval Warm Period are some of the most well documented late Holocene palaeoclimate changes. Despite the debate over the specific causes (see section 1.3.6), these events are recorded at sites in Siberia. LIA aged moraines are found in the Sayan Mountains (Mackay *et al.*, 2012), and response to both the LIA and the Medieval Warm Period (MWP) are documented in changing diatom assemblages in Lake Baikal sediments, which are triggered by alterations in the Siberian High (Mackay *et al.*, 2005). Other sites in the Siberian region, however, do not show evidence of these events (Bezrukova *et al.*, 2010), which could be due to chronological controls, sampling resolution or due to a limited effect of these events in this region, and further research is required to resolve this.

Studies in Siberia are now focusing on human effects on the environment, with increases in pastoral farming being highlighted by nutrient enrichment at sites including Lake Khall (Ol'khon region) since AD1845 (Mackay *et al.,* 2013), while other sites including Lake Shira only document changes from humans over the recent past, from 1955, despite the long history of mobile pastoralists in the region (Hildebrandt *et al.*, 2015).

1.5.5 Additional Factors

These studies demonstrate there is significant complexity in the region's responses to climatic changes. Issues with dating control may explain some

of the differences between records (Colman *et al.*, 1996; Lowe and Walker, 2000), however, it is also possible that low resolution studies are preventing understanding of multiple abrupt events during this period, and therefore it is possible these signals are being merged in some lower resolution sites. Therefore, understanding of the Holocene will require further higher resolution studies to resolve these issues.

Alongside the need for higher resolution, well dated sites, palaeoenvironmental research requires a multiproxy approach, as this can ensure different elements of the ecosystems can be considered. For example, using C/N ratios can inform about the source of organic matter (Meyers, 1994; Meyers and Lallier-Vergès, 1999), and using this alongside a diatom assemblage record can allow consideration of how changes in the catchment may be influencing processes within a lake. Multi-proxy studies therefore have the potential to provide a much more detailed and integrated reconstruction of past conditions, encompassing both lake and catchment environments.

1.5.6 Summary of Siberian Literature

Despite a growing number of studies (Tarasov *et al.*, 2009) there are still significant discrepancies between sites. These may result from real variations in responses across Siberia, as suggested by the influence of the Selenga on whether the Younger Dryas is recorded in Lake Baikal (Shichi *et al.*, 2013) or problems with proxies, such as lag time responses and preservation issues (Kostrova *et al.,* 2013b). Additionally, issues with resolution of sites may prevent detection of some of the abrupt events. Chronological problems, such as radiocarbon reservoir offsets, hard-water error and large measurement uncertainties, limit the potential to test synchronicity of responses between sites and detection of real regional time discrepancies (Colman *et al.*, 1996; Lowe and Walker, 2000).

There is also still a heavy bias to studies based on Lake Baikal, and it is now apparent that work on smaller sites with high deposition rates, will allow a wider understanding of the regional responses to palaeoclimatic changes in Siberia. Additionally, these smaller sites may be more sensitive to some of these changes, due to smaller catchments, which will prevent the responses

being buffered, as has been suggested for Lake Baikal due to its large catchment (e.g. Kostrova *et al.,* 2013b).

In summary, there is a clear need for palaeoenvironmental and palaeoclimatic reconstructions in the Siberian region, to provide essential context for current global warming, which has implications for the global carbon cycle and the region's hydrology, and hominin and faunal dispersal, evolution and occupation histories. Despite the importance of the region, several knowledge gaps exist in the potential contribution of palaeoclimate studies to these areas. Further work is needed to understand how interactions between the North Atlantic, westerlies and monsoons affect Siberian ecosystems (Oberhansli and Mackay, 2005), and additionally understanding of the regional variations in responses to these changes is needed. Understanding of localised ecological responses is required to allow better preparation for future variability, while exploring the pressures that have affected past communities within this region are also important for considering future challenges. Further, and perhaps most importantly, establishing a robust data set of past palaeoenvironmental records for the region is also required to aid the construction and testing of climate models. For example, palaeoecological studies can provide essential data for reverse modelling exercises, where models are tested in their ability to retrodict periods of abrupt change in the palaeo-archive.

1.6 Aims and Objectives

Research in southern Siberia is clearly of paramount importance. Therefore, this project aims to reconstruct the lacustrine ecological history of Lake Baunt over past ~30 ka BP, in order to consider responses to climatic change and add to the understanding of how these changes are reflected in wider southern Siberia.

To achieve this aim, several objectives will be addressed.

- Evaluate the **lacustrine ecological and isotopic records** in Lake Baunt back to ~30 ka BP.
- Integrate and analyse the **multiple proxies** generated with ecological, stratigraphic and palaeoclimatic data provided by colleagues.

- Compare with data from **the surrounding region**, to assess expression of palaeoenvironmental change recorded in each site.
- Compare the regional data with **key global archives** to understand the pattern of abrupt changes in the context of global climate forcing mechanisms.
- Examine this in the **context of ad-hoc and computer model simulations** to test hypothesis of key climate and environmental forcing factors.

2 Site Description and Context, Core collection and Stratigraphy

2.1 Lake Baunt Site Description and Context

Lake Baunt is situated in central Asia, southern Siberia (55°11'15"N, 113°01'45"E) (figure 2.1). The lake is located in the Transbaikal mountains, in the administrative district of the Republic of Buryatia. It was formed due to tectonic activity, making up one of the Baikal Rift Zone (BRZ) hollows (Bezrukova *et al.*, 2017), although glacial thawing action has also been implicated in its formation (Yakhnenko *et al.,* 2008). Lake Baunt makes up the largest of several lakes in the Tsipikan-Baunt limnic morphosystem (Shchetnikov, 2007; Yakhnenko *et al.,* 2008) and is located at ~1050m a.s.l. and measures approximately 111km^2 (19km length on a SW-NE elongation and 9km width), with an average depth of 17 meters and a maximum depth of 33 meters (Krainov *et al.*, 2017). The lake's catchment predominantly lies to the south, east and west (Krainov *et al.*, 2017), and the region is bounded by the Ikat and Tsipikan highlands (Solotchin *et al.,* 2015) (Figure 2.1B). Lake Baunt receives inputs from the Verkhnyaya Tsipa and Tsipikan Rivers (Krainov *et al.*, 2017) and, unusually for the lakes in this area, Baunt is an open lake, discharging into the Nizhnyaya Tsipa (Lower Tsipa) River, which is a result of the lake lying above the local trough (Ufimtsev *et al.*, 2009) (see figure 2.1.C). At the current time, Lake Baunt is an oligotrophic lake, meaning that the lake has limited productivity, with well-oxygenated bottom waters (Horne and Goldman, 1994). The surface water has a neutral pH value between 7 – 7.2, which is temperature dependant, with cooler temperatures of 4°C allowing a pH of 7, while warmer temperatures of 19°C raise the pH to 7.2 (Kozhov, 1950). Baunt undergoes thermal stratification during the summer months, while during the wintertime (October-May) the lake surface is frozen (average March ice thickness ~1.8 meters).

The lake basin's morphology, shown in figure 2.2 (and corresponds to the A-B transect on figure 2.1C), follows the general slope seen on the coastline, with steepest sides on the northern side of the lake (nearest point 'A' – see figure 2.1C). The maximum depth of the lake is not found centrally, but is offset to the south-east of the centre (Krainov *et al.*, 2017). Normally basins in the

Baikal Rift Zone are asymmetrical, with the deepest areas corresponding to the fault zone where the maximum rate of tectonic settling was observed, however Baunt's morphology does not conform to this general pattern (Krainov *et al.*, 2017). Baunt instead is pushed into the fault zone slope, which results in the lake lying above the local trough, allowing discharge to run into the Lower Tsipa river (Ufimtsev *et al.,* 2009). The eastern side of the lake is bordered by accumulative plains (figure 2.3A), suggesting previous periods of lake aggradation, with 12 ancient beach ridges being identified (Krainov *et al.*, 2017), while the western side has many small lakes present (see figure 2.4).

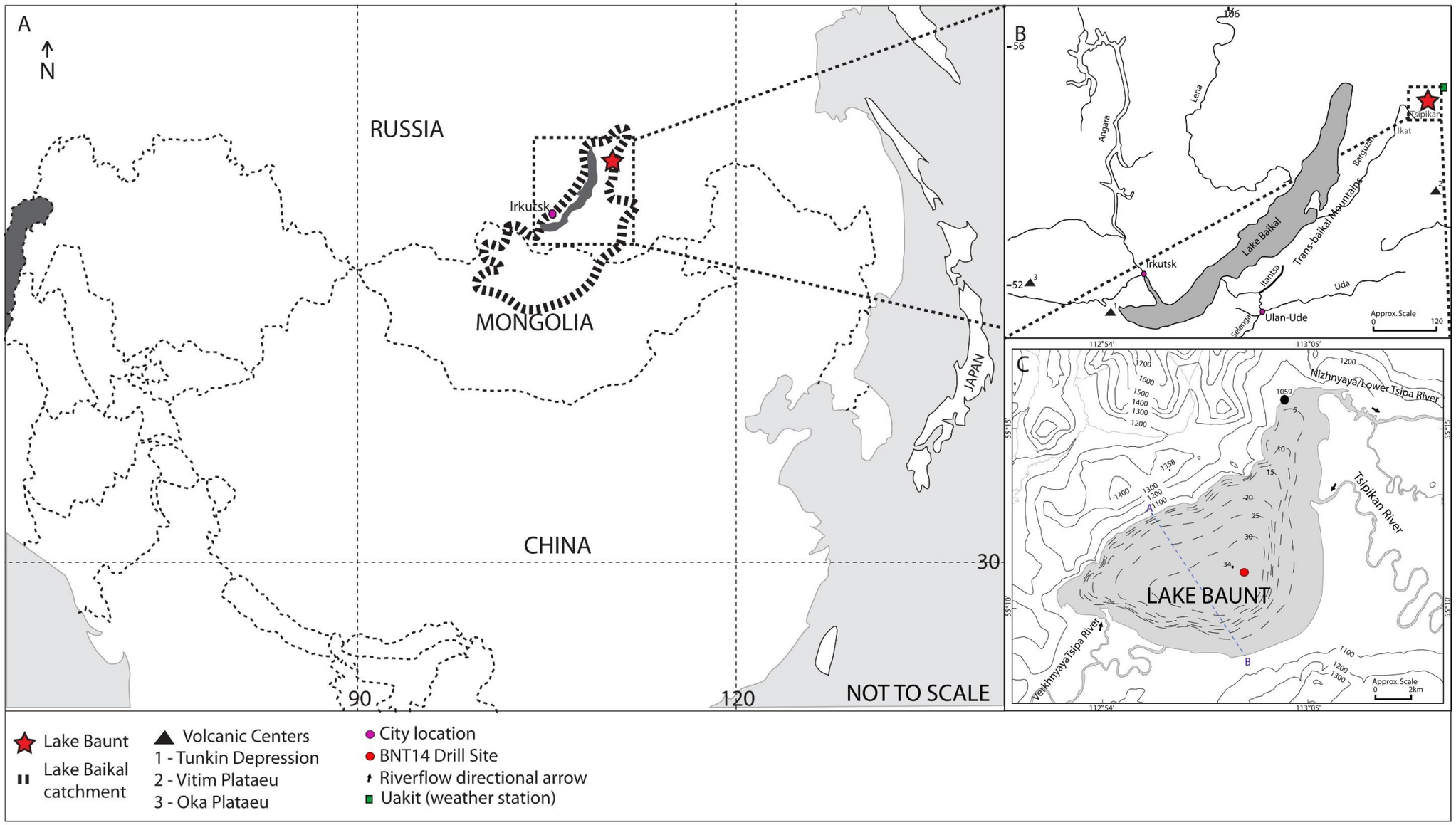

Figure 2.1: (A) Schematic Map of Asia highlighting the position of Lakes Baunt (red star) and Baikal. Lake Baikal's catchment area is shown. **(B)** Closer image of the Lake Baikal region, showing Lake Baunt and Uakit (weather station location). Major rivers in the region are shown alongside volcanic centres. **(C)** Close image of Lake Baunt highlighting basin topography and the regional topography. Drill location of the BNT14 core is shown. River inflows and outflow are shown with directional arrows. A-B Blue dashed line highlights where figure 3.2 basin morphology corresponds to.

Figure 2.2: Basin Morphology of Lake Baunt from Krainov *et al.,* 2017 (page 1403). The A-B transect is marked on figure 3.1.C (blue line).

Figure 2.3: Photographs of Lake Baunt sourced from:
(A & B): Vasiliy Tatarinov through Wikipedia.ru (Russian Wikipedia)
Showing the regions surrounding Lake Baunt, including accumulative plains **(A)** and highlands **(B)**.

Figure 2.4: Photograph of Lake Baunt sourced from:
https://maps.google.com/maps/contrib/107272866542069064224/photos
showing rocky mountainous outcrops and the high quantities of small lakes in the surrounding region.

2.1.1 Regional Climate Controls

Lake Baunt is situated in one of the most continental regions on the planet, dominated by the influence of the wintertime Siberian High. The pressure differences caused by the Siberian High induce significant seasonality in temperature and precipitation within the region. When the Siberian High dominates during the winter months, pressures reach high levels of over ~1030mb (Tubi and Dayan, 2013), while during the summer months, when the anticyclone is not active, pressures drop to ~1005mb. As a result, the highest levels of precipitation are observed during the summer months (see figure 2.3.B) (Huhne and Slingo, 2011), although a small amount reaches the region as snowfall over the winter months (Huhne and Slingo, 2011). Despite this level of seasonality, the total precipitation reaching the region is limited to ~300mm a year, although there is year to year variability. Temperatures show strong seasonality, reaching highs of ~20°C during July, while cooling occurs during the winter months, reaching lows of –30°C (see figure 3.3.A), allowing lake surface freezing.

Figure 2.3: Climate Data summaries for Uakit (nearest weather station to Lake Baunt) **(A)** Annual Average Temperature (°C) **(B)** Annual Average precipitation (mm/day) obtained via the KNMI Climate Explorer (http://climexp.knmi.nl/)(Trouet and Van Oldenborgh, 2013).

2.1.2 Regional Geology

The region's geology is predominantly the Barguzin and Vitimkan igneous granitic complexes, which are part of the Angara-Vitim batholith (see figure 2.4), which makes up the largest batholith in the western Transbaikal region, incorporating 130,000km^2 of granitoids (Nenakhov and Nikitin, 2007; Rytsk *et al.*, 2007; Tsygankov *et al.*, 2007). Within the lake basin itself, Neogene-Quaternary sediments including sands, clays and gravels dominate (Bezrukova *et al.*, 2017; Krainov *et al.*, 2017; Shchetnikov, 2007), while Holocene sediments are documented as lacustrine, fluvial and peat deposits (Bezrukova *et al.*, 2017). There are no carbonate rocks found within the Lake Baunt catchment. Baunt is located in a region with geothermal activity, notably hot springs, found as part of the Mogoi (Tsipin) springs (Solotchin *et al.,* 2015). These mineral springs are controlled by deep faults, with those in the Baunt region being related to the southeastern hydrothermal line of the Baunt basin (Solotchin *et al.,* 2015).

This climatic regime means continuous permafrost is a key feature of the region (Bezrukova *et al.*, 2017), although Baunt is close to the boundary with discontinuous permafrost. Permafrost in this region has a lower boundary between 100-250m, with an average active layer thickness of 2m (Solotchin *et al.,* 2015). This means that there is a high risk of it being affected by modern day climate changes, and additionally, means the site is influenced by landscape processes including weathering, erosion and solifluction (Bezrukova *et al.*, 2017). These processes will therefore have important influences on the lake, affecting the materials being in-washed into the lake, the sediments that are preserved within it and additionally they will affect processes including carbon and silicon cycling within the catchment.

Figure 2.4: Geological Map of the Baikal region adapted from Shatsillo *et al.,* (2014) (p866). Lake Baunt's approximate location is shown with the green star. Fields in the legend are as follows: *1,* Cambrian-Silurian and superposed Jurassic basins; *2*, Late Precambrian; *3*, Early Precambrian basement outcrops; *5*, Mesozoic complexes *6*, Caledonides from the Caledonian orogeny; *7*, Baikalides of the Baikal–Muya belt, Central Asian Orogenic belt; *8*, Late Paleozoic granitoids; *9*, Middle Paleozoic granitoids.

2.1.3 Regional Vegetation and Soils

The Transbaikal region to the east of Lake Baikal incorporates forest and steppe ecotones, with forest mosaics being dominated by Birch stands, although some areas are dominated by pine and larch species. Generally the region has forested areas on northern slopes up to 1200 meters, while southern slopes are often covered by grass communities (Kharuk *et al.*, 2013).

The regions vegetation is currently being heavily influenced by increased frequency of wildfires in some locations and also due to drought conditions between 2000-2010 when summer precipitation decreased by ~25%, which reduced birch stand areas by ~5% (Kharuk *et al.*, 2013).

Lake Baunt sits within the western area of the Transbaikal Mountains, which consists of boreal forests and taiga. The region is generally forested below 1400 meters, with the dominant trees in the Lake Baunt area including *Pinus sylvestris* (Scots Pine) and *Larix sibirica* (Siberian Larch). Mountain slopes in this region are often dominated by *Pinus sibirica* (Siberian Pine) alongside *Abies sibirica* (Siberian fir) and *Picea ovobata* (Siberian spruce) (Müller *et al.*, 2014)**.**

Soil cover in the western Transbaikal region and taiga zones are poorly understood (Tsybzhitov *et al.*, 2006), although soils in the Transbaikal region are generally rocky podzols with low water content. In regions with permafrost, including Lake Baunt, soil moisture is generally higher, due to periods of permafrost thaw (Kharuk *et al.*, 2013). Soil cover in this region is influenced by the local topography, slope steepness and aspect alongside the height of the territory, groundwater depth and water permeability alongside the homogeneity of the soil forming rocks (Tsybzhitov *et al.*, 2006).

2.1.4 Justification for the site study

The Transbaikal region is an essential area for palaeoenvironmental studies, being positioned on the boundary between the sensitive taiga and steppe-tundra biomes, and at the southern permafrost margins. Yet, the Transbaikal Mountains have very limited palaeoenvironmental data (Biskaborn *et al.*, 2012), with most regional studies being based on Lake Baikal or smaller lakes to the south and central regions of Transbaikalia (Krainov *et al.*, 2017). While these studies have been central in allowing improvements in the understanding of the region's palaeoenvironmental and palaeoclimatic responses, additional studies are required from smaller lakes to provide more detailed evidence for localised responses. Lake Baunt is a useful addition to this increasing network of sites, allowing study of a site which is over 285 times smaller than Lake Baikal and, the much smaller catchment of Lake Baunt

means that there is the potential for a clearer atmospheric signal in certain proxies (e.g. isotopes), as opposed to one influenced by fluvial input. Baunt's specific position at the edge of continuous permafrost make it highly susceptible to influences of climate change, and also make it highly susceptible to degradation as a result of permafrost thaw (Gordov and Vaganov, 2010). Low precipitation levels within the region means glaciation was restricted to the high mountains during the LGM, allowing accumulation of long archives for palaeoenvironmental reconstruction (Biskaborn *et al.*, 2012). Moreover, by studying a network of lakes with long sedimentary records, Lake Baunt provides a valuable addition by allowing the testing of whether abrupt changes seen in Lake Baikal, for example, are localised to the lake, or are part of a wider response to extrinsic forcing in the region (Williams *et al.,* 2011).

2.2 Sample Collection

Exploratory work at Lake Baunt began in November 2013, when a short core was collected from the site and bathymetric surveys were carried out using a Hummingbird Matrix 748 x 3D 6-beam echo sounder (Krainov *et al.*, 2017), by a team from the Russian Academy of Sciences in Irkutsk. This initial work led to a further expedition to Lake Baunt in March 2014 when a long core (BNT14) of 13.66 m was extracted from the site.

BNT14 was collected using a UWITEC gravity corer while the lake was frozen (ice thickness maximal – up to ~2 meters with limited movements) (see figure 2.5) (Krainov *et al.*, 2017). The UWITEC system used hammer action with inner 63mm PVC liners to extract the 13.66 m core in 8 liners over 3 days, with a 95% recovery rate (Krainov *et al.*, 2017). The core location (55°11'15"N, 113°01'45"E) was chosen following the bathymetric surveys, which highlighted this as the region with most regular sedimentation rates, due to it being situated over 1km from the steep sides of the basin (see figure 2.1.C). This reduced the risk of the core being influenced by slumping and turbidites, although the potential influence of these must be considered when studying this core, due to the steep sided nature of the basin (see figure 3.2), and due to the risk of tectonic movements triggering faulting within the lake sediments.

The water depth at the drilling location is 33 meters deep, which is the deepest area of the lake (Krainov *et al.*, 2017). This core was taken to the Institute of Geochemistry, Russian Academy of Sciences in Irkutsk where it was split and described. Loss-on-ignition (LOI), total organic carbon (TOC) and biogenic silica (BSi) analyses were undertaken, to provide downcore information on the varying material contents of the core and will be discussed further in section 2.3 and 2.4. For this project, research samples were subsampled from the BNT14 core in April 2015 at a 5cm resolution, with additional samples being collected in April 2016 to allow increased resolution of some sections of the core (to every 2.5cm), and for additional dating to be carried out.

Figure 2.5: UWITEC coring system set up on Lake Baunt. Photo taken by A. Shchetnikov (25/03/2016).

2.2.1 Lake Baunt Stratigraphy

2.2.1.1 Lithostratigraphic Description

Understanding a core's lithostratigraphy is essential to provide context for proxies from within the archive to be studied. This is because they provide valuable information about changes to sediment delivery to the lake system and can highlight periods of increased in-washing or reworking within a core (Klaar *et al.*, 2015; Marston, 2010). Figure 2.6 highlights the litho-stratigraphic results from the BNT14 core from Lake Baunt.

The base of BNT14 consists of silty clay with frequently occurring hydrotroilite ($FeS\dot{n}H_2O$), a hydrous sulphide of ferrous iron (Ferronsky *et al.*, 2014) and sand enriched areas from 1366-1170cm (Krainov *et al.*, 2017) (Fig 3.5). Diatoms are observed in low concentrations through this section (see chapter 4), after which there is a gradual change into silty clay with abundant diatoms, which persists until ~620cm, with periods of increased clay and silt enrichment. Within this section of the core, two faults are noted, at c.990cm and 660cm (Krainov *et al.*, 2017). These were taken into account during data analyses and interpretation, as they could indicate areas where the sediments may have been shifted by tectonic activity, and, thus, the sediments may be stratigraphically deformed. Hydrotroilite ($FeS\dot{n}H_2O$) is also observed at intervals across this section (Krainov *et al.*, 2017) (Fig 2.6). Sedimentological changes are observed during a short ~40cm section made up of diatomaceous ooze between ~620-580cm, with the unit at ~600cm also containing charred wood fragments (Krainov *et al.*, 2017). After this, the sediments return to silty clay with diatoms until ~540cm, although this is interrupted by interbedded clayey silt throughout the section (Krainov *et al.*, 2017). From ~540cm there is a return to diatomaceous ooze, which continues to the core top but is sporadically interrupted with charred wood fragments between ~480-380cm (Krainov *et al.*, 2017) (Fig 3.5). It is also known that charcoal occurs in high abundances through the BNT14 core, with particularly charcoal rich areas documented between 0-180cm, 820-920cm and 1200-1300cm (Bezrukova, pers. com.).

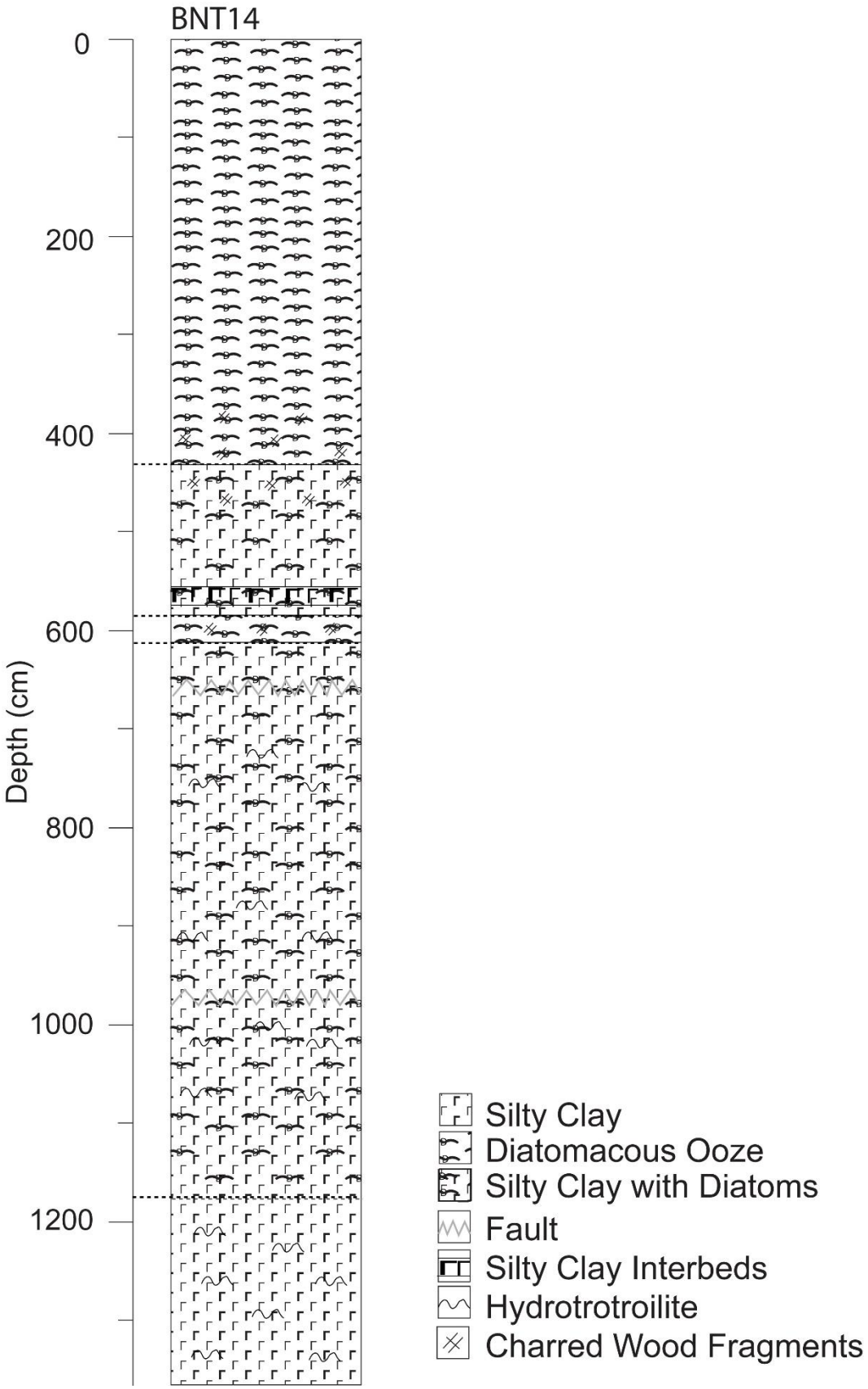

Figure 2.6: Detailed lithostratigraphy of the BNT14 core (see Krainov *et al.,* 2017 for published stratigraphy).

2.2.2 Additional Stratigraphic Methods

2.2.2.1 Loss-On-Ignition (LOI) and Total Organic Carbon (TOC)

Alongside the lithostratigraphy, a loss-on-ignition (LOI) curve has been produced, allowing consideration of the organic content of the sediments. LOI provides a rapid, inexpensive technique (Dean 1974; Konen *et al.,* 2002; De Vos *et al.*, 2005), and is widely used to estimate the organic content of samples by oxidising organic matter to CO_2 and ash (Heiri *et al.,* 2001).

The LOI (%) record was produced by collaborators at the Russian Academy of Sciences, Irkutsk. Samples were studied at a 3cm resolution, with analyses following Heiri *et al.*, 2001: samples were weighed, dried at 105°C in an air circulation oven for 12 hours, and then reweighed to determine dry weight (formula 2.1). Samples were placed in weighed crucibles before undergoing ashing at 550°C for 2 hours, which combusts organic carbon (Heiri *et al.,* 2001). Samples were cooled to room temperature and placed in a desiccator, before being re-weighed to allow the LOI to be established as outlined in equation 2.2. Estimates of the carbonate content, made by heating to 950°C (Heiri *et al.,* 2001) were not carried out on the BNT14 core as initial testing with 50% hydrochloric acid demonstrated that there were few, if any, sedimentary carbonates present.

Equation 2.1:

Dry weight (g) = Wet sediment weight – Dried sediment weight

Equation 2.2:

$$\textbf{Loss-on-Ignition} = \frac{(\text{Dried weight (g)} - \text{Ashed weight at 550°C (g)})}{\text{Dried weight (g)}} \times 100$$

2.2.2.2 Total Organic Carbon

Alongside the LOI, the Total Organic Carbon (TOC) content of the samples every ~6cm was established by Russian collaborators. This was measured at the Russian Academy of Sciences, Novosibirsk, using a NC1500 elemental analyser (Prokopenko *et al.*, 1999; Prokopenko and Williams, 2004).

2.2.2.3 Biogenic Silica

The biogenic silica (BSi) concentrations in the BNT14 sediments were measured by the Institute of Geochemistry, Russian Academy of Sciences (RAS), Irkutsk Branch, following the alkaline digestion method outlined by Mortlock and Froelich (1989). Samples were studied at 5cm intervals, following the standard technique, which involves dissolving the sediment using an alkaline reaction. Briefly, freeze-dried samples were lightly crushed (but not powdered), and then returned to room temperature for 24 hours. Aliquots ranging between 25 to 200mg were weighed into 50ml polypropylene centrifuge tubes, and samples masses are adjusted so no sample can contribute more than 25mg of pure biogenic silica (Mortlock and Froelich, 1989). 5ml of 10% H_2O_2 was added for 30 minutes, followed by 5ml of ~1 M HCl solution. The samples were sonified and left for 30 minutes, before 20ml of deionised water was added and samples were centrifuged for 5 minutes at 4300rpm. Supernatants were decanted and the remaining residue in the centrifuge tubes were dried at 60°C overnight (Mortlock and Froelich, 1989). Following this, 40ml of 2M Na_2CO_3 solution (Baker reagent grade) was added and the centrifuge tubes were capped, mixed and sonified before being placed into a constant temperature water bath at 85°C. Every 2 hours samples were mixed, and after 5 hours they were removed, centrifuged at 4200 rpm for 5 minutes, and the 20ml of the clear supernatant was transferred to a polyethylene scintillation vial (Mortlock and Froelich, 1989). The alkaline reaction was followed by spectrophotometry analysis of the suspension, using a UNICO 1200/1201 (Krainov *et al.*, 2017) with ammonium molybdate colour reaction, which allows determination of the dissolved silica (Mortlock and Froelich, 1989). This wet chemical digestion using a hot alkali is one of the most common techniques for measuring BSi, making it highly comparable between sites and is also seen as a straightforward and reproducible technique (Street-Perrott and Barker, 2008).

2.3 Stratigraphy Results

The loss-on-ignition (LOI), total organic carbon (TOC) and biogenic silica (BSi) results are shown against the site lithostratigraphy in figure 2.7, while figure 2.8 documents the same datasets shown as deviations from the mean,

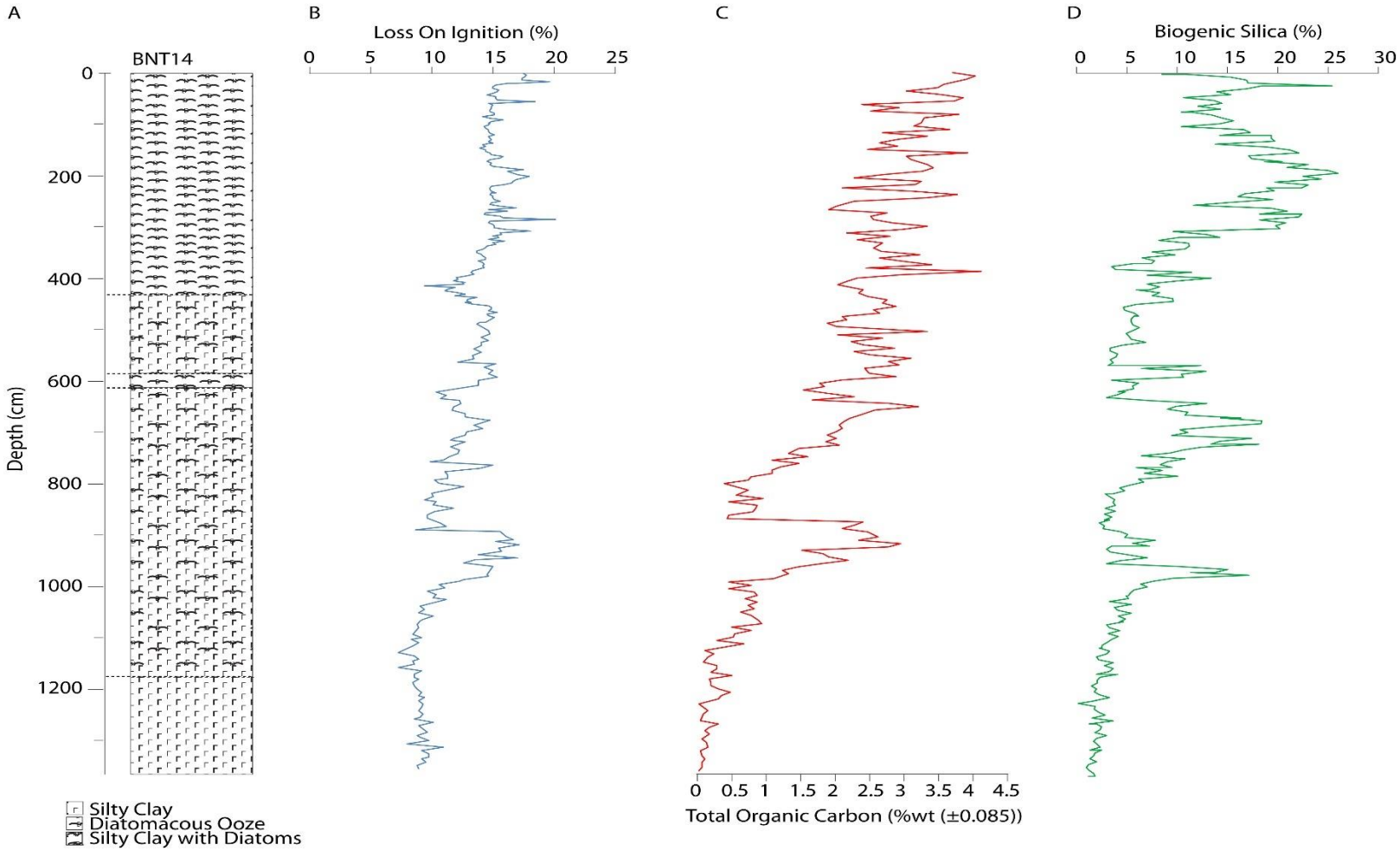

Figure 2.7: (A) Simplified lithostratigraphy of BNT14 core **(B)** Loss-On-Ignition (%) (LOI) record for BNT14 against depth **(C)** Total-Organic-Carbon (% wt) (TOC) for BNT14 against depth and **(D)** Biogenic Silica (%) (BSi) for BNT14 against depth.

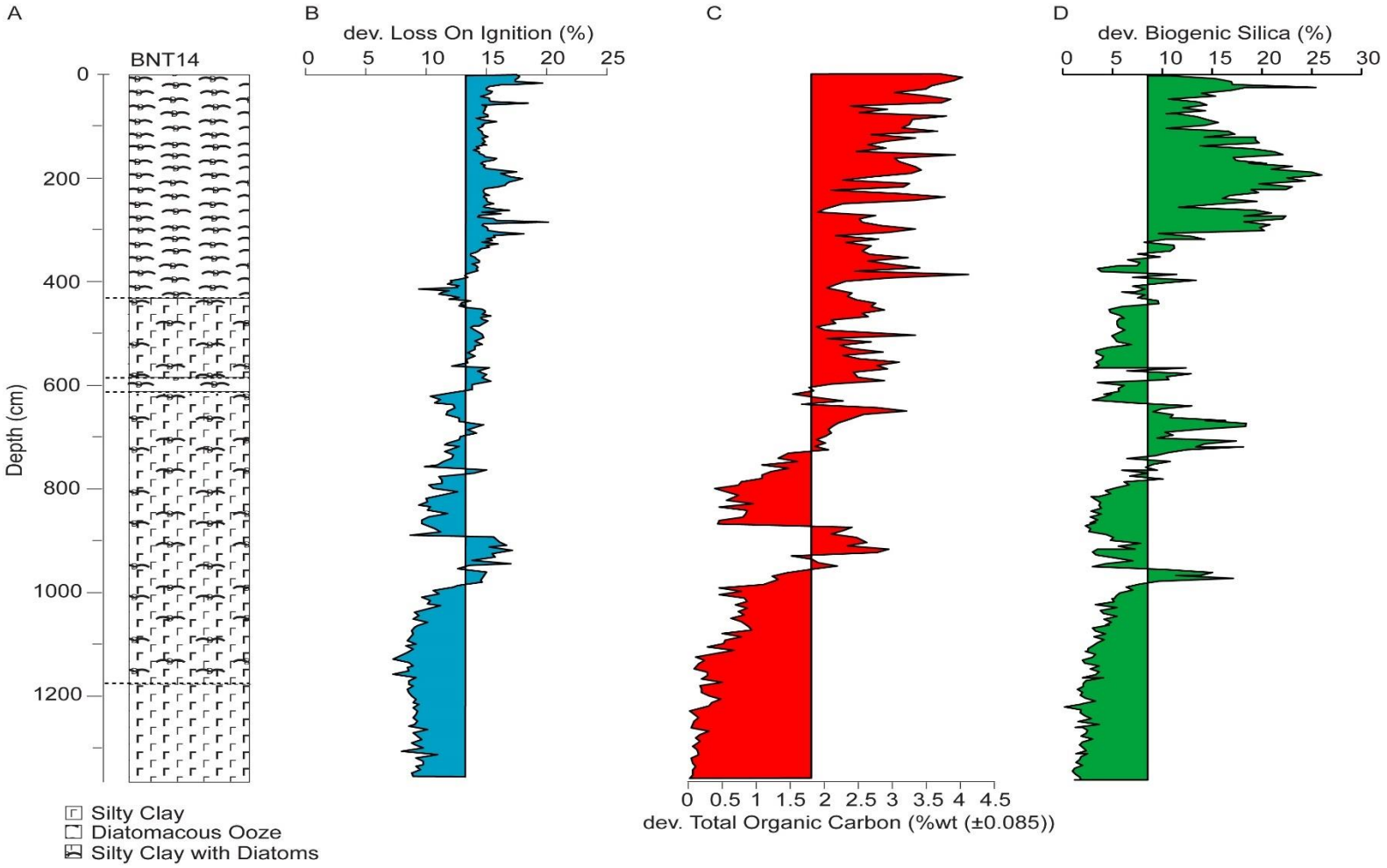

Figure 2.8: (A) Simplified lithostratigraphy of BNT14 core **(B)** Loss-On-Ignition (%) (LOI_{550}) record shown as deviations from the mean **(C)** Total-Organic-Carbon (% wt) (TOC) shown as deviations from the mean and **(D)** Biogenic Silica (%) (BSi) shown as deviations from the mean.

revealing variations in the LOI, TOC and BSi values. Figure 2.7.b shows several shifts in the LOI curve across the core, with initial values between 13.66-10.00m of around ~10%. After this there is an increase to above average levels (figure 2.8.b), which reach a peak of 17.2% at ~9.24m. Values then decline to ~10% again by ~8.94m. Following this, levels remain between 10-11%, until a short-lived peak of 15.0% at ~7.68m, and this is followed by levels fluctuating around the mean. From around 4.00m values consistently sit above the mean, with peaks reaching ~18-20% occurring at ~3.08, 2.87, 2.01 and 0.15m.

The TOC values are generally low, with an average of 1.8%wt (±0.085) (see figure 2.8), however, the record documents several variations. As with the LOI, the lowest values, are documented at the base of the core and these continue until ~9.50m, later than the low values observed in the LOI, before they increase in values to a peak of 2.609%wt (±0.085) at ~9.04m. These higher values persist until ~8.77m where they decline again, showing structural similarities to the LOI record, which is not unexpected given the close correspondence between TOC and LOI data (Meyers & Lallier-vergés, 1999; Heiri *et al.,* 2001). Unlike the LOI, this record steadily increases after the low, rising to a peak of 3.2%wt at ~6.52m. After this, TOC becomes more unstable with shifts across a general range of ~2-4%wt, although levels remain above the mean values for almost all the record after 7.00m, with larger peaks reaching over 4%wt at ~3.88 and ~0.06m. To test the apparent relationship evident from the figures, pairwise or where necessary nearest neighbour samples (n=199), were compared using a Spearmans rank correlation (rho), returning a value of 0.582 and a two-tailed significance value of 0.00 at 2 sigma, meaning they have a moderate but statistically significant relationship.

The BSi record demonstrates considerable variation across the core, with average values sitting at ~8.6%, while the range covers 0.2-26.1%. The lowest values are recorded in the earliest section of the core, where they remain under 5% until ~10.00m. After this the BSi values rise rapidly to a peak of 15.1% at 9.45m. This peak above average values occurs earlier in the BSi than the TOC and LOI records, however above average values are sustained longer in both TOC and LOI (see figure 2.7 and 2.8), with the initial occurrence

of above average values being documented earlier in the LOI (see figure 2.8). Following this period, BSi values again decline, remaining below mean values until ~8.00m, after which they increase, rising to peaks at ~7.10m, ~6.95m and 6.70-6.65m of 18.2%, 17.5% and 18.5% respectively (see figure 2.7 and 2.8). After these peaks, values drop below average levels to lows between 3-6%, which is followed by a small increase to ca. 11% between ~580-570cm and then a decline back to previous levels. Between 5.0-3.0m BSi fluctuates within a few percent of the mean (figure 2.8.D), while after ~3.0m values increase, remaining above average for the remainder of the record and reaching their highest deviations from the mean at peaks of 26.1% at ~190cm. This is followed by a gradual fluctuating decline, to levels between 10-15% in the depth range ~100-30cm, after which there is a rapid shift to 25.5% at ~20cm depth.

The three records all differ from each other, however, as shown in figures 2.7 and 2.8 and described above, there appears to be a general similarity in the structures of the records. All three document the lowest values in the basal sections of the core, with a switch to above average values occurring broadly between 9-10m in all three records. After this level they fluctuate around the mean, and then towards the upper sections of the core all of the records switch to sitting above their mean values. This switch occurs at differing times in all the records, with the TOC values sitting generally above the mean much earlier from ~7.0m compared with the switch at ~4.0m in the LOI and ~3.0m in the BSi.

2.4 Discussion

Variations in the TOC, LOI and BSi records from BNT14 as described in section 2.3, have several major trends that are important for understanding the nature of the core and informing the interpretation of the proxy records in later chapters. One of the most notable factors shown in figures 2.7 and 2.8 is the similar structure seen between the TOC and LOI records, and the statistical relationship between these is discussed below. This is because in producing an LOI curve record, the organic content of the material is approximated (Heiri *et al.,* 2001), while TOC is a bulk value representing the fraction of organic carbon that escapes remineralisation during sedimentation (Meyers and

Lallier-Vergès, 1999), and this makes it an essential parameter for considering the abundance of organic matter preserved within sediments (Meyers and Lallier-Vergès, 1999). In essence, both are methods for estimating the organic content of the sediment, however, TOC estimates are considered more accurate than LOI for understanding organic carbon levels. However, both records are considered here due to the higher resolution (double) of the LOI, which is a result of these analyses being cheaper and more rapid to carry out (Heiri *et al.,* 2001). Figure 2.9 documents the TOC as deviations of the mean against the LOI after Dean (1974)'s correction factor of 0.469 has been applied to allow the LOI curve to represent carbon content (Dean, 1974; Anderson *et al.,* 2009). Figure 2.9 shows a clear difference in the estimated TOC from the LOI correction versus the initial TOC, with the corrected LOI predicting much higher TOC values, giving an average of 6.1 versus the measured TOCs average of 1.8. This discrepancy, possibly due to the lower accuracy of the LOI method, means that, despite its lower resolution, the measured TOC record will be considered in this thesis as the most accurate record for estimating the organic carbon content of the cores.

2.4.1 TOC

As documented in figures 2.7 and 2.8, TOC shows several shifts around the mean, although values remain fairly low at under 5% throughout the record. The variation in the amount of organic carbon preserved in lake sediments is controlled by several factors, with changes in primary production rates altering the amount of organic carbon available for preservation (Meyers and Lallier-Vergès, 1999) and the source and molecular composition of the organic material affecting preservation (Meyers and Lallier-Vergès, 1999; Sobek *et al.*, 2009). For example, autochthonous material is considered less prone to accumulation as it is easily decomposed by heterotrophic microbes, fuelling respiration in the sediments (Sobek *et al.*, 2009). Allochthonous inputs on the other hand have been documented to drive high organic carbon burial rates (Sobek *et al.*, 2009). Therefore, the source and type of organic matter is highly influential on the organic carbon content preserved in lacustrine sediments.

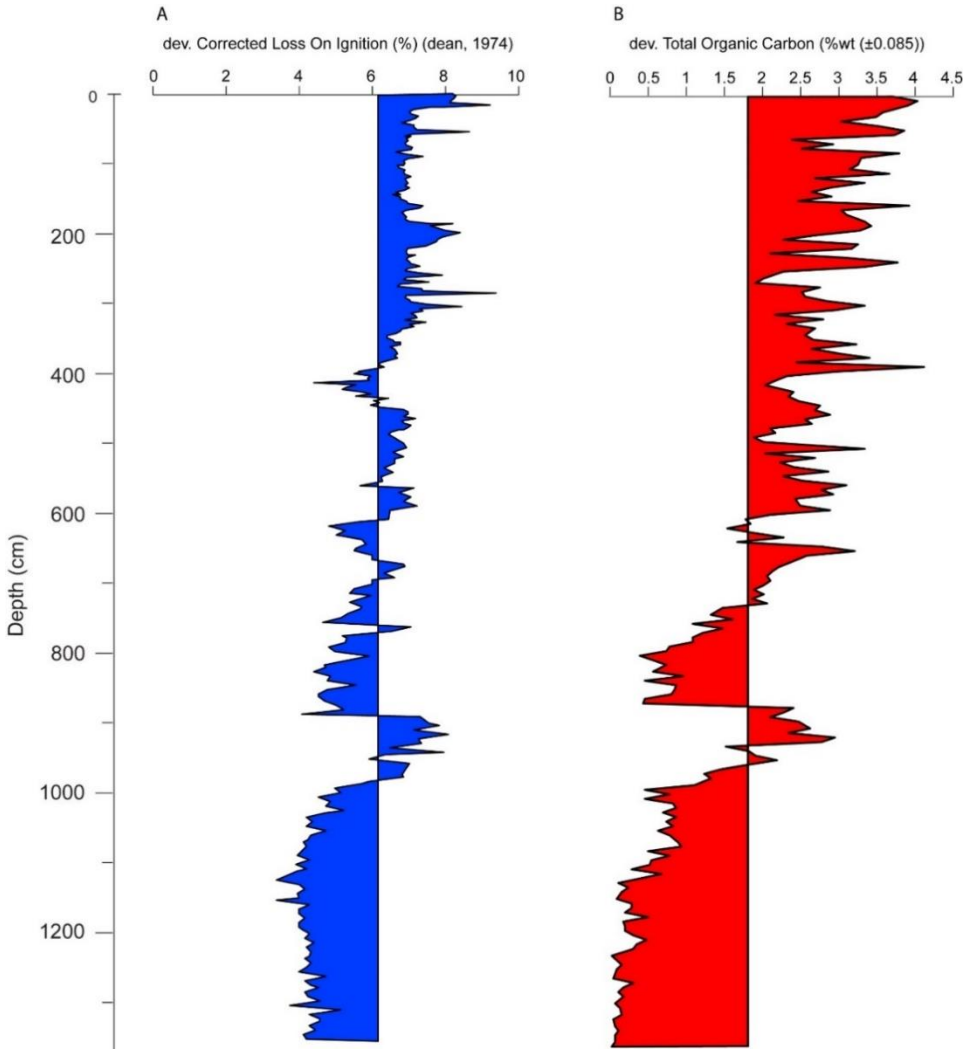

Figure 2.9: (A) - Corrected LOI (using Dean, 1974's correction factor) as deviation from its mean. **(B)** - TOC as deviations from the mean.

Changes in the type and abundance of plant life within and around the lake, will influence the amount and nature of organic matter delivered to the lake sediments (Meyers and Lallier-Vergès, 1999). It is also possible that variations within the TOC record are driven by changes in the source of the organic matter, potentially with more autochthonous inputs from within lake productivity during periods when TOC values are very low, such as at the base of the record, while allochthonous sources may become more influential during the upper sections, and this may suggest changes are driven by source material variations. There is potential to differentiate the sources of organic matter through study of C:N ratios (Sobek *et al.*, 2009), and these will be considered in chapter 6.

Alongside the quantity and source of organic carbon initially produced, TOC values are affected by a range of taphonomic processes, with microbial activity playing an important role. As organic matter is deposited onto lake sediments it may be subject to microbial reworking, which, in turn, can alter the molecular composition (Meyers and Lallier-Vergès, 1999). After deposition, the organic carbon molecules can undergo microbial remineralisation, into inorganic compounds such as CO_2 or CH_4, preventing it being preserved in the sediments (Anderson *et al.,* 2009; Sobek *et al.*, 2009). Mineralisation is strongly influenced by the oxygen concentrations of bottom water, as oxygen is consumed from the lake waters during mineralisation, to convert the carbon into CO_2 or CH_4, and this can make bottom waters anoxic (Sobek *et al.*, 2009). The mineralisation, therefore, causes TOC concentrations to decrease as the carbon is removed from the lake and emitted to the atmosphere (Meyers and Lallier-Vergès, 1999). Thus, once waters are depleted in oxygen, remineralisation is limited, and organic carbon is preserved within the sediments, and therefore anoxic conditions are seen to favour organic carbon preservation (Sobek *et al.*, 2009). The source of the organic carbon also influences remineralisation rates, with autochthonous sediments mineralisation occurring at similar rates in oxic and anoxic conditions, while rates with allochthonous organic carbon are suppressed under anoxic conditions. Thus, if bottom waters alter in their oxygen concentration, it will alter the amount of allochthonous carbon being preserved within the sediments. Mineralisation rates are also limited by organic matter absorbing onto mineral particle surfaces, allowing it to be preserved within the sediments (Sobek *et al.*, 2009).

Another important driver of changes in the preservation of organic carbon within sediments are variations in sedimentation rates (Sobek *et al.*, 2009). This is due to TOC being expressed as percentage weights, and, thus, they are influenced by the overall sediment composition and changes in sediment supply from the catchment, and, therefore, the record can become diluted by clastic sediment particles. This can lead to an apparent reduction in organic carbon, while conversely the dissolution of carbonate materials can cause the record to be concentrated in TOC (Meyers and Lallier-Vergès, 1999).

Therefore, the subsequent shifts seen in figure 2.7 and 2.8 may result from variations in the sedimentation rates, potentially with high clastic sediment delivery occurring during the base of the core, and less clastic being delivered during the upper sections where values are well above the mean. This is supported by shifts in the lithostratigraphy (see figure 2.6), which highlights that the sediments are made up of clastic silty-clay at the base of the record, while in the upper sections the shift to diatomaceous ooze is shown in a period of increased TOC. The use of carbon mass accumulation rates (CMARs) can help to overcome the impacts of variable sedimentation rates and will be discussed in chapter 6.

2.4.2 BSi

As with the TOC record, variability is evident in the BSi record for BNT14 (see figures 2.7.d and 2.8.d). BSi is an amorphous form of silica, biologically precipitated by a range of siliceous organisms, which in freshwaters include diatoms, chrysophytes and sponges, and it is often considered as a proxy for palaeoproductivity (Conley, 1988; Street-Perrott and Barker, 2008). However, for BSi to be utilised in this manner, several requirements must be met, including that there has been no change in the BSi preservation over the record (Conley, 1988) and that the preserved BSi is representative of the productivity of the overlying water (Conley, 1988).

The lithostratigraphy shown in figure 2.6 highlights the increase in diatoms found within the sediment, as one moves from the base of the core to the upper sections. Diatoms are one of the key sources of BSi in lake sediments, particularly due to their widespread occurrences in a range of aquatic habitats, flow conditions and water chemistries (Street-Perrott and Barker, 2008). As such, BSi has often been used to estimate the quantity of diatom silica in sediments (Conley, 1988). The variations in the BSi record may fluctuate as diatom production changes. This could highlight one source of increasing BSi across the BNT14 core, as diatoms are not observed in large concentrations at the base, where BSi values are well below their mean value. However, the upper sections of the BNT14 sediments contain high concentrations of diatoms, and this may explain why the upper section of the core has BSi values

well above the average for the core as a whole. That said, the variations documented across the BNT14 do not only vary as the lithostratigraphy changes, and, thus, other factors could be affecting the BSi signal. These factors could include variability within the diatom composition of the core, as individual species of diatoms have varying silica contents (Conley, 1988), with some taxa, such as *Aulacoseira* being much more heavily silicified than others (Chen *et al.*, 2012; Kilham *et al.*, 1986). This can lead to the case that BSi values rapidly increase where larger and more silicified diatoms are part of the assemblage, rather than when diatom concentrations increase (Conley, 1988). This will therefore be considered as a driver of BSi changes later in the thesis (see chapter 4), where these are also considered alongside biovolumes. Where shifts do not appear to correlate to diatom composition or concentration changes the BSi may be reflecting alterative amorphous silica sources. It is of note that sponge spicules can contain an order of magnitude more silica than diatoms, and their higher aluminium content is thought to make them more resistant to dissolution (see below) (Conley, 1988; Street-Perrott and Barker, 2008), and it is then possible that a period of high sponge spicule concentration could significantly increase BSi values.

An additional factor that must be considered when interpreting a BSi record is the influence of silica dissolution (Conley, 1988). As discussed above, diatom species vary in their cell's silica content, and dissolution can exacerbate this by removing the more delicate and less silicified species from the sediments, thus, reducing the BSi levels at these points, as dissolution rates are known to have varied due to different volumes and surface areas of diatoms (Barker *et al.,* 1994). The more silicified species are more likely to be preserved into the BSi record (Ryves *et al.,* 2003), and, therefore, it is possible that particular species may significantly influence the BSi record. Diatoms are susceptible to dissolution as they are deposited into sediments, as their organic membrane and, in some cases a thick polysaccharide gel layer protecting the frustule from dissolution, is rapidly decomposed (Street-Perrott and Barker, 2008), with bacterial activity thought to hasten digestion, meaning the BSi may not accurately record the diatom productivity of a water body. The pH of a water body can also be highly influential in dissolution rates, with a pH of 9 or above

showing an exponential increase in dissolution rates, while pressure and temperature are also positively related to increases in dissolution (Barker *et al.*, 1994). This highlights that shifts in the alkalinity, temperature and pressure have substantial influence on how much BSi is preserved in sediments and, therefore, changes in these parameters will influence the BSi record. It is clear that diatom dissolution is a complex process and, as such, will be considered further in chapter 4.

2.4.3 TOC versus BSi

As mentioned in section 2.3, structural similarities are seen between the TOC and BSi records (see figures 2.7 and 2.8). This may mean the records are documenting responses to changes driven within the ecosystem. To allow more consideration of this, statistical analyses have been undertaken and a bivariate plot of the two datasets is shown in figure 2.10. Initially the datasets were tested for normality using a Shapiro-Wilk W test alongside an Anderson Darling A test, in PAST (Hammer *et al.,* 2001). Both tests highlighted the data were non-normal, thus, a Spearman's Rank correlation analysis was carried out in SPSS, giving a correlation coefficient of r_{SR} = 0.636 and a two-tailed significance value of 0.00 at 2 sigma, meaning they have a moderately strong statistically significant relationship. It is worth noting that the sample intervals and sample locations are not completely paired for these data so pairwise time analyses were not possible without the removal of BSi data.

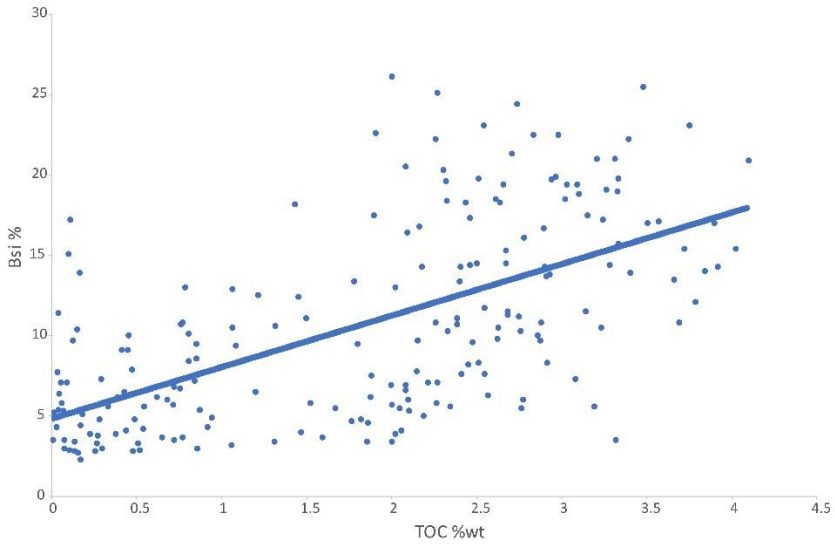

Figure 2.10: Bivariate plot of TOC (%wt) and BSi (%) with line of best fit.

The correlation between TOC and BSi highlight that both proxies are covarying to some extent, and this may suggest that a similar factor, such as ecosystem productivity may be influencing them (Horiuchi *et al.*, 2000). This may suggest that the overall environmental system is influencing both data sets, with high levels in the BSi record demonstrating high productivity within Lake Baunt, while co-occurring high values in the preserved TOC values may document a more productive landscape. The moderate nature of the correlation between the two records also highlight the complexity affecting the TOC and BSi data, with additional factors as discussed in sections 2.4.1 and 2.4.2 both influencing the records.

2.4.4 Additional Factors

As discussed in previous sections, other drivers may be causing the shifts documented within the TOC and BSi records, and these will be discussed in later sections of this thesis, where chronological controls allow wider discussion. Of particular importance here though are the two faults that are shown in figure 2.6 at ~990cm and ~660cm, which may relate to unconformities in the sediments. The lower of these at 990cm occurs close to shifts from below average to above average values in TOC, LOI and BSi, and it is possible that faulting may have influenced the sediments at this depth, potentially by reworking them, or causing slumping within the lake. Rapid shifts are also seen in all records during the section of the core around ~660cm where the second faulted area is identified. In both cases care must be taken when considering the drivers of changes in these particular areas. The implications of these faults are considered during the interpretation of the proxy records in later chapters.

Section 2.2.2 also documents the occurrences of increased charred wood fragments between 480-380cm and increased charcoal in some sections of the core, and this is also important to consider for the BNT14 archive. These periods may document increased fire frequency in the landscape (Earle *et al.*, 1996), which would have implications for the carbon content entering the lake and for the catchment development in general, such as impacts on vegetation development. These periods may, therefore, document instability on the

landscape. It has also been observed that under current warming conditions fire frequency has been shown to increase (Tchebakova *et al.*, 2016), and it may be that these periods may also document shifting climatic conditions. These factors will be considered alongside the proxies produced as part of this project to consider the drivers of these increased charcoal and charred wood fragments later in the thesis.

2.5 Stratigraphy Summary

The sedimentary records from BNT14 demonstrates variability in the BSi, TOC and LOI records. These will be considered with respect to the proxy records produced as part of this thesis to allow a detailed multiproxy record to be produced for Lake Baunt. It is of particular importance, to consider the faulting documented in the core during proxy analyses, as this may have caused changes within the sediments, while periods with increased charcoal fragments must be considered when studying the carbon content within the core. Overall, however, the majority of the core is stratigraphically sound for undertaking palaeoenvironmental studies.

3 Chronological Controls at Lake Baunt

3.1 Introduction

Palaeoenvironmental studies rely on accurate and precise chronologies to investigate responses to abrupt climatic changes, regional signals and to detect leads and lags between the response in different regions (Lane *et al.*, 2011). Late Quaternary studies focused on the past 50 ka most commonly utilise radiocarbon dating to provide chronological controls (Brauer *et al.*, 2014), however, other techniques including ^{210}Pb, luminescence dating, U-Series, palaeomagnetic dating and astronomical tuning (Mackay, 2007) have all been used to provide chronological controls in central Asia, while newly developed techniques such as the application of cryptotephra (the use of volcanic ash horizons not visible to the naked eye) are well developed in other regions including Northern Europe and the Mediterranean (Lowe *et al.,* 2015).

3.2 Radiocarbon Dating

Radiocarbon dating was developed 7 decades ago this year (Brauer *et al.*, 2014), by Libby and co-workers (Libby *et al.*, 1949). The technique is based on the principle that there are 3 different isotopes of carbon, ^{12}C, ^{13}C and ^{14}C. Of these isotopes, only ^{14}C is radioactive (Libby, 1955; Libby *et al.*, 1949), with a half-life of 5730±40 years (Godwin, 1962). Radiocarbon is produced in the upper atmosphere by cosmic ray bombardment, although atmospheric concentrations of ^{14}C are very low (Browman, 1993), at 1 part per trillion (Libby, 1955), and it is oxidised into $^{14}CO_2$, after which it is able to enter the carbon cycle by incorporation into carbon bearing materials. At the time of death, radioactive decay starts the clock (Brauer *et al.*, 2014). Radiocarbon dating generally relies on the material selected for dating being in isotopic equilibrium with the atmosphere at the time of death of the organism. However, as there are other carbon reservoirs, such as the oceans, cryosphere and some deep lakes, there can be a residence time for old carbon (where ^{14}C is lower) that can lead to a reservoir effect, inducing an apparent older radiocarbon age than would be expected for a given sample. This issue can be tested, in part by examining the δ^{13}C values for a lake record (discussed below), or for very deep lakes such as Baikal, radiocarbon dating

of modern material. Additionally, the technique needs a reliable calibration curve, due to changes in cosmic ray flux over time, and thus radiocarbon production (Walker *et al.,* 2001; Blockley *et al.*, 2007).

Since its development, radiocarbon dating has undergone several improvements, including the ability to apply the method to any carbon bearing material, where carbon was laid down in the last ~50-60 ka, permitting the sample of direct interest to be analysed (Brauer *et al.*, 2014). For larger samples of sediment, in the size range of 1-10 g, the sample is suitable for dating by conventional radiocarbon dating, using beta decay or liquid scintillation (Bowman, 1990). For charcoal, this ranges between 10 g and as little as 0.1 g of material. Required sample sizes have been reduced through the development of accelerator mass spectrometry (AMS), which for most samples required 0.1 to 0.01g of material. This has allowed the utilisation of a wider range of materials, including smaller macrofossils, pollen and compound specific dating to target specific carbon molecules. This has enabled a refinement of the dating at particular sites, and higher resolution studies (Brauer *et al.*, 2014), although it is also fair to reiterate that if larger sample sizes are available, older conventional counting techniques can yield good results on different chemical fractions of sediment (e.g. Walker *et al.,* 2014). Additional improvements in the application of radiocarbon dating are linked to improved calibration (discussed in section 3.2.3), precision, and age modelling (see section 3.6) (Blockley & Housley, 2009; Reimer *et al.*, 2013; Brauer *et al.*, 2014).

3.2.1 Radiocarbon limitations

3.2.1.1 Bulk Samples

Despite its wide usage, radiocarbon dating has several limitations. In areas of poor macrofossil preservation, such as in Siberia, many chronologies are established using total organic carbon (TOC) bulk dates (Colman *et al.*, 1996). Bulk radiocarbon samples are problematic as they can be affected by issues including, *inter alia,* incorporation of older carbon through mineral carbon error, humic acid percolation in the sediments, and lacustrine reservoir offsets in deep lakes (Blockley *et al.*, 2007; Colman *et al.*, 1996). Several techniques

have been used to attempt to prevent the issues associated with bulk samples, including extracting pollen from samples, which was attempted on samples from Lake Baikal (Piotrowska *et al.*, 2007). This technique has the advantage of avoiding issues associated with bulk samples, however, mixing of microfossils in a profile can potentially rework mixed age material leading to erroneous radiocarbon ages (Blockley *et al.*, 2007). If bulk samples do need to be used, the calcium carbonate content of the lake or the isotopic ratio of $\delta^{13}C$ of bulk carbonate can be used to assess any lake reservoir issues, with, for example, influence of magmatic sources causing a $\delta^{13}C$ value to sit around ~ -8‰ (Walker *et al.*, 2008), or chalk bedrock detrital input having a $\delta^{13}C$ value ~ 0-1‰ , while organic terrestrial sample values are normally in the range of ~ -25-28‰ (Blockley *et al.*, 2018).

3.2.2 Freshwater Reservoir Offsets

Radiocarbon chronologies for lake and marine settings can also be affected by reservoir effects (Lowe *et al.*, 2007). This occurs where there is an offset in radiocarbon ages of organisms that gain their carbon from these sources, compared to those which derive their carbon from the atmosphere (Reimer & Reimer, 2001). In settings and samples where there is potential for a reservoir influence, it is necessary to treat the dating with caution, and ideally use terrestrial macrofossils as the sampling material, where carbon has been photosynthesised from the air, preventing any influence from a reservoir effect. However, even in these circumstances it is necessary consider the potential for fossil recycling and contamination when undertaking age modelling, to ensure the produced chronologies are robust. In a lacustrine setting there is still the potential for either contamination of a fossil sample, the need to date bulk material or misidentification of macrofossil material. In these cases, if there is a reservoir offset this can significantly affect radiocarbon ages. This can often be a result of the in-washing of detrital carbonates of geological age or in some deep lakes it can be the result of long residence time of carbon in lake-bottom waters, changing lake surfaces and a lack of overturning. Either way, this can lead to ages that are apparently too old by several hundred to thousands of years (e.g. Blockley *et al.,* 2018), even in some macrofossils where there has been some sub aqueous photosynthesis (such as reeds). In

these cases, a sound assessment of the potential for a reservoir effect, such as testing for inorganic carbon content and interrogation of $\delta^{13}C$ values, as discussed above with reference to bulk samples, can be a useful indicator of reservoir problems. For larger lakes with the potential for deep bottom waters with a long residence time, and the potential for mixing between bottom waters and the surface, there is the potential for a reservoir offset, similar to in a marine system. In these settings, sampling of modern material for radiocarbon dating, is recommended to calculate the offset. For example, recent studies of Lake Baikal have estimated a reservoir offset of ~500 years for both modern and Holocene archaeological studies of paired aquatic and terrestrial material (Nomokonova *et al.*, 2013). A similar average offset of ~500 to ~775 years has been reported for different locations around Baikal by comparing bulk and pollen radiocarbon ages (Piotrowska and Oberhänsli, 2009).

3.2.3 Radiocarbon Calibration

Radiocarbon calibration is now routinely undertaken, being considered an essential stage of radiocarbon dating, and is an area that is undergoing continual improvements (Bronk Ramsey *et al.*, 2010). It is required due to natural variations in atmospheric production and carbon exchanges between ^{14}C reservoirs (Stuiver & Kra, 1986). Calibration also provides an opportunity to correct for the underestimation of Libby's original half-life for ^{14}C, which was 5568 years as opposed to 5730±40 (Godwin, 1962). The original half-life is still used to provide consistency with dates produced in the early days of the method, and a correction for this is incorporated into the calibration process (Brauer *et al.*, 2014). It is undertaken by using independently dated archives, which record atmospheric ^{14}C, or can be converted using a reservoir correction to an atmospheric signal (Reimer *et al.,* 2009; Reimer *et al.*, 2013).

3.2.3.1 Calibration Curves

Several calibration curves exist, although the majority of the radiocarbon community recommend the use of the consensus IntCal curves (Brauer *et al.*, 2014) . The current curve, IntCal13, utilises Northern Hemisphere tree rings back to 13.9 ka BP (Reimer *et al.*, 2013), and this section of the curve is considered to be particularly robust as a result of this. Beyond this period the

record uses corals, macrofossils, speleothems and varved lakes, including the long Lake Suigetsu record to extend the curve to ~50 ka BP, and greater uncertainty is more likely during this section (Brauer *et al.*, 2014). Despite being recommended as the best tool for terrestrial calibration over the radiocarbon timescale (Bronk Ramsey *et al.,* 2013), IntCal13 does have several limitations and should be considered as a best representation of the present understanding of several datasets, which have inconsistencies between them. Due to these factors it is best that IntCal13 is viewed as a work in progress, with changes anticipated as additional datasets become available (Ramsey *et al.*, 2013). At some points over the radiocarbon timescale, IntCal13 can give over-precise calibrated ages, with fluctuations seen in the individual records being treated as noise, where in fact they may be real fluctuations (Bronk Ramsey *et al.*, 2013).

Despite issues with IntCal13, radiocarbon calibration has undergone several significant improvements over the past decades, linked to the development of Accelerator Mass Spectrometry, reductions in required sample sizes and improvements in precision (Bronk Ramsey *et al.*, 2013). Inconsistencies between the archives used to construct previous curves have prevented calibration of some samples; for example IntCal04 only extended to 26ka BP, due to inconsistencies between 26-50 ka BP (Bronk Ramsey *et al.*, 2013). The Lake Suigetsu varve record has been key to improvements in terrestrial calibration, allowing the full ^{14}C dating range to be covered from a terrestrially derived curve (see reservoir offsets 3.2.1.2). The use of dendrochronology in the most recent ~13.9 ka BP years of the record are considered to make the most robust section, evidenced by the small standard deviations across this section (Reimer *et al.*, 2013).

3.2.4 The Lake Baunt Radiocarbon Strategy

In an ideal world, the best practice for a radiocarbon chronology would consist of picking known species of terrestrial macrofossils for radiocarbon dating, while also using independent dating methods/isochrons such as those produced by tephra horizons to test the ^{14}C dates. The radiocarbon dates need to be calibrated using the most up to date calibration curve available, in this

case IntCal13 (see section 3.2.3), and then dates require statistical treatment through modelling (see section 3.6). In the case of this study, macrofossils were not preserved within the core, and therefore bulk samples had to be utilised for radiocarbon dating. As a result of this, it was essential to assess the dates robustly, and this can be done by considering the $\delta^{13}C$ values that have been measured from samples across the core. This is important as samples could contain detrital carbonate, which causes the radiocarbon dates to be contaminated. The most likely sources of error for Lake Baunt come from humic acid percolation, which can cause the dates to be too young, or from methane gas venting, as a result of the site's geothermal influences, which causes dates to be older. In the latter two cases bulk $\delta^{13}C$ values would highlight this, with methane venting having much more negative $\delta^{13}C$ values (~$-40^{0}/_{00}$) (Reimer and Reimer, 2001), and much less negative for geothermal sources (~ $-8^{0}/_{00}$) (Walker *et al.*, 2008).

For Lake Baunt, radiocarbon dating was carried out on bulk sediments, at either the Poznan radiocarbon labs (BNT codes) or Queens University Belfast (UBA codes), and the results are shown in table 3.1. These dates were calibrated using the recommended IntCal13 calibration curve (Reimer *et al.*, 2013) in OxCal 4.3, and they have been Bayesian age modelled to produce the most robust age model (see section 3.6). In order to test the issues relating to bulk dates discussed above, through some form of geological carbon input, from magmatics, ^{14}C depleted carbonate rocks (which are not present in the catchment – see chapter 2), glacial flour formed from carbonate rocks overridden by glaciers from outside the local catchment, but delivered to the site by glacial processes (Lowe and Walker, 2000), or by dust (Dietze *et al.*, 2014), it would be ideal to check the offline $\delta^{13}C$ measurements on the radiocarbon samples. In the case of the Baunt, AMS dates measured ^{13}C was used for mass correction, as is common in many laboratories, and this is not useful for assessing the potential for geological carbonates to have induced a reservoir offset. However, for Baunt an extensive set of bulk $\delta^{13}C$ values are available, and these (chapter 6) were checked across the core and conformed to the range expected for primary terrestrial organic material (~-25 - $-28^{0}/_{00}$). This suggests that a geological carbon reservoir offset would be highly unlikely

in this site. One additional source of old carbon that it is essential to consider in a Siberian context is CH_4 as release of CH_4 into the atmosphere from melting Arctic permafrost and thermokarst lakes has been observed to be a major contributor to global atmospheric CH_4 concentrations (Fisher *et al.*, 2011). From a radiocarbon dating point of view, old carbon supplied through released CH_4 would be a problem, but as discussed in chapter 6, the Baunt bulk $\delta^{13}C$ values do not show any likely influence of CH_4 as the $\delta^{13}C$ of measured modern CH_4 in modern Siberian Thermokarst lakes is ~–57- –80$^{0}/_{00}$ (Walter *et al.*, 2006), whereas the Baunt isotope range is within the range expected of the terrestrial baseline (Fernandes *et al.*, 2014).

Name of Date	Depth (cm)	Uncalibrated ^{14}C date	Error (±)	Nearest bulk $\delta^{13}C$	Nearest bulk $\delta^{13}C$ depth (cm)
BNT14-52	52	5590	35	-27.3	276
UBA-32755	97.5	5049	40	-27.3	276
BNT-200	200	5775	30	-27.3	276
BNT-400	400	9000	50	-26.9	400
UBA-32756	497.5	11489	60	-26.6	497
BNT-600	600	11620	50	-26.4	599
BNT-692	691	14090	80	-27.8	694
BNT-800	800	14930	70	-25.4	799
BNT-950	950	18220	80	-26.7	948
BNT-1110	1110	18850	120	-24.6	1027
BNT-1150	1150	20680	140	-24.6	1027
BNT-1172	1172	21670	140	-24.6	1027
BNT-1195	1195	21720	140	-24.6	1027
BNT-1277	1277	24760	190	-24.6	1027
BNT-1350	1350	25350	180	-24.6	1027

Table 3.1: Uncalibrated radiocarbon dates and error available for Lake Baunt, shown alongside the nearest bulk $\delta^{13}C$ value and its associated depth.

3.3 ^{210}Pb, ^{137}Cs, ^{241}Am Dating

Alongside radiocarbon dating, ^{210}Pb (Lead-210) offers one of the most utilised dating techniques for studies considering a range of environmental systems, since its introduction in the 1960's by Goldberg (MacKenzie *et al.*, 2011). The technique is the most widely used isotope system for dating recent sediments

(Baskaran *et al.*, 2014; Hansson *et al.*, 2014), up to ~150 years, due to the short half-life of ~22.23 years (Sanchez-Cabeza & Ruis-Fernandez, 2012), and, thus, been used successfully for many studies considering the influence of recent climatic and environmental changes. ^{210}Pb is a naturally produced radionuclide, and is part of the ^{238}U decay series (Schelske *et al.*, 1994) with ^{226}Ra decaying (1622year half-life) to ^{222}Rn, an inert gas in sediment (Appleby & Oldfieldz, 1983). Some of the ^{222}Rn produced enters the atmosphere where it undergoes decay with a short half-life of 3.83 days, through a series of short lived isotopes to form ^{210}Pb (Appleby & Oldfieldz, 1983). ^{210}Pb is removed from the atmosphere through precipitation or dry fallout, and on entering a lake the ^{210}Pb is scavenged by the sediments, where the unsupported ^{210}Pb in each sediment layer declines as it undergoes radioactive decay (Appleby & Oldfieldz, 1983), as opposed to supported ^{210}Pb, which is derived from authigenic material and is assumed to be in equilibrium with the parent isotope ^{226}Ra (Appleby, 2002).

Several methods exist for determining ^{210}Pb, including measurements by direct gamma assay. One of the main advantages of this method is that on lake sediments the method is non-destructive, and allows for simultaneous assay for other environmental gamma emitting radioisotopes, including ^{137}Cs and ^{241}Am (Appleby *et al.*, 1986). Other methods including alpha counting have been utilised, however this is a destructive method (Appleby *et al.*, 1986), and is, therefore, problematic for studies where sediment quantities are limited.

^{210}Pb is often used in conjunction with ^{137}Cs (Cesium-137) and ^{241}Am (Americium-241). These are both artificially produced radionuclides, which have come to exist in the atmosphere following nuclear weapon testing (Oldfield *et al.*, 1995). These anthropogenic radionuclides have been globally dispersed, and have been incorporated into lake sediments as they undergo atmospheric fallout (Yang & Turner, 2013), initially starting in 1951-1952, with intensive atmospheric testing leading to a peak of these radionuclides in the atmosphere in 1963, where after they undergo a decline (Yang & Turner, 2013). These additional radionuclides can provide an independent age marker, alongside ^{210}Pb, with ^{137}Cs potentially allowing detection of the

caesium atmospheric peak in 1962-1963 (Schelske *et al.*, 1994). Despite these benefits, care must be taken due to the ability for ^{137}Cs to be mobilised in lake sediments, which means in some sites it is unsuitable to act as an independent age marker (Yang & Turner, 2013).

3.3.1 Lake Baunt ^{210}Pb Methodology

Four samples from the upper 10cm of Lake Baunt cores were air dried and then analysed for ^{210}Pb, ^{137}Cs, ^{226}Ra and ^{241}Am by direct gamma assay, in the Environmental Radiometric Facility at University College London, using a ORTEC HPGe GWL series well-type coaxial low background intrinsic germanium detector. ^{210}Pb was determined from its gamma emissions at 46.5keV, while ^{226}Ra was determined by the 295keB and 352keV gamma rays, which are emitted by its daughter isotope ^{214}Pb, following 3 weeks storage in sealed containers, which allow radioactive equilibration (Appleby *et al.*, 1986). ^{137}Cs and ^{241}Am were determined by their emissions at 662keV and 59.5keV (Appleby *et al.*, 1986). The detector efficiencies were measured using calibrated sourced and sediment samples of known activity, with corrections being made for the effect of self-absorption of low energy gamma rays within the sample (Appleby, 2002).

3.3.2 Lake Baunt ^{210}Pb Results

The results of the ^{210}Pb profile from Lake Baunt show that the BNT14 core did not have good unsupported ^{210}Pb activity (calculated by subtracting ^{226}Ra activity – supported ^{210}Pb – from the total ^{210}Pb activity), as these results show large negative numbers (see table 3.2). This means a ^{210}Pb chronology for these sediments could not be established. Small sample sizes, particularly in the 0.5cm sample, is likely to be the cause of big negative unsupported ^{210}Pb activity levels. Additionally, artificial fallout radionuclides were measured for ^{137}Cs and ^{241}Am), but were not detectable in the sediments from the BNT14 core (see table 3.3).

Depth	Pb-210					
	Total		Supported		Unsupported	
Cm	Bq Kg^{-1}	±	Bq Kg^{-1}	±	Bq Kg^{-1}	±
0.5	56.38	41.93	145.11	10.91	-88.73	43.33
1.5	63.78	8.38	78.06	2.4	-14.28	8.71
2.5	64.75	13.36	73.39	4.04	-8.64	13.96
8.5	61	14.26	73.42	3.87	-12.42	14.77

Table 3.2: ^{210}Pb concentrations in core BNT14.

Depth	Cs-137		Am-241	
Cm	Bq Kg^{-1}	±	Bq Kg^{-1}	±
0.5	0	0	0	0
1.5	0	0	0	0
2.5	0	0	0	0
8.5	0	0	0	0

Table 3.3: Artificial fallout radionuclide concentrations in BNT14.

This data suggests that the Lake Baunt BNT14 core does not contain sediments deposited over the past 100-150 years, or potentially that sedimentation rates are very high, causing dilution of the ^{210}Pb signal. When considered alongside the calibrated radiocarbon dates, this may suggest that there is a hiatus in the core after ~6 ka BP, or that the uppermost section of the core has been lost during coring, which is possible due to the difficult conditions of core extraction in Siberian environments.

3.4 Palaeomagnetic Excursions

The Earth's geo-magnetic field (GMF) has fluctuated between periods of normal polarity (as during the present time), and periods when it had opposite polarity, and these periods form 'chrons'. These last between thousands and millions of years (Nami *et al.*, 2016), with the current time period being included in the Bruhnes Chron, which started ~780 ka BP (Nami *et al.*, 2016). On shorter timescales of decades to millennia (Nami *et al.*, 2016) palaeomagnetic excursions are known to occur, and are defined as where the geomagnetic field direction changes with an amplitude that is 3 times greater than the secular variation for the given time interval (Petrova & Pospelova, 1990). Bruhnes Chron excursions are, therefore, characterised as brief geomagnetic

instabilities, where intensity is decreased and there is a large directional shift from the dipolar field direction, followed by a return to the pre-excursion conditions (Kissel *et al.*, 2011). These palaeomagnetic excursions are of particular interest for palaeo researchers, as these events impact on cosmogenic isotopes (e.g. ^{14}14C, ^{10}Be) and have the potential to provide precise time markers (Nöel & Tarling, 1975; Kissel *et al.*, 2011). Several excursions have been documented in late Quaternary records, including the Laschamp, Mono Lake, Gotherburg, Solovki and Etruria-Sterno excursions, which are now discussed.

The Laschamp geomagnetic excursion is the most widely recognised Late Quaternary palaeomagnetic excursion, and is generally documented to have an age of ~41 ka BP (Kent *et al.,* 2002; Lund *et al.*, 2005, 2017; Nowaczyk *et al.*, 2012). The palaeomagnetic excursion was first observed in lava flows in the Chaîne des Puys (France) (Bonhommet & Babkine, 1969), and has been seen to cause declination changes of ±120° and inclination changes of 140° at some sites, including in the North Atlantic (Lund *et al.*, 2005). Over decades of investigation, the age of the event has been wide ranging (Kent *et al.,* 2002), however, studies have continued to allow these to be refined, assisted by factors including the documentation of the event in Black sea sediments, where they are found below the Campanian Ignimbrite tephra (Nowaczyk *et al.*, 2012), which is dated to 39.28±0.11 ka BP (De Vivo *et al.*, 2001).

The Mono Lake Excursion was first documented at Mono Lake, California (Denham & Cox, 1971), and has subsequently been identified at many other sites including in the Atlantic and Arctic oceans (Channell, 2006), in the Great Basin of North America (Channell, 2006), and in the ^{36}Cl and ^{10}Be signals in the GRIP ice core (Greenland) (Wagner *et al.*, 2000). The wide documentation of this event indicates that it has significant potential to act as a time marker across multiple sites, allowing correlation of their records (Benson *et al.*, 2003), although chronological estimates have been wide ranging for this event. At its type locality, the Mono Lake Excursion was placed around ~24 ^{14}C ka BP, ~28 ka BP (Denham & Cox, 1971), although this was later revised to ~28 ^{14}C ka BP, ~32 ka BP (Kent *et al.,* 2002). Peaks in the GRIP ice core ^{36}Cl data are thought to reflect higher production rates of cosmogenic radionuclides, and

these occur alongside palaeomagnetic field intensity minima (Wagner *et al.*, 2000). One such of these events occurs between D-O events 6 and 7, at ~32 kyr BP (Wagner *et al.*, 2000), and this is thought to be a record of the Mono Lake Excursion, with a corresponding event also documented for the Laschamp between interstadials 9 and 10 (Raisbeck *et al.*, 2017). Kent *et al.,* (2002) suggested that the event at the type locality is much older, overlapping the Laschamp excursion, and they concluded that they should be considered at this site as the same excursion, supported by the occurrence of only one palaeomagnetic excursion during this period (Kent *et al.,* 2002). Tephrochronology was utilised by Benson *et al.*, (2003), and their results discredited the Kent *et al.,* (2002) theory, suggesting that there were issues with the reservoir correction used, and with ostracod reworking. Benson *et al.*, (2003) assigned the event an age of 31.5-33.3 GISP2 yrs BP, due to the palaeomagnetic excursion occurring during a period of tephra deposition at the site. More recently Lund *et al.*, (2017) supported this, suggesting that the Mono Lake Excursion and the Laschamp are distinct events, with two palaeomagnetic excursions being documented in the Pyramid Lake core record between ~17-47 ka BP, with an event at ~34.1 ± 0.4 ka being linked to the Mono Lake Excursion, while an additional event at 40.9 ± 0.5 ka BP is correlated to the Laschamp (Lund *et al.*, 2017). These events are also similar in timing to two events ages defined in the GLOPIS global palaeo-intensity stack (Laj *et al.,* 2014), and for the events in the 10-75ka record from the Chaîne des Puys (Laj *et al.,* 2014).

The Gothenburg magnetic excursion was originally documented as a period of irregular polarity, covering the period 13.7-12.3ka BP, ending with a period of full magnetic reversal known as the Gothenburg Flip, which occurred between 12.4-12.3ka BP (Mörner, 1977). It has been found in several localities, including the South China Sea where the excursion dates to ~12.9 ± 0.39 ka BP (Yuan *et al.*, 1991), while in the central Russian Plain it is documented to occur between 13-12.3ka BP (Gus'kova *et al.*, 2012a). The rapid nature of the event means it requires sites to have high sedimentation rates to record it, and its short occurrence has also been suggested to make it a useful chronological marker. However, it has been suggested that the

Gothenburg palaeomagnetic excursion may occur at varying times in different localities (Gus'kova *et al.*, 2012b), and this has implications for its use as a chronological isochron. Its existence at its type locality was also questioned by Verosub and Banerjee (1977), as a separate paper on the core where the Gothenburg was first documented, highlighted the occurrence of diagentic FeS (Morner *et al.,* 1973). This was stated to be able carry a signal of chemical remanent magnetisation, which would have formed post deposition, preventing confident identification of the excursion, with further evidence being required (Verosub & Banerjee, 1977). These factors must therefore be considered when correlating a palaeomagnetic event to the Gothenburg excursion.

More recent palaeomagnetic excursions have also been documented in some localities. These include the Solovki excursion, which is suggested to have occurred between ~7-4.5 ka BP, and the Etrussia (also known as the Sterno-Etrussia) excursion between ~3-2.2 ka BP (Dergachev *et al.*, 2004). These are thought to be extremely short lived events with ~100 year durations (Dergachev *et al.*, 2004), potentially meaning that evidence of these events is rare, requiring high resolution studies. Despite this, a number of sites have documented the Sterno-Etrussia, including in Tahiti sea cores (Lund *et al.*, 2007; Nami *et al.*, 2016), Baltic sea records and the Ob river in Russia (Dergachev *et al.*, 2004), and it is generally thought to have occurred at ~2.8ka BP (Dergachev *et al.*, 2004). This event is argued to be the magnetic field reversal documented by Giuseppe Folgheraiter in 1896, which was recorded archaeological samples (Ransom, 1973), highlighting the potential widespread use of these excursions as chronological markers.

Over the time period of this study, there appear to be several palaeomagnetic excursions that could be recorded in the lake sediments. Despite this, the dating around these palaeomagnetic excursions requires further work, and caution should be taken when assigning an age. This is particularly important for the shortest duration events; it is possible that they will only be documented in limited material (Bol'shakov, 2017), making their detection difficult in some sites, while processes including reworking can easily erase the events (Verosub & Banerjee, 1977). Lake sediments have been considered one of

the better localities to study these events, as they are less likely to undergo reworking than marine sediments (Nöel & Tarling, 1975; Avery *et al.*, 2017), however, there are still several factors that must be considered when identifying palaeomagnetic excursions (Verosub & Banerjee, 1977; Langereis *et al.*, 1992; Bol'shakov, 2017). Misinterpretation can occur due to sediment overprinting, seismic activity, disturbances in the sediments post deposition and during coring, and due to limited consideration of core stratigraphy (Verosub & Banerjee, 1977). Cores should be closely examined with particular attention given to lithostratigraphic changes and sediment structures that must highlight that there has been no deformation (Verosub & Banerjee, 1977). Even in the case of regional excursions, there should be a degree of spatial and temporal coherence, with the event being documented in more than one locality (Verosub & Banerjee, 1977), and in multiple cores from a site, as practiced by Avery *et al.*, (2017) where 4 cores were correlated from Lake Windermere (England), using independent chronologies.

Clearly there are multiple factors to consider before assigning a palaeomagnetic shift in a lake core. Despite this, there is significant potential to utilise palaeo-magnetic excursions to provide chronological markers. For Lake Baunt, this was studied by colleagues at the Russian Academy of Sciences in Irkutsk, and the results are documented in Krainov *et al.*, (2018, 2017). Below these are outlined, and their results and significance for the chronological of Lake Baunt are discussed.

3.4.1 Palaeomagnetic Methodology

Samples studied from Lake Baunt for palaeomagnetic changes are outlined in Krainov *et al.*, (2017, 2018), but are briefly described here. In total 277 samples were collected (initially at 5cm resolution, with 18 additional samples taken later) and analyses were carried out on an AGICO JR-6 spinner magnetometer. Sample demagnetisation was performed in a magnetic vacuum, in the Earth's magnetic field. Natural remnant magnetisation (NRM) was measured on all the studied samples. The validity of the samples for palaeomagnetic study was considered through a detailed stepwise demagnetisation with an alternating magnetic field on 25 samples (2, 5, 10,

15, 20, 30, 40, 50, 60, 80, 100 mT). The remaining samples were demagnetised with an alternating magnetic field (10, 20, 40 mT), and then remagnetised using the same magnetic field values. This allowed a anhysteretic remanent magnetisation (ARM) to be calculated for three values of the alternating magnetic field (Krainov *et al.*, 2017).

3.4.2 Palaeomagnetic Results

Krainov *et al.,* (2017; 2018) identified three periods of palaeomagnetic reversals, at 225cm, 590cm and 1190cm, although the first was only identified in one sample. Kravinov *et al.,* (2017; 2018) have suggested that the latter two are responses to the Gothenburg excursion and the Mono Lake Excursion (see table 3.4). The identification of these two events means these two events may be able to make up independent marker horizons in the Lake Baunt chronology. These markers will be assessed as part of the age modelling for the site with reference to the quality assurance criteria discussed above (see 3.6.3).

Sample Depth (cm)	**Krainov *et al.,* (2017; 2018) age (ka BP) of sample**	**Measured Inclination (10 mT) (Krainov *et al.,* 2017; 2018)**	**Correlated Palaeomagnetic Excursion**
225	-	~ 40	Solovki – unconfirmed.
588	13.2	~ -25	Gothenburg
1190	25.8	~ -35	Mono Lake

Table 3.4: Palaeomagnetic results for Lake Baunt published by Krainov *et al.,* (2017; 2018).

3.5 Tephrochronology

Tephrostratigraphy and tephrochronology have become widely used in Quaternary studies to provide a means of stratigraphically linking and synchronising sites, and in some cases where a tephra is independently dated, it can allow the transfer of an age between sites. Volcanic ash, known as tephra lends itself to this, as one eruption can produce microscopic ashes that travel thousands of miles, and primary tephra layers are deposited over a rapid

time period, usually less than 1 year (Lowe, 2011). These tephra layers are then geochemically identified using Electron Microprobe Analysis (EPMA – Electron Probe Micro Analyses), to allow their source volcano to be determined, and in many cases these layers have now been independently dated to allow an age to be assigned to the layer.

In areas that now have detailed tephrostratigraphies, such as Northern Europe and the Mediterranean, tephra layers have been utilised to allow detailed correlation and in some cases the transfer of dates between sites, where a well dated tephra layer has been identified (e.g. Lane *et al.,* 2013). Detailed tephrostratigraphies, including that compiled for North Atlantic and Western European records by the INTIMATE group, which reaches back to ~80ka BP, incorporating 88 tephra isochrons (Blockley *et al.*, 2014), demonstrate the widespread nature of these isochrons. In some cases, tephras have provided a means to consider leads and lags between sites, such as between Meerfelder Maar and Kråkenes, where Lane *et al.*, (2013), via the presence of the Vedde Ash in both sites, determined a 120 year offset between the sites during the Younger Dryas, driven by a gradual northward retreat of the polar front.

Southern Siberia is a region significantly affected by tectonic adjustments, with the Transbaikal region being formed through a tectonic rift. The landscape close to Lake Baunt has several volcanic fields (see figure 3.1) and is noted for its geothermal energy. Due to the presence of these features, rangefinder microtephra scans were carried out on the top meter of Lake Baunt core.

3.5.1 Tephrostratigraphy Methodology and Results

Ten rangefinder samples were prepared in conjunction with Royal Holloway, University of London, following Blockley *et al.*, (2005). This method includes sieving and density separation using sodium polytungstate ($3Na_2WO_4 \cdot 9WO_3 \cdot H_2O$) (SPT, at 1.95 and 2.5 gm), before samples were mounted in Canada Balsam and counted using an Olympus BH2 microscope at x100 magnification. The full sample was checked, including residues, and the cleaning float, to determine if basaltic shards were present at the site.

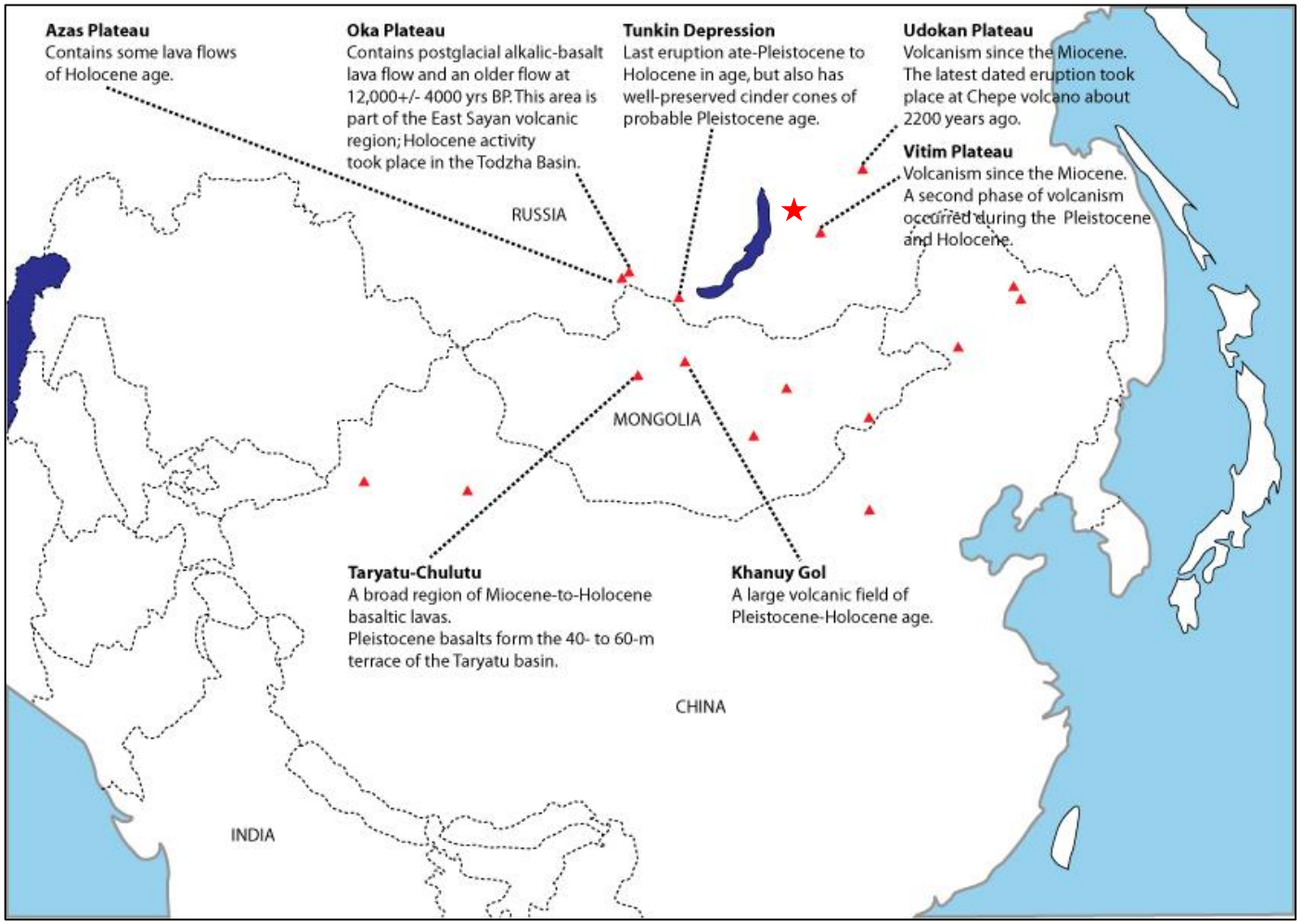

Figure 3.1: Schematic Map of Siberia showing volcanic regions as potential tephra sources. Red star shows approximate position of Lake Baunt. Information from Volcanoes of the World 2018.

No shards were detected in the top 1 meter of the BNT14 core. Despite this, shards were found at a separate point in the project during isotopic preparations following density separation. Shards were detected in water and are shown in figure 3.2.

Figure 3.2: Microtephra shards detected in the lower section of the Lake Baunt (BNT14) core. Photographed at x100 in water.

Despite these results, it is anticipated that tephrochronology has significant potential in this region due to the presence of several volcanic fields and it is anticipated that further sites should be studied for microtephra, as a tephra lattice for the Siberian region would significantly improve the area's chronological controls, by allowing sites to be independently linked by tephra isochrons and this will improve studies looking at abrupt changes, as leads and lags may be detected. The detection of shards in the lower sections of Lake Baunt suggest that further microtephra work should be undertaken to determine if specific tephra horizons can be identified.

3.6 Age modelling

3.6.1 Bayesian Age modelling

Calibration of radiocarbon dates is necessary to allow the production of meaningful calendar ages, undistorted by variations in ^{14}C production. It can also be problematic, however, causing additional uncertainties to be introduced, including the problem that the resultant calibrated probability distributions are not normally distributed, and, thus, require statistical

treatment (Lowe *et al.*, 2007). For palaeoenvironmental and palaeoclimatic studies, Bayesian analysis has become routinely used for age modelling radiocarbon chronologies, to improve chronological precision (Blockley *et al.*, 2007; Bronk Ramsey, 2008).

Using a Bayesian approach has many advantages, including being able to develop *Priors* that incorporate additional information into the age model, such as through marking stratigraphic changes by inputting boundaries, to constrain the chronological record (Bronk Ramsey, 2009). The ability to input additional known information is beneficial, as it allows any bias that may be introduced by large gaps in sequences to be corrected and this prevents overestimation of the oldest dates (Blockley *et al.*, 2004). Moreover, it is now possible to incorporate a model for the sediment deposition process in many of the Bayesian software packages (see below).

One program that is widely utilised for Bayesian age models is OxCal (Bronk Ramsey, 2008), which was first released in 1994 to allow calibration and various analysis of groups of radiocarbon events (Bronk Ramsey, 2001). Since its development, the program has undergone significant improvements (Bronk Ramsey, 2001), and the current version OxCal 4.3, has several modelling options, including a *P_Sequence* Poisson-process to model sediment deposition, which incorporates depth information and the law of stratigraphy and succession to constrain ages, and uses the Poisson distribution to model sediment built up as the deposition of discrete packages of sediment (Bronk Ramsey, 2008; Brooks *et al.*, 2012). Several of OxCal 4.3's features allow the production of age models alongside identification of errors (Bronk Ramsey & Lee, 2013), with outlier analysis allowing operator bias to be removed (Bronk Ramsey, 2009). Outlier detection is based on a prior assumption that there is a given chance of a percentage of the dates being outliers. Thus, if working at 95% confidence, this is usually set to 5% outliers being acceptable. If a date falls outside the expected range beyond 5%, based on all of the other dates in the model and the stratigraphic information, then its probability is proportionally down-weighted in its contribution to the model. Bayesian age models in OxCal 4.3 can also include automatic interpolation, which allows the uncertainty in an age model between radiocarbon dates to be documented and accounted for

(Bronk Ramsey & Lee, 2013). Further flexibility in Bayesian age models have been incorporated in OxCal through changes to the *k* parameter, which determines model rigidity (Bronk Ramsey & Lee, 2013). The parameter gives the number of accumulation events per unit depth (Bronk Ramsey, 2008) and is usually defined exactly, however, from version 4.2 onwards it has been possible to allow for reasonable variations in the *k* values, as opposed to a fixed value, which allows a wider range of variability (Bronk Ramsey & Lee, 2013). This means that where deposition is increasingly variable, the posterior value for *k* declines and the model's uncertainty will increase. This is considered as a model averaging approach and allows for a more realistic average over different situations of deposition to be included in the model (Bronk Ramsey & Lee, 2013).

3.6.2 Lake Baunt Age Models

Chronological control is an essential part of this research project, as reliable and precise dating is essential to allow detection of regional shifts and responses to abrupt climatic changes. Age models for Lake Baunt have been constructed based on 15 ^{14}C dates and a ^{210}Pb dating profile, while a tephrostratigraphic framework has been created for the upper meter of the BNT14 core, and palaeomagnetic excursions have also been studied (see Krainov *et al.*, 2017), and data from this have also been incorporated into some of the models. The age models have been constructed following Bayesian approaches in OxCal 4.3 (Bronk Ramsey 2009a; Bronk Ramsey *et al.,* 2010; Bronk Ramsey & Lee 2013), and all radiocarbon dates have been calibrated using IntCal13 (Reimer *et al.*, 2013).

Several age models have been produced for Lake Baunt in OxCal 4.3, and these are shown in figures 3.3-3.6. All the models utilise a *P_sequence* deposition model, with automatic outlier detection using the 'General' model, which assumes there are a range of potential sources of error in the sample, including contamination and sediment reworking (Bronk Ramsey, 2009). Despite this, the models have several variations, linked to changes in the model's rigidity, interpolation and the use of boundaries. All ^{14}C dates have been calibrated in the modelling process using IntCal13 (Reimer *et al.*, 2013).

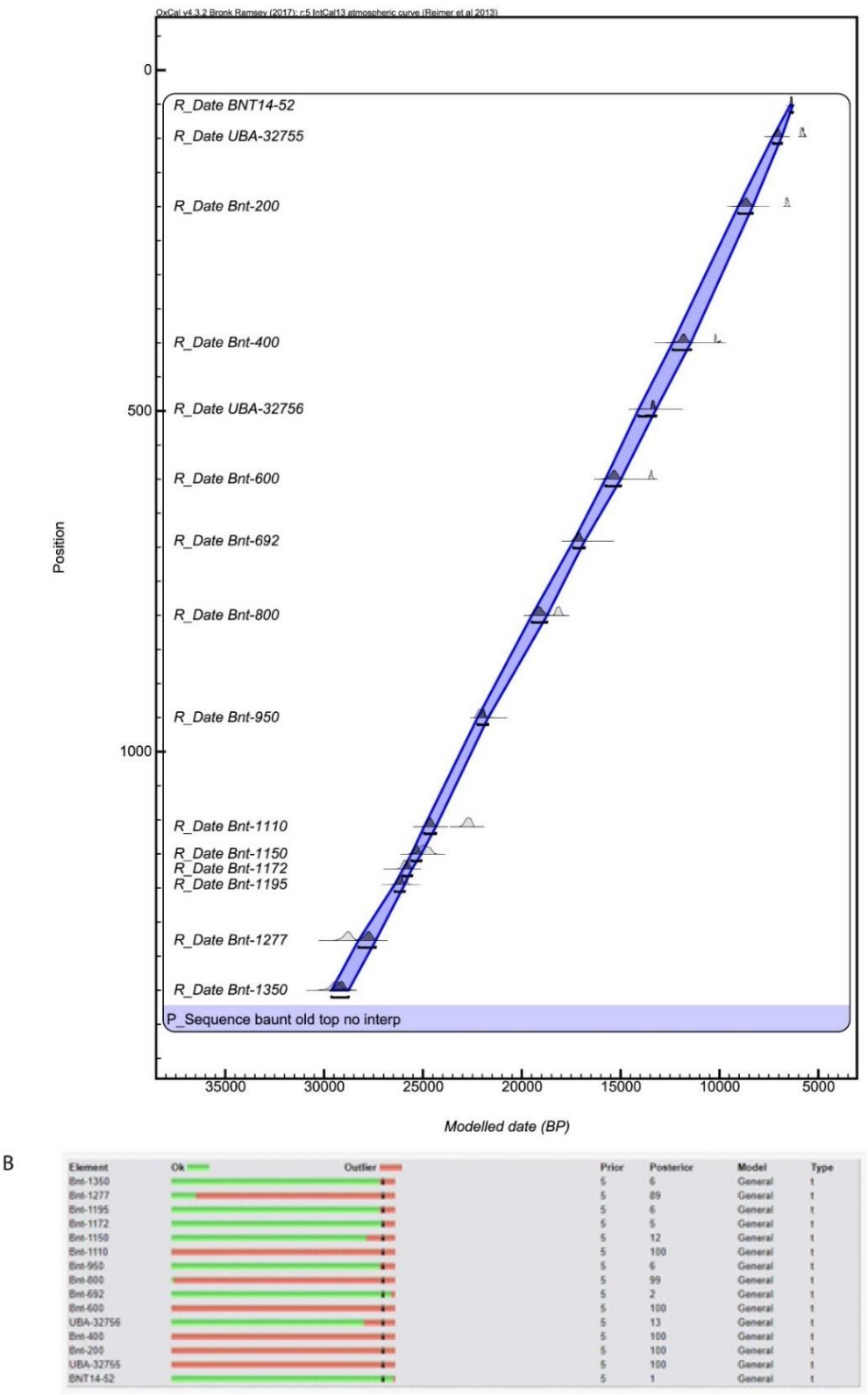

Figure 3.3: (A) Initial Bayesian Age model for Lake Baunt in OxCal 4.3. Dates calibrated using IntCal13 (Reimer *et al.,* 2013). Model run with fixed *k* parameter of 1 and no interpolation between dates. **(B)** Outlier Analysis Output showing, which dates have been downweighed by the general outlier model.

A

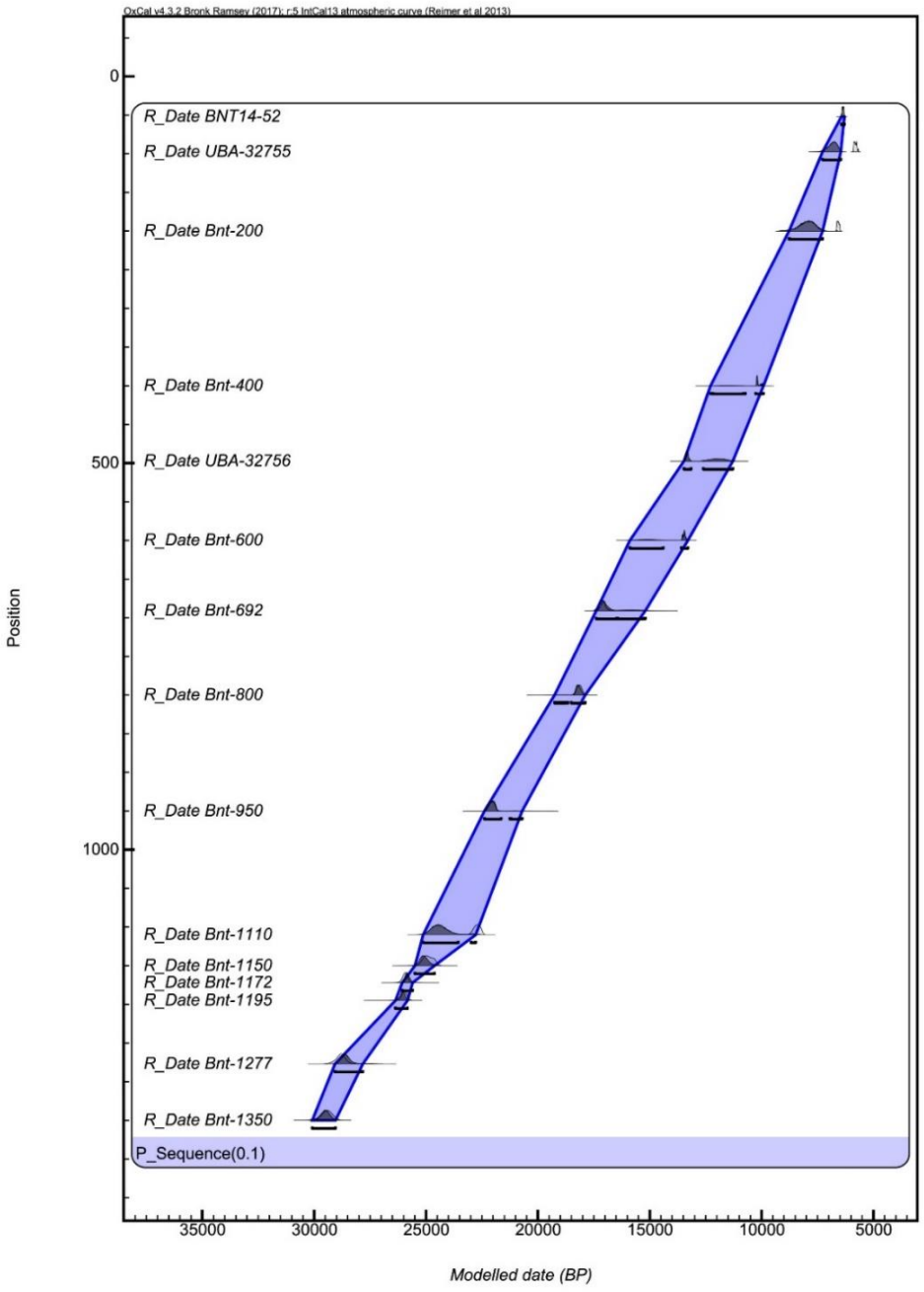

B

Element	Ok	Outlier	Prior	Posterior	Model	Type
Bnt-1350			5	3	General	t
Bnt-1277			5	10	General	t
Bnt-1195			5	3	General	t
Bnt-1172			5	3	General	t
Bnt-1150			5	4	General	t
Bnt-1110			5	96	General	t
Bnt-950			5	9	General	t
Bnt-800			5	8	General	t
Bnt-692			5	24	General	t
Bnt-600			5	44	General	t
UBA-32756			5	59	General	t
Bnt-400			5	29	General	t
Bnt-200			5	100	General	t
UBA-32755			5	100	General	t
BNT14-52			5	1	General	t

Figure 3.4: (A) Bayesian Age model produced for Lake Baunt in OxCal 4.3. Dates calibrated using IntCal13 (Reimer *et al.,* 2013). Model running with less constrained *k* parameter of 0.1 to allow greater flexibility. **(B)** Outlier Analysis Output showing which dates have been downweighed by the general outlier model.

A

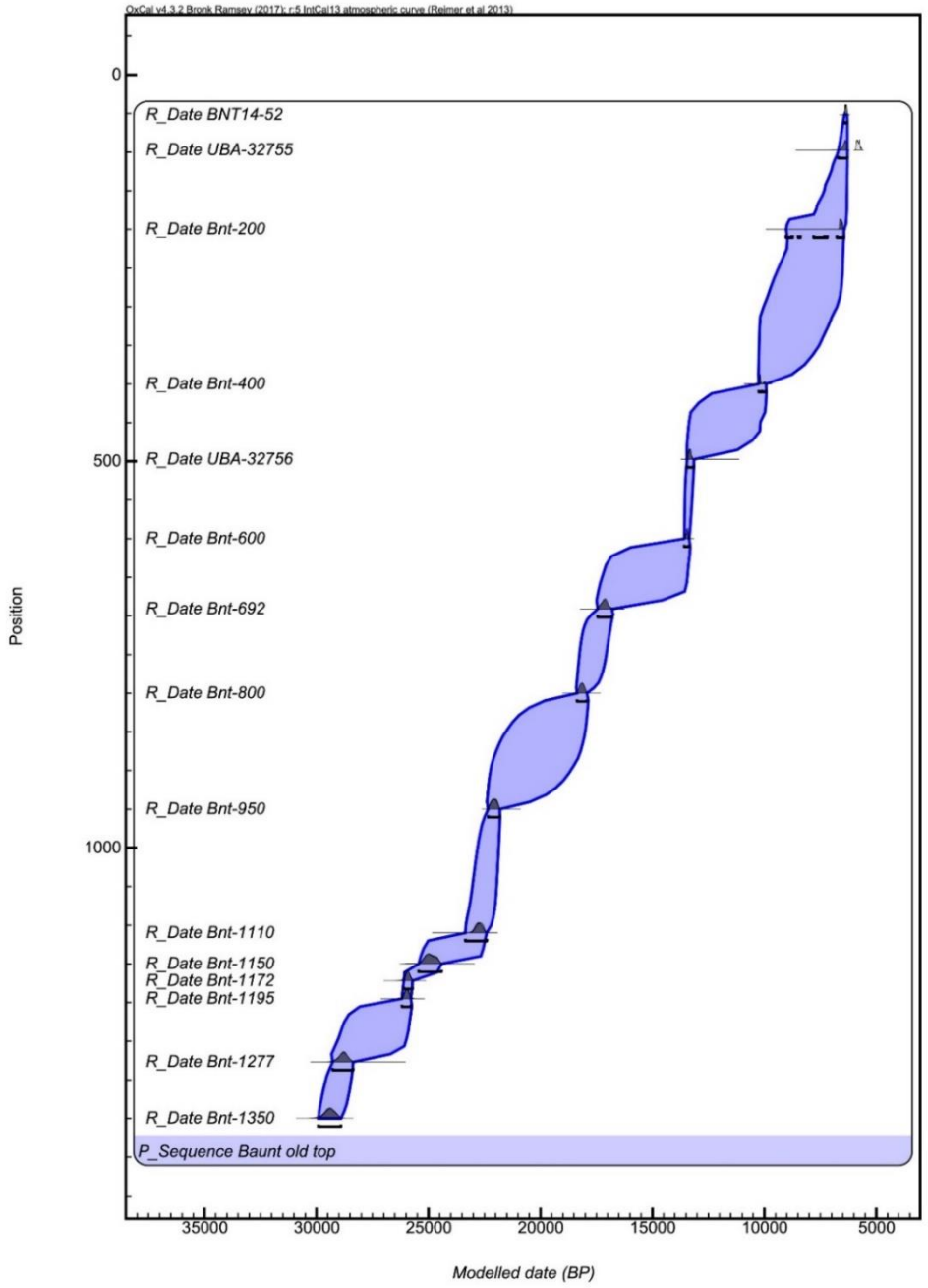

B

Element	Ok	Outlier	Prior	Posterior	Model	Type
Bnt-1350			5	3	General	t
Bnt-1277			5	4	General	t
Bnt-1195			5	2	General	t
Bnt-1172			5	2	General	t
Bnt-1150			5	5	General	t
Bnt-1110			5	7	General	t
Bnt-950			5	4	General	t
Bnt-800			5	3	General	t
Bnt-692			5	3	General	t
Bnt-600			5	2	General	t
UBA-32756			5	5	General	t
Bnt-400			5	3	General	t
Bnt-200			5	10	General	t
UBA-32755			5	100	General	t
BNT14-52			5	1	General	t

Figure 3.5: (A) Bayesian Age model produced for Lake Baunt in OxCal 4.3. Dates calibrated using IntCal13 (Reimer *et al.,* 2013). Model includes interpolation with a variable *k* parameter between 2 to -2. **(B)** Outlier Analysis Output showing which dates have been downweighed by the general outlier model.

A

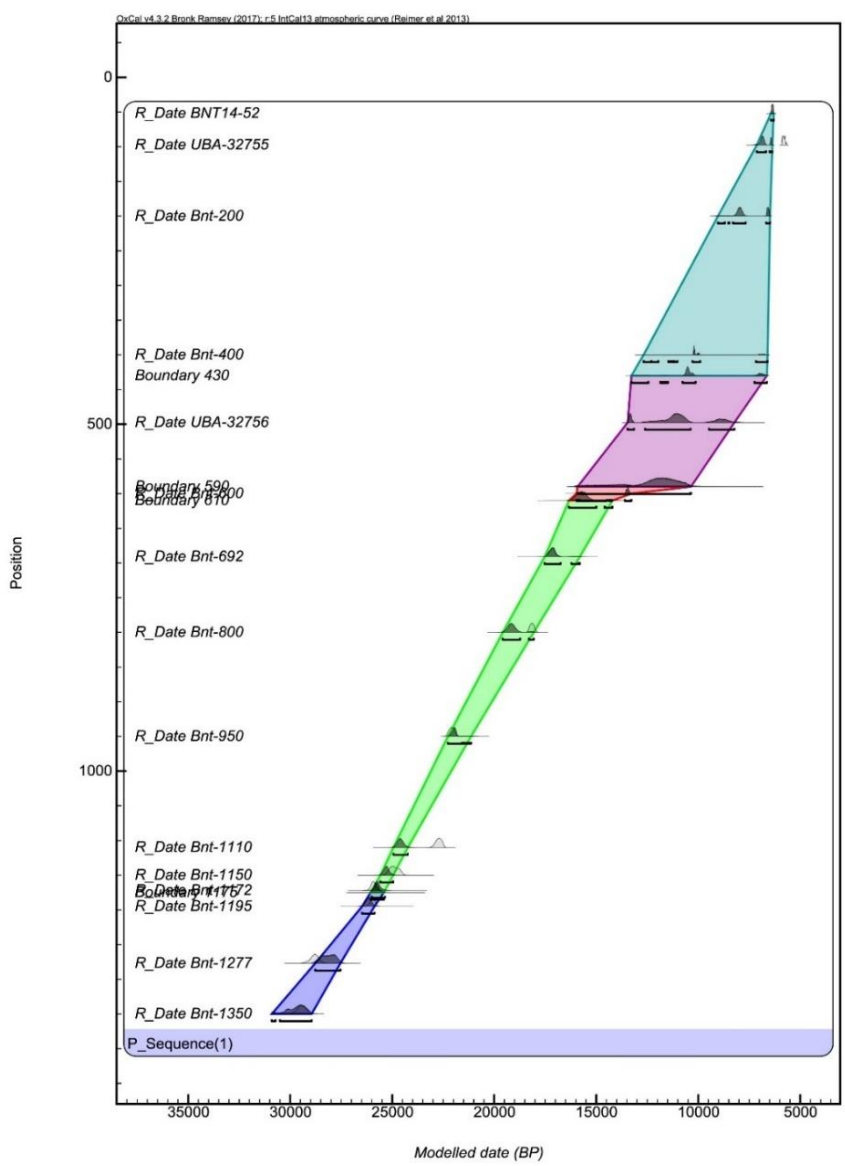

B

Element	Ok / Outlier	Prior	Posterior	Model	Type
Bnt-1350		5	12	General	t
Bnt-1277		5	50	General	t
Bnt-1195		5	6	General	t
Bnt-1172		5	15	General	t
Bnt-1150		5	9	General	t
Bnt-1110		5	100	General	t
Bnt-950		5	11	General	t
Bnt-800		5	94	General	t
Bnt-692		5	8	General	t
Bnt-600		5	26	General	t
UBA-32756		5	90	General	t
Bnt-400		5	34	General	t
Bnt-200		5	77	General	t
UBA-32755		5	100	General	t
BNT14-52		5	1	General	t

Figure 3.6: **(A)** Bayesian Age model produced for Lake Baunt in OxCal 4.3. Dates calibrated using IntCal13 (Reimer *et al.,* 2013). Model includes boundaries at changes identified in the core stratigraphy (see figure 2.6) and the *k* parameter is fixed (no interpolation). **(B)** Outlier Analysis Output showing which dates have been downweighed by the general outlier model.

A

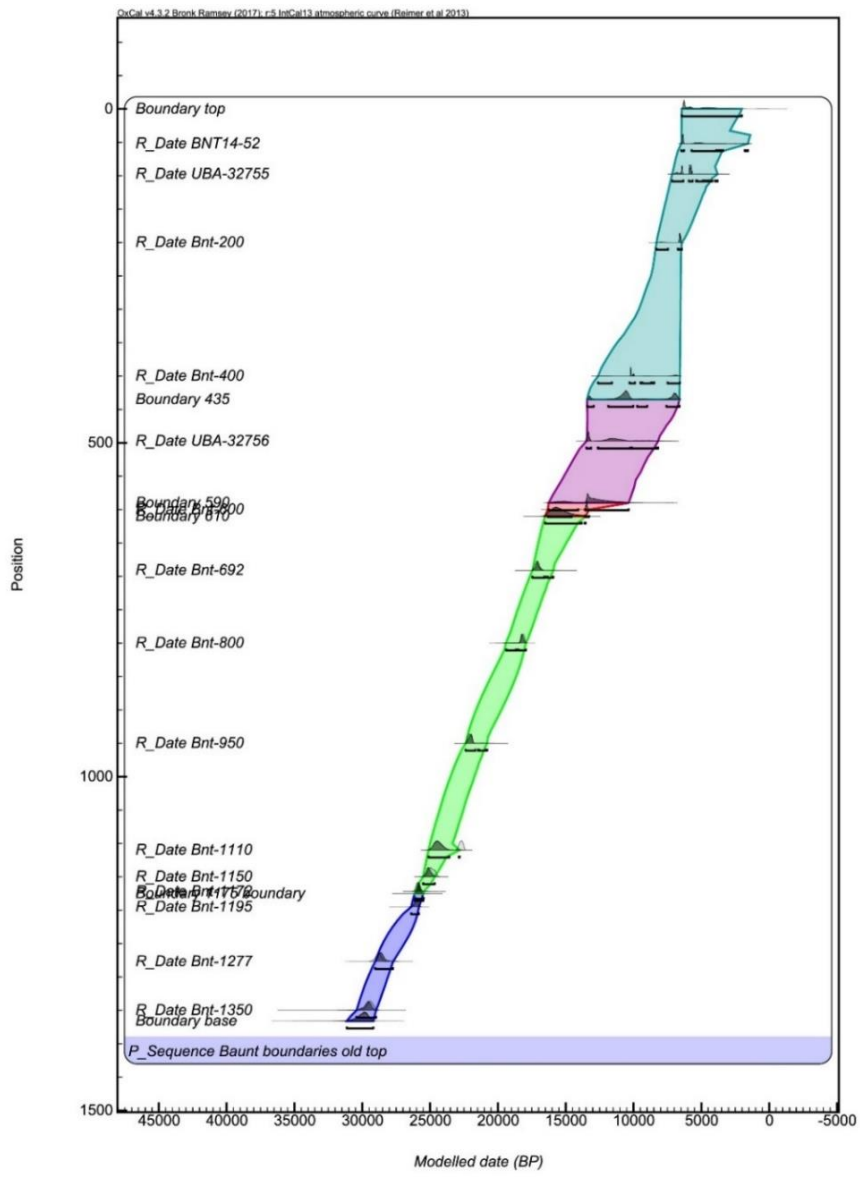

B

Element	Ok	Outlier	Prior	Posterior	Model	Type
Bnt-1350			5	8	General	t
Bnt-1277			5	12	General	t
Bnt-1195			5	4	General	t
Bnt-1172			5	7	General	t
Bnt-1150			5	4	General	t
Bnt-1110			5	97	General	t
Bnt-950			5	12	General	t
Bnt-800			5	18	General	t
Bnt-692			5	11	General	t
Bnt-600			5	24	General	t
UBA-32756			5	77	General	t
Bnt-400			5	44	General	t
Bnt-200			5	21	General	t
UBA-32755			5	60	General	t
BNT14-52			5	53	General	t

Figure 3.7: (A) Bayesian Age model produced for Lake Baunt in OxCal 4.3. Dates calibrated using IntCal13 (Reimer *et al.,* 2013). Model includes boundaries at changes identified in the core stratigraphy (see figure 2.6) and the model allows interpolation through a variable *k* parameter of 2 to -2. **(B)** Outlier Analysis Output showing which dates have been downweighed by the general outlier model.

Figure 3.3A is perhaps the simplest of the models, with a *k* parameter of 1, which means the model is rigid, and interpolation was not allowed between dates. No additional stratigraphic information was incorporated into this model, for example by applying boundaries. This model has been rejected as an appropriate age model for the Lake Baunt sediments for several reasons. The high rigidity of the model means that sedimentation rates are highly constrained, and it is felt that this is inappropriate, as it is unlikely that there have been no significant shifts in terrestrial sediment supply, during the time the core has been deposited. This is supported by the site stratigraphy (see figure 2.6), where several changes are described in the core's lithostratigraphy, suggesting alterations in material being deposited. Additionally, 12 of the radiocarbon dates have been significantly down-weighted (figure 3.3B), with suggestion that they are outliers at 95% confidence. There is no additional information (unusual ^{13}C values etc) to support this, thus, it is likely this is a function of the highly constrained model parameters.

To allow more flexibility in the model, figure 3.4 has been produced. This model runs under the same conditions as the model in figure 3.3, however the *k* parameter has been reduced to 0.1, allowing an order of magnitude more flexibility in the model. This is potentially more realistic for a site that has undergone several changes in sedimentation rate, however, the model still suggests that 10 of the 15 dates are outliers (figure 3.4B).

The initial two models (figures 3.3 & 3.4), although useful, are potentially preventing a clear picture of the chronology of the site being developed. This is because they both assume linear sedimentation between the calibrated radiocarbon dates, rather than showing periods without dating as being more uncertain (Bronk Ramsey & Lee, 2013). One of the key newer features of OxCal 4.3 is the ability to allow interpolation between dates and the calculation of the additional uncertainty of interpolation, and this feature has been added to the model shown in figure 3.5. As discussed in section 3.6, models with interpolation allow a range of *k* parameter values from -2 to 2, and therefore the models are much more flexible. This is shown immediately within figure 3.5B, where the number of dates down-weighted declines to just 3, and only 1

date has a posterior outlier probability larger than 10. This suggests that the earlier models are indicating dates are outliers because the models are too strongly constrained, and that there is in fact no issues with the majority of dates. It is possible, therefore, to view this model as more realistic than the first two.

After these initial models more complex models were run, allowing the incorporation of Lake Baunt stratigraphy through the use of boundaries. These 'boundaries' inform the model that there is a potential change in the system at these points, and this may mean a shift in the deposition at the site and, thus, chronological changes. Both figures 3.6 and 3.7 show models with boundaries, which have been added where the core stratigraphy is known to change at 430, 590, 610 and 1175cm (see figure 2.6). These locations have been chosen as the shifts in the sedimentary composition at the core at these points indicate that there may be significant changes in deposition at these points, and, thus, the age model may need to account for this. These models both demonstrate shifts in the depositional rates between the different sections. The first (figure 3.6) does not contain interpolation but suggests that uncertainties are greatest in the upper 600cm of the core, particularly between 600-400cm. This differs significantly to the previous model (figure 3.5), where the section between 600-500cm was the most constrained section. As with the earlier models, which did not allow interpolation, this model down-weights 14 of the 15 dates (figure 3.6B), suggesting that the increased rigidity of the model with a fixed *k* parameter is not accurately representing the sites sediment deposition. Unlike this, figure 3.7 shows the same model run with interpolation, which increases its flexibility, although it still has a high rate of date down-weighting, with 13 of 15 dates considered to be potential outliers, suggesting that this may not be the most accurate interpretation of the sediments deposition. Despite allowing interpolation, these models are highly similar, both suggesting the lower sections of the core are constrained more robustly that the upper sections, where uncertainties are larger.

3.6.3 Testing Palaeomagnetic Event Ages using Bayesian Analysis

After the initial age models were produced for Lake Baunt, the additional palaeomagnetic data from Krainov *et al.,* (2017, 2018) have been considered and added to the model. Initially, the depths that were assigned by Krainov *et al.*, (2017, 2018) have been marked as having a palaeomagnetic event during them, to allow the ages provided by the models produced as part of this project to be compared to Krainov *et al.*, (2017, 2018) ages, produced by their age model (based on radiocarbon dating using a smaller dataset (some dates are included in both age models)). The produced ages are shown in table 3.5 and were determined using the same model setup as shown in figure 3.5. The dates produced between this work and that of Krainov *et al.,* (2017, 2018) are similar, and the uncertainties from this age model mean they overlap, however, it should be noted that the Krainov *et al.,* (2017; 2018) study have not documented the error associated with the levels where palaeomagnetic excursions have been documented.

Palaeomagnetic Excursion	**Krainov *et al., (*2017, 2018) age (ka BP).**	**Age produced (this study) (ka BP).**	**Published Ages, dating method and references. Original Identification Age shown in red.**
Gothenburg	13.2	13.4 ± 230	12.35 ± 0.05 ^{14}C years (Mörner, 1977).
			11800 ± 1400 ^{14}C years (Guskova *et al.*, 2007).
			12675 ± 325 ^{14}C years (Gus'kova *et al.*, 2012b).
Mono Lake	25.8	26.0 ± 400	24000 ± 300 ^{14}C years (Denham and Cox, 1971).
			27000 ± 1000 ^{14}C years (Guskova *et al.*, 2007).
			34100 ± 400 cal years BP (age model including 20 ^{14}C dates, 4 tephras and GISP2 correlation) (Lund *et al.*, 2017).
			32400 ± 900 GISP2 years BP (Benson *et al.*, 2003).
			34200 ± 1200 (^{40}Ar/^{39}Ar) cal years BP (Laj *et al.*, 2014).
			34250 ± 626 years b2k GICC05 (Svensson *et al.*, 2008).

Table 3.5: Ages for palaeomagnetic excursions produced by Krainov *et al.,* (2017, 2018) and for the same depths using this studies age models.

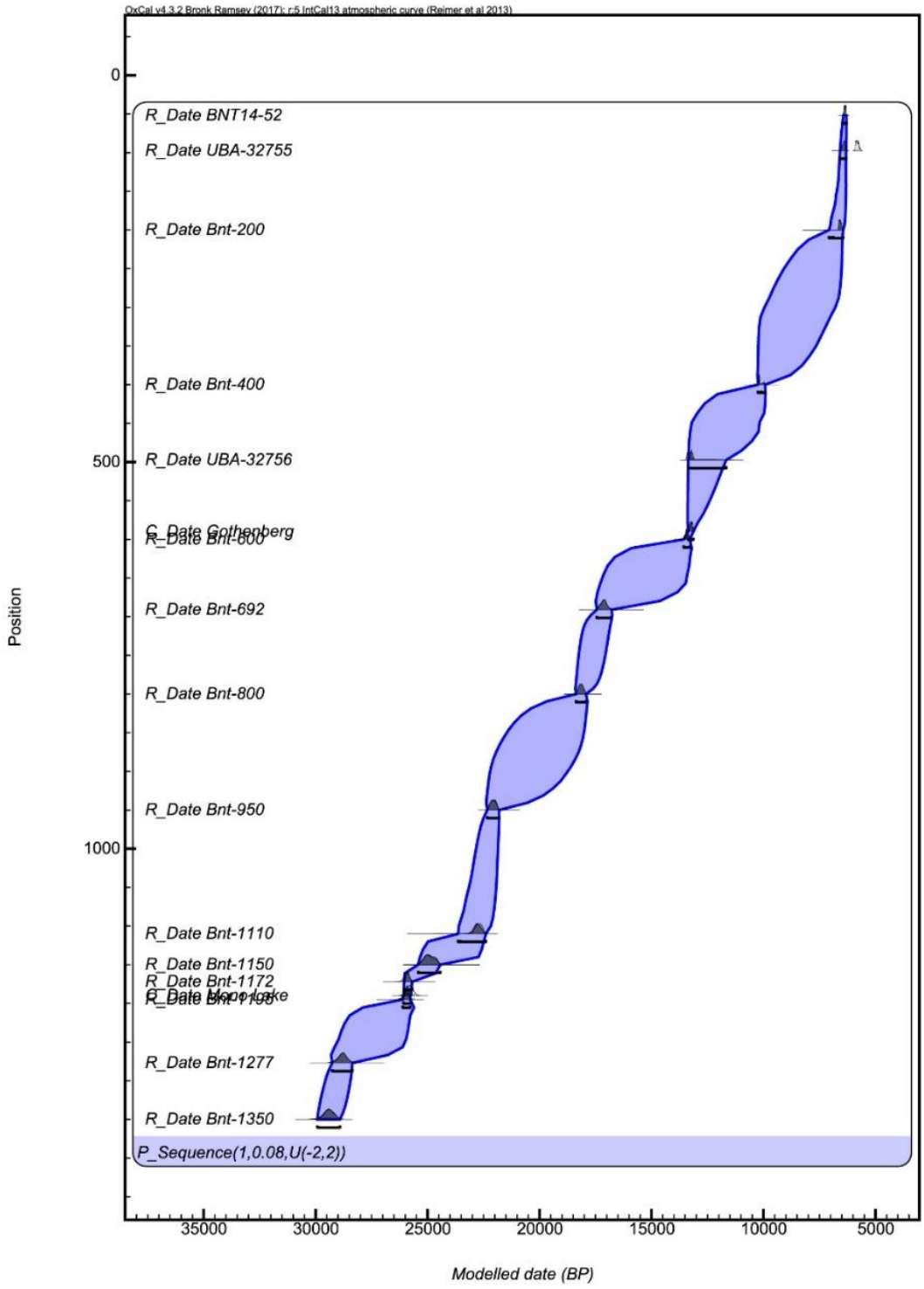

Figure 3.8: Bayesian age model produced in OxCal 4.3 (Bronk Ramsey, 2017) and calibrated using IntCal13 (Reimer *et al.,* 2013) with the depths stated by Krainov *et al.,* (2017) to show palaeomagnetic excursions (Gothenbury and Mono Lake) marked. Model run using with interpolation but no boundaries.

Following this, several models were run using published dates of the events (Mono Lake and Gothenburg) to which, Krainov *et al.*, (2017) correlate, and

additional dates from published literature (see table 3.4). These models were run under the same conditions as several of the age models discussed in section 3.6.2, with interpolation allowed between dates and with automatic outlier detection operating. The published dates were incorporated as either R-dates (uncalibrated radiocarbon dates) or C-dates (calendar dates for Ice core and Ar/Ar dates, or pre-calibrated radiocarbon dates), depending on the individual studies. All the events were assigned the same depth (z value) and were also included in the automatic outlier detection. These are documented in figures 3.9 (Gothenburg) and 3.10 and 3.11 (Mono Lake).

It is immediately noticeable in figure 3.9:A that the Gothenburg dates add significant uncertainty to the Lake Baunt age model. The wide spread of the ages is largely due to the wide errors on some of the included dates (table 3.4), however, these should allow the model to be flexible enough to incorporate the dates. Figure 3.9:B however, documents that several of the dates have been down-weighted in this model, as opposed to the model shown in figure 3.5, which ran under the same parameters with the exception of the inclusion of the Gothenburg dates. It may be that the original date from (Mörner, 1977), was previously given too precise an age estimate, and potentially, given the improvements documented in radiocarbon dating (see section 3.2), this date should be utilised cautiously. This date is the most down-weighted of the incorporated Gothenburg dates, and thus this could be an indication of contamination, and potentially that the other dates for the Gothenburg, which have much lower posterior values are better dates to utilise. Additionally, with the Gothenburg palaeomagnetic excursion we must be cautious of the suggestion that the excursion occurs at varying times at different localities (Gus'kova *et al.*, 2012a), as this may mean incorporating a date from a different locality is inappropriate, particularly as Lake Baunt is located ~8000 km from southern Scandinavia, the locality where Krainov *et al.,* (2017) have correlated the excursion.

Figure 3.10 documents an age model incorporating 6 published dates for the Mono Lake palaeomagnetic excursion. Figure 3.10:B demonstrates that this model is problematic, with most dates being down-weighted. The model in figure 3.5 was run under the same parameters with the exception of not

including the Mono Lake published ages, so it appears that including these dates is problematic for the Baunt chronology. As discussed in section 3.4, the original date of ~24 ka BP for the Mono Lake excursion was revised (Denham & Cox, 1971; Kent *et al.,* 2002) and, therefore, this model was also run excluding some of the oldest studies of the event, to see if, potentially, dating issues from these earlier dates may be introducing the problems causing many dates to appear as outliers. This additional model is shown in figure 3.11, with figure 3.11:B documenting that all the dates have been down-weighted to some extent in this model.

This is strikingly different to figure 3.5, and, thus, we assume that the age of the palaeomagnetic shift at Lake Baunt occurs at a different time to those demonstrating the Mono Lake excursion elsewhere. This makes sense, as the most recent estimates of the Mono Lake excursion tend to place it between ~32-34 ka BP (Benson *et al.*, 2003; Svensson *et al.*, 2008; Laj *et al.,* 2014; Lund *et al.*, 2017), and the previous models for Lake Baunt in section 3.6.2 tend to suggest the record only covers the last ~30 ka BP, and, thus, the occurrence of this palaeomagnetic excursion at Lake Baunt would be inconsistent with all the other dating and Bayesian age modelling carried out at Lake Baunt.

A

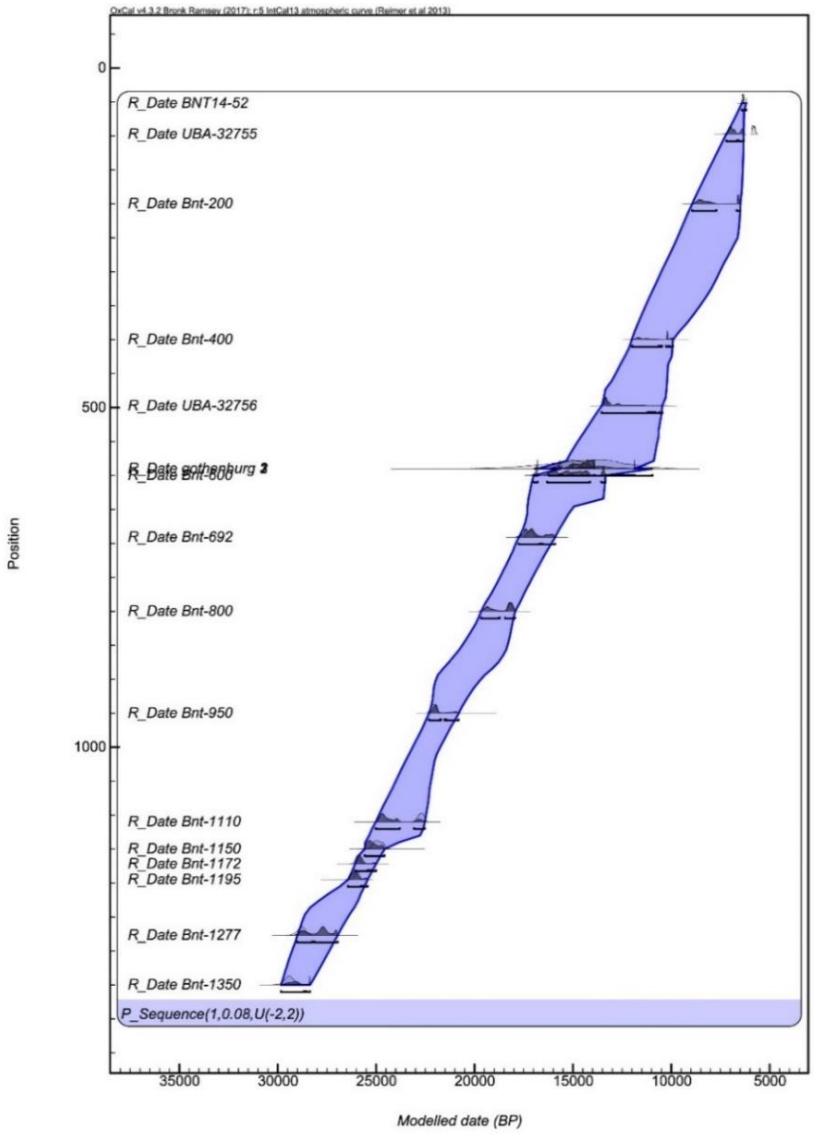

B

Element	Ok	Outlier	Prior	Posterior	Model	Type
Bnt-1350			5	19	General	t
Bnt-1277			5	64	General	t
Bnt-1195			5	10	General	t
Bnt-1172			5	18	General	t
Bnt-1150			5	9	General	t
Bnt-1110			5	82	General	t
Bnt-950			5	26	General	t
Bnt-800			5	48	General	t
Bnt-692			5	32	General	t
Bnt-600			5	91	General	t
gothenburg 3			5	5	General	t
gothenburg 2			5	19	General	t
gothenburg 1			5	46	General	t
UBA-32756			5	51	General	t
Bnt-400			5	64	General	t
Bnt-200			5	77	General	t
UBA-32755			5	100	General	t
BNT14-52			5	13	General	t

Figure 3.9: (A) - Bayesian Age model for Lake Baunt including 3 published ages for the Gothenburg Palaeomagnetic Excursion (Morner *et al.,* 1977, Guskova *et al.,* 2007 and 2012.). Model run allowing interpolation but no boundaries. **(B)** Outlier Analysis Output showing which dates have been downweighed by the general outlier model.

A

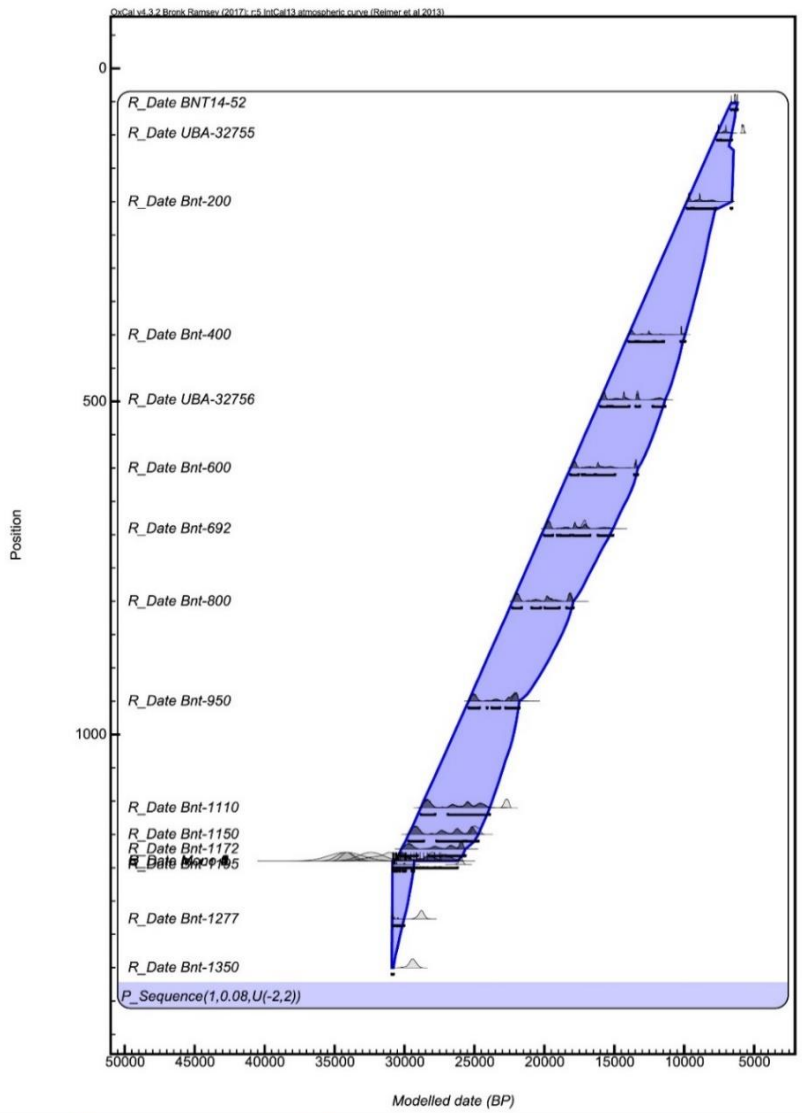

B

Element	Ok	Outlier	Prior	Posterior	Model	Type
Bnt-1350			5	100	General	t
Bnt-1277			5	100	General	t
Bnt-1195			5	100	General	t
Mono 6			5	100	General	t
mono 4			5	98	General	t
mono 5			5	4	General	t
mono 1			5	100	General	t
mono 2			5	53	General	t
mono 3			5	75	General	t
Bnt-1172			5	67	General	t
Bnt-1150			5	76	General	t
Bnt-1110			5	99	General	t
Bnt-950			5	58	General	t
Bnt-800			5	75	General	t
Bnt-692			5	77	General	t
Bnt-600			5	82	General	t
UBA-32756			5	85	General	t
Bnt-400			5	79	General	t
Bnt-200			5	98	General	t
UBA-32755			5	100	General	t
BNT14-52			5	51	General	t

Figure 3.10: (A) - Bayesian Age model for Lake Baunt including 6 published ages for the Mono Lake Palaeomagnetic Excursion (1: Lund *et al.,* 2017, 2: Benson *et al.,* 2003, 3: Laj *et al.,* 2014, 4: Denham & Cox, 1971, 5: Guskova *et al.,* 2012, 6: Svensson *et al.,* 2008). Model run allowing interpolation but no boundaries. **(B)** Outlier Analysis Output showing which dates have been downweighed by the general outlier model.

A

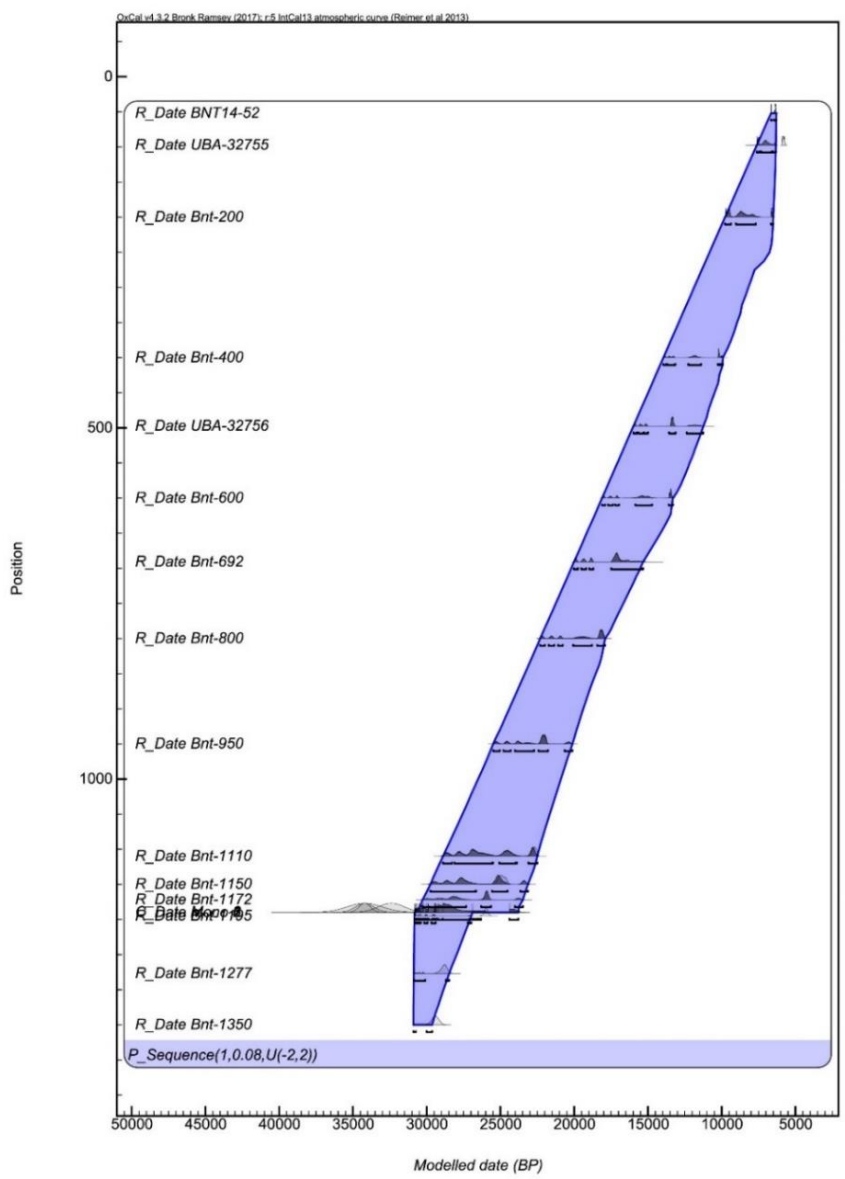

B

Element	Ok	Outlier	Prior	Posterior	Model	Type
Bnt-1350			5	91	General	t
Bnt-1277			5	91	General	t
Bnt-1195			5	100	General	t
Mono 6			5	100	General	t
mono 1			5	100	General	t
mono 2			5	32	General	t
mono 3			5	77	General	t
Bnt-1172			5	67	General	t
Bnt-1150			5	69	General	t
Bnt-1110			5	82	General	t
Bnt-950			5	52	General	t
Bnt-800			5	57	General	t
Bnt-692			5	49	General	t
Bnt-600			5	71	General	t
UBA-32756			5	52	General	t
Bnt-400			5	69	General	t
Bnt-200			5	91	General	t
UBA-32755			5	100	General	t
BNT14-52			5	28	General	t

Figure 3.11: (A) - Bayesian Age model for Lake Baunt including 4 published ages for the Mono Lake Palaeomagnetic Excursion (1: Lund *et al.,* 2017, 2: Benson *et al.,* 2003, 3: Laj *et al.,* 2014, 6: Svenssen *et al.,* 2008). Model run allowing interpolation but no boundaries. **(B)** Outlier Analysis Output showing which dates have been downweighed by the general outlier model.

Other factors to the dating must be considered before the palaeomagnetic shifts documented by Krainov *et al.,* (2017, 2018) at Lake Baunt can be correlated to the Gothenburg and Mono Lake palaeomagnetic excursions. The site stratigraphy must be considered (Verosub & Banerjee, 1977), and lithostratigraphic shifts are documented at 5.9m, where the Gothenburg excursion was suggested to occur, while the Mono lake correlation was made at 11.90cm, and lithostratigraphic changes are seen gradually around ~11.75cm. It appears, therefore, that the shifts seen in the Lake Baunt record may be reflecting sedimentological changes, and these must be considered before an excursion can be identified.

In addition to stratigraphic issues, the core also records interlayers of hydrotroilite from depths below 540cm (see figure 2.6) (Krainov *et al.*, 2017). Hydrotroilite, a hydrous sulphide of ferrous iron (Ferronsky *et al.*, 2014), could potentially cause alterations in the magnetics of the core. As discussed in section 3.4, the occurrence of diagentic FeS at Gothenburg was suggested by Verosub and Banerjee (1977) to be a reason for the sediments to carry a signal of chemical remnant magnetisation, which they used to question the occurrence of the palaeomagnetic excursion. Therefore, we must consider that the presence of hydrotroilite in Lake Baunt could also affect the sites magnetic records and, thus, caution must be taken when considering the results. A final stratigraphic factor must also be considered for the Lake Baunt palaeomagnetic excursions to be identified, and this is the potential influence for sampling on the core's signal. Figure 3.12 highlights the Krainov *et al.,* (2017) magnetic record alongside the sites stratigraphy, and it is immediately noticeable that the two inclination shifts occur at drive core ends. It is, therefore, possible that coring may have disturbed the sediments, inducing a change in their inclination (Verosub & Banerjee, 1977). As discussed in section 3.4, due to these factors with the Lake Baunt core the magnetic field shifts need to be documented in more than one core from the site (Verosub & Banerjee, 1977), to demonstrate coherence, and to highlight these changes occur away from core ends. Therefore, based on multiple lines of evidence it appears that the palaeomagnetic excursions documented by Krainov *et al.,*

(2017) cannot confidently be assigned to the Mono Lake or Gothenburg excursions, and will not be utilised to constrain the sites chronology.

Figure 3.12: Magnetic field inclination and NRM of the BNT14 sediments from Krainov *et al.,* (2017) with added dashed red lines highlighting shifts in the inclination record and drive end positions.

3.7 Assessing the Lake Baunt Models

There are several key trends that need to be considered in all the initial age models produced from Lake Baunt. The upper date in all models suggests that the age of the site at 52cm depth is approximately 6.2 ka BP, similar to the 97.5cm dates age. In some of the models, the age range produced for these dates can cause a reversal to be found in the sequence, however, in the more flexible models, these dates can be accommodated. In all the models, if the sedimentation rate from the upper section of the core is extrapolated, the

sedimentation rate is too low to for the core to cover the full Holocene period, potentially stopping around ~6 ka BP. This raises a number of questions and means several factors must be considered to allow this issue to be resolved. It is possible that either the 100cm or 52cm date has been contaminated and is not, therefore, allowing a reliable age model to be produced. Despite this being possible, as discussed in the strategy for Lake Baunt radiocarbon dating (section 3.2.2/3.2.4), there is no detrital carbonate found at the site and a lake reservoir offset seems unlikely, and, thus, it is not thought to be that probable for the dates to be too old.

A different option is the consideration that the site has a hiatus at some period. The ^{210}Pb, ^{137}Cs and ^{241}Am dating indicate that the upper section of the core does not contain sediments deposited during the last 150 years, although in at least one lake in the region ^{210}Pb ages are viable for the last ~60 years (Adams *et al.*, 2018). It is unexpected that the lake system would not have deposited sediments over this period, so is possible to suggest that the core top may have been lost during collection in 2014. This would explain the models suggesting the record stops at ~6ka BP. The work of Krainov *et al.*, (2017), may lend support for the loss of the upper section of the core as during the Holocene they only detect what they suspect to be the Solovki excursion in 1 sample and they do not detect the more recent Etruria excursion (Krainov *et al.*, 2017), which dates to 3-2.2 ka BP (Dergachev *et al.*, 2004). The lack of these palaeomagnetic excursions could be attributed to the upper part of the core being lost, which would allow the presence of earlier events but not the most recent one. It is possible, however, that this point may be circular, given the difficulty in resolving magnetic excursions in other parts of the core. Thus, the dates in the upper part of the model are examined in more detail below.

In order to investigate the upper sections of the model further, a fully interpolated model for the core with variable *k* and outlier detection was run, with the insertion of a ‘date’ function at a depth of 1cm. This function inserts the age calculated for a particular depth returned from the whole model (Bronk Ramsey, 2008). It is also possible to derive the same age from viewing the full deposition output from the model, but the ‘date’ function is used here for ease of viewing. The model shown in figure 3.13 uses all of the available dates and

predicts an age for a depth of 1cm as 6322-4003 ka BP. Suggesting that unless one or more of the dates above 200cm are incorrect, then part of the upper section has been lost in sampling, as suggested above.

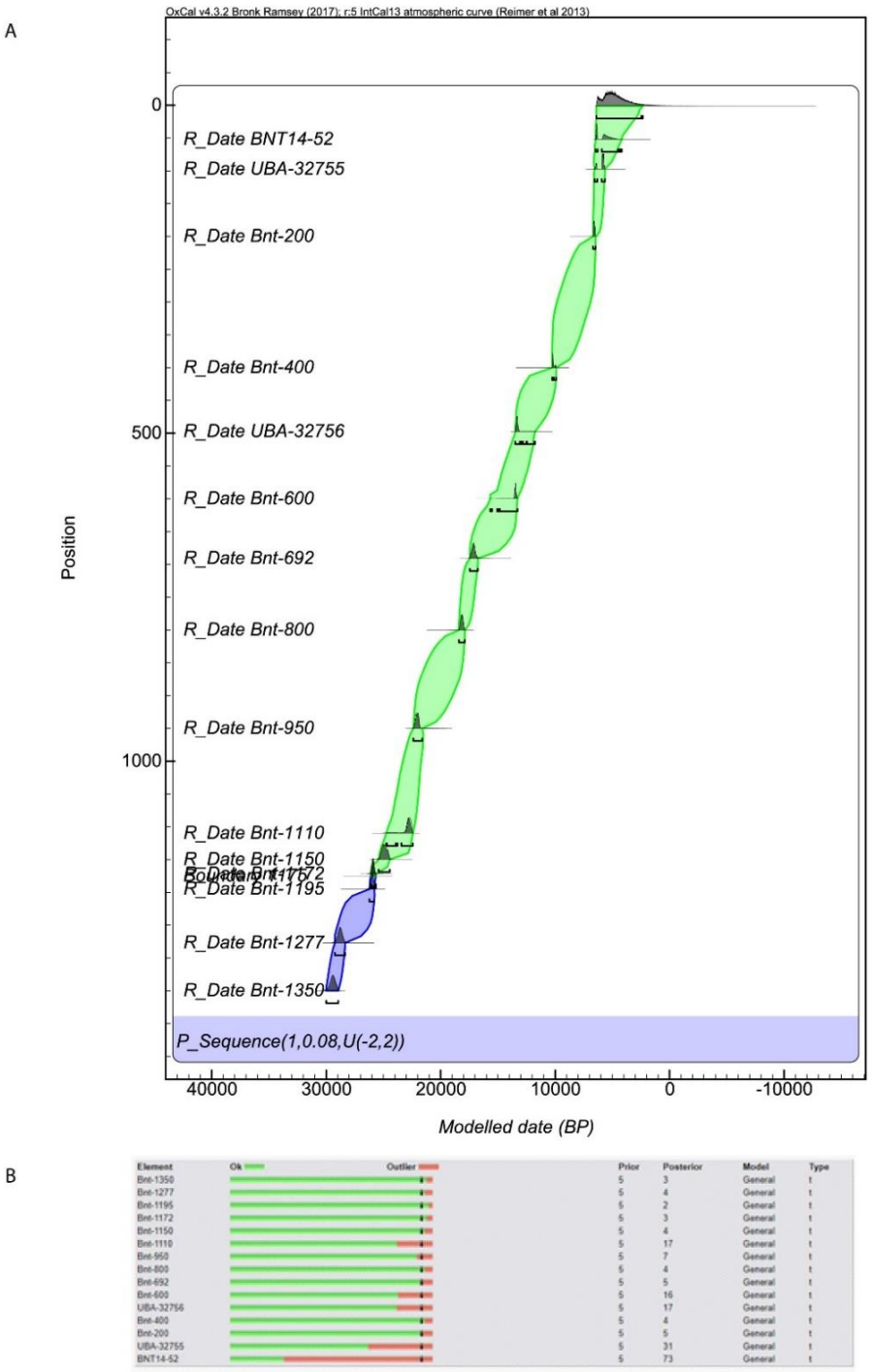

Figure 3.13: (A) - Bayesian Age *P_sequence* model for Lake Baunt with interpolation and outlier detection with the insertion of a date function for 1cm, which reports age if 6322-4003 ka BP. Model run allowing interpolation with 1 boundary. **(B)** Outlier Analysis Output showing which dates have been downweighed by the general outlier model.

To fully test this problem, a series of model experiments were run in OxCal, by progressively removing the upper dates and running a *P_Sequence* model with variable *k* and outlier detection and a 'date' function at 1cm (Bronk Ramsey, 2008). Interpolation modelling was not undertaken in this case, as this is not an attempt to construct a final age model, but to test the influence of specific dates and it the reduced uncertainty ranges of a more simple deposition model to allow a clearer view of the contribution of the dates. The first iteration of this experimental model (figure 3.14) does not use the new Belfast date at 97.5cm but keeps all of the original Poznan ages. Running this model gives an age for the 1cm depth of 6407-5205 ka BP. Running the model again figure 3.14 with the upper Poznan age at 52cm means that there are now no age constraints above 2m and the model is allowed to extrapolate from the ages below this depth. Doing so gives an age for the 1cm depth of 5830-1045 ka BP. The large age range is due to the long extrapolation over 2m and no constraints, but even so, this model cannot achieve a modern age for the top of the core. Thus, these experimental runs suggest that the upper ~6000 years of the core have not been captured. One final supporting point for this interpretation of the BNT14 core comes from a short core taken from the upper basal sediments in the site in 2013 (Bezrukova *et al.*, 2017). The coring location is the same as that is reported as for BNT14, and analyses of initial proxy data were carried out in the same laboratories. The base of the short core is reported at 147cm and has a radiocarbon age of 5990 $\pm$ 35 years. As such, if the BNT14 core did indeed cover a period younger than ~6000 ka BP it would be reasonable to expect some consistency between the two records. Two data sets available for both cores were undertaken by Russian collaborators and, therefore, some equivalence would be expected. In TOC for both cores this is the case with values ~15% above 2m for BNT14, and for the whole record in the short core. However, a shift to higher percentage values seen in BNT14 is not apparent at the top of the short core. A clearer issue between the cores, however is the completely different values in Biogenic Silica % with the short core having values of between 54-60% (Bezrukova *et al.*, 2017, Figure 2), whereas for BNT14 they vary between 10-25% for the upper 200 cm. This clear offset between the two cores suggests

that the interpretation derived from the radiocarbon ages, that the upper sections of the core have not been captured during the 2014 coring, seems valid.

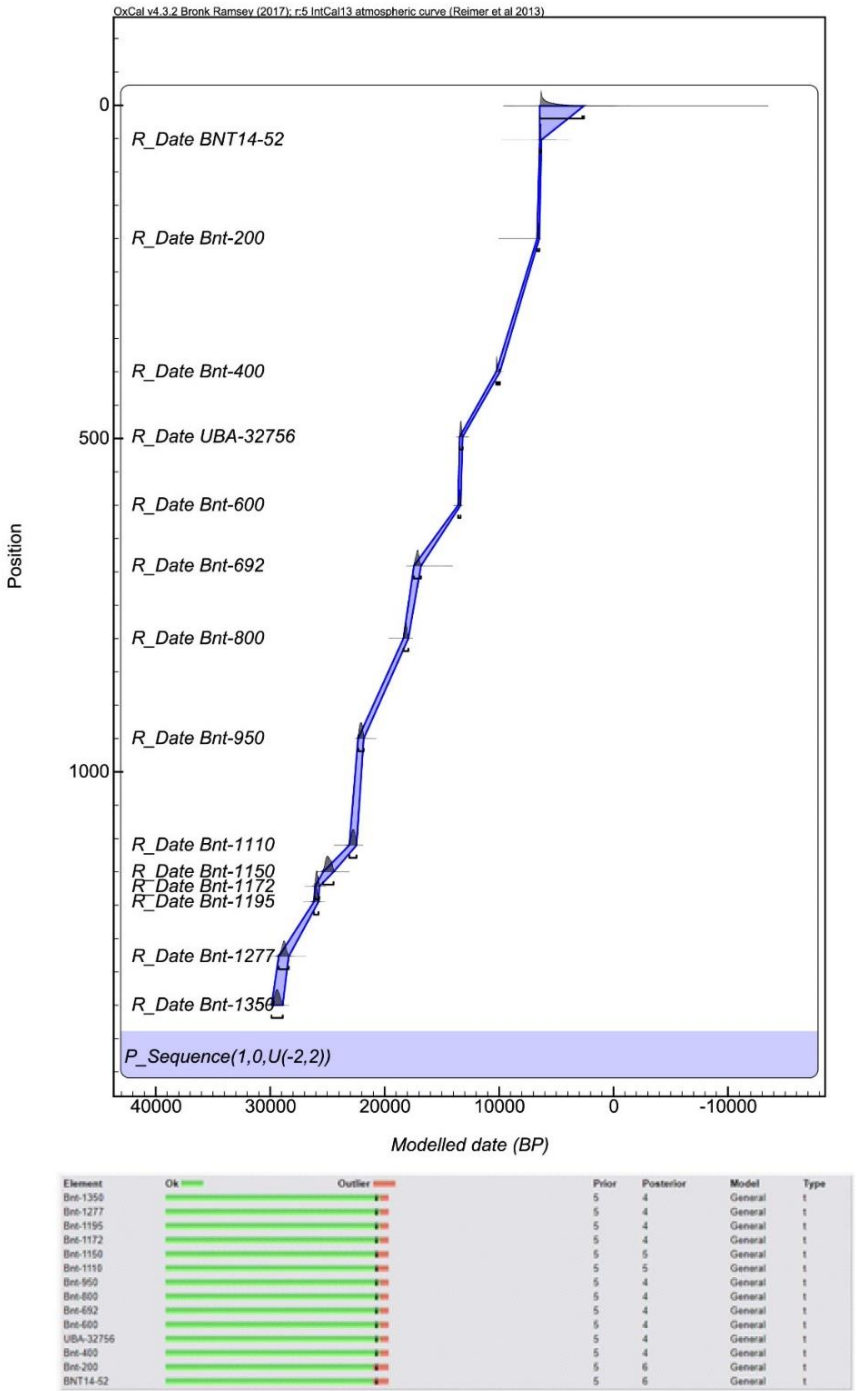

Figure 3.14: (A) - Bayesian Age model for Lake Baunt with the Belfast UBA-32755 date removed. No interpolation or boundaries are included. **(B)** Outlier Analysis Output showing which dates have been downweighed by the general outlier model.

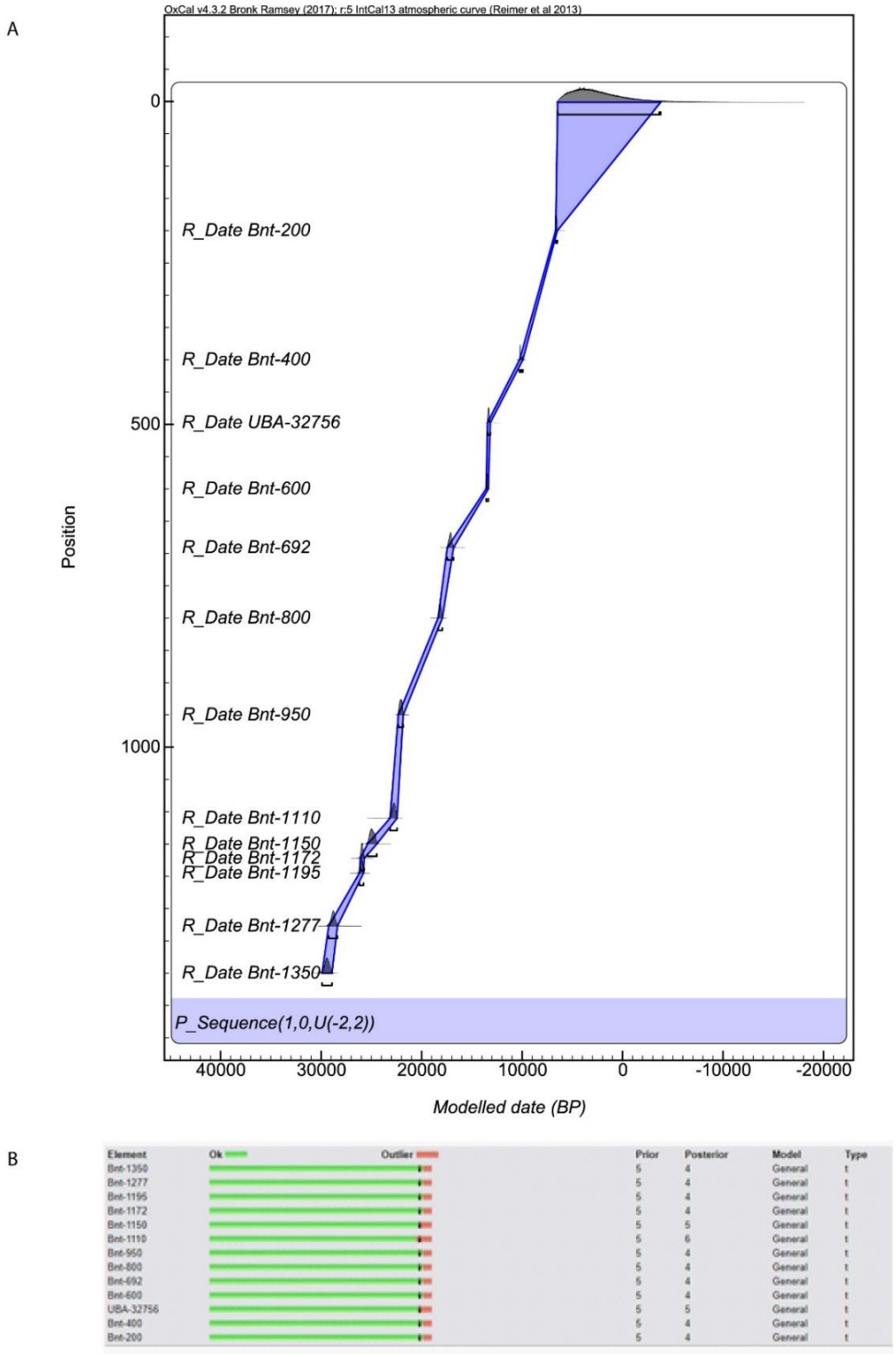

Figure 3.15: (A) - Bayesian Age model for Lake Baunt with the Belfast UBA-32755 and BNT14-52 dates removed. No interpolation or boundaries are included. **(B)** Outlier Analysis Output showing which dates have been downweighed by the general outlier model.

The different models for Baunt also highlight significant differences between how the models interpret the sediments between 600cm and 450cm. The first 2 models (figure 3.3 & 3.4) show very little variation in sedimentation rates over this period, while the third model (figure 3.5) is tightly constrained between 600-500cm, despite allowing interpolation between the dates. The models incorporating boundaries (figures 3.6 & 3.7) are much less constrained for this period, irrespective of whether the models allow interpolation. This period of the Lake Baunt core contains the most significant changes in the lithostratigraphy, so it is possible that sediment deposition underwent major changes during this period. Potentially then, the models using boundaries are more realistic for these periods, compared to those without boundaries, where the model lacks prior knowledge that there are sedimentological changes at these depths. Despite this, the model in figure 3.5 can be considered preferable as this model does not down-weight as many of the dates, and as there is no supporting information to suggest the dates should be considered as outliers. Therefore, it may be the case that the boundaries are introducing additional uncertainty, and it is necessary to consider if the lithostratigraphic changes documented are sediment source changes, or just minor changes in the sediment deposition.

In order to consider the issue of where to place boundaries in this record, it is necessary to take a strategy that considers the lake stratigraphy but also the robustness of the whole model, with respect to outliers. At this point, it is useful to review the combined stratigraphic information for the core presented in chapter 2 (figure 2.7). There are a number of fluctuations within the various productivity signals for the lake (LOI, TOC, Biogenic silica), and these generally co-vary. These fluctuations in the lake productivity signal do not really conform in any clear way to the changes in recorded sediment, with the largest shift across all indicators occurring at ~1000-800cm and this sits well within any reported boundaries. It is taken here to suggest that the logged changes in stratigraphy 600-400cm are related to clay content and would not necessarily have an impact on sedimentation rates. Thus, in the final model, below, the upper boundaries are omitted to allow the lowest number of outliers in the age model. One boundary that is retained is the lowest boundary,

between silty clay and silty clay with diatoms. The lowest section has the lowest diatom concentration and is the least productive part of the record. This suggests that the regime in the lake is very different and this boundary may be more significant than the other boundaries. Incorporation of this boundary also gives the lowest level of outlying elements of the probability ranges.

Large uncertainties on some of the dates in the core may also be a function of the calibration process. All the radiocarbon dates in the Lake Baunt age model are calibrated using the IntCal13 curve (Reimer *et al.*, 2013), and although this is essential, it may introduce some of the larger uncertainties documented in some of the models. This can be due to variations in past atmospheric concentrations of ^{14}C, which mean that there is significant variation in the shape of the calibration curve. As discussed in section 3.2.3, calibration of two dates with a similar error can result in large variations in the range of the calibrated ages, due to variations in the shape of the IntCal13 calibration curve. In Lake Baunt's case, some of the dates including UBA-32755 have a much wider range than some of the others, including BNT-1195, due to plateauing areas on the IntCal13 curve (see figure 3.16). In general, the dates below 600cm are less affected by plateauing of IntCal13, and this may explain why uncertainties are smaller in these sections of the model, and why these areas are more consistent between models.

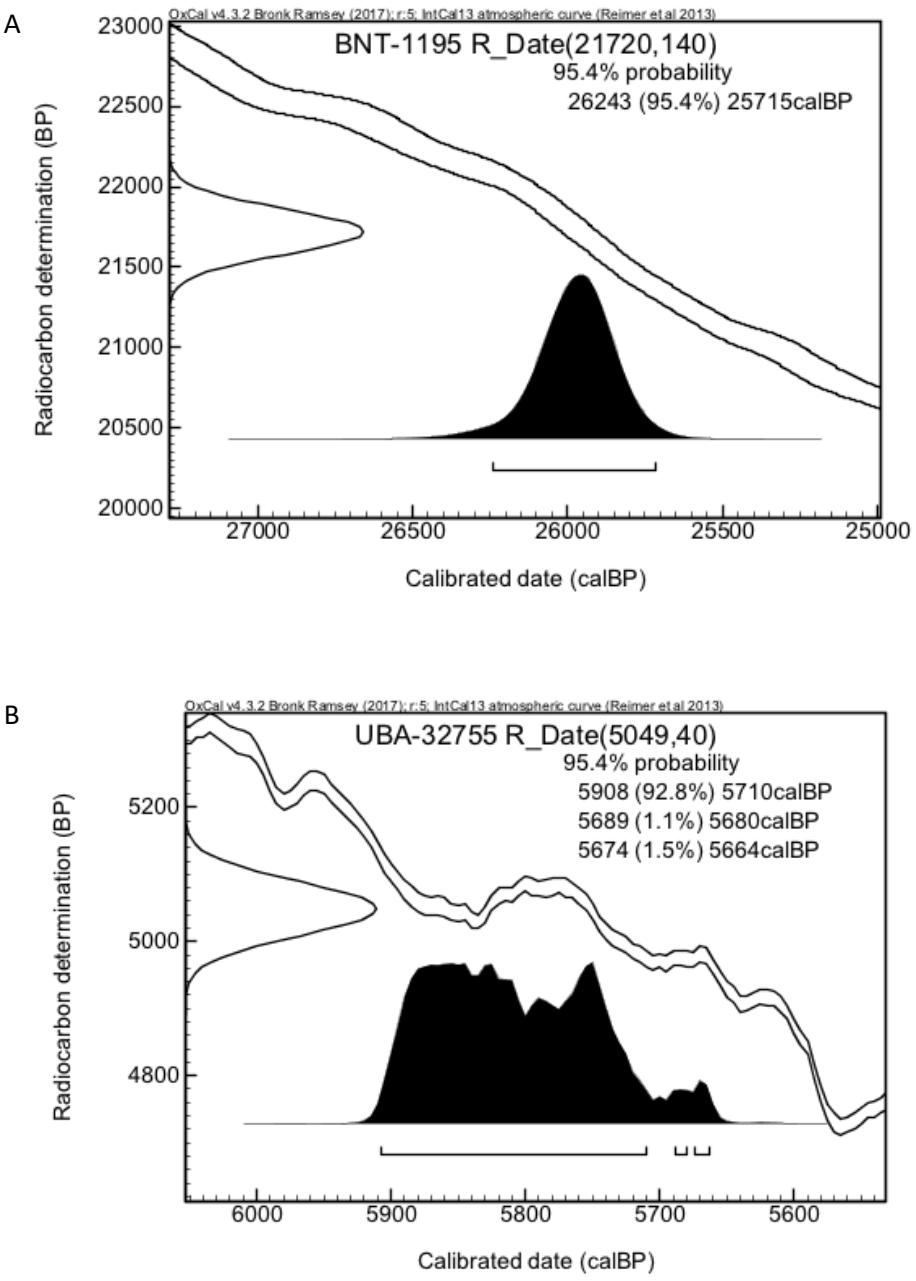

Figure 3.16: Radiocarbon date and calibrated probability density function of calibrated ages from Lake Baunt shown with the relevant section of the IntCal13 curve (Reimer *et al.,* 2013) **(A)** BNT-1195 **(B)** UBA-32755.

3.8 The complete Lake Baunt age model

The final Bayesian Age Model for Lake Baunt is shown in figure 3.17. The model uses a *P_sequence* deposition with interpolation model, with automatic outlier detection. The model allows for interpolation between the dates, as this most accurately reflects the current knowledge of the age of sediments between the dates and allows for more flexibility within the model. This also

prevents dates being down-weighted due to the model being too rigid. The model includes the full set of 15 radiocarbon dates, and it is assumed, based on the ^{210}Pb dating, that there is a hiatus above ~6 ka cal BP, supported by the modelling experiments and comparison to the short core above and, thus, the record does not extend beyond the early mid Holocene. Figures 3.6 and 3.7 highlighted that models produced for Lake Baunt, which incorporate boundaries, have had a higher number of dates down-weighted as potential outliers, than those without. To consider this, the site stratigraphy required careful scrutiny, to determine periods of sediment supply change. As a result, the final age model from Lake Baunt (figure 3.17) incorporates only one boundary at 1175cm, where there is a significant shift to a more organic dominated system, from a system were the minerogenic fraction is greater (see figure 2.6), which suggests there are different sedimentary sources and supply regime at this time. As discussed in section 3.6.3, the palaeomagnetic excursions documented by Krainov *et al.,* (2017) from Lake Baunt are not included in the final model as further work is required to determine the robustness of these excursions.

The model indicates fairly consistent sedimentation at the site from ~30 ka cal BP and is considered to be the most realistic representation of deposition of the Lake Baunt sediments. Interpolation between dates within the model allows a more realistic representation of model uncertainty, and the variable *k* factor has given the model enough flexibility to incorporate almost all the dates with very limited down-weighting. This is ideal, as the site's δ^{13}C record suggests that we do not anticipate a high number of outliers. One date (UBA-332755) is fully down-weighted, suggesting that this date is 100% outlying, and further dating in this area of the core in the future may help to resolve this. The remaining dates are either fully contributing to the model at 95% confidence, or within 1-3% of this, and therefore the model is performing very well.

The model suggests an average deposition of ~30-100 years per centimetre (0.03-0.01 cm/yr), which suggests that the site is suitable for considering abrupt climatic shifts throughout the later Quaternary period.

A

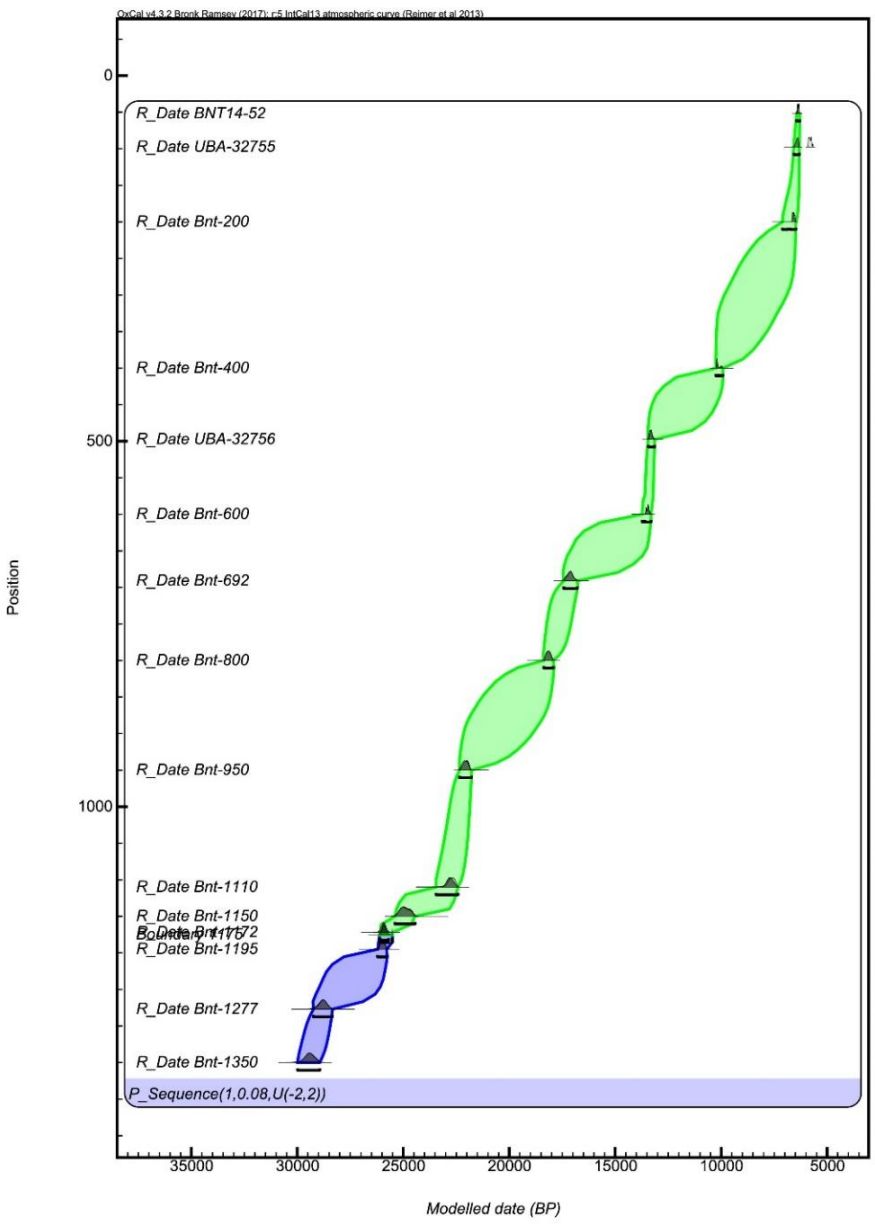

B

Element	Ok	Outlier	Prior	Posterior	Model	Type
Bnt-1350			5	3	General	t
Bnt-1277			5	4	General	t
Bnt-1195			5	2	General	t
Bnt-1172			5	2	General	t
Bnt-1150			5	4	General	t
Bnt-1110			5	8	General	t
Bnt-950			5	5	General	t
Bnt-800			5	3	General	t
Bnt-692			5	3	General	t
Bnt-600			5	6	General	t
UBA-32756			5	4	General	t
Bnt-400			5	2	General	t
Bnt-200			5	8	General	t
UBA-32755			5	100	General	t
BNT14-52			5	1	General	t

Figure 3.17: (A) Final Bayesian Age model for Lake Baunt incorporating 15 ^{14}C dates calibrated using IntCal13 (Reimer *et al.*, 2013), and modelled in OxCal 4.3. Outlier analysis and interpolation (variable *k* parameter of 2 to -2) has been used and one boundary is included at 1175cm depth. **(B)** Outlier Analysis Output showing which dates have been downweighed by the general outlier model.

Due to the lack of dates above 52cm, this upper section of the core will only be discussed with reference to the extrapolated age range for the upper 52cm from the final model.

Although issues remain with the Lake Baunt chronology, it is the best and most comprehensively considered available chronology for the site, and the different techniques used have supported several of the chronological findings, including the potential hiatus or upper core loss. Despite the issues raised about the late Holocene, for the period covered by this study, it provides one of the best chronologies for palaeoenvironmental studies in southern Siberia. By comparison with the only currently published chronology for BNT14 (Krainov *et al.*, 2017), the model presented here now has a fully defined age range over the full depth of the core with fully defined uncertainties, as the only published age model focusses on attempting to define palaeomagnetic changes in the core at a small number of specific depths. Therefore, the model from this project is the best available age depth model for understanding changes in the Baunt record over time.

In a number of proxies, changes in sedimentation rate can influence the apparent influx of material. It is common, therefore, to convert some parameters, such as % organic carbon or the biovolume, to account for accumulation rates (Rioual and Mackay, 2005). The first step is to calculate the Dry Bulk Density for each individual sample. Dry Bulk Density is calculated by weighing each wet sample, drying in an oven overnight at 105˚C and then re-weighing the cooled sample. Dry Bulk Density is wet mass –dry mass of sample. To obtain sediment Mass Accumulation Rates this is then multiplied by the linear sedimentation rate between dated points. The MAR for Lake Baunt is shown in 3.18.

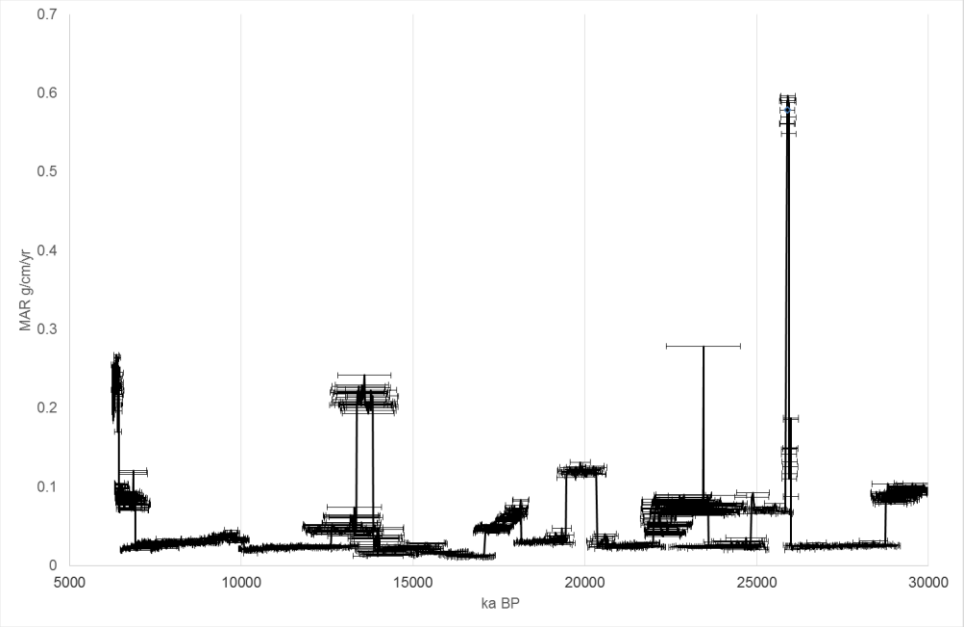

Figure 3.18 MAR's for Lake Baunt in g/cm^2/year from for the whole record on the final Baunt age model with 2 sigma uncertainty ranges on the chronology.

3.9 Future Chronological Work

Lake Baunt has one of the best well constrained age models for a site in southern Siberia. Although the site has not preserved macrofossils, the bulk-radiocarbon samples are considered sound. The sedimentation rates documented through the core allow high resolution palaeoenvironmental and palaeoclimatic studies to be undertaken at the site. It is anticipated that several areas of the Lake Baunt chronology may undergo refinement, potentially linked to improvements to radiocarbon calibration, which may allow uncertainties in some areas of the core to be reduced. The use of additional techniques including tephrochronology, in the future, may assist chronological controls, by providing the ability to link records from regional sites, and if a microscopic tephra can be linked by geochemical characteristics to a known eruption, an argon-argon date may be used and provide an independent age for a site. The palaeomagnetic work carried out at Lake Baunt by Krainov *et al.,* (2017, 2018) requires further work to determine if core factors and sampling are causing the magnetic field shifts, or if these are indeed true palaeomagnetic excursions.

4 The Lake Baunt Diatom Assemblage

4.1 Diatoms as Palaeoenvironmental Indicators

Diatoms are unicellular, photosynthetic algae (Barber and Haworth, 1981; Round *et al.,* 1990), belonging to the class Bacillariophyceae of the algal kingdom (Barber and Haworth, 1981; Battarbee *et al.*, 2002). They are found in almost all aquatic environments (Jones and Mann, 2004), in some cases making up 98% of silicic material in sediments (Swann and Mackay, 2006). Diatoms make excellent indicators for palaeoenvironmental, palaeolimnological and palaeoclimatic studies for many reasons, including their ability to respond rapidly to environmental changes, as a result of their short life cycles (Kilham *et al.,* 1986; Rioual *et al.*, 2007), which makes them ideal for studying responses to abrupt climatic change. They provide essential insight into aquatic environments, which is aided by the longstanding studies of diatoms over the past two centuries, meaning that in many cases their ecological preferences are well documented (Barber and Haworth, 1981; Jones, 2013).

Diatoms are known to respond to a wide range of environmental variables, including changes in pH, salinity, nutrients and oxygen availability, which make them useful for reconstructions of these environmental indicators at a range of geographic and temporal scales. Diatoms are a key tool in modern ecological studies of single lakes, to multiple lakes in a broad region, and over daily and seasonal timescales (e.g. Pan *et al.*, 1996; Maier *et al.*, 2018), but at the same time are used to examine ecological and environmental change over much longer Quaternary records, from the last millennium through to glacial to interglacial cycles (e.g. (Mackay, 2007; Rioual *et al.*, 2007; Wang *et al.*, 2013). As such, diatoms are an incredibly useful and diverse proxy record. However, diatom studies also require knowledge of ecological preferences to e.g. lake chemistry and an understanding of secondary and taphonomic influences on diatom preservation, so the reconstructions can be robustly evaluated (Barker *et al.,* 1994).

A key feature of diatoms, which makes them an excellent environmental indicator, are their intricately patterned siliceous cell wall structure (Barber and

Haworth, 1981; Zurzolo and Bowler, 2001). Diatom cells are encased in two siliceous frustules, which are essential for allowing identification of species, due to the variations in the patterning, which are usually species specific and reproduced identically during cell division (Zurzolo and Bowler, 2001). The two frustules consist of a larger epitheca, which fits over the smaller hypothea, and they are linked by copulae (Round *et al.,* 1990). The rigid amorphous biogenic silica (Zurzolo and Bowler, 2001), which comprises the frustules, is able to withstand harsh environments, allowing diatoms to be well preserved in sedimentary deposits. The biogenic silica is comprised of inner tetrahedrally bonded silica oxides (Si-O-Si) surrounded by a hydrous layer (-Si-OH), which is freely exchangeable with the surrounding environment (Leng and Barker, 2006; Leng and Swann, 2009). To form their frustules, diatoms utilise silicic acid from their environment, using their specialised silica deposition vesicles to polymerize the acid (Zurzolo and Bowler, 2001). Diatom cell replacement primarily occurs as asexual vegetative replacement, however, this results in progressively smaller cells (O'Farrell *et al.,* 2001), and as a result sexual reproduction also occurs (Kaczmarska *et al.*, 2013).

One of the most important issues that can affect the reliability of diatom reconstructions is dissolution of diatom frustules, both within the water column, and post deposition. This can be a significant issue for palaeoenvironmental reconstruction, as dissolution of diatoms, in the worst cases, can cause complete removal of diatoms from a record. More commonly, a diatom assemblage becomes biased, as a result of partial dissolution, with the smaller or more delicately silicified species (Battarbee *et al.*, 2005; Ryves *et al.*, 2003), being preferentially removed from the record, preventing them from being documented. In many cases, the more robust species undergo less dissolution, which may mean they are more easily identified in the record, again introducing bias (Ryves *et al.,* 2009). Effects of dissolution on palaeolimnological reconstructions are well documented, with evidence of dissolution shown clearly in Lake Baikal, where the water column is always undersaturated in silica (Mackay, 2007), and only 1-3% of valves are preserved.

Diatom dissolution in aqueous environments is known to be primarily influenced by temperature, pH (Swann and Mackay, 2006), salinity and the silica content of water (Cohen, 2003; Flower and Ryves, 2009). Through laboratory experiments, high pH environments have been shown to be most conducive for diatom dissolution, with saline solutions generating the greatest solubility of diatom frustules in these environments (Barker *et al.,* 1994). Temperature is an important control on all solution reactions and in general colder waters would promote diatom preservation (Kamatani, 1982), in part by reducing bacterial influence on dissolution (Bidle *et al.*, 2003), although these effects have been most studied in marine environments. Additionally, other factors are important, including the oxygenated nature of bottom waters, silica in pore waters, carbonate content and meromixis, especially in saline lakes (Ryves *et al.*, 2006).

Effects of dissolution are not linear through time, or within water bodies, with factors such as lower diatom concentrations, for example during colder glacial periods (e.g. in Lake Baikal, Mackay (2007)), exacerbating the effects. Additionally, coarser sediments, often associated with increased erosion in cold conditions, are found to damage diatoms more readily (Lowe & Walker 2015). Additional factors, such as increased grazing, both in the water column and on the lake bed, can fragment the frustules making them easier to dissolve (Mackay, 2007).

Diatoms have been well utilised in Siberia as a proxy, as discussed in chapter 1.4. Their widespread use is primarily due to their ability to preserve well in aquatic environments, and the relatively low salinity and relatively cold conditions in most Siberian lakes gives generally good diatom preservation. Moreover, as discussed below, techniques have been developed to assess diatom dissolution and potential bias in a diatom assemblage, allowing greater confidence in diatom based environmental reconstructions (Ryves *et al.,* 2001).

Despite the issue of dissolution, diatom assemblage data has been generated from many studies in order to understand paleoenvironments. Diatom assemblage data are presented in many ways. Most commonly, percentage

relative abundances are used, allowing raw count data to be rapidly converted to a more comparable form. This is particularly important where the exact number of values varies, as without converting to percentages, raw counts could identify a species as increasing when it could be due to larger count numbers. Despite this, without careful consideration, percentage change values still need to be considered carefully. This is because as one species declines, it automatically increases the proportion of other species, where they may not have actually increased in the assemblage, and this is a common problem across a range of compositional data (Aitchison, 1986). Diatom concentrations have been used to overcome this (Battarbee and Kneen, 1982), preventing species being given a higher value due to proportional reductions in other species. Despite this, concentration data can also be difficult to interpret, as concentrations within a core may increase rapidly, as a result of factors external to the diatom assemblage, such as changes to sedimentation rates. This has increasingly led to diatom concentrations being converted to diatom fluxes (e.g. Battarbee *et al.*, 2001) or diatom biovolumes (Rioual and Mackay 2005). Diatom fluxes take account of sedimentation accumulation rates, and, therefore, rely on a robust chronology to provide an accurate view of periods of increased diatom concentrations over time. Biovolumes are also able to accommodate accumulation rate shifts (e.g. Rioual and Mackay, 2005), but they require accurate size measurements of the taxa. This in itself can be problematic due to the wide variety of morphologies and sizes seen in diatom assemblages (Hillebrand *et al.*, 1999). Therefore, to allow the most detailed understanding of an assemblage it appears that using a range of these techniques to consider an assemblage is advantageous.

4.1.1 Functional Groups

The use of ecological guilds and functional groups are increasingly popular for understanding ecological status (Passy, 2007a, 2007b; Tapolczai *et al.*, 2016). However, they have not yet been extensively applied to studies considering palaeoenvironmental shifts (Riato *et al.*, 2017). The reason for considering species traits and functional adaptations when studying assemblages is due to issues that can arise in understanding the ecosystem with a large variety of

species; trait analyses requires identification of taxa only to genus level, overcoming issues with hard to identify species, or species that are extinct (Riato *et al.*, 2017; Tapolczai *et al.*, 2016). Grouping taxa according to their functional adaptations allows the complexities of the environment to be better understood (Riato *et al.*, 2017). This is because certain traits will enable some groups to thrive (Tapolczai *et al.*, 2016), and changes in the proportions of these can give distinct responses to changing environments (Passy, 2007b).

Functional groups are, therefore, a useful way to extract additional information from a complex diatom assemblage. As a result, several grouping classifications have previously been developed, although Passy's (2007b) four ecological guilds grouping is the most widely known (Tapolczai *et al.*, 2016). Passy (2007) based guilds on tolerance to resource use, nutrient limitations and physical disturbance (Passy, 2007b; B-Béres *et al.*, 2017), however, this has been viewed as problematic as the definition of 'disturbance' is unclear (Tapolczai *et al.*, 2016). Additionally, the use of only four groups is thought to be insufficient to cover the main habitat types, and, therefore, newer classifications of eco-morphological groups have been developed to allow species-environmental correlations to be revealed (B-Béres *et al.*, 2017). These have adapted Passy's (2007b) guilds with the addition of a planktonic group suggested by Rimet and Bouchez (2011), and size separations within groups, which improve detection of correlations between different environmental factors and cell size (B-Béres *et al.*, 2016).

4.1.2 Diatoms in Cold Environments

Cold regions provide a particular set of conditions, which strongly influence their diatom communities. Factors that are of particular note for influencing diatoms in these regions are the duration of ice cover, stratification of the water column, intensive seasonality, and lake level (Kilham *et al.,* 1996). Slight year-to-year changes can have significant impacts on an assemblage, as shown by Malik *et al.,* (2018), where variations in the timing of the start of the ice free season influenced whether *Lindavia bodanica* (Eulenstein ex Grunow) T.Nakov, Guillory, Julius, Theriot & Alverson - or *Discostella stelligera* (Cleve & Grunow) Houk & Klee, became dominant. The timing and duration of the

ice-free season are also critical in how much these regions can warm during summer months, with the timing of ice cover and spring overturning controlling nutrient delivery from the hypolimnion to the epilimnion, through mixing of deep water (Kilham *et al.,* 1996), which in turn influences the diatom community. Additionally, the duration of ice cover will cause particular requirements to be beneficial to some diatom species, with early ice free conditions causing early and prolonged spring overturning, and this favours species that can tolerate low light conditions (Kilham *et al.,* 1996). Reduced ice cover is also linked to higher biomass conditions, as a result of reduced loss of diatom cells through erosive abrasion and higher primary productivity, due to increased nutrients, substrate and light (Snoeijs, 1990). This means that when the ice free duration changes, it can impact the niches that are available for diatoms to occupy, with earlier ice free conditions promoting large diatom blooms (Snoeijs, 1990). On the other hand, when ice durations are extended, productivity is often significantly lower, with increased minerogenic inputs promoting erosive abrasion which damages the diatoms (Lowe and Walker, 2015; Snoeijs, 1990), making them more susceptible to dissolution , as seen during glacial periods in Lake Baikal (Mackay 2007). Therefore, it is essential to carefully consider these specific features when considering diatom assemblages in cold environments, as in cold regions, such as southern Siberia, assemblages reflect strongly seasonal conditions, with long, cold and arid winter environments and short, warm, moist summers.

4.1.3 Aims and Objectives

The aim of this component of the project is to produce a high-resolution record of change in lake ecology from Baunt. This has been achieved using several objectives including the production of a high-resolution diatom assemblage record for the BNT14 core, which is considered alongside additional datasets from Baunt to consider how the lake has changed over the past ~30 ka BP. External drivers of palaeoclimatic change have been considered to determine their influence on the ecosystem.

4.2 Methodology

4.2.1 Sample Preparation

Diatom samples were taken at 5cm resolution across the BNT14 core, with additional infilling at 2.5cm at key areas of the core. In total 327 samples were prepared for compositional analyses following Battarbee's (2001) digestion procedure. The method comprised sampling 0.1g of wet sediment and adding 5 ml of H_2O_2 (laboratory grade). The samples were placed in a water bath and warmed to 80°C. Care was taken while heating, to ensure a violent reaction was avoided. Samples remained in the water bath until all organics had been removed and additional H_2O_2 was added as required. Following this, a few drops of 5% HCl were added to remove any carbonates. Samples were then topped up with distilled water and centrifuged at 1200 RPM for 4 minutes. The supernatant was poured off and additional distilled water added. The process was repeated 4 times to ensure all H_2O_2 is removed. During the last two rinses NH_3 was added to keep the clays in suspension and to stop the diatoms clumping. Blank samples were added at each stage of the preparation, to provide a means of checking samples were not contaminated.

Additionally, divinylbenzene (DVB) microspheres were added after the final rinse to allow determination of diatom concentrations (Battarbee and Kneen, 1982). Once microspheres were added to the samples, they were diluted and pipetted onto the cover slips, which were covered and left to dry. Once dried, a hotplate was heated to 130°C in a fume cupboard. A drop of Naphrax mounting medium (resin) (refractive index 1.65), was placed on the slide and the cover slip inverted. This was followed by heating the slide until the toluene was driven off the Nahrax, causing the refractive index to rise to 1.73, making it ideal for fixed diatom slides.

Each sample was studied at X1000 magnification and had a minimum of 300 diatoms counted and identified, using a Lecia DMBL. Identifications principally followed Krammer and Lange-Bertalot (1986, 1988, 1991a, 1991 b)**,** supplemented with Lange-Bertalot, (2001) and Krammer (2002) and was supplemented by web based resources (http://craticula.ncl.ac.uk and https://diatoms.org), alongside published literature on particular taxa (e.g.

Duleba *et al.*, 2015; Genkal and Popovskaya, 2008b; Koppen, 1978, 1975). Light microscope photos and scanning electron microscopy images were used to record and classify hard to identify species. Additionally, advice was sought from diatom experts at the International Diatom Symposium 2018 (Berlin) to help resolve difficult to identify taxa.

Raw counts were transformed to percentages to provide relative abundances, while concentrations were determined using microspheres. Concentrations were calculated as:

$$\frac{\text{Number of Microspheres Added x Number of Diatoms Counted}}{\text{Number of Microspheres Counted}}$$

Equation 4.1: Diatom Concentration

The concentration data has been converted to diatom fluxes as this incorporates variations in sedimentation rates, as determined in chapter 3. Expressing data as a flux reports quantity through an area over time. In the case of diatom flux this can be the quantity of diatoms in a sediment trap collected over a period of weeks or months (e.g. Hausmann and Pienitz, 2009), or, as in this case, diatom concentrations derived from microspheres (Battarbee and Kneen, 1982) are expressed as units per cm against time:

$$\text{Diatom Concentration x } 10^6/\text{cm}^2/\text{time}$$

Equation 4.2: Diatom Flux

Abundances were expressed as concentrations $x10^6$ by dividing the calculated values by 1,000,000. As samples were not taken at every cm, the sedimentation rate was derived by dividing the difference between average ages from the calibrated radiocarbon chronology for Baunt, by the difference in relative depth between each diatom sample. Reporting diatom flux in such a way relies on a relatively linear sedimentation rate, and the average of the Baunt age depth model (figure 4.1) supports the reporting of the diatoms as flux, as well as concentrations.

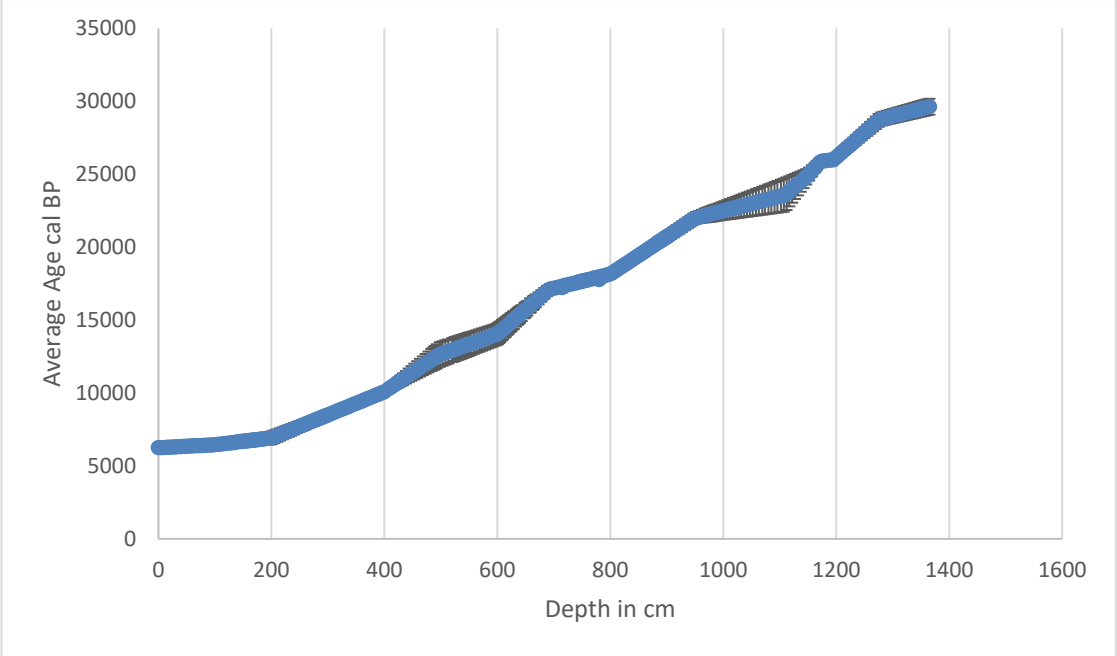

Figure 4.1: Age depth model for Lake Baunt (see chapter 3).

Additionally, diatom biovolumes have been studied for the main planktonic taxa, *A. granulata* and *P. ocellata*, which usually make up >60% of the assemblage and are, therefore, likely to provide a good representation of the Baunt assemblage. The biovolumes of the main taxa have been studied as this can allow the size differences between the main species to be considered more clearly. Biovolumes were calculated by using a micrometre eyepiece to measure the lengths and widths of *A. granulata*, while the diameter was measured for *P. ocellata,* and the cell depth was inferred from this using the radius (Anderson, 1994). A minimum of 50 valves were measured per taxa. Mean and median biovolumes were then calculated using the Hillebrand *et al.,* (1999) geometric shape guidelines. The median biovolumes were converted to biovolume accumulation rates (BVAR) by calculating the diatom cell concentration (diatom valve concentration divided by two, and expressed in millions of cells per gram of dry matter), as outlined by Rioual and Mackay (2005). Median biovolumes were multiplied by the diatom cell concentration, the dry bulk density, and sedimentation rate.

Diatom dissolution of the dominant diatom taxa, *A. granulata* and *P. ocellata* was quantified with individual frustules being classified into 1 of 4 stages (see figure 4.2): (1) pristine, (2) little dissolution, (3) very dissolved, and (4) almost

unrecognisable. 76 of the 327 samples were classified for dissolution at regular intervals across the core. Dissolution quantifications were carried out under light microscope at X1000 magnification. Dissolution was quantified for the first 100 frustules of these taxa found per sample, to ensure the sample was random.

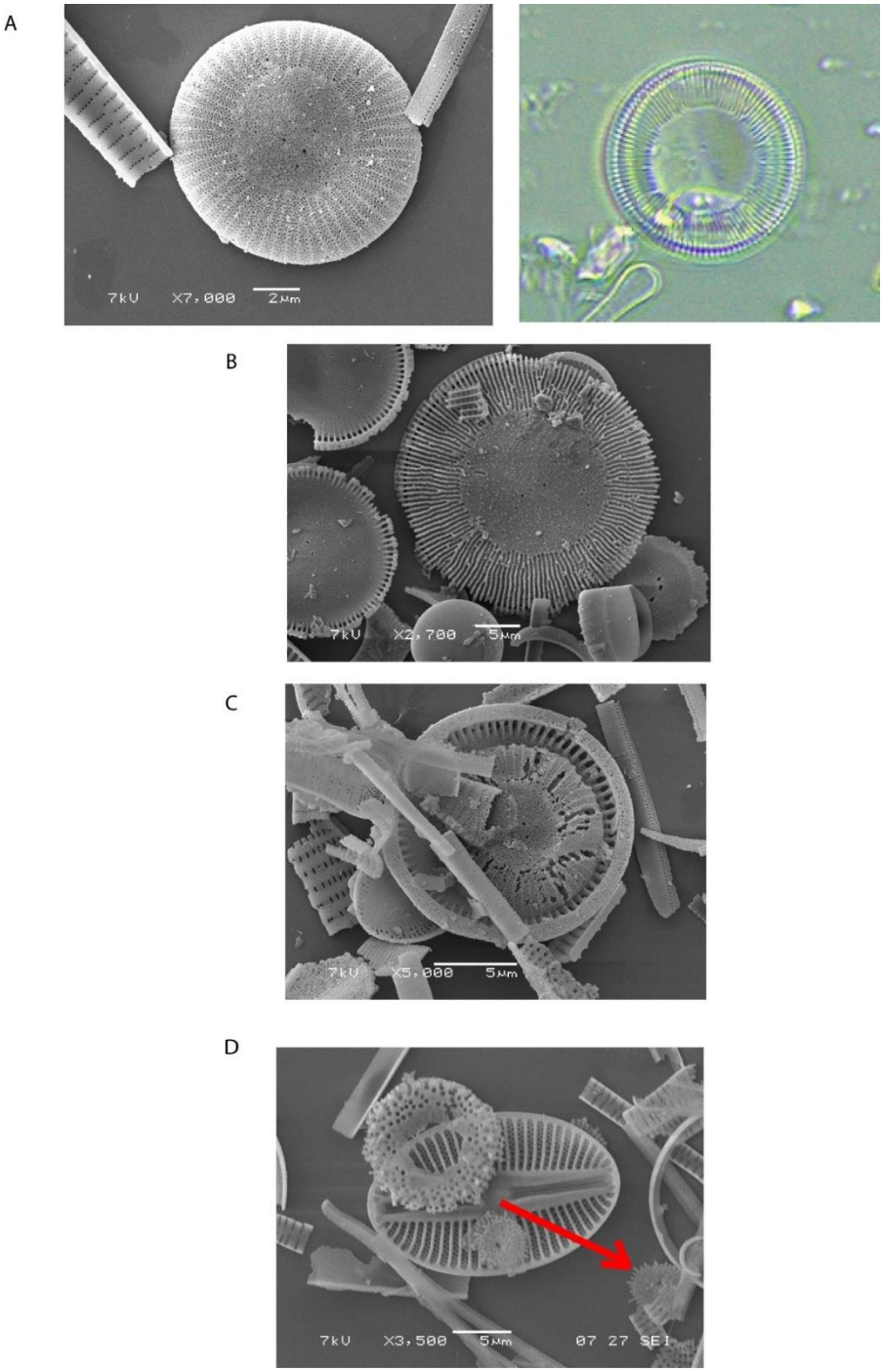

Figure 4.2: Dissolution stages of *P. ocellata* **(A)** pristine (under SEM and LM) **(B)** little dissolution -concentrated around valve edges, **(C)** very dissolved with dissolution towards the mantel and **(D)** almost unrecognisable.

Dissolution was not quantified for *T. flocculosa* as this is not present during the lower sections of the core, and because it is difficult to consistently quantify dissolution for this morphology. Additionally, *T. flocculosa's* morphology meant that it is more liable to breakage than dissolution, making calculations of biovolume difficult too.

Dissolution stages were converted to a dissolution *F*- index following Ryves *et al.*, (2001) and Flower and Ryves (2009), as an objective assessment of diatom preservation. In this case, from the same observations above, a ratio of pristine valves for a given species for each sample against total counts (pristine and non-pristine) for the same species was calculated, expressed as:

$$Fi = \sum_j^m nij / \sum_j^m N \ /$$

Equation 4.3: *F*- Index

Where F_i is the *F*- index for sample i, n is the sum of the pristine valves for species j in the sample, and N is the sum of the total number of valves in the same sample. This has been calculated for every sample in the Baunt core for *A. granulata* and *P. ocellata*.

4.2.2 Statistical Analyses

Initially, a detrended correspondence analysis (DCA) was undertaken in Canoco5 (ter Braak and Smilauer, 2018), to estimate the beta diversity of the dataset. DCA is a form of indirect gradient analysis, with gradient length (or beta diversity) estimated in standard deviation units (Lepš and Šmilauer 2003). The gradient length of the DCA's first axis was 1.35**,** and, therefore, it was decided that a linear ordination method would be most appropriate for the dataset, as a short first axis gradient < 3 generally indicates that many species have a linear relationship to their environment (Lepš and Šmilauer 2003). Therefore, principal components analysis (PCA) was also undertaken in Canoco5. The species were centred and standardised, to stabilise variance

for the PCA (Lepš and Šmilauer 2003). PCA provides an approximation of the greatest variance within the data using ordination (Lepš and Šmilauer 2003).

The Baunt record has been divided into 6 diatom assemblage zones (DAZ's) (see figure 4.5/4.6), based on the shifts identified in the PCA (see section 4.2.2), and these are used to assist description of the changes seen in the Baunt record.

4.2.3 Functional Groups

The main species from Lake Baunt were grouped into functional groups following B-Béres *et al.*, (2017), where species are primarily divided into 4 groups – low profile, high profile, motile and planktonic, as originally outlined by Passy (2007b), and following species information based on species specific wider literature and databases (e.g. Algalbase; (Guiry and Guiry, 2018), http://craticula.ncl.ac.uk and https://diatoms.org). Species are then sub-divided into size ranges as follows: (1) 5–99µm^3, (2) 100–299µm^3, and (3) 300–599µm^3, based on their mean cell biovolume as described by B-Béres *et al.*, (2017). The four main functional groups define different conditions, with the low-profile group occupying the base of the benthic layer, where they are at risk of resource stress due to low light conditions and limited nutrients (Passy, 2007b; Stenger-Kovács *et al.*, 2013). The high profile guild on the other hand have better access to light and nutrients, but are at risk of 'disturbance' due to grazing or water flow in the phytobenthos, while motile species are able to select their own microhabitat, minimising resource limitation (Passy, 2007b; Stenger-Kovács *et al.*, 2013). The addition of the planktonic group allows guilds to be considered across the wider assemblage, as planktonic species are not always affected by the same factors as the taxa placed into the other guilds, and placing planktonic taxa into these guilds can obscure these groups changes (B-Béres *et al.*, 2017).

4.3 The Lake Baunt Diatom Record

The Lake Baunt diatom record includes 290 known species from 79 genera, and 3 unresolved taxa, two of which are broadly linked to the genus *Navicula*, and one further unresolved taxa. Due to the rarity of these individuals, images

of these taxa were not obtained. SEM and light-microscope images of some of the taxa from Lake Baunt are shown in figures 4.3 and 4.4.

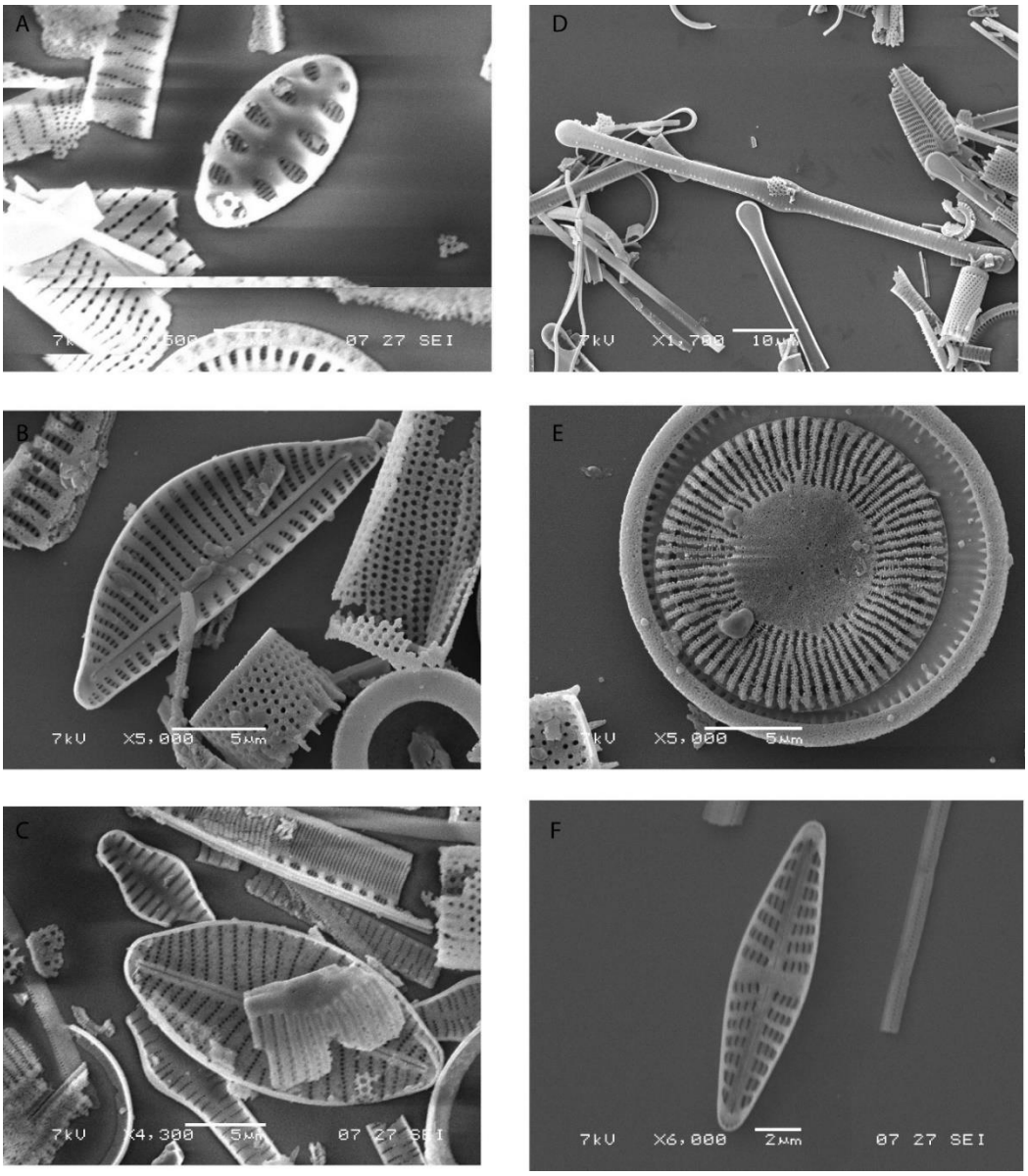

Figure 4.3: SEM images of diatom taxa observed in Lake Baunt sediments. **(A)** Staurosirella pinnata **(B)** Encyonema silesiacum **(C)** Placoneis clementis **(D)** Tabellaria flocculosa **(E)** Pantocsekiella ocellata **(F)** Hippodonta costulata.

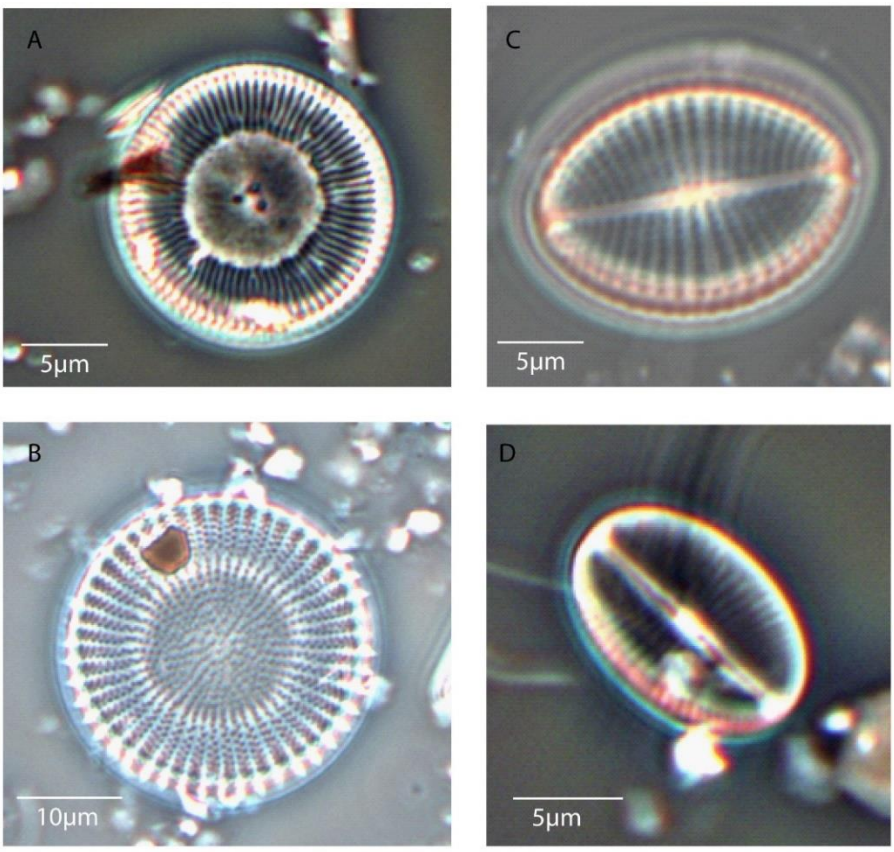

Figure 4.4: Light Microscope images of diatom taxa observed in Lake Baunt sediments. **(A)** *Pantocsekiella ocellata* **(B)** *Stephanodiscus alpinus* **(C)** *Khursevichia jentzschii* **(D)** *Cavinula jaernefeltii.*

Figure 4.5 documents the relative percentage diatom assemblage record for Lake Baunt, against depth, including all species which make up a minimum of 2% of the assemblage. The diatom flux, quantified dissolution and planktonic benthic ratio is also shown. The record has been divided into 6 diatom assemblage zones (DAZ's) (see figure 4.5/4.6), based on the shifts identified in the PCA (see section 4.2.2). Figure 4.4 documents the same data against age, highlighting that the assemblage covers the period ~29.0-6.2 ka BP based on the final age model presented in chapter 3. Figure 4.6 documents the >2% assemblage as flux data.

4.3.1 DAZ 1 – ~ 29.0 – 22.5 ka BP

DAZ 1 shows a clear dominance of *Pantocsekiella ocellata* (Pantocsek) K.T.Kiss and E.Ács, with values starting around 60% and gradually rising to approximately 80% by ~24 ka BP (figure 4.6). The zone also documents

consistent, low values (<10%) of several benthic species, including *Pseudostaurosira brevistriata* (Grunow) D.M.Williams and Round, *Staurosira pseudoconstruens* (Marciniak) Lange-Bertalot, *Planothidium lanceolatum* (Brébisson ex Kützing) Lange-Bertalot, *Encyonema silesiacum* (Bleisch) D.G.Mann and *Cavinula jaernefeltii* (Hustedt) D.G.Mann & A.J.Stickle. *Staurosirella pinnata* (Ehrenberg) D.M.Williams and Round is documented in higher levels (~20%) at the start of the zone, declining to ~10% by ~24 ka BP. The PCA first axis sample scores (see figure 4.6) are stable across this zone, highlighting limited change. The diatom flux across this zone is low, with some dissolution being identified (see figure 4.6). BVAR are low throughout this zone, although there is a peak of ~5751 $\mu m^3 cm^{-2} yr^{-1}$ at ~25.9 ka BP, which is driven by rapid increases in sedimentation rate at this time (see figure 3.18).

4.3.2 DAZ 2 – ~ 22.5 – 20.5 ka BP

Zone 2 shows a rapid shift from the assemblage seen in DAZ1 (section 4.3.1) (see Fig). *P. ocellata* drops to below 40%, while *Aulacoseira granulata* (Ehrenberg) Simonsen rapidly becomes the dominant species, with levels reaching around 60%, with a peak of 84.5% at ~22 ka BP. All the benthic species discussed in DAZ1 show reductions across this zone, while *Tabellaria flocculosa* (Roth) Kützing, *Stephanodiscus alpinus* Hustedt in Huber-Pestalozzi and *Achnanthidium minutissimum* (Kützing) Czarnecki, show small peaks during this zone. Large shifts are documented in the PCA here, with a change from 2 to -0.05 between ~22.5-22.3 ka BP, and a further shift at the end of the zone from -1.2 to 2.5 at ~20.5 ka BP.

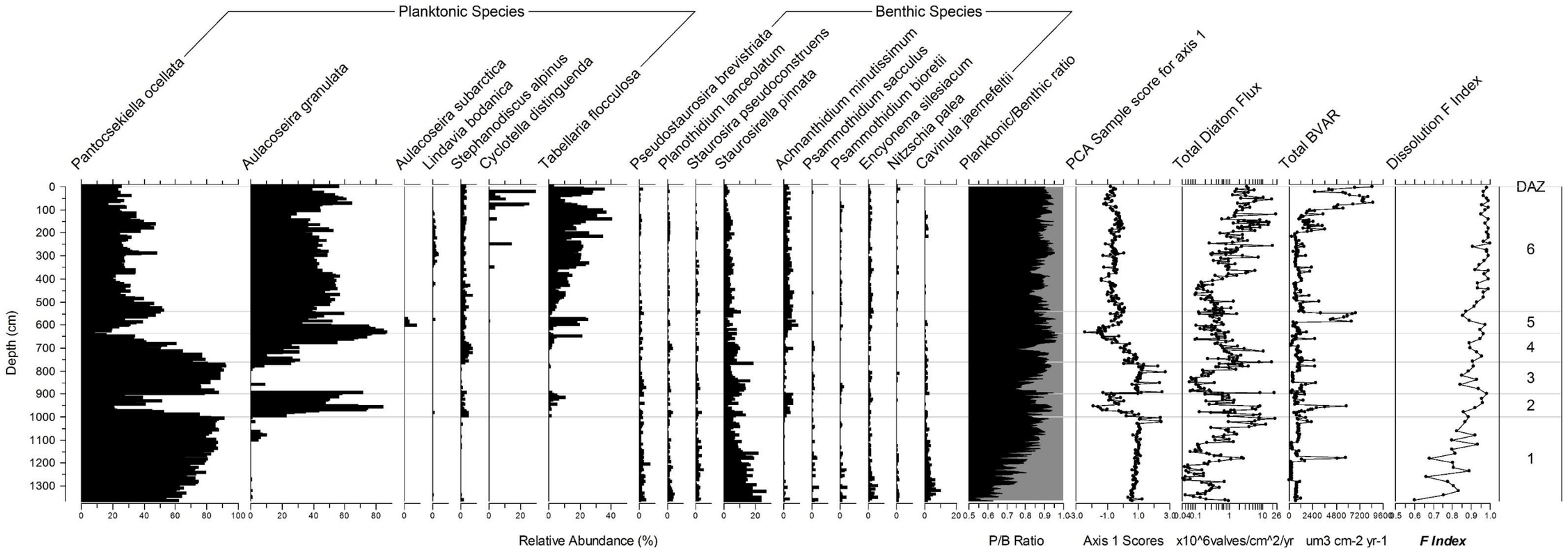

Figure 4.5: Diatom Stratigraphy for Lake Baunt (BNT14) shown as relative abundances against depth (cm). Rare species <2% have been removed. Planktonic Benthic Ratio, PCA Axis 1 Sample Scores, Total Diatom Flux (x10^{6}valves/cm^2/yr) shown on a logged x-axis, total Biovolume accumulation rate (BVAR) (µm^{3}cm^{-2}yr^{-1}) and the Dissolution *F* index are also shown.

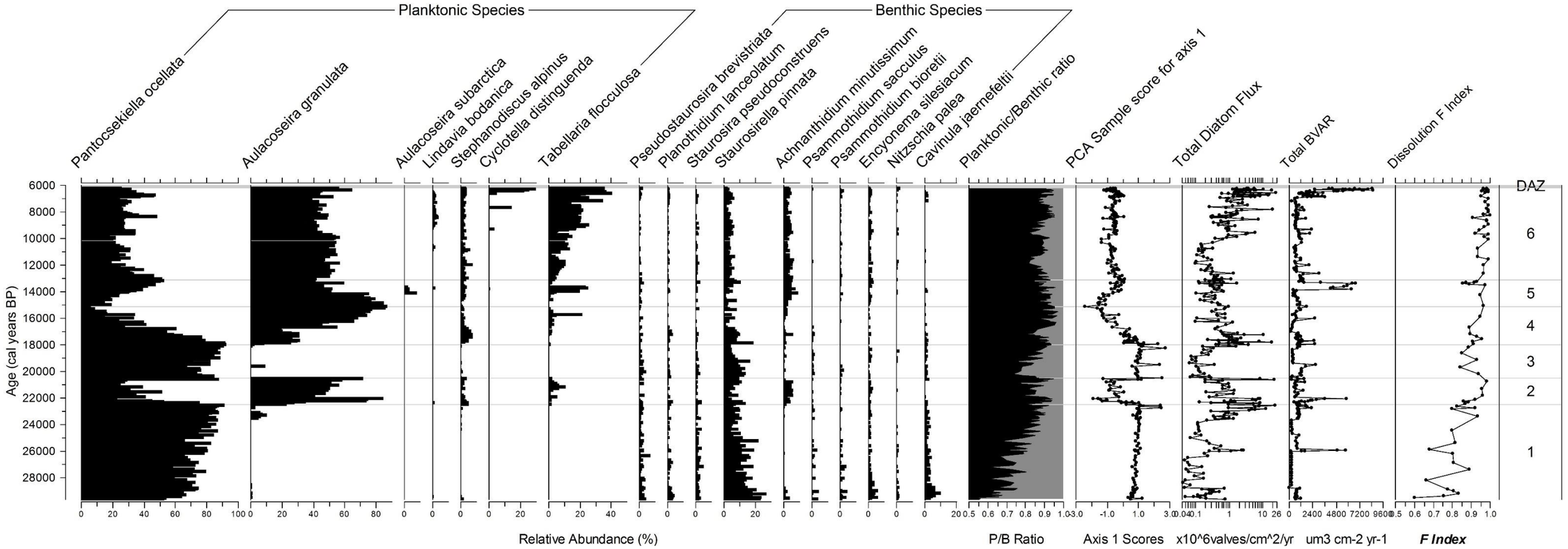

Figure 4.6: Diatom Stratigraphy for Lake Baunt (BNT14) shown as relative abundances against age (years BP). Rare species <2% have been removed. Planktonic Benthic Ratio, PCA Axis 1 Sample Scores, Total Diatom Flux (x10^{6}valves/cm^2/yr) shown on a logged x-axis, total Biovolume accumulation rate (BVAR) (µm^{3}cm^{-2}yr^{-1}) and the Dissolution *F* index are also shown.

4.3.3 DAZ 3 – ~ 20.5 – 18.0 ka BP

The third assemblage zone shows a return to an assemblage similar to that recorded in DAZ1, with a dominance of *P. ocellata*, although benthic species remain in lower levels. *S. alpinus*, *T. flocculosa* and *A. minutissimum* all become absent in this zone. PCA sample scores all shift back towards values more similar to those seen earlier in the record. BVAR return to lower values generally <1000 $\mu m^3 cm^{-2} yr^{-1}$, while the *F* index highlights limited dissolution. Diatom flux peaks are observed at the transitions between DAZ2 to DAZ3 and between DAZ 3 to DAZ4.

4.3.4 DAZ 4 – ~ 18.0 – 15.1 ka BP

DAZ4 documents a more gradual transition where *P. ocellata* declines and *A. granulata* increases to a peak of 88% at ~15.1 ka BP. *S. alpinus* and *T. flocculosa* reappear in the record, while benthic values remain low, despite a slight peak in *S. pinnata* at the start of the zone around ~17.5 ka BP. *T. flocculosa* has a rapid (1 sample) peak at ~15.7 ka BP. Diatom biomass rises gradually across the zone, while fluxes show peaks at ~17.7 and ~17.2 ka BP. The PCA axis one sample scores document gradual decline across this period.

4.3.5 DAZ 5 – ~15.1 – 13.1 ka BP

Assemblage zone 5 starts with a rapid decline in *A. granulata,* with a corresponding rise in *P. ocellata* to a peak at ~ 13.1 ka BP. *S. alpinus* and *S. pinnata* are present in stable values through the zone, while *T. flocculosa* documents a short-term peak at ~ 14.0 ka BP. *A. minutissimum* is present in larger quantities in this zone. Diatom biovolumes decrease down this zone, while diatom flux is relatively stable. PCA scores increase gradually across the zone.

4.3.6 DAZ 6 – ~ 13.1 – 6.2 ka BP

The uppermost zone of the Baunt record shows more stable values of *P. ocellata* and *A. granulata*, although slight fluctuations are seen. Throughout this zone *T. flocculosa* undergoes a gradual increase. *S. alpinus*, *S. pinnata* and *A. minutissimum* are stable across this section. *Lindavia bodanica* (Eulenstein ex Grunow) T.Nakov, Guillory, Julius, Theriot &

Alverson, appears in its most consistent quantities during the upper section of this zone, while *Encyonema silesiacum* (Bleisch) D.G.Mann has a consistent presence across this zone. Species biovolumes fluctuate and diatom fluxes document large peaks at ~6.7-6.5 and ~6.3 ka cal BP. The PCA axis 1 scores are also more stabilised across this zone, although as with the diatoms, slight fluctuations are present.

4.3.7 Diatom Fluxes and Biovolume

Figure 4.7 shows the diatom flux data for the main species found in Lake Baunt against time, and the diatom zones outlined above. Additionally, the biovolume accumulation rates (BVAR) are shown for *P. ocellata* and *A. granulata* and then for all diatoms. The data are plotted on an x axis log scale to allow the variability in the minor assemblages to be discussed in relation to the dominant species. In zone 1 (~29.6-22.5 ka BP) benthic species and *P. ocellata* co-vary but other planktonic species show no real change, apart from the end of the zone when the majority of the diatoms show an increase in flux from ~23.5 ka BP. The BVAR across this zone are relatively low, except at ~25.9 ka BP, where they rise to ~5000 $\mu m^3 cm^{-2} yr^{-1}$ due to a change in sedimentation rate. In zone 2 the greatest change is a rise in both *A. granulata* and *S. alpinus* to ~5 and 0.1 respectively. This change is accompanied by a shift to high BVAR, reaching 5826 $\mu m^3 cm^{-2} yr^{-1}$ at 22 ka BP. In the third zone these two species show a reduced flux and there is relatively little change across the other species, while BVAR are also lower. The onset of zone 4 shows a rapid change in the diatom flux seen across all species, and this is centred around 17 ka BP, with total diatom flux reaching 19 $x10^6$ valves/cm^2/yr at 17.8 ka BP. In zone 5 there is little variability across most of the species fluxes, however the total BVAR and *A. granulata* BVAR show a large shift at ~13.3 ka BP, which reaches a total biovolume of 6832 $\mu m^3 cm^{-2} yr^{-1}$. Zone 6 documents little variability in the first 2-3k of the zone until ~ 10 ka cal BP, after which increases are observed in the fluxes of most taxa. BVAR are generally lower in this zone but increase rapidly during the latter sections. Care must be taken when considering the biovolume taxa, as median values have been used, however, the upper and lower values in table 4.1, highlight there is a wide range in both species biovolume ranges.

Species	***A. granulata* (µm^3)**	***P. ocellata* (µm^3)**
Median Biovolume	339.1	95.8
Mean Biovolume	364.3	144.2
Upper Biovolume	3692.6	2103.5
Lower Biovolume	62.8	21.5

Table 4.1: Biovolume size ranges for *A. granulata* and *P. ocellata.*

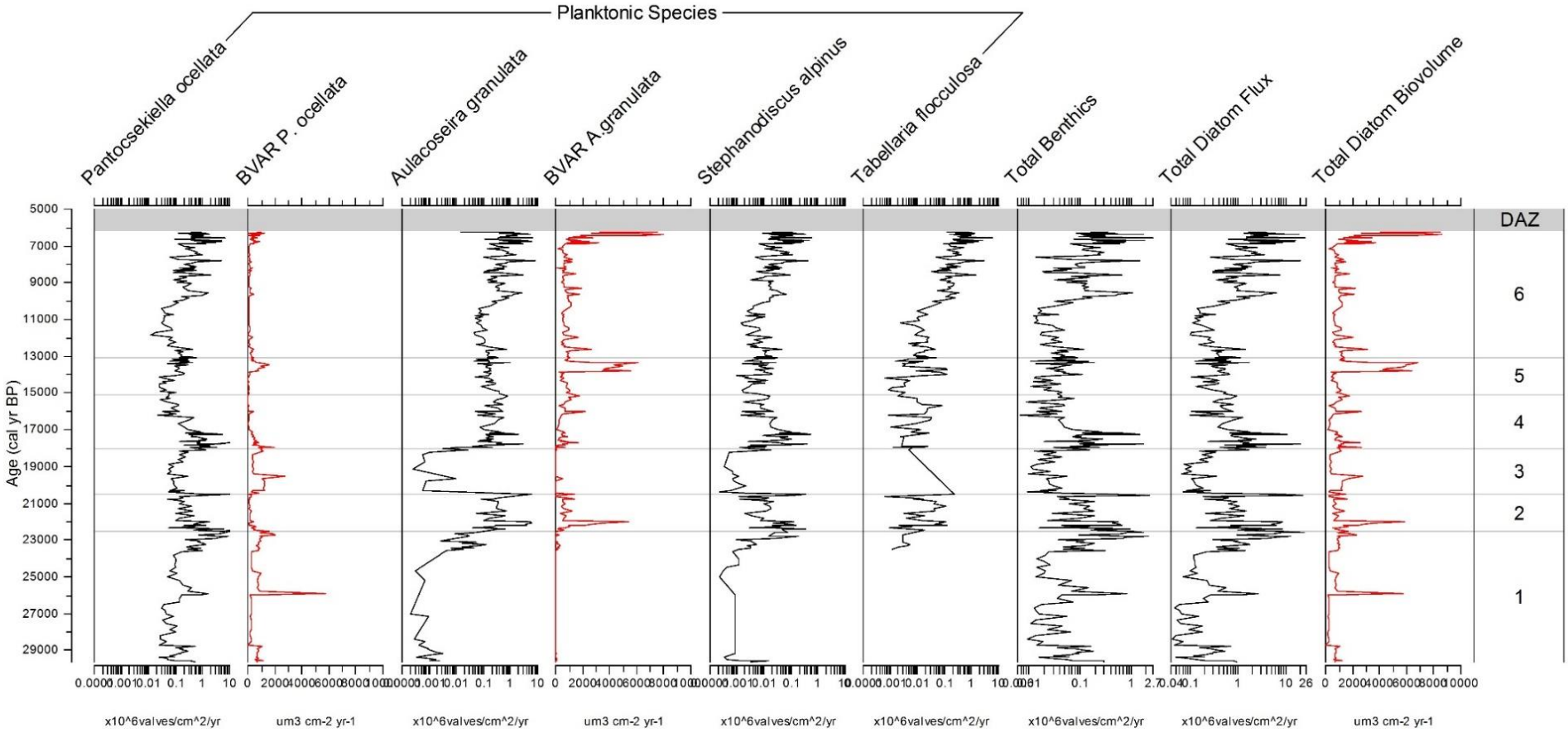

Figure 4.7: Diatom fluxes summary. X-axis is on a Log scale to draw out less abundant species changes.

4.3.8 Functional Groups

Figure 4.8 documents the results of the main functional group classifications, while table 4.2 shows how the taxa present in above 2% have been classified. Figure 4.9 highlights the dominance of planktonic species across the core, as a result of the dominance of *P. ocellata* and *A. granulata* in the diatom assemblage. The dominance of these two species, even when grouped with additional species in the Baunt record is clear, with PS2 reflecting changes in *P. ocellata,* while PS3 reflects *A. granulata* changes (see figure 4.9). Low profile, high profile and motile species are limited throughout the core, however, they have higher relative proportions at the base of the core.

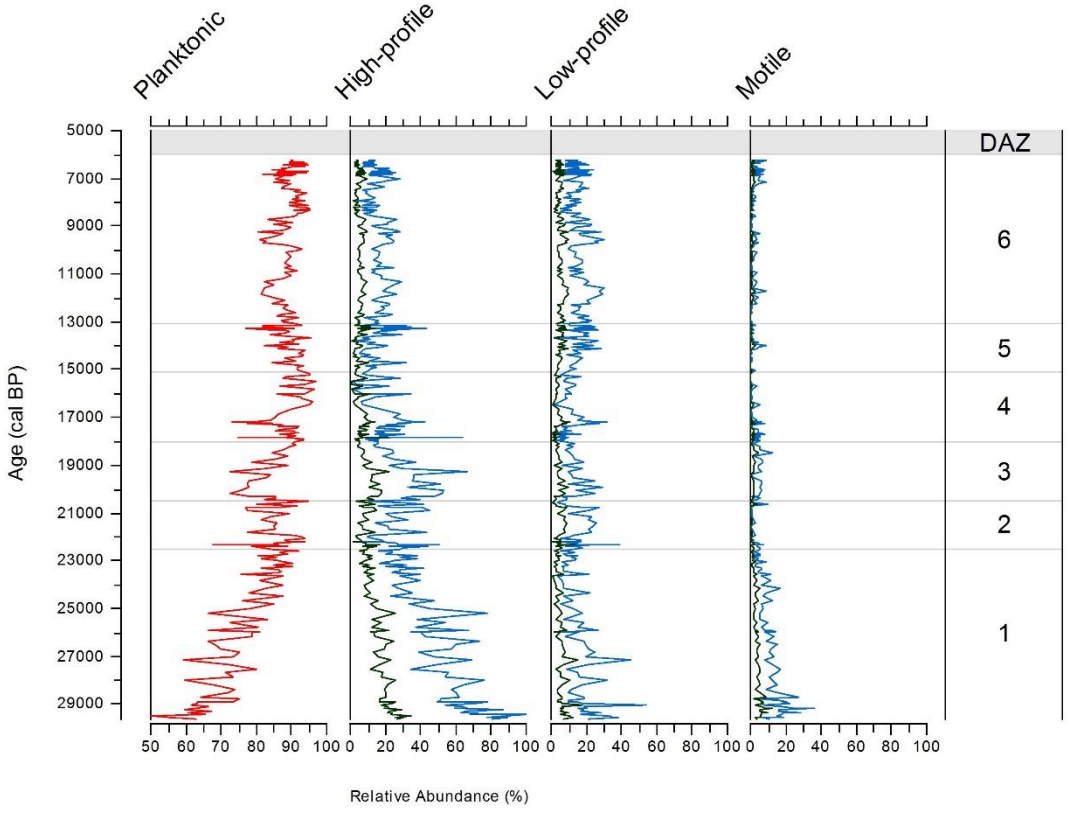

Figure 4.8: Lake Baunt main Functional Groups (species sizes grouped) against age. High-profile, Low-profile and motile species also show a x3 exaggeration line (blue).

Species	Classification	Basic Species Information
Psammothidium bioretii	LS2	Slight motile, solitary species, attachment by mucilage pad.
Achnanthidium minutissimum	LS1	Slightly motile species with attachment by mucilage pad (prostrate).
Psammothidium sacculus	LS2	Non-motile.
Aulacoseira granulata	PS3	Non motile, common in colonies, unattached planktonic species.
Aulacoseira subarctica	PS3	Non motile, common in colonies, unattached planktonic species.
Lindavia bodanica	PS4	Non motile, solitary, unattached, planktonic species.
Cyclotella distinguenda	PS3	Non motile, solitary, unattached planktonic species.
Pantocsekiella ocellata	PS2	Planktonic solitary species.
Encyonema silesiacum	HS2	Often attached in mucilage tubes.
Cavinula jaernefeltii	MS2	Motile species.
Nitzschia palea	MS2	Moderately motile species, attachment by mucilage pad. Pedunculate.
Planothidium lanceolatum	LS1	Solitary, low profile benthic species.
Pseudostaurosira brevistriata	HS1	Non-motile species, attachment vertically by stalks. Colonies common.
Staurosira pseudoconstruens	LS1	Non-motile, occasional colony forming species, attachment by prostrate mucilage pad, but also unattached. Low profile species.
Staurosirella pinnata	HS1	Non-motile species that can attach vertically using stalks.
Stephanodiscus alpinus	PS3	Planktonic species, unattached life form. Non-motile.
Tabellaria flocculosa	PS2	Non motile species, common in colonies. Attachment by mucilage pad.

Table 4.2: Main diatom species from Lake Baunt shown against their functional group classification alongside basic information about the species. Classifications were based on Passy (2007) and Béres *et al.*, (2017).

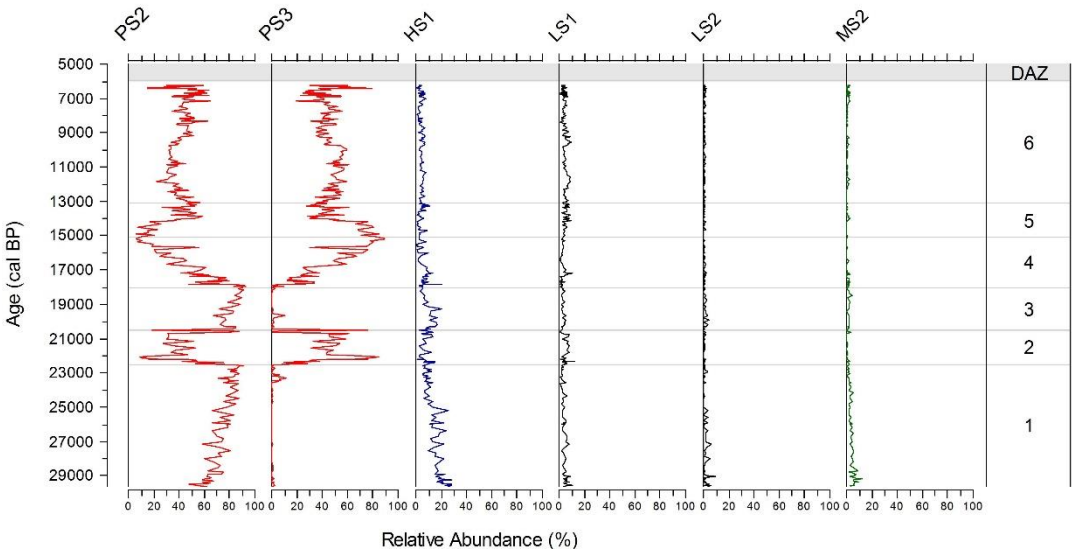

Figure 4.9: Key Functional Groups shown in sizes ranges (1-5) for Lake Baunt.

4.4 Discussion

The Lake Baunt diatom assemblage shows a high-resolution record of palaeolimnological change, from ~29 ka BP, through to the mid-Holocene. Caution is needed when examining this upper section due to the potential hiatus at the top of the core, as discussed chapter 3. As a result of this, the mid Holocene period is carefully considered and, where necessary, it is studied against depth. Additional caution is also required when considering the record, due to radiometric dating uncertainties, which means shifts in the assemblage can have large ranges, particularly towards the base of the core. These are quantified where relevant, with particular care needed in the sections around 5.0m and 10.0-11.0m, where errors are in excess of ±800 and ±1000 years (95% confidence), respectively. This makes linking changes in the diatom assemblage to shifts in other records at these times more tentative, and further dating work is recommended, to improve this in the future.

4.4.1 Integrity of the diatom record

Estimation of the extent of dissolution of the dominant taxa, highlights that diatoms from Lake Baunt are generally very well preserved. The oldest sections of the core show the highest quantities of dissolution, however, most cells are still considered as pristine with high *F*-index scores (Fig 4.4) down the whole core profile (Flower and Ryves, 2009; Ryves *et al.*, 2001). The

average *F*- index for the major taxa across the whole core is 0.91 ± 0.083, and the average for the oldest 10,000 years, overlapping broadly with the LGM, has an *F*- index of 0.84, which is within 1s.d. of the group mean. It could be that the dominance of *P. ocellata* in the older sections of the core could be a result of other delicate species being dissolved, however, non-pristine frustules in the older zones were generally only quantified as stage 2 'little dissolution', and it would be expected that more frustules would be classified in stages 3-4 'very dissolved to almost unrecognisable' if dissolution was severely affecting the assemblage, and causing this bias. Additionally, *P. ocellata* is a small species with high surface area, and, thus, is quite susceptible to dissolution itself (Barker *et al.,* 1994), so it is interesting that valves of this taxon are generally very well preserved. This indicates that the diatom assemblage from Lake Baunt does not suffer with any significant species bias, and this, therefore, allows sound palaeoenvironmental considerations to be undertaken from the data. The excellent preservation in Baunt may result from several site-specific factors. Firstly, site pH, which for Baunt is 7-7.2, with the minor range being driven by seasonality. Thus, Baunt has a neutral pH and is, therefore, good for biogenic silica preservation, with high pH ranges (>pH9) most associated with biogenic silica dissolution in freshwater lacustrine environments (Barker *et al.,* 1994). Secondly, temperature is also a significant factor, which may have been buffered around Lake Baunt due to its close proximity to geothermal springs (Solotchin *et al.*, 2015), and this may have allowed a more stable thermal range and also limit ice cover and ice-melt induced erosion. Taken together this may enhance preservation, despite the continental conditions that occur in Siberia. Salinity is an additional factor that can affect diatom dissolution (Ryves *et al.*, 2006) and for Baunt, the water chemistry, diatom species mix, and non-evaporative nature of the lake suggest it is a very freshwater environment, and, thus, less susceptible to dissolution. It must, however, be noted that levels of dissolution were quantified under the light microscope, whereas had quantification been undertaken using an SEM it may have been easier to detect dissolution characteristics (see figure 4.10), and, therefore, the extent of pristine valves may have been lower. Despite this, the low quantities under the light microscope give confidence that dissolution is not inducing large changes in

the assemblage, allowing a reasonable level of confidence that the ecological data derived from the Baunt assemblage is not being biased by dissolution.

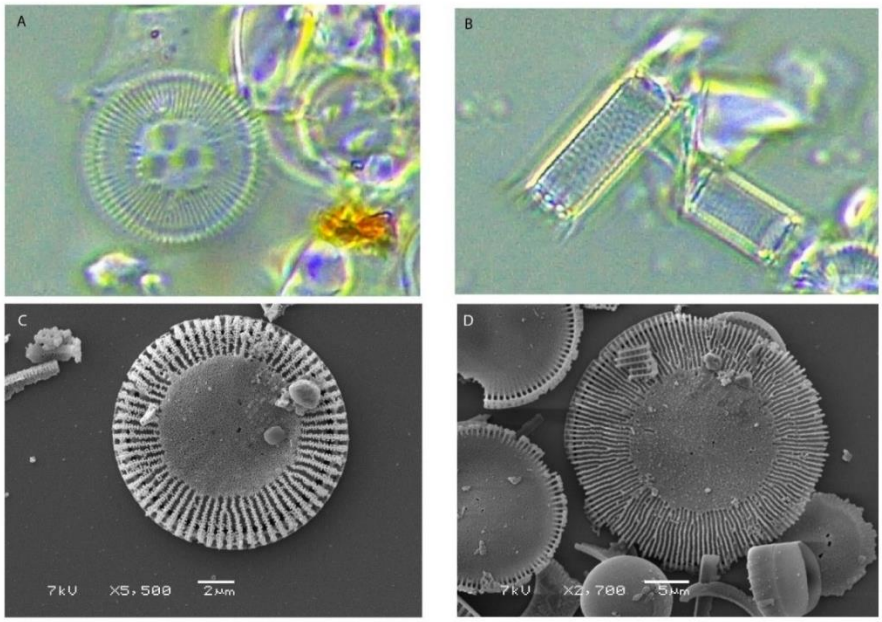

Figure 4.10: (A + B): Light microscope images showing vision achievable for quantifying dissolution against **(C + D)**, showing frustules under the SEM where dissolution is much easier to detect.

The excellent preservation of diatoms in Lake Baunt is one reason for the limited number of taxa, which are not able to be assigned to a species. The few of these that have not been able to be assigned in the Baunt record are not considered to be highly detrimental to the interpretation of the assemblage, as they all make up <2%. The Lake Baunt diatom record also benefits from high quantities of cosmopolitan taxa, which are well documented in many sites (e.g. Edlund *et al.*, 2003; Genkal and Popovskaya, 2008b; Kilham and Kilham, 1975; Kostrova *et al.*, 2014; Lamb *et al.*, 2005; Prokopenko *et al.*, 2007), allowing identifications to be made robustly. Despite this, one dominant species, *P. ocellata* shows significant morphological variability, and this will be explored further in section 4.4.3.

4.4.2 Functional Groups

Figure 4.8 documents the dominance of planktonic species in the functional groups from Lake Baunt. This is primarily due to the dominance of *A. granulata*

and *P. ocellata* in the diatom assemblage. The key changes in the planktonic group are driven by proportional changes between two size ranges (PS2: 100–299μm^3 and PS3: 300–599μm^3 (based on median biovolumes)). The changes between larger and smaller planktonic species is likely to suggest that conditions are altering to support larger species at certain times. This is likely to be linked to changes in turbulence, with increased turbulence supporting larger species to remain in the photic zone (Winder and Hunter, 2008), while increased nutrients may also be required to support the larger planktonic species during their periods of dominance (Kilham *et al.*, 1986, 1996).

Other than the dominance of planktonic species, the functional group's higher proportion of high-profile species e.g. tall stature species (Passy, 2007b), in the lower section of BNT14, suggest steady environmental conditions, as these species are very sensitive to disturbances, including flow conditions, so it is likely that the base of the core records a period of low turbulence, potentially with limited overturning (Passy, 2007b; Stenger-Kovács *et al.*, 2013), and this potentially supports the suggestion that turbulence is influencing the planktonic species, as the period with high proportions of high-profile taxa occurs alongside high proportions of smaller PS2 planktonic species, which may indicate that lake conditions are less turbulent at this time, preventing larger planktonic species being able to remain in the photic zone.

4.4.3 Morphological variability of *Pantocsekiella ocellata*

P. ocellata is a complex species (Cremer and Wagner, 2003). This is primarily due to the wide morphological variability that this species shows (Cherepanova *et al.*, 2010; Cremer and Wagner, 2003; Duleba *et al.*, 2015; Genkal and Popovskaya, 2008), which means it has also been considered as a species complex (Cremer and Wagner, 2003; Duleba *et al.*, 2015), potentially incorporating several species (Cremer and Wagner, 2003). *Cyclotella comensis, Cyclotella rossii* and *Cyclotella Krammeri*, (Cremer and Wagner, 2003; Hegewald and Hindáková, 1997; Udovič *et al.*, 2017) are often incorporated into this complex, although *Cyclotella tripartita* and *Cyclotella kuetzingina* have been included in other studies (Genkal and Popovskaya, 2008). The range of variability, with many intermediate forms across this

complex, is considered to mean that splitting the morphotypes under a light-microscope is unfeasible (Knie and Hübener, 2007).

It has been suggested that these morphological variations may be the result of the lake environment, with large initial cell sizes in Lake Hovsgul being linked to favourable conditions (Genkal and Popovskaya, 2008), while others have suggested that morphological changes are a result of climate change. For example, in Lake El'gygytgyn, Cherepanova *et al.,* (2010), suggested that certain morphotypes of *P. ocellata* are favoured at certain periods, with the *P. ocellata-ocellata* morphology replacing the *P. ocellata-kuetzingina* morphotype during the Late Pleistocene, as a result of changes in the waters conditions (e.g. temperature and nutrient changes), driven by palaeoclimatic shifts (Cherepanova *et al.*, 2010).

The morphological variability of *P. ocellata* in Lake Baunt is shown in figures 4.11 and 4.12. Cell sizes range considerably in Lake Baunt (~4-30µm), as documented in other sites (Cherepanova *et al.*, 2010), however caution must be taken when considering size variations as evidence of different morphologies, as vegetative replacement drives cell size reductions from the initial cell, which can make these cells up to three times smaller (Perez-Martinez *et al.,* 1992; Cherepanova *et al.*, 2010). Additionally, cell size changes in diatoms can also be linked to water conditions, with lowered silica supply driving smaller cell sizes being associated with reduced precipitation and runoff (Jewson, 1992)**.** The size variations across *P. ocellata* in Baunt could reflect changes in the regional precipitation and the nutrients being washed into the lake. The large range in *P. ocellata* size in Baunt does not, however, show any clear trend across the record, with the wide range documented across the core.

Alongside the wide-ranging sizes, variations documented in Baunt include valve relief, central area diameter, and the arrangement of rimoportulae. This morphological variability is potentially the reason that *P. ocellata* is found in many sites, and this has led to it being considered to have uncertain ecological characteristics (Cremer and Wagner, 2003). It appears to thrive in a range of environments, suggesting tolerance across broad ecological conditions, from

ultra-oligotrophic, as seen in Lake El'gygytgyn (Cremer and Wagner, 2003), to meso- and eutrophic conditions in British Columbia (Canada) (Cremer and Wagner, 2003; Cumming *et al.*, 1995). It is thought to be able to thrive in silicate poor waters (Perez-Martinez *et al.,* 1992), and this is partly due to its small size.

The morphological variability seen in *P. ocellata* (see figures 4.11 and 4.12), is, therefore, not unexpected and may reflect the occurrence of a species complex within the lake. As further work is carried out, it is likely that the morphological variations of the *P. ocellata* morphotypes will become clearer and their ecologies will become better constrained. Despite these issues, *P. ocellata* is still able to inform about paleoenvironmental and palaeoclimatic shifts within Lake Baunt, as its ecological information is considered alongside that of the other key other taxa from Baunt, allowing it to assist palaeolimnological understanding.

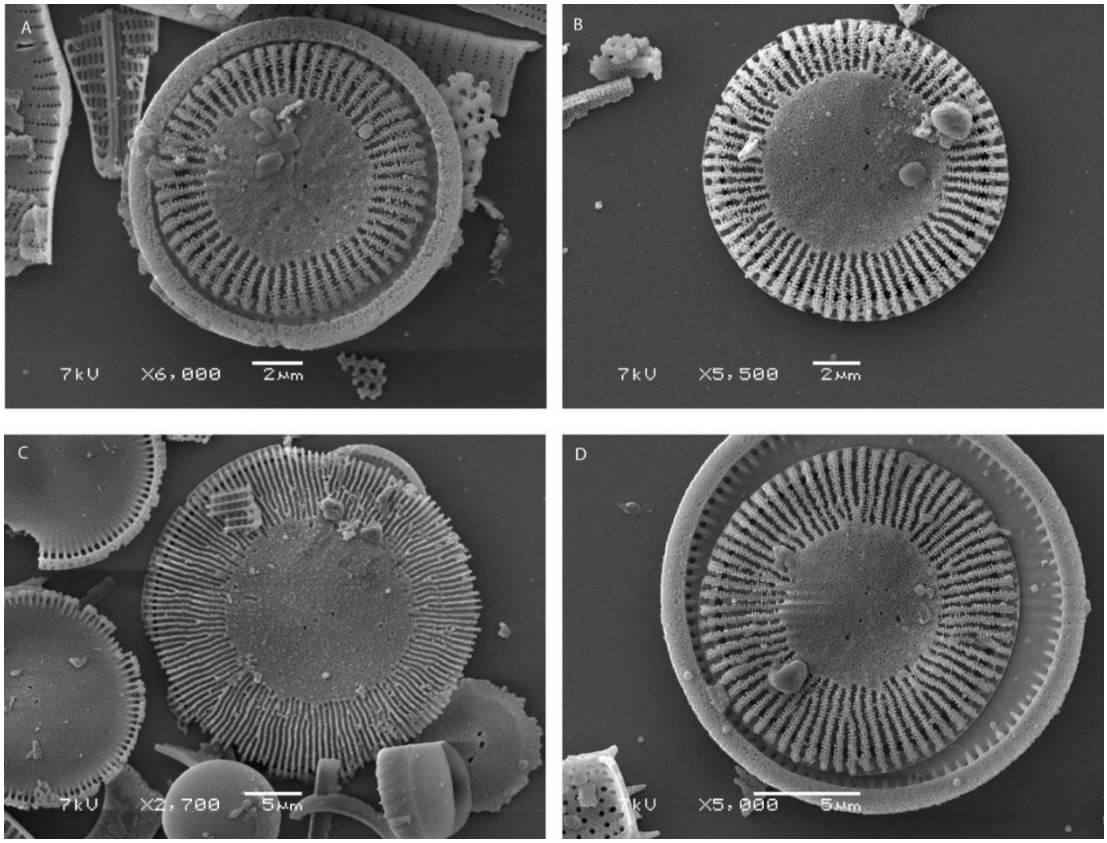

Figure 4.11: Scanning Electron Microscopy (SEM) images of *P. ocellata* from Lake Baunt sediments.

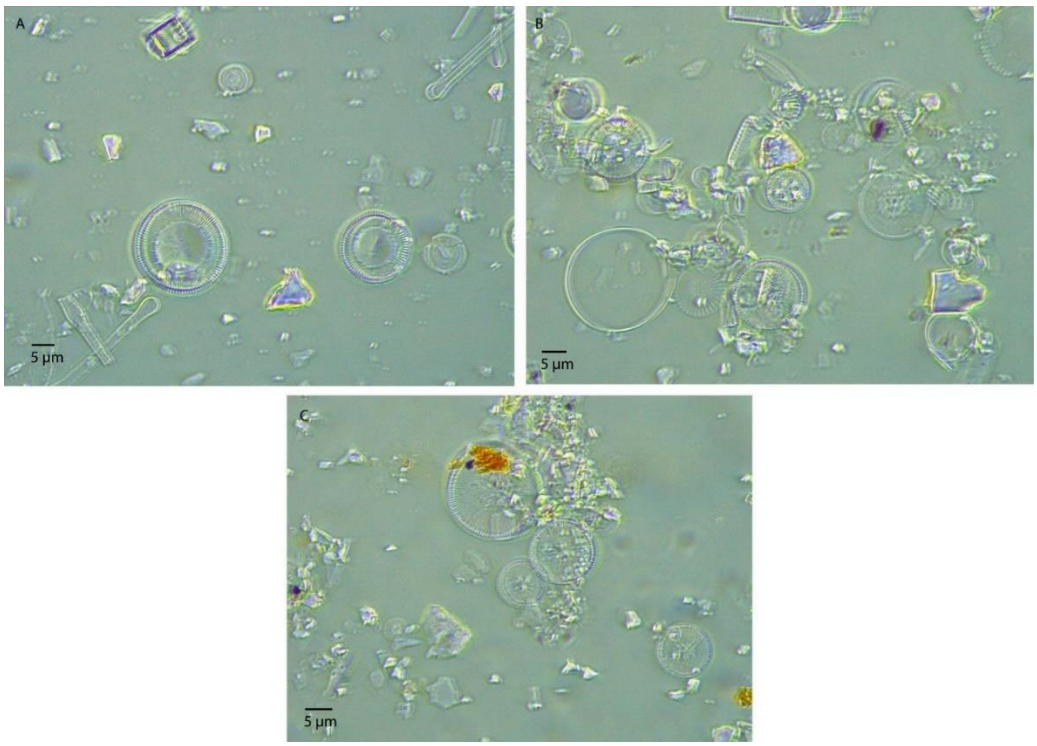

Figure 4.12: Light Microscope Images of *P. ocellata* from varying depths of Lake Baunt sediments - **(A)** 0.75m **(B)** 7.08m and **(C)** 8.18m.

4.4.4 Morphological variability of *Tabellaria flocculosa*

T. flocculosa, like *P. ocellata*, includes a wide range of morphologies (Koppen, 1978, 1975), with three morphotypes existing . The *T. flocculosa* species from Lake Baunt are thought to be predominantly the IIIp strain, due to their long lengths, which reach over 83µm in many cases, however, there is some caution with the interpretation of *T. flocculosa,* as distinguishing these forms is difficult (Koppen, 1978). If none of the frustules were over 83µm, these species would have been classified as benthic strain III (Koppen, 1978, 1975). Additionally, although *T. flocculosa* is known to be colony forming, in its planktonic form, it is not expected that more than 5 cells will be found in a stellate colony (Koppen, 1975). In Baunt, it may be that there is a mix of groups III and IIP, as apart from differences in length, both types have with marginal spines, and ~14-17 striae per 10µm, although IIIp has fewer intercalary bands, and this means that caution should be applied when considering this species as a purely planktonic form (Koppen, 1975). Figure 4.13 documents the varying morphologies identified by Koppen (1975), while figure 4.14 highlights a *T. flocculosa* species from Baunt. This highlights the clear similarities between morphotypes of *T. flocculosa* and demonstrates that strain III is the most appropriate classification of these species in Baunt.

Figure 4.13: Plates of *T. flocculosa* taken from Koppen, 1975 (p.241 figures 30-45) taken under x1000 magnification, except for figure 46, which is x430. Figures 37-43 highlight strain IIIp, while 45, shows strain IIIp in a colony in girdle view. 44 shows strain II in girdle view.

Ecologically there are slight differences in the environments preferred by the different strains of *T. flocculosa,* with strain III (including subset IIIp) considered to have the widest tolerances, although the species are generally considered to be cosmopolitan. Their widespread distributions may be due to the range in their morphologies, which may allow them to thrive in varied environments.

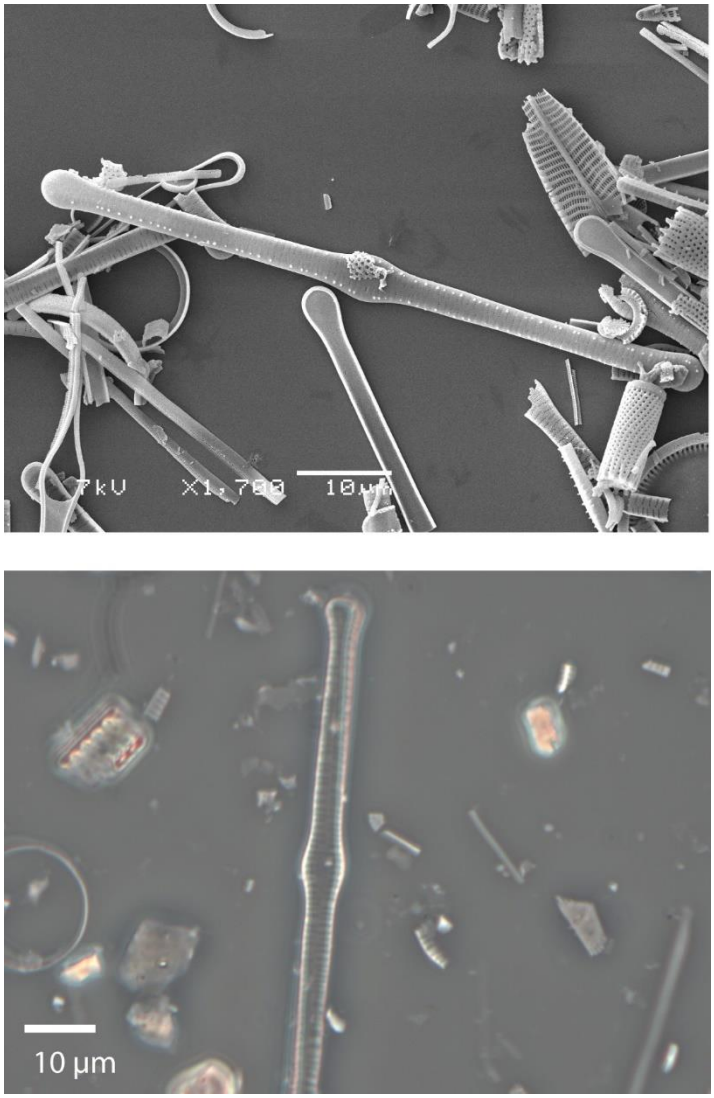

Figure 4.14: *T. flocculosa* found in Lake Baunt under SEM and Light-Microscope.

4.4.5 The Diatom Assemblage

Of the 290 species identified from the sediments of Lake Baunt only 17 species make up over 2% each of the assemblage. Understanding the ecological

information from the more dominant of these species is essential, allowing consideration of the drivers of the assemblage shifts documented by the DAZ's. Table 4.3 provides key ecological information for the most prominent of these species from the BNT14 record.

The Lake Baunt diatom assemblage shows a high-resolution record of palaeolimnological change, from ~29 ka BP, through to the mid-Holocene (~6 ka BP). The diatom assemblage changes will now be considered against additional Lake Baunt data (TOC and BSi) (see figure 4.15), and potential external drivers of change (figure 4.16)

4.4.5.1 The Middle and Late Pleniglacial, Heinrich 2 and the Last Glacial Maximum

The boundary between MIS3 and MIS2 is often placed around ~29 ka BP (LR04) (Lisiecki and Raymo, 2005), however, there is some debate that is could begin as late as 24 ka BP (Tzedakis *et al.*, 2013), and, therefore, the earliest part of the Lake Baunt record, from ~29 ka BP, is considered to cover the transition between the more unstable MIS3 to the more stable period of early MIS 2. This period of late MIS3 and early MIS2 encompass Heinrich Event 2 and the Last Glacial Maximum (LGM) between ~26-21 ka BP (Lisiecki and Raymo, 2005), although the timing of the local response can vary within an individual region (Clark *et al.*, 2009). In Siberia, the timing, nature and duration of ice extent has been debated (Clark and Mix, 2002), with potentially later maximum ice extent than further west, but the LGM is broadly defined in the Transbaikal region as 24.6-22.9 ka BP (Kostrova *et al.*, 2014). The period covered by late MIS3 and early MIS2 in the Baunt diatom assemblage (see figure 4.15), is one of the most stable periods over the past ~30 ka BP. This stability is also documented in the BSi and TOC records, suggesting that the system is potentially relatively unproductive for much of the last glacial period. Diatom fluxes and BVAR for the dominant species are low across this period, again suggesting a period of very low primary productivity. Low diatom productivity may explain the higher quantity of dissolution seen in this section, with processes leading to dissolution acting with greater pressure on the fewer valves present.

The climate around Lake Baunt is heavily influenced by the relative strength of the Siberian High (Park *et al.*, 2014; Tubi and Dayan, 2013). This GISP2 K+ (potassium) signal (see figure 4.16) is thought to provide a record of Siberian High strength changes (Mayewski *et al.*, 2004), and this shows that during the LGM, Siberian High strength is at its highest for the whole period covered by the Baunt assemblage. Towards the end of this period, the GISP2 record shows particular strengthening of the Siberian High, which is likely to be due to Heinrich 2, which occurs ~25 ka BP (Cascalheira, 2013). It also occurs at a time when solar insolation (figure 4.16) declines to its lowest values. These forcings are suggestive of intensified cold conditions, potentially with limited precipitation, as a result of the blocking high (Park *et al.*, 2014; Tubi and Dayan, 2013). This data supports the idea of limited productivity in the Lake Baunt system during this period, indicated by the low TOC, BSi and restricted species within the assemblage.

These external forcings also support the diatom evidence for cool and arid conditions across this period. Despite difficulties in identifying *P. ocellata, as* discussed in section 4.4.3, this species is tolerant of low nutrient conditions, assuming that light availability is high. This species could, therefore, thrive in an unproductive environment, with limited nutrients. This is supported by low BVAR's, which indicate that algal productivity is limited, while low TOC may suggest limited in-washing, which, in turn, could ensure the clarity of the water. *P. ocellata* is also known, however, to develop under ice surfaces, provided solar insolation is able to be transmitted through the ice (Cherepanova *et al.*, 2010). This could, therefore, allow the species to survive in cold periods with long durations of ice cover, and accompanying arid conditions induced by a strong blocking Siberian High, ensuring high light conditions within Lake Baunt. DAZ1 (figure 4.6) corresponds to a cold arid period that corresponds broadly in time to the latter stages of MIS3 and the early stages of MIS2 (Lisiecki and Raymo, 2005), as well as the Northern Hemisphere expression of the LGM (Clark *et al.*, 2009) and Heinrich 2**.**

Diatom Species	Planktonic or Benthic	Ecological Information	Key References
Pantocsekiella ocellata	P	Small centric taxa, with wide ecological tolerances. Often associated with high light requirements, particularly in nutrient poor waters. Considered able to develop on ice surfaces, assuming ice can easily transmit solar rays under low humidity, and, thus, sometimes associated with lower temperatures. Slow sinking rates. Good competitor for nitrogen and always found in alkaline waters. Blooms across the summer season, with site specific variations. Discussed to have been favoured by erosion and soil leaching in some systems. This species shows significant morphological variability, which may explain the wide ecological tolerances.	Schmidt *et al.*, 2002; Cremer and Wagner, 2003; Edlund, *et al.,* 2003; Winder and Hunter, 2008; Cherepanova *et al.*, 2010; Duleba *et al.*, 2015; Malik and Saros, 2016; Pérez-Mejías *et al.*, 2017; Genkal and Popovskaya, 2008.
Aulacoseira granulata	P	A heavily silicified centric taxon that is associated with turbulent waters, to assist it to remain in the photic zone and to allow resuspension. Cells able to survive in a vegetative state on the lake bottom, before being resuspended and this assists them in avoiding nutrient limitation. Associated with nutrient rich waters (particularly silica and phosphorous) as a poor competitor for these nutrients. Tolerates low light conditions. Often considered to be thermophilic	Kilham and Kilham, 1975; Kilham, Kilham and Hecky, 1986; O'Farrell *et al.,* 2001; Lamb *et al.*, 2005; Reynolds *et al.*, 2006; Zalat and Vildary, 2007

		diatom as requires temperatures of 15°C, meaning it often blooms in the late summer, although it is also thought to bloom during overturning periods when mixing occurs (spring/autumn), due to increased nutrients being bought to the epilimnion and due to windiness. Preference for low conductivity waters with pH lower than 9. Often in moderate to high productivity waters.	
Tabellaria flocculosa	P	Species with 3 morphotypes. In Lake Baunt species are classified as strain IIIp, as species length ranges between 37-123µm. Colony forming species, often associated within increased water acidity. Has been linked to regions with snowmelt, bringing higher acidity water pulses to sites, but also documented to tolerate range of pH conditions. Cosmopolitan species, generally blooming in spring, with smaller autumn bloom.	McGowan *et al.,* 2017; Koppen 1975; Knudson and Kipling 1957; (Koppen, 1978)
Lindavia bodanica	**P**	Requires high water temperature if nutrients are in low concentrations, compared to other Cyclotella type species (e.g. *P. ocellata*).	Maliz & Saros, 2016
Stephanodiscus alpinus	**P**	*Stephanodiscus* requires high phosphorous but grows under low silica and light regimes. Often found in oligotrophic to mesotrophic lakes.	Kilham, Kilham and Hecky, 1986; Wunsam, Schmidt and Klee, 1995
Staurosirella pinnata	**B**	A pioneer species, found in sites with cold conditions, short open water seasons and high erosion. Influenced by changes in pH,	McGowan *et al.*, 2017; Finkelstein and Gajewski,

		summer water temperatures and dissolved organic carbon concentrations of the lakewaters.	2008; Kostrova *et al.*, 2014; Schmidt *et al.* 2004.
Achnanthidium minutissimum	**B**	Considered as an alkaliphilous species, an early coloniser, resistant to disturbance including lake level changes, low nutrients, sheer stress and a high affinity for Na^+ dominated lakes.	Koivo and Seppälä, 1994; Riato *et al.*, 2017

Table 4.3: Ecological Information concerning the main diatom species preserved in sediments from Lake Baunt.

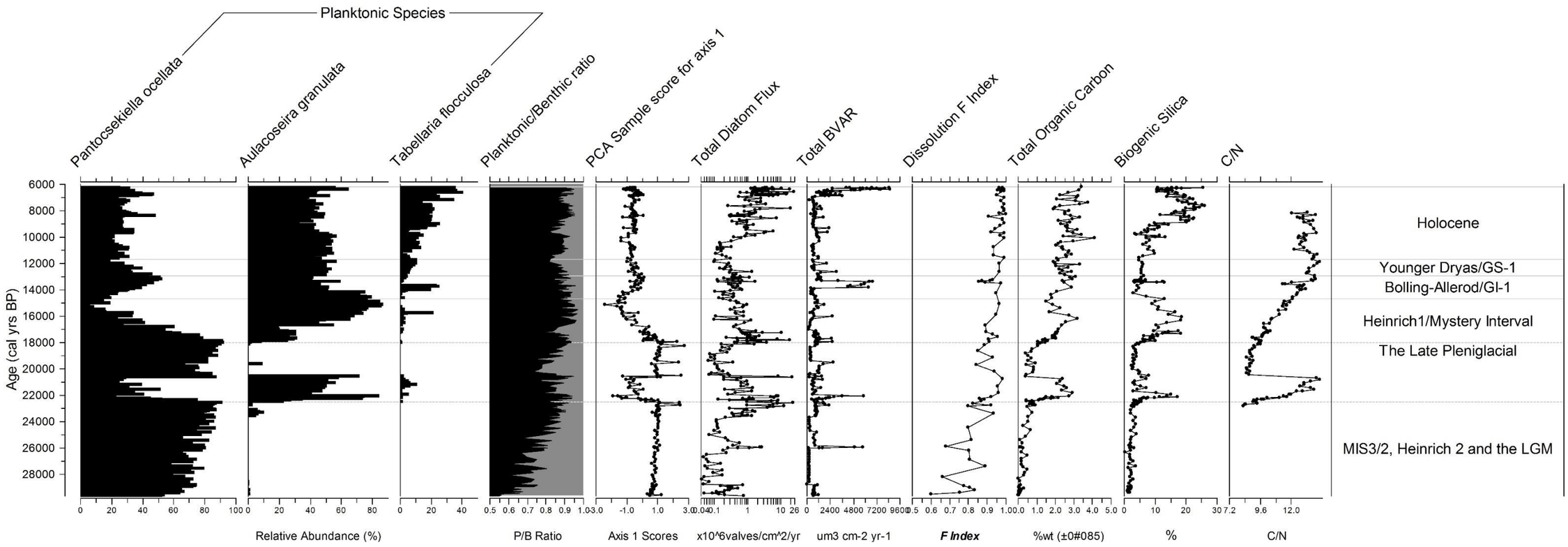

Figure 4.15: Summarised Lake Baunt diatom assemblage alongside Planktonic/Benthic ratio, total diatom flux (x10^6valves/cm^2/yr) shown on a logged x-axis, biovolume accumulation rates (BVAR) ($\mu m^3 cm^{-2} yr^{-1}$), Dissolution *F* index, Total-Organic-Carbon (TOC) (%weight), Biogenic silica (BSi) (%) and C/N ratios plotted on the Baunt chronology.

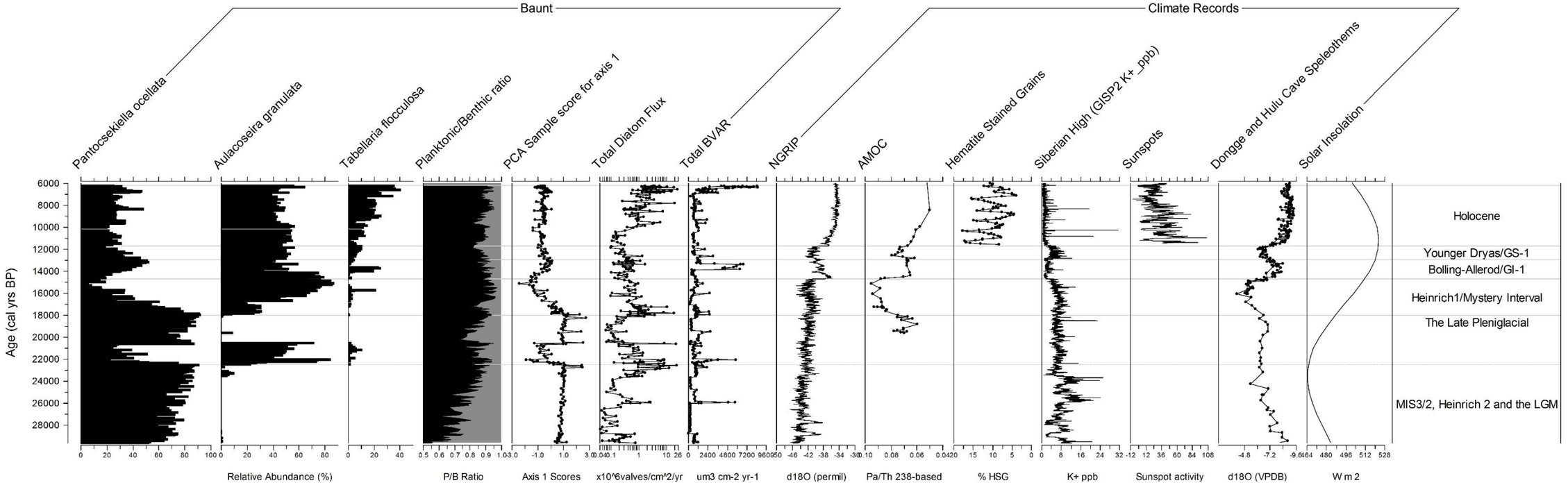

Figure 4.16: Summarised Lake Baunt diatom assemblage, P/B ratio, PCA axis 1 scores, Total diatom flux (x10^{6}valves/cm^2/yr) shown on a logged x-axis and biovolume accumulation rates (BVAR) (µm^{3}cm^{-2}yr^{-1}), shown against proxies for external climate forcing's including NGRIP $\delta^{18}O$ signal (Greenland air temperature) (Rasmussen *et al.*, 2014), Pa/Th^{238} record (AMOC strength) (McManus *et al.*, 2004), Hematite Stained Grains (%) (IRD signal) (Bond *et al.*, 2001), GISP2 K+ signal (ppb) (Siberian High strength) (Mayewski *et al.*, 2004), Sunspots, Hulu (Wang *et al.*, 2001) and Dongge Caves ($\delta^{18}O$ signal) (Dykosko *et al.*, 2005) and Solar Insolation from 60^{0}N for June (W m^2)(Berger and Loutre, 1991).

4.4.5.2 The Late Pleniglacial and Heinrich 1

The Late Pleniglacial period (24-14.6 ka BP), following the LGM until the LGIT (Tzedakis *et al.*, 2013), shows major variability within the Lake Baunt diatom assemblage. The time period also includes some of the largest abrupt Hemispheric climate shifts seen in the period, including Heinrich Event 1 (Alvarez-Solas and Ramstein, 2011; Hemming, 2004; Keigwin and Lehman, 1994).

The first of the large amplitude changes documented at this time occurs at ~22.5 ka BP, with a switch to dominance of *A. granulata*. The heavily silicified nature of *A. granulata* means it requires much higher silica concentrations within the lake waters to form its frustule, while it also requires high levels of phosphorous (Kilham *et al.,* 1986; O'Farrell, *et al.,* 2001)**.** It also implies much faster sinking rates (Chen *et al.*, 2012), particularly when compared to the smaller *P. ocellata.* This is particularly clear when the biovolumes of the two species are compared (see figure 4.7). This results in the species requiring turbulent water conditions, to allow it to remain in the photic zone (Biskaborn *et al.*, 2012; Hampton *et al.*, 2014; Rühland *et al.*, 2015).

Turbulent water conditions may be brought about through several factors in the lake, including increased mixing, potentially as a result of reduced ice cover and increased windiness. Increased turbulence is also likely to drive the shift from *P. ocellata* to *A. granulata* through light availability within the lake, with increased turbulence reducing light, which is an important factor for *P. ocellata* (Malik and Saros, 2016)*,* while *A. granulata* can thrive in low light conditions (Kilham *et al.*, 1986). Increased nutrient concentrations are also required to allow *A. granulata* to dominate the assemblage, and potentially this could be driven by both increased mixing and regeneration of nutrients (Winder and Hunter, 2008), but also landscape changes bringing increased nutrients to the lake (McGowan *et al.,* 2017). This may be a result of more abundant vegetation on the landscape, which is supported by increased C/N ratios, which have higher values when more carbon comes from allochthonous sources. This is because vascular plants contain more cellulose, and,

therefore, have higher C/N ratios (see figure 4.15) (Meyers, 1994), and, thus, indicate more carbon is from allochthonous sources at this time.

The large shifts seen in the Baunt diatom assemblage during the start of this zone (22.5-20.5 ka cal BP) (figures 4.15, 4.6), are concomitant with increases in TOC, BSi and diatom biovolumes (see figure 4.15). These increases may suggest improved within-lake or catchment productivity, with changes seen within the BSi potentially being linked to the short-lived increase in diatom flux at the start of this shift, or it may reflect the greater biovolume of silica across this period, that is a result of the shift to the more silicified *A. granulata* from *P. ocellata* (see figure 4.6) (Kilham *et al.,* 1986; O'Farrell *et al.,* 2001). However, these transitions may also be a result of external forcing. Interestingly C/N ratios also show rapid increases from being predominantly sourced from algal productivity, to a shift to allochthonous sources external to the lake (see figure 4.15) (Meyers, 1994; Meyers and Lallier-Vergès, 1999). This all may indicate a time transgressive response to post LGM conditions, across the ecosystem, and within the Baunt catchment, as it is possible that the initial rise in BSi reflects the onset of increased diatom productivity, during the early part of this period, following the LGM, with a slightly delayed response in the wider landscape, as indicated by the C/N ratios.

Either way, these factors suggest increased productivity within Lake Baunt and its catchment at this time. This is likely to have provided additional nutrients to the lake, allowing *A. granulata* to become dominant. These shifts are indicative of warmer temperatures after the LGM, supported by the thermophilic nature of *A. granulata*, with it requiring warm summer temperatures of 17-25°C (Fedotov *et al.*, 2012). Thus, the first part of DAZ 2 is defined here as reflecting lacustrine and local catchment response to warming coincident with the end of the LGM.

When external forcing factors are considered as potential drivers for these shifts, there are several complexities to consider. Solar insolation is low at this time, making the required warm temperatures needed by *A. granulata* harder to explain. It is possible, however, that continental conditions, may mean summer temperatures are warm, despite low total insolation. *A. granulata* has

previously been suggested to thrive under cooler, unstable conditions (Biskaborn *et al.*, 2012), however, the support of the additional data from Baunt does not necessarily indicate a cooler period, supporting continental summer warming. Additionally, if turbulence is increased due to overturning and reduced ice cover, it is again difficult to explain cold conditions. Generally, colder waters are easier to mix, however, the requirements of *A. granulata* suggest that this is unlikely. Other forcings do, however, support a potentially warmer, more productive period, with the GSIP2 K+ signal suggesting a weaker Siberian High (Mayewski *et al.*, 2004), and corresponding strong East Asian Summer Monsoon (Tubi and Dayan, 2013). In Greenland, the period following Heinrich 2 stadial is followed by two short lived interstadial episodes (GI-2.2 and GI-2.1), and these are followed by generally warmer conditions (Rasmussen *et al.,* 2014). The greater productivity in Baunt could, therefore, be linked to these warmer episodes, and these factors may drive the reduced Siberian High strength and increased East Asian Summer Monsoon strength, discussed above. The diatom flux data (figure 4.7) also support interpretations of DAZ2 as a warming episode within the core sequence, following the LGM (see figure 4.15), as there is an increase in total diatom flux across this period of time (22.5-20.5 ka BP). Therefore, it appears this stage of the Pleniglacial is more productive at Lake Baunt, potentially as a weaker Siberian High allows increased precipitation and nutrient in-washing and increased turbulence, to drive these assemblage shifts. The interpretation of this part of the Baunt record as a warming transition is consistent with the regionally defined end of the LGM (Kostrova *et al.*, 2014).

The onset of DAZ3, from ~20.5 ka cal BP sees a further major shift documented in the Baunt assemblage, returning to similar conditions in the diatom assemblage as those in DAZ1. As DAZ1 is thought to correspond to the LGM, Heinrich 2 and the transition from MIS3 to MIS2, with cold arid conditions, this suggests a major climate shift may have driven the fluctuation. When external drivers are considered as a potential factor to explain this reversal in the diatom assemblage, there appear to be few major climatic shifts reported for this period. Slight increases are seen in Siberian High strength, but Greenland air temperatures, the East Asian Monsoon and AMOC are

relatively stable (figure 4.16). The shifts in Baunt may, therefore, be linked to more localised factors. C/N ratios (see figure 4.15) decline to values ~9, suggesting that these are being driven by within lake algal productivity (Meyers, 1994; Meyers and Lallier-Vergès, 1999), and this may, therefore, indicate that the catchment is no longer a key source of organic carbon, and, potentially, nutrients delivered to the lake from the catchment may have reduced. Reduced allochthonous carbon could improve water clarity and this would provide conditions supporting *P. ocellata's* return to dominance, while reduced nutrients from the catchment, could provide a limiting factor affecting *A. granulata's* ability to thrive (Kilham *et al.,* 1986; O'Farrell *et al.,* 2001). These factors, alongside a slight increase in Siberian High strength suggested by the GISP2 K+ record (figure 4.16), could allow the switch between the two species, with the slight increase in Siberian High strength potentially preventing waters warming enough during the short continental summer to allow *A. granulata* to continue to dominate the assemblage (figures 4.15 and 4.6). The very limited change in the Siberian High, that could be an influence behind this shift, may indicate the sensitivity of the Baunt assemblage and ecosystem to fairly minor external climate forcing. This is considered again as part of the discussion of the whole Baunt proxy archive in chapter 7.

P. ocellata peaks at ~18.0 ka BP and then starts to decline. During this period, potential external drivers of these shifts are notable, in the form of a large decline and potential cessation of AMOC (McManus *et al.*, 2004) as a result of Heinrich 1 cooling (see chapter 1.2), which is considered to start at ~18ka cal BP (Hemming, 2004) and ends ~15 ka cal BP (McManus *et al.*, 2004). Alongside the changes in AMOC, the East Asian Winter Monsoon strengthens, although the response in the GSIP2 K+ record of Siberian High strength is more limited. These changes could, therefore, cause some of the alterations seen in the assemblage. It is notable that the changes in AMOC (McManus *et al.*, 2004), show similarity to the PCA scores (figure 4.16), with a rapid decline at ~18 ka BP and a shift to higher values at ~15.1 ka BP. This suggests shifts within the diatom assemblage are in line with the changes in AMOC and may, therefore, be showing a response to Heinrich 1.

The changes seen in Baunt, therefore, appear to reflect a response to Heinrich 1, however, this period of change globally is complex, and in many records, following the initial weakening in AMOC, a period of short lived warming is documented (Hodell *et al.*, 2017)**.** The complexities in this period (~17.5-14.5 ka BP), have led to it being termed the mystery interval (Denton *et al.,* 2006). In Baunt, this complexity is also reflected in the changes in the lake, which suggest this period is more productive (see table 4.4). This may reflect a limited expression of Heinrich 1 at Baunt, due to the less clear response in the Siberian High. However, given the similarities in changes in the AMOC signal and the diatoms (as highlighted by the PCA), which suggest there is a response to Heinrich 1, this is locally complex. Changes may be linked to increased nutrients being washed into the lake, following increased erosion, following Heinrich 1 (McGowan *et al.,* 2017). It is also worth noting, however, as discussed in section 4.4, dating uncertainties in some sections of the core are relatively large, and in places around this section are ±700 years BP, and therefore, it could be that these responses occur at a period of time offset from H1. Further dating would help to allow improved understanding of responses to this well documented event. The wider significance of this complex period in the Baunt record is discussed further in chapter 7, with reference to the suite of proxies generated for Baunt, and the records from the wider region, which can assist with understanding this period.

4.4.5.3 The Last-Glacial-Interglacial-Transition

The Last-Glacial-Interglacial-Transition (LGIT) is well studied in many regions of the Northern Hemisphere, with the pattern of interstadial warming, after the instability around H1, followed by the abrupt cooling of the Younger Dryas, being well documented. LGIT warming is recorded earliest in the Greenland Ice Cores at ~14.7 (GICC05 timescale) and is referred to the late-glacial-interstadial, or often as the Bølling-Allerød in Europe, or GI-1 in Greenland (Rasmussen *et al.,* 2014). The period is characterised by warmer Northern Hemisphere air temperatures, during a time where solar insolation is increasing between ~14.7 – 12.9 ka BP. The Siberian High appears to have reduced strength across this period, although there is some variability, while the East Asian winter monsoon is also reduced in strength (Dykosko *et al.*,

2005; Mayewski *et al.*, 2004; Tubi and Dayan, 2013). North Atlantic overturning also strengthens following its cessation through Heinrich one (McManus *et al.*, 2004) (see figure 4.16), highlighting that across the Northern Hemisphere atmospheric and ocean systems are responding and driving changes.

This period covers the latter stages of DAZ5 in the Baunt assemblage zone, during a period of increasing TOC and a short-lived BSi peak (figure 4.15). C/N ratios have continued to rise through this period (figure 4.15), suggesting increasing allochthonous sources of organic carbon. There is a short-term peak in the C/N ratios during this zone, which may indicate a period of rapid in-washing from the catchment, however, this value is only reflected in one sample and may be an outlying result and is, therefore, considered with caution. During the LGIT, *A. granulata* declines, while *P. ocellata* increases suggesting potential shifts in light levels within the lake (O'Farrell *et al.,* 2001; Malik and Saros, 2016)**.** These light variations could be driven by increased thermal stratification (Winder and Hunter, 2008), as a result of increased warming, and this would reduce turbulence causing the decline in *A. granulata* while favouring *P. ocellata* (Winder and Hunter, 2008; Winder *et al.,* 2009). The short-term peak in *T. flocculosa* may suggest increased snowmelt, as a result of warming, which could increase nutrients and allow this species to bloom within the lake (McGowan *et al.*, 2017). It is notable that the shifts seen through this section are more muted than those seen during the earlier sections of the Baunt assemblage, and this may suggest that, although climatic events are influencing the site, the forcings may be relatively limited in their strength, or the ecosystem may be better buffered against them.

The Younger Dryas/Greenland Stadial 1 period is considered to occur between ~12.9 ka BP and 11.7 ka BP (Rasmussen *et al.*, 2014b). During this period there are changes in several of the potential forcings that could influence the diatom assemblage. AMOC again decreases, as the stadial is thought to be driven by freshwater input into the North Atlantic, although this is substantially smaller than the response seen during Heinrich 1 (McManus *et al.*, 2004). In addition, Greenland air temperatures decline (Rasmussen *et al.,* 2014) and the East Asian Winter Monsoon increases in strength (Dykosko

et al., 2005), which also co-occurs alongside Siberian High strength increases (Mayewski *et al.*, 2004).

Shifts within the diatom assemblage are however less clear; there is a small decline in abundance of planktonic taxa, mainly due to the decline in *P. ocellata* (figure 4.6). This could be driven by increased Siberian High strength, however, as this species is seen to thrive during the cold and arid period of MIS3/MIS2, this is not necessarily straightforward. C/N ratios in Baunt show a small fluctuation at the start of DAZ 6, which may suggest there are slight changes in the catchment, reducing the input of organic carbon to the lake, however, this shift is of small magnitude. BSi and TOC values remain fairly stable, again highlighting a fairly limited response to climatic changes induced by the Younger Dryas. The flux data show little variability between ~13-11.7 ka BP, suggesting stable conditions across all taxa, although there is a slight increase in flux of *P. ocellata* and some of the benthic species from ~13 ka BP, which may reflect a weak Younger Dryas/Greenland Stadial 1 signal. At the same time, it is worth noting that this is far from clear. The signal from Baunt is interesting, as a range of records covering this time period, as discussed above (see figure 4.16), show significant variability.

Other factors may, however, be able to explain the limited diatom responses. It has been suggested by Schenk *et al.*, (2018), that during the Younger Dryas, a blocking high caused warm summers to be a feature of European climates at this time. This could, therefore, mean that conditions are still warm during summer months, allowing the lake waters to remain productive. These warmer temperatures are supported by the continued presence of *A. granulata*, as summers must have reached ~17°C to support this thermophilic species (Fedotov *et al.*, 2012). Although this could sound contradictory to a strengthened Siberian High, it is possible for summers to remain warm as this system dissipates during the summer months (Schenk *et al.*, 2018). This warming could generate conditions allowing both *A. granulata* and *P. ocellata* to remain in large proportions, with initial warming providing stratification and high light quantities for *P. ocellata* (Winder and Hunter, 2008), while later overturning and windiness during the late summer and autumn would provide the turbulence required by *A. granulata* (Winder and Hunter, 2008). It is only

possible to fully consider this question when all of the proxy data from Baunt are considered and this is discussed in chapter 7.

4.4.5.4 The Holocene

The Holocene epoch is defined as starting at ~11.7 ka BP (Walker *et al.*, 2009), and although it was once considered to be climatically stable (Dansgaard *et al.*, 1993; deMenocal and Bond, 1997), the last few decades of research have highlighted several periods of instability, particularly during the Early to Mid-Holocene, which is encompassed with the Lake Baunt assemblage. Generally, the Baunt record shows greater stability across this period, as inferred from PCA axis 1 samples scores (figure 4.15), potentially as a result of reduced Siberian High strength, increased East Asian Summer Monsoon strength and greater insolation (Berger and Loutre, 1991), causing reduced climate extremes (e.g. aridity and temperature), as a result of reduced Northern Hemisphere ice sheets (see figure 4.16). Reduced Siberian High strength may also be driving assemblage fluctuations, by increasing the precipitation entering the region (Tubi and Dayan, 2013) allowing in-washing of nutrients. This could be causing the higher TOC levels in the sediments (figure 4.15), as more carbon is washed into the lake, and this agrees with the C/N ratios, which are consistently between 12-14 throughout the Holocene, suggesting mixed sources from both algal communities and from the catchment (Mackay *et al.*, 2012).

Although it appears there is more stability across this period, the Siberian High strength is interrupted by occasional short-term periods of increased strength, suggesting potential climatic instability. These occur alongside rapid fluctuations in the hematite stained grains (HSG) record, which highlight periods of increased ice-rafted debris in the Atlantic (Bond *et al.*, 2001) (figure 4.16). The close occurrence of the events in the HSG and Siberian High records may suggest that these factors may be propagated to Baunt from the North Atlantic (e.g. see Mackay *et al.,* 2011, 2017), and potentially they may be driving some of the short-term fluctuations seen in the diatoms, such as the peaks in *P. ocellata* seen at ~6.7-6.5 and ~6.3 ka BP. This instability may also be represented in the rapid fluctuations in total diatom flux, seen in the Early

Holocene Baunt record. Additionally, figure 4.16 highlights the variability seen in sunspots across this period, although dating uncertainties prevent secure correlations between specific events. It is possible that increased resolution in future studies from Baunt across this period, alongside refined dating, could allow the responses to Baunt to these external drivers to be better understood.

4.4.6 Local and Regional responses

The main shifts seen at Lake Baunt, and the potential environment and climatic implications of these, are shown in table 4.4. Examining the record in this table it is clear that the site and the diatom assemblage is responding to a range of drivers, including localised within-lake and close catchment influences, as well as external factors that relate to the wider environment. For example, it is possible to explain some of the TOC variability as being driven solely by productivity and local organic carbon supply. However, many of the changes seen in Baunt seem unlikely to be a localised signal, especially in relation to temperature, light levels, ice cover etc. If some of the changes documented in Lake Baunt are driven by external forcings, then other local sites may show responses.

Lake Kotokel, to the south of Baunt, provides a suitable comparison, being influenced by similar external drivers. Lake Kotokel's diatom assemblage is immediately different from Lake Baunt's, with the periods between ~31.9 - 24.7 and ~22 - 17 ka BP having too low concentrations to allow further analyses (Kostrova *et al.*, 2014), and this highlights the quality of the preservation in Lake Baunt. Kotokel does, however, have a period of enhanced productivity during MIS2, between ~24 - 22 ka BP, which is documented to have had warmer and wetter conditions(Bezrukova *et al.*, 2010). This varies in timing from the more productivity period in Baunt, which is later, between ~22.5 - 20.5 ka cal BP, however, with the dating uncertainties associated with both sites, more of these periods could be overlapping. This may therefore suggest a regional period of enhanced productivity following the LGM, and this will be explored more in chapter 7.

The LGIT and Holocene periods are better preserved and highlight complex conditions, with cold periglacial landscapes being suggested by pollen, while

the diatoms, including dominance of *A. granulate*, suggest warm summers occurring alongside the solar insolation peaks between ~12 - 9.5 ka BP. Thus, in the Kotokel record there are some similarities to Baunt. Other much more detailed records also exist for the region in the form of Lake Baikal (Mackay, 2007), however, direct comparison between the diatom assemblages in Baunt and the multiple studies for Baikal are difficult, as the Baikal diatoms are highly endemic (Mackay *et al.*, 2006). While it is problematic, however, to compare these records purely on their diatom assemblages with Baunt, there are proxies discussed in this thesis that can be compared independently with the Baikal and Kotokel records, such as oxygen isotopes, and these are considered in the next chapter.

Moreover, to gain a much clearer insight into the whole record and how it relates to the wider region chapter 7 considers all of the available data for Baunt together and discusses it against the regional archives discussed above. Furthermore, factors that may be driving change in Southern Siberia during the Late Quaternary, as discussed with relevance to the diatom archive in section 4.4.5, are potentially linked to the abrupt and long term transitions seen across the Northern Hemisphere. Thus, in later chapters the whole Baunt record is also considered against key wider scale records of climate change.

Diatom Assemblage Zone	Age (ka cal yrs BP)	Diatom Assemblage summary	Lake Baunt Sedimentological Information Averages (means)			Indicated Environment and Climate
			BSi (%)	TOC (%)	Diatom Flux (10^6valves/cm^2/yr)	
1	~29-22.5	*P. ocellata* dominates alongside the highest observed values of *S. pinnata.*	2.4	0.3	1.28	Low productivity, and low nutrients (particularly silica) within the lake waters. Very limited preservation of TOC, highlighting well oxygenated water column, and potentially a lack of organic carbon being generated within and around the lake.
2	~22.5-20.5	*A. granulata* dominates with occurrences of *T. floccuosa* and *A. minutissimum.*	6.6	1.8	2.96	*A. granulata* suggests increased nutrient in-washing, and potentially reduced ice cover causing increased turbulence. Higher BSi may suggest increased productivity or be a result of more silicified

						diatom species. Warmer summer conditions indicated by thermophilic *A. granulata* (Fedotov *et al.*, 2012).
3	~20.5-18.0	*P. ocellata* dominants, *S. pinnata* increased from previous zone. Absence of *A. granulata* and *A. minutissimum*.	3.8	1.0	0.62	Potential change in nutrients and turbidity driving change from *A. granulata* to *P. ocellata* (Kilham, *et al.,* 1986; Donk and Kilham, 1990; O'Farrell, *et al.,* 2001; Malik and Saros, 2016). Lower BSi may reflect change from *A. granulata* to *P. ocellata* or suggest reduced productivity. Lower TOC may reflect reduced organic carbon being available in the catchment and lake.
4	~18.0-15.1	Gradually rising *A. granulata* to peak at ~15.1 ka cal BP and declining *P. ocellata*.	10.9	1.8	1.80	Potential increase in nutrients (silica, phosphorous) and increased turbulence within the lake and warmer summer

		Peak levels of *S. alpinus.*				temperatures (Kilham *et al.,* 1986; O'Farrell, Tell and Podlejski, 2001; Fedotov *et al.*, 2012). Higher BSi may be linked to increased diatom productivity, reflected in the higher total diatom flux values, or *A. granulata* reappearance due to higher biovolumes. Increasing TOC due to increased organic carbon sourced from catchment.
5	~15.1-13.1	Declining *A. granulata* and gradually increasing levels of *P. ocellata.*	6.2	2.4	0.42	Declining *A. granulata* potentially due to increased light availability and potentially reduced nutrients, as a response to greater summer stratification (Winder and Hunter, 2008). Continued presence during late-summer overturning.

6	~13.1-6.2	More stabilised quantities of *A. granulata* and *P. ocellata* with increasing *T. flocculosa.*	14.0	2.9	2.63	Higher productivity system. Increasing quantities of *T. flocculosa* can indicate shifts in the acidity of the lake waters, potentially due to snowmelt pulses resulting from increased temperatures driven by stronger solar insolation and weaker Siberian High (McGowan *et al.*, 2017). Co-occurring *P. ocellata* and *A. granulata* linked to thermal stratification allowing P. ocellata to bloom in the spring and summer, while *A. granulata* blooms during autumn overturning.

Table 4.4: Summary of the main changes in Lake Baunt and the indicated climate/environment.

4.5 Lake Baunt Limnological Summary

The Lake Baunt diatom assemblage highlights several periods of change between ~29.0 - 6.2 ka BP, which are broadly divided into 6 diatom assemblage zones on the basis of PCA. These shifts are linked to within lake changes, including turbidity and ice duration, alongside catchment driven changes influencing nutrient availability. Consideration alongside additional Baunt datasets (TOC and BSi) demonstrate that changes co-occur in many of the records, and there is suggestion that the same forcings may be influencing these records. These are potentially the result of external climatic forcing, with changes in solar insolation and AMOC all potential drivers of these shifts. These issues are considered in chapter 7 of the thesis in relations to isotopic and chemical evidence from the lake.

5 The Lake Baunt Oxygen Isotope Record

5.1 Introduction

Understanding palaeohydrology in the past is very important for assessing how hydrological systems can respond to climate change, due to the potential impacts of current warming on global hydrological systems (Swann *et al.*, 2018). Alongside this, there is a need to extend palaeohydrological records to allow testing of whether hydrological changes occur on local (site only), or regional (multiple sites) scales. Understanding palaeohydrological changes at different scales allows detailed consideration of their drivers, with site specific changes potentially highlighting responses to intrinsic drivers, while multiple sites responses can indicate extrinsic drivers, including factors such as climate.

Isotopes are a well-established technique to study palaeoclimate, with the study of $\delta^{18}O$ of carbonates being most commonly used (Leng and Barker, 2006). Over recent decades, use of the isotopic composition of biogenic silica in freshwater environments has grown, providing a direct replacement for carbonates where they are absent from sedimentary environments (Leng and Barker, 2006). Of the use of isotopes in biogenic silica, the study of the isotopic composition of diatom frustules is the most common (see chapter 4). Oxygen diatom isotopes are the most utilised, although others including silicon, carbon and nitrogen isotopes are increasingly being studied. Diatom oxygen isotopes are controlled by several factors, including the $\delta^{18}O_{lakewater}$ in which the diatom frustule was formed, and the water temperature (Leng and Barker, 2006) (see figure 5.1). This means when external events induce variability in these factors, the $\delta^{18}O_{diatom}$ values change, and, thus, such records have been used for palaeoclimatic reconstruction, as an atmospheric temperature shift can lead to changes in the water temperature, which in turn affects the $\delta^{18}O_{diatom}$. In addition, a change in the precipitation received in a catchment, or the amount of evaporation, will also affect the $\delta^{18}O_{lakewater}$ and, in turn, the $\delta^{18}O_{diatom}$ values. The technique, consequently, provides an ideal tool for considering changes in precipitation, evaporation and temperature, and, in turn, palaeohydrological and palaeoclimatic changes (Chapligin *et al.*, 2012a;

Hernández *et al.*, 2011; van Hardenbroek *et al.*, 2018), as long as there has been little internal changes in the system over the studied period, such as lake level and catchment dynamics (Leng and Barker, 2006). It is, therefore, necessary to consider a site's individual characteristics to interpret the signal. For example, open lakes usually reflect the isotopic composition of precipitation (snowfall and rainfall), which is, in turn, affected by air temperature, while closed lakes are more influenced by the balance between precipitation and evaporation (Leng and Barker, 2006; Leng and Swann, 2009).

Figure 5.1: Controls on diatom oxygen isotopes adapted from Leng & Barker (2006) to highlight specific factors affecting the signal from southern Siberia.

$\delta^{18}O_{diatom}$ studies have now been undertaken in many regions. For example, at Lake Chungará (central Andes) $\delta^{18}O_{diatom}$ is influenced by changes in the lakewaters, due to shifts in the P/E balance (Hernández *et al.*, 2011), as is documented at other tropical sites, including Lake Tipo (Ethiopia) (Lamb *et al.*, 2005), while at Lake Malawi $\delta^{18}O_{diatom}$ records highlighted wet-dry intervals every ~2.3ka for the past ~25 ka BP (Barker *et al.*, 2007). Diatom isotopes

have also been used extensively in southern Siberia, as a direct replacement for freshwater carbonate isotopes, which tend not to preserve well in this region (Mackay *et al.*, 2013b). They have provided a useful technique to assess hydrological and climatological changes, generating records from key sites, including Lake Baikal (Kalmychkov *et al.*, 2007; Mackay *et al.*, 2013b, 2011, 2008; Swann *et al.*, 2018), and Lake El'gygytgyn (North East Siberia) (Chapligin *et al.*, 2012b; Swann *et al.*, 2010), and smaller lakes including Lake Kotokel (Kostrova *et al.*, 2016, 2013). Although the number of studies is limited at present, LGIT and Holocene records do highlight several isotopic shifts. These have been linked to several factors, including fluvial input into Baikal (Mackay *et al.*, 2013b), and the interplay of evaporation and the $\delta^{18}O$ of precipitation, which is linked to air temperature, at Lake Kotokel (Kostrova *et al.*, 2013; Kostrova *et al.*, 2016). Diatom oxygen isotopes, therefore, have great potential for furthering our understanding of palaeoclimate and palaeohydrology in the region.

The aim of producing a $\delta^{18}O_{diatom}$ record from Lake Baunt is to add to the growing network of $\delta^{18}O_{diatom}$ records from sites in southern Siberia. This will allow consideration of intrinsic and extrinsic forcings on the regions palaeohydrology. Additionally, this information will provide essential context for modern day climatic and hydrological shifts, while the data will be useful to test models of modern day hydrological variations, which are very uncertain for this region at the current time. Consideration of local versus regional hydrological changes, alongside testing of climate models, will help to refine understanding of teleconnections between atmospheric systems, which may be driving these changes.

5.2 Methodology

5.2.1 Water samples

In 2014 water samples were collected from Lake Baunt and its fluvial inflows, and a small nearby lake, by collaborators from the Institute of the Earth's Crust, Russian Academy of Sciences. These were collected in Spring (23-Mar-14; n=3), while the lake was frozen, and during summer, post ice melt (21-Aug-14; n=6). These samples were sent for analyses at the Isotope Laboratory

(AWI Potsdam), where they underwent hydrogen and oxygen isotope analysis with a Finnigan MAT Delta-S mass spectrometer. Three additional water samples were collected by collaborators in March 2016 and also analysed at AWI Potsdam, including one bottom water sample taken from the deepest point of the lake at ~34 meters depth.

5.2.2 $\delta^{18}O_{diatom}$ analyses

59 samples have been analysed to produce the BNT14 $\delta^{18}O_{diatom}$ record. As $\delta^{18}O_{diatom}$ measurements are easily influenced by detrital grain contamination (e.g. Leng and Marshall, 2004; Brewer *et al.*, 2008; Leng and Swann, 2009), the samples were purified prior to analysis. This is necessary as other components, including clay, silt, tephra and carbonates, which could be present in a sample if vigorous cleaning is not undertaken, contain a high proportion of oxygen, and, consequently, have high potential to influence the $\delta^{18}O_{diatom}$ measurement, as all the oxygen in the sample is liberated during analysis (Morley *et al.*, 2004; van Hardenbroek *et al.*, 2018). Cleaning of the Lake Baunt samples followed the protocols outlined by Morley *et al.*, (2004), which are summarised below. Samples were first treated in hydrogen peroxide (H_2O_2) for ~4 hours to disaggregate the sediment, before undergoing a three-stage heavy liquid separation using sodium polytungstate (SPT) ($3Na_2WO_4 \cdot 9WO_3 \cdot H_2O$). Organics are removed from the samples using hydrogen peroxide, with samples being placed in a water bath at ~75ºC for 1 week. What few carbonates there were, were removed using 5% hydrochloric acid (HCl), and finally samples were filtered through cellulose nitrate membranes to remove any remaining contaminates and chemical residues (e.g. SPT), before drying for analyses (Morley *et al.*, 2004).

Sample purity prior to analyses was assessed using elemental analyses by energy dispersive spectroscopy (EDS) by Russian collaborators, to estimate the extent of contaminants remaining in the samples post cleaning, particularly silt quantities. These were used for the mass-balance correction detailed below. For EDS analyses, approximately 1 mg of purified diatom material was diluted and pipetted onto conductive tabs, mounted on aluminium stubs. Once dried these stubs were carbon coated (Chapligin *et al.*, 2012a). Sample purity

was further assessed using scanning electron microscopy (SEM) imaging in the Department of Earth Sciences, University College London.

Isotopic analyses for Lake Baunt were carried out at the stable isotope facility British Geological Survey, Keyworth, UK. The samples from Lake Baunt have undergone a step-wise fluorination method, as described by Leng and Sloane (2008), which is briefly described here. First, the samples are 'outgassed' (dehydrated) at room temperature in the reaction tubes, which removes loosely bound water. Samples, secondly, underwent pre-fluorination, involving a stoichiometric deficiency of the reagent (bromine pentafluoride, BrF_5), at a low temperature (Leng and Sloane, 2008). This step removes loosely bound water and the hydroxyl layer, which is necessary, as this outer hydrous layer is freely exchangeable and, thus, does not reflect the isotopic composition of the frustule at the time of burial (Leng and Barker, 2006). Finally, the samples are fully reacted at 450ºC for 12 hours, with an excess of reagent. After this, the oxygen from the samples is liberated by opening the next section of the fluorination line, while liquid nitrogen is used to trap the other products. The oxygen is converted to CO_2 by exposure to a graphite rod, while 2 additional waste traps are cooled using liquid nitrogen to ensure purity of the gas (Leng and Sloane, 2008). Once converted to CO_2 the CO_2 yield is calculated using a calibrated capacitance manometer and the CO_2 is collected into vessels. After this the line is pumped down to $<1 \times 10^{-5}$ mbar to ensure residual gases are removed. The CO_2 produced was analysed using IRMS, on a Finnegan MAT253 (Leng and Sloane, 2008).

Despite vigorous cleaning processes, $\delta^{18}O_{diatom}$ samples may still contain small levels of contaminants, particularly due to ability of contaminants to become electro-statically charged to the diatom frustules (Brewer *et al.*, 2008). Samples containing contaminates can significantly alter the record, due to their different isotopic composition, for example, samples containing silt have lower $\delta^{18}O$ values. To compensate for contaminants potentially affecting the Lake Baunt $\delta^{18}O_{diatom}$ record, a mass balance correction was applied to the original data, following Swann and Leng, 2009 (equation 5.1), outlined below:

$\delta^{18}O_{corrected} = (\delta^{18}O_{measured} - (\%contamination./100)) * \delta^{18}O_{contamination}) / (\%purity/100)$

Equation 5.1: mass balance correction.

where $\delta^{18}O_{corrected}$ is the measured value after it has been corrected for contaminants, $\delta^{18}O_{measured}$ is the original measured value, %contamination is the percentage of the known contaminant (Al_2O_3), while %purity is the percentage of diatom material, established by geochemical methods (Swann and Leng, 2009).

Silt samples were obtained by dissolving diatoms from 4 samples in NaOH and retaining the residues (Swann and Patwardhan, 2011). These end members have very similar values and are, therefore, used to create a signal end member (Swann and Patwardhan, 2011).

5.3 Results

5.3.1 Water Isotopes

Isotope results from analysed water samples are shown in table 5.1, while, figure 5.2 documents the positioning of each of these samples. The contemporary water isotope samples, δD and $\delta^{18}O$, have been plotted alongside the Global Meteoric Water Line (GMWL), and are shown in figure 5.3. The local water meteoric water regression line (LMWL) is $\delta D = 7.64\delta^{18}O + 5.7$, indicating that Baunt is influenced by local sources of water, with a limited effect of evaporation (Leng and Marshall, 2004). The average $\delta^{18}O$ value from Lake Baunt waters is –16.0‰, with higher values during the summer (–15.9‰), than under ice (–16.3‰) (2016 data included). Figure 5.4 shows the Baunt samples colour coded according to the timing of their collection. This demonstrates that although the averaged $\delta^{18}O$ values are similar, the data from the different seasons plot on different LELs, highlighting a slight seasonal variation. In spite of these differences, figure 5.5 shows that all Baunt data plot in the expected region for cold region freshwater lakes (Leng and Marshall, 2004).

Rivers flowing into Lake Baunt have a wider range of $\delta^{18}O$ values, and it should be noted that the water temperatures of these rivers vary substantially, from 5°C to 19.6°C, despite only being taken over 3 days during the summer period (August), and this may be influencing the values. The small lake site of Lake Sary has also been included, and has less negative $\delta^{18}O$ values than Baunt, however, there is only 1 reading from this lake and, thus, its yearly variations are not able to be considered.

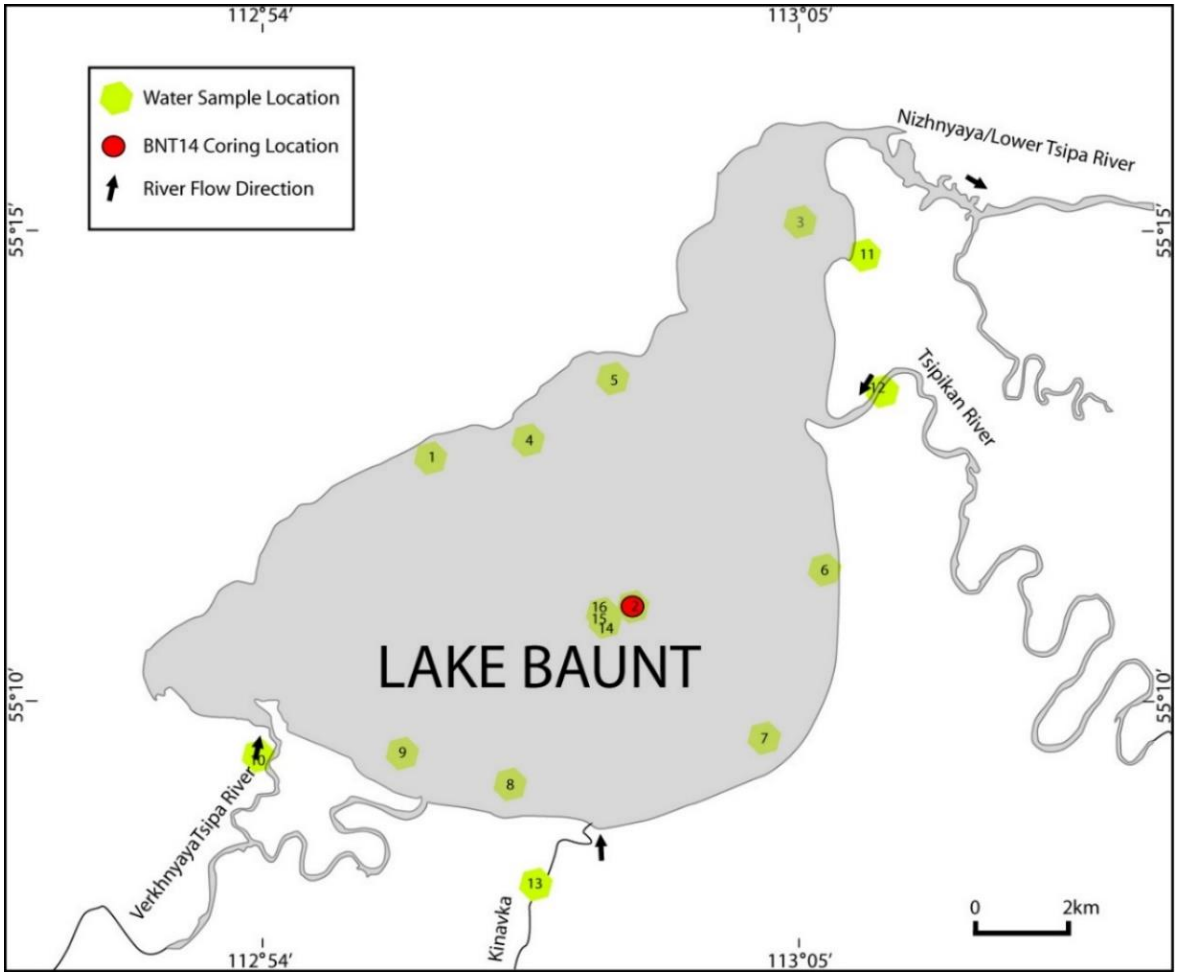

Figure 5.2: Schematic map showing locations of water samples taken from Lake Baunt and surrounding locations.

Sample Name	Sample Location	Collection Date	Water Temperature (°C)	$\delta^{18}O_{vsmow}$	δD_{vsmow}[‰]	Mean values
BA-N1	N55°12'53.0" E112°57'45.1"	26.03.14	1.0	-15.96	-123.0	-
BA-N2 (coring site)	N55°11'15.2" E113°01'45.1"	26.03.14	1.0	-16.23	-124.0	-
BA-N3	N55°14'55.7" E113°04'53.1"	26.03.14	1.0	-16.48	-125.5	-16.2 (March 2014)
BA-N4	N55°13'02.1" E112°59'12.8"	21.08.14	17.5	-15.99	-122.3	-
BA-N5	N55°13'23.7" E113°00'54.1"	21.08.14	18.0	-15.91	-131.5	-
BA-N6	N55°10'58.2" E113°05'29.1"	21.08.14	20.0	-16	-121.5	-
BA-N7	N55°08'59.9" E113°03'07.9"	21.08.14	20.0	-15.96	-121.6	-
BA-N8	N55°08'44.7" E112°59'08.8"	21.08.14	20.0	-16.05	-122.3	-

BA-N9	N55°09'10.3" E112°56'47.1"	21.08.14	20.0	-15.46	-117.9	-15.9 (Aug 2014)
BA-N10 River Tsipa	N55°09'38.1" E112°54'14.7"	21.08.14	15.5	-16.31	-123.7	-
BA-N11 Lake Sary Sary	N55°14'36.8" E113°05'55.6"	21.08.14	19.6	-15.21	-116.9	-
BA-N12 River Tsipican	N55°12'57.6" E113°06'01.9"	21.08.14	16.0	-14.39	-111.1	-
BA-N13 River Kinavka	N55°07'34.6" E112°59'35.6"	24.08.14	5.0	-15.61	-115.0	-15.4 (Riverine systems and nearby lakes) (Aug 2014)
BA-N14	N55°11'10.90" E113°01'33.55"	27.03.16	1.0	-16.26	-124.6	
BA-N15 (Bottom water)	N55°11'11.85" E113°01'32.85"	30.03.16	1.0	-16.14	-123.7	-16.1 (Bottom Water – Aug 16)
BA-N-16	N55°11'11.85" E113°01'32.85"	30.03.16	1.0	-16.46	-124.8	-16.3 (All Baunt March) -16.4 (March 16)

Table 5.1: Table showing water isotope data from Lake Baunt and surrounding water sources.

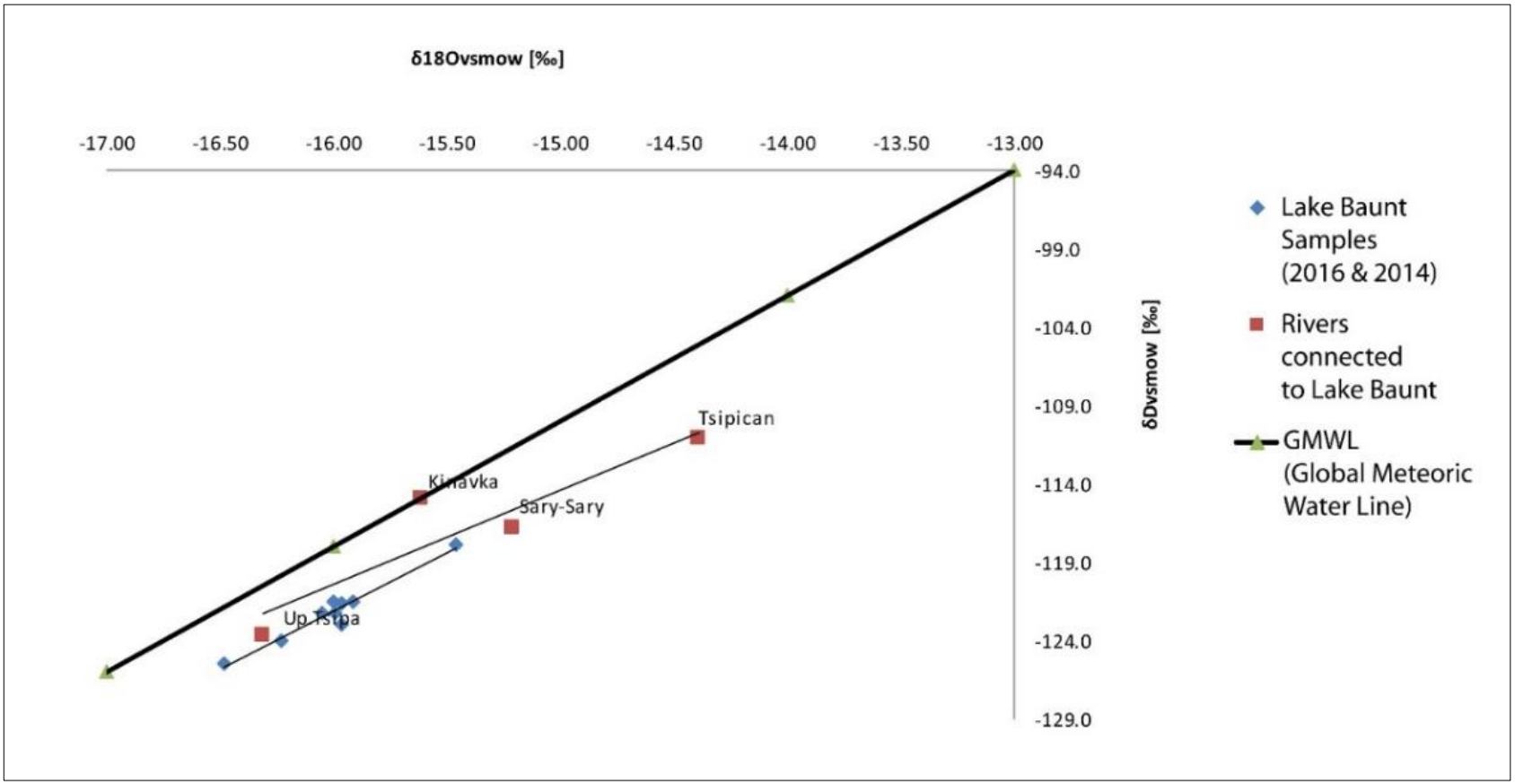

Figure 5.3: Graph plotting the GMWL against the Lake Baunt and nearby water sources.

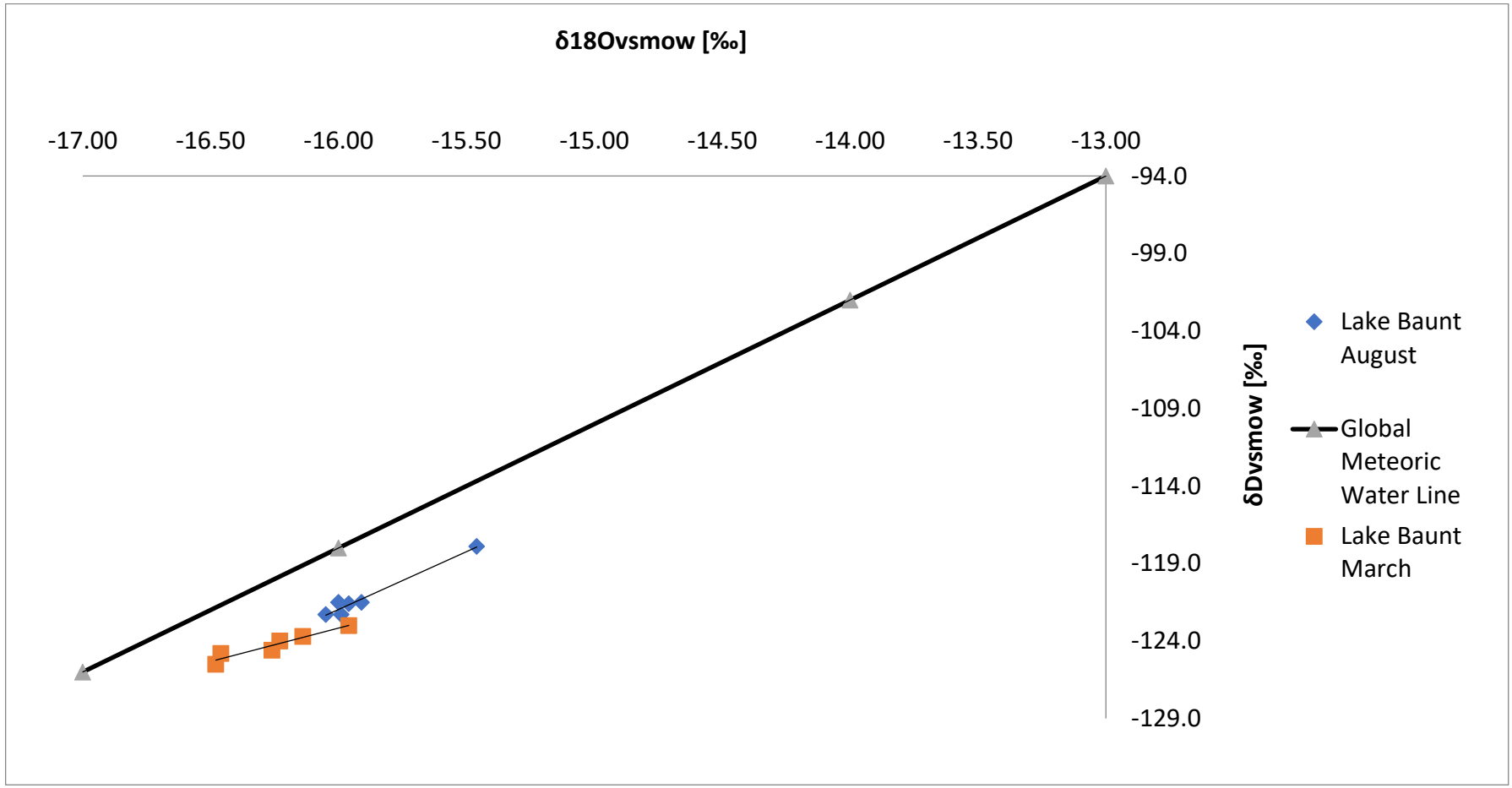

Figure 5.4: Graph plotting the Lake Baunt seasonal water data against the GMWL.

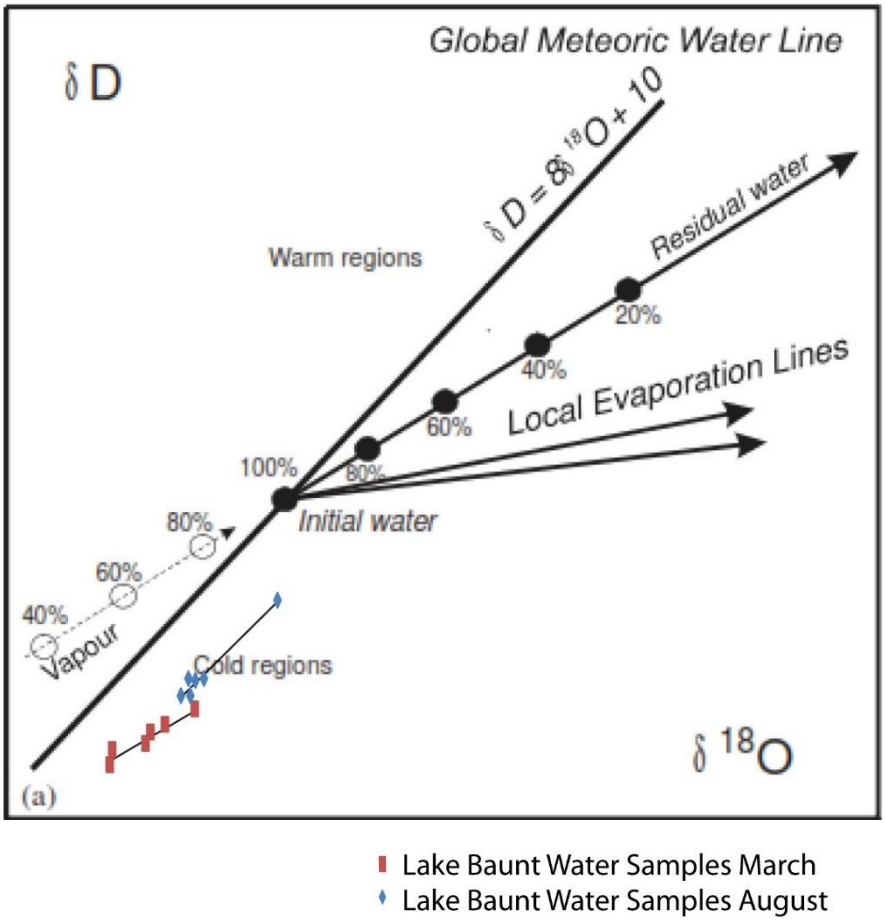

Figure 5.5: Figure adapted from Leng and Marshall (2004) (pp813) showing the Global Meteoric Water Line (GMWL). Lake Baunt's seasonal water sample data has been added and sits within the area associated with cooler regions, close to the GMWL indicating its isotopic similarity to precipitation.

5.3.2 $\delta^{18}O_{diatom}$ Results

Figure 5.6 shows the unmodelled versus corrected $\delta^{18}O_{diatom}$ values, and the percentage silt found within the samples, while figure 5.7 shows the modelled (corrected) $\delta^{18}O_{diatom}$ record for BNT14, all plotted using the Lake Baunt chronology, developed in chapter 3. The Baunt record covers ~12.5-6 ka BP and shows several distinct shifts in isotopic composition between +22.7 and +32.1‰, with a general decline in the isotopic composition of diatoms of around 3.0‰, from the lower section of the core to the core top.

The earliest section of the record is relatively stable sitting between +26.5 and +27.5‰ between ~12.4 and ~10.8 ka BP (figure 5.7). Following this stability,

the record documents the largest and most frequent isotopic changes in the Lake Baunt record, with peaks reaching, in excess of +31.0‰, at ~10.0, 9.4 and 8.5 ka BP, although these higher values are interrupted by declines to ~+25.0‰ at ~9.8, and 8.9 ka BP.

Following the high value of 32.0‰ at ~8.5 ka BP there is a decline until ~7.6 ka BP, after which values rise slightly until ~7 ka BP. Changes during this period are less variable, remaining around +24.0‰, which continues until a low of +22.6‰ is observed at ~6.2 ka BP. These samples have undergone the largest corrections due to the highest levels of contamination from silt (see figure 5.6), which in one sample reached almost 24% (see figure 5.6). This sample also has the highest $\delta^{18}O_{corr}$ value of the Late Holocene and it is possible that this is due to the correction factor, rather than being a real peak in the record during a period of relative stability.

The record, therefore, appears to show three zones, with the LGIT-Holocene transition period (~12.4-10.0 ka BP) having values ranging between 26-28‰; the period between 10.0-8.0 ka BP then shows a period of rapid large amplitude changes, before a final shift to lower, declining values after 8 ka BP.

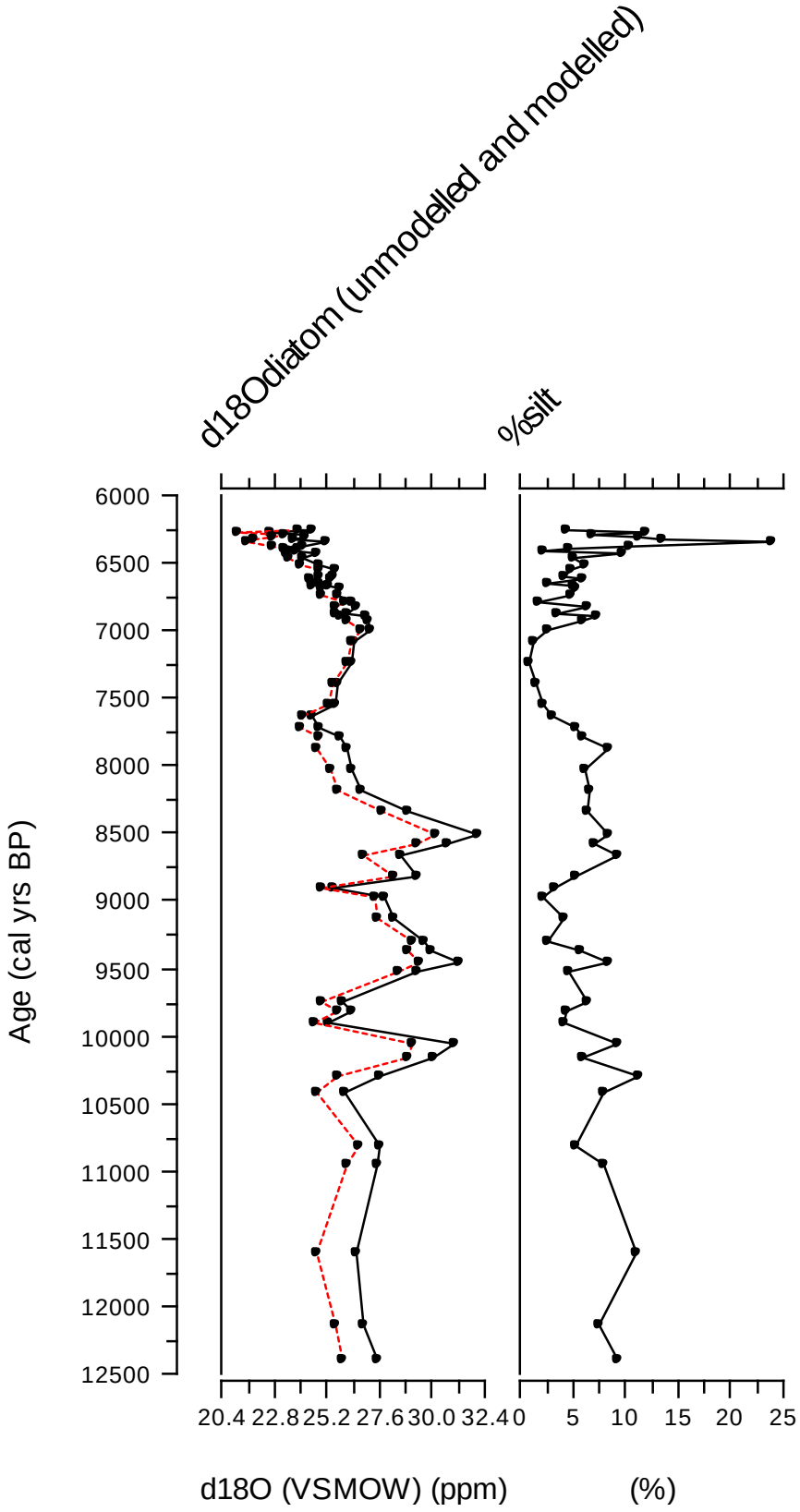

Figure 5.6: Uncorrected $\delta^{18}O_{diatom}$ record from BNT14 (red dashed) against Corrected $\delta^{18}O_{diatom}$ record (black) against percentage Silt values (%), all shown against calibrated years BP.

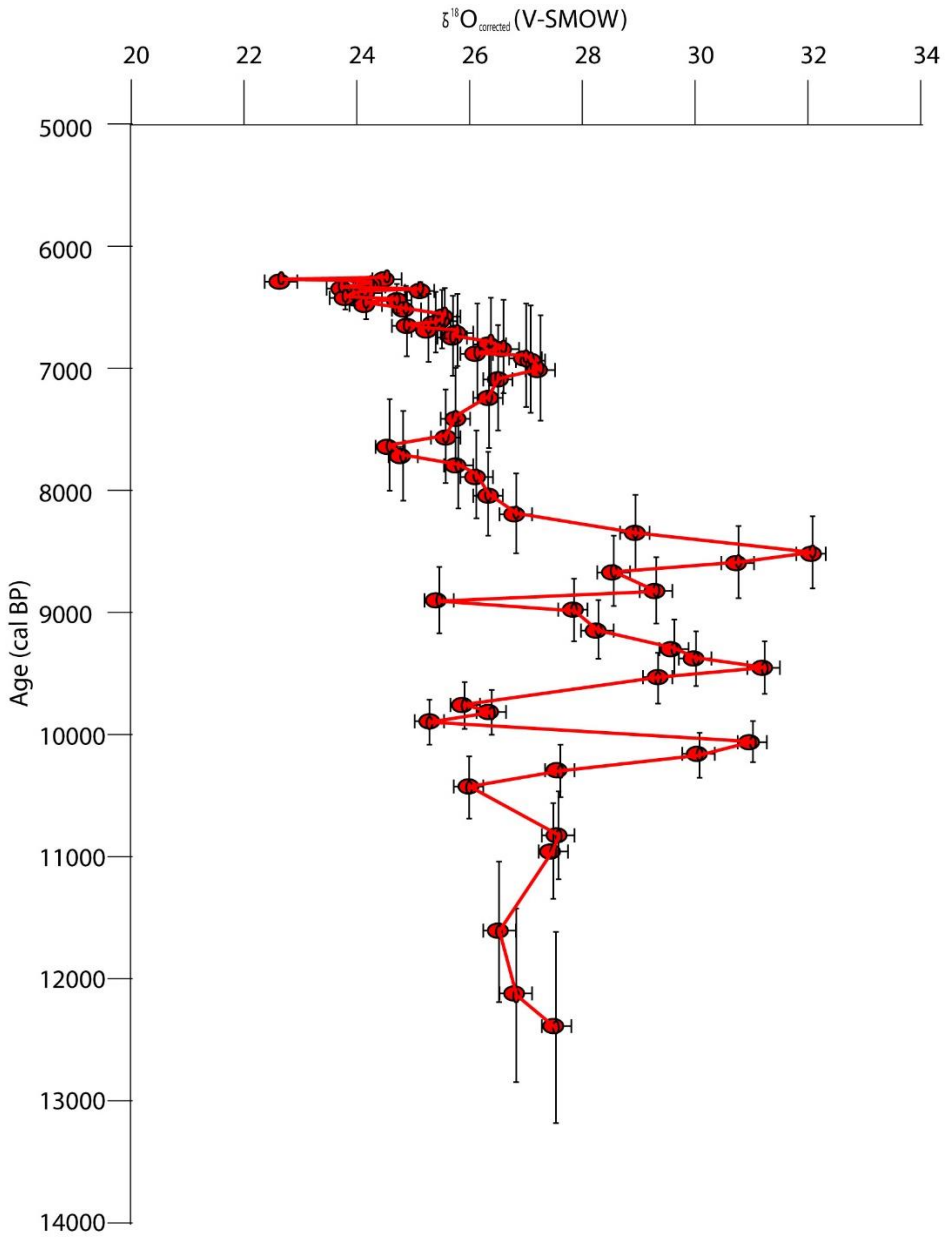

Figure 5.7: Corrected $\delta^{18}O_{diatom}$ record from BNT14 plotted along the BNT14 Chronology produced as described in chapter 3, shown with chronological uncertainty and analytical errors.

5.4 Discussion

5.4.1 Integrity of the isotope record

$\delta^{18}O_{diatom}$ measurements are highly susceptible to the influence of sample contamination (Brewer *et al.*, 2008; Morley *et al.*, 2004; Wilson *et al.*, 2014). Figure 5.8 highlights cleaned purified diatom samples from across the BNT14 record, and these demonstrate that the cleaning process outlined in section

5.2.3 has removed the majority of contaminants. Alongside the mass balance remodelling of the $\delta^{18}O_{diatom}$ data, it is believed that contaminants have been adequately accounted for. Despite the success of the sample cleaning, it must be noted that the $\delta^{18}O_{diatom}$ results from BNT14 are associated with low O_2 yields (the standards yields were normal), suggesting that something within the samples contains less oxygen than normal diatom samples (Leng, pers.com.). This is difficult to explain, particularly as the SEM images, shown in figure 5.8, highlight that detrital material has been removed. One possibility is that the cleaned BNT14 diatom samples contain a different form of biogenic silica, potentially sponges, chrysophyte cysts (Leng, pers. com.) or tephra. Sponge spicules and chrysophyte cysts were not, however, documented in large quantities in the Baunt samples, and although rangefinder scans were carried out for some sections of the core for tephra, only occasional shards were located, and these appeared in samples from depths not studied for isotopes. Despite this, it is not thought that the $\delta^{18}O_{diatom}$ measurements have been affected, with the smaller samples covering the complete $\delta^{18}O_{diatom}$ range seen in the larger sized ranged samples, from BNT14 (Leng, pers. com.).

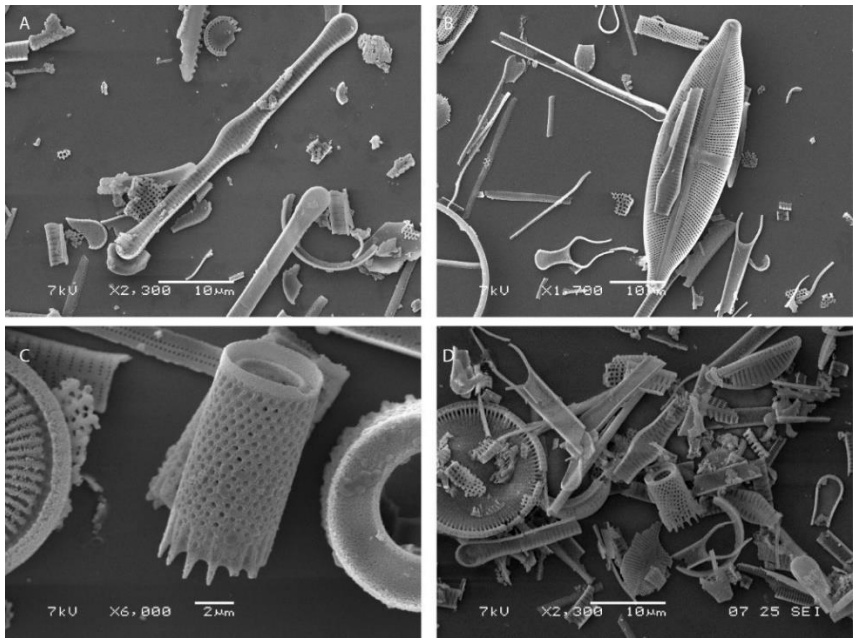

Figure 5.8: Scanning Electron Microscopy Images of cleaned isotope samples from varying Lake Baunt Depths: **(A)** 0.05m, **(B)** 1.90m, **(C)** 3.75m, **(D)** 4.20m.

One of the assumptions that is made when using diatom isotopes for palaeoclimate and palaeohydrological studies is that the diatoms have

precipitated in isotopic equilibrium with the lakewater (Swann *et al.*, 2007; van Hardenbroek *et al.*, 2018). However, it is known from the study of other biological organisms (e.g. ostracods, foraminifera) that this is not always the case (Xia *et al.,* 1997; Bemis *et al.*, 1998; Swann *et al.*, 2007), with interspecies and intraspecies offsets affecting the signal (Swann *et al.*, 2007). As a result, isotope/disequilibrium vital effects have been discussed as having potential influences on $\delta^{18}O_{diatom}$ records in many papers (Brandriss *et al.*, 1998; Chapligin *et al.*, 2012a; Swann *et al.*, 2010, 2007), and they are thought to be linked to a range of habitat and taxonomic processes (Schiff *et al.*, 2009), such as vertical migration in the water column, benthic/planktonic (and other spatial effects) precipitation rate changes, micro-environment changes, metabolic fluid variations and pH alterations (Swann *et al.*, 2007). Species effects are thought to be caused by species specific fractionation (Chapligin *et al.,* 2012a), due to the range of conditions which diatoms occupy (Schiff *et al.*, 2009). Studies have, therefore, been undertaken to consider if vital or other species effects influence $\delta^{18}O_{diatom}$ signals (e.g. Schmidt *et al.*, 2001; Schiff *et al.*, 2009), and these are now thought to have a limited influence on lacustrine samples, where species influence is thought to be smaller than the analytical error associated with each sample (Swann *et al.*, 2007, 2010; Leng and Swann, 2009; van Hardenbroek *et al.*, 2018). Therefore, it appears unlikely that species effects have a significant influence on the BNT14 record, and this is further supported by the dominance of only three species, *Aulacosiera granulata*, *Pantocsekiella ocellata* and *Tabellaria flocculosa*, all of which are considered to be planktonic species, and, thus, representing mainly open water environments. The dominance of open water diatoms, particularly through the period covered by $\delta^{18}O_{diatom}$ samples (see figure 5.9) reduces the potential influence of a species effect further.

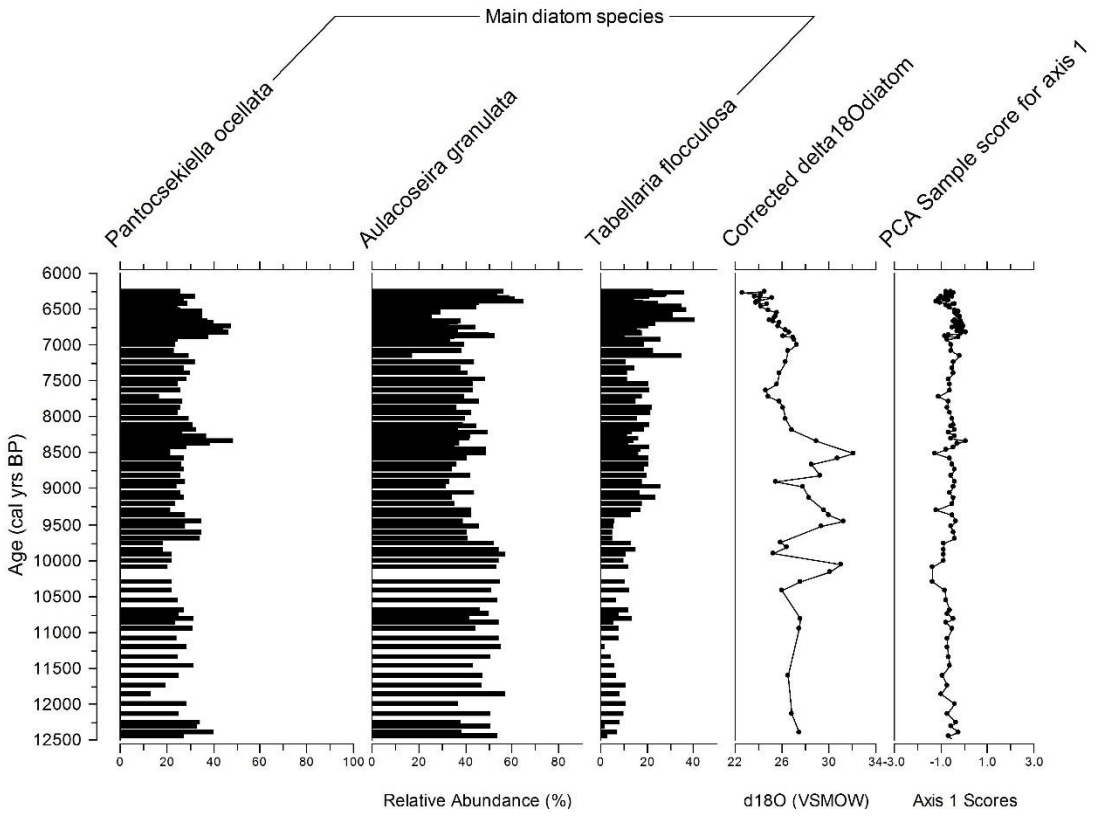

Figure 5.9: Summary diatom data showing percentage abundance of the three-dominant species against the PCA 1st axis scores and the corrected $\delta^{18}O_{diatom}$ record.

Additionally to vital effects, diatom dissolution has been considered to influence measurements of $\delta^{18}O_{diatom}$ (Leng and Swann, 2010; Swann *et al.*, 2010). Dissolution can influence this, as it may exacerbate any species effects by preferentially removing some species (Leng & Swann, 2009). Dissolution can alter $\delta^{18}O$ values, causing a small negative effect of up to 0.56‰ beyond analytical error (Smith *et al.*, 2016). The isotopic ratio changes are usually due to kinetic fractionation, which preferentially dissolves certain parts of the diatoms frustule, causing rapid shifts in the $\delta^{18}O$ signal (Smith *et al.*, 2016). Silica maturation is also thought to influence $\delta^{18}O_{diatom}$ values (Leng & Swann, 2009; Swann *et al.*, 2010), however, the extent this affects the use of $\delta^{18}O_{diatom}$ for palaeoenvironmental reconstructions remains unknown (Leng & Swann, 2009). Despite this, the effects of dissolution and silica maturation are thought to be limited for the BNT14 core, as diatoms are well preserved, with few frustules showing signs of dissolution down the core (see chapter 4).

Therefore, it is likely that the variations in the $\delta^{18}O_{diatom}$ record are not driven by these factors.

As an open lake, and with no evidence of species effects or dissolution affecting the record, it is expected that Lake Baunt's $\delta^{18}O_{diatom}$ record will reflect changes in $\delta^{18}O_{precipitation}$ values (Leng and Barker, 2006; Leng and Marshall, 2004; Leng and Swann, 2010). For this region, precipitation includes summertime rainfall sourced from the North Atlantic, and brought to the region by the Westerly winds during the months when the Siberian High dissipates (Park *et al.*, 2014; Tubi and Dayan, 2013), and snowfall/snowmelt, which enters the lake during springtime melting. Summertime precipitation is likely to be more influential during periods when the Siberian High is weaker, as this allows the westerly winds to bring increased precipitation to the region, while periods with a strong Siberian High will receive less summer precipitation (Park *et al.*, 2014; Tubi and Dayan, 2013), and, thus, the lakewaters will be influenced more by the $\delta^{18}O$ of the snowmelt. Snowmelt $\delta^{18}O$ values vary within the Transbaikal area, as documented in figure 5.10, however, it is significantly lower (mean values ~-29.07‰) (data from Chishchov *et al.,* 2015) than the current summer (JJA) precipitation $\delta^{18}O$ values, which for this region sit around ~-12.8‰. Modern day annual average precipitation values sit at -16.9‰ and the close similarity to the average of Baunt's $\delta^{18}O_{lakewater}$, which is -16.0‰ (see section 5.3.1), highlights the well mixed nature of Lake Baunt's water, suggesting the lake's $\delta^{18}O$ is closely related to the annual average $\delta^{18}O$ of precipitation. The seasonal variations in the $\delta^{18}O_{precipitation}$ is influenced by air temperature changes, alongside the air mass source region (Seal and Shanks, 1998). Baunt's well mixed nature is highlighted by the similar modern day water samples, both across the lake and between surface and bottom waters (see section 5.3.1). This, along with its similarities with average annual precipitation, is an important characteristic for understanding the $\delta^{18}O$ signal, as it is essential for lakewaters $\delta^{18}O$ to have averaged out (Leng and Marshall, 2004). The slight seasonal difference shown in August versus March $\delta^{18}O_{lakewater}$ values do indicate a minor seasonal influence, however, this is not unexpected as seasonal differences are known to be greater in smaller lakes (Leng and Marshall, 2004), and will need to be considered to interpret the

record further. Additionally to the variations in precipitation, the $\delta^{18}O_{diatom}$ record will be influenced by site specific factors, including the catchment size in comparison to the lake size (Leng and Marshall, 2004).

Figure 5.10: $\delta^{18}O$ values of bulk snowmelt from southern Siberia from Chizhova *et al.,* (2015), with red dot showing approximate location of Baunt.

5.4.2 Scales of Change

It is important to consider the $\delta^{18}O_{diatom}$ trends across different timescales, and, therefore, before the details of the BNT14 record are discussed, it is notable that the general trend of the $\delta^{18}O_{diatom}$ record follows a general decline from the earliest part of the record ~12.5 ka BP to the upper section of the record after 6.5 ka BP. This may be recording a response to declining solar insolation levels through the Holocene. Figure 5.11 highlights the Baunt $\delta^{18}O_{diatom}$ record against solar insolation, and it is clear that the gradual trend appears to follow

this signal. This may, therefore, represent a response to declining temperatures or changing hydrology from the Early Holocene to the Mid-Holocene, however, while noteworthy here, this is discussed in later sections of the thesis, when it is considered against a range of evidence. The Baunt $\delta^{18}O_{diatom}$ data are first considered in the wider climatic context of the transition from the last glacial to the early Holocene.

5.4.3 LGIT-Holocene Transition (~12.4-10.5 ka BP)

$\delta^{18}O_{diatom}$ values vary little during the period between the latter stages of the Younger Dryas and the early Holocene, ~12.4-10.5 ka BP, and there may be several reasons for this. The first factor to consider is that this period of apparent stability may be a function of the limited sampling resolution over this section, due to insufficient material for analysis being available. The limited resolution may mean that rapid shifts, if occurring over timescales of only a few hundred years, are not being captured by in the Baunt record. Nevertheless, isotope values for the late Younger Dryas are similar to those from the early Holocene. It has been suggested for continental Europe, on the basis of pollen transfer functions and climate models, that while overall conditions were cold, summers in the Younger Dryas were warm (Schenk *et al.*, 2018). The second factor to consider is that conditions were cool until after 10.5 ka BP, as Baunt is in the north of the Baikal region.

When considered against other Northern Hemispheric climate records for this time period, the limited shifts in the $\delta^{18}O_{corr.diatom}$ record could be considered unusual, as it incorporates ages normally associated with the Younger Dryas/Greenland Stadial 1 (GS1; Rasmussen *et al.*, 2014), alongside the transition from the Late Pleistocene to the Holocene, and additional climate oscillations, such as the Pre-Boreal-Oscillation and 11.1ka BP events (Blockley *et al.*, 2018). During GS1 and the Younger Dryas, cold conditions are documented in Greenland and at many Northern Hemisphere sites (Brauer *et al.*, 2008; Brooks *et al.*, 2012; Coope *et al.*, 1998; Heiri and Millet, 2005), and as discussed in chapter 1, these shifts are thought to be driven by changes in North Atlantic meridional overturning circulation (AMOC) (Lane *et al.*, 2013), which are triggered by freshwater inputs from melting ice sheets altering ocean

salinity and temperature (Bond, 1997). These AMOC shifts induce large scale ocean circulation reorganisation, which is in turn propagated to the atmosphere (Bakke *et al.*, 2009), causing responses across the globe, although there is variation in the expression of these events. It could, therefore, be expected that an expression of these events should be shown in the $\delta^{18}O_{diatom}$ records from Siberia, driven by atmospheric changes propagated from the North Atlantic to Siberia, through the Siberian High. It could be anticipated that the Siberian High should increase in strength, inducing cooler and more arid conditions in southern Siberia, triggering alterations in the isotopic composition of the lakewater and in turn of diatom frustules. The Baunt record does, however, not appear to demonstrate this, and several factors may be responsible.

One of the reasons for the absence of a YD signal in the Baunt isotope samples, could be a function of the seasonality produced by the diatom record, as the diatom's isotopic signal is reflective of their growing season (Leng and Swann, 2009), with bulk samples tending to be averaged across the spring to the autumn. Figure 5.9 highlights that during this period diatoms in Lake Baunt are dominated by *A. granulata and P. ocellata., and A. granulata* blooms predominantly in the summer-autumn period, usually alongside conditions including high turbulence and abundant silica (Rioual *et al.*, 2001). Therefore, this species may be less likely to document a cooling event, as the seasonality induced by the Siberian High means that even during cold stadial conditions, summer temperatures in this region may not be influenced, and, thus, the $\delta^{18}O_{diatom}$ signal that is contributed by *A.granulata* is likely to document summer temperatures, rather than colder winters bought about by a stronger Siberian High. As this period occurs just before perihelion in the Northern Hemisphere, this would support extreme continentality at this time, potentially with warm moist summers. In Lake Baikal, the second half of the stadial shows a rise in isotopic values. Moreover, it has been argued that warm summers during the Younger Dryas (GS-1 in the Greenland event stratigraphy) (Rasmussen *et al.*, 2014) may be a feature of continental records, as opposed to North Atlantic climates (Schenk *et al.*, 2018), with the main cooling occurring in winter, and, thus, if the diatom record reflects a summer bias, these colder

and potentially more arid conditions may not be well documented by the $\delta^{18}O_{diatom}$ record. Pollen based evidence for increasing precipitation by ~12 ka BP suggests, at least from summer dominated proxies, that precipitation in the second half of the Younger Dryas (GS-1) was high (Tarasov *et al.*, 2007). It is also possible that there is significant enhancement of the East Asian Winter Monsoon at this time, suggested by evidence from Lake Suigetsu, Japan (Schlolaut *et al.*, 2017), and this would imply a strengthening of the Siberian High (Tubi and Dayan, 2013). For Japan there is also a weakening of the summer monsoon, but this is less clear than for the winter proxies. Figure 5.11 shows the $\delta^{18}O_{diatom}$ record against the GISP2 potassium (K+) record, which is considered to be a proxy for Siberian High strength (Mayewski *et al.*, 2004), alongside other records of climate drivers, and this clearly shows that the Siberian High is strong through this period. The increased cooling and aridity bought about by this may only have limited effects on the region's hydrology, with wintertime precipitation being very low, and ecosystems already being adapted to cold conditions. If summertime conditions remain warm in continental settings, as suggested by Schenk *et al.,* (2018), the period when the Siberian High dissipates would still allow westerly winds to propagate to the region, bringing precipitation and, thus, the $\delta^{18}O$ of precipitation would not be altered that much meaning a large change would not be apparent in the $\delta^{18}O_{diatom}$ record.

The issue with this theory is that *A. granulata* dominates the diatom assemblage throughout the whole $\delta^{18}O_{diatom}$ record discussed in this chapter (figure 5.9), and, thus, if the species was preventing abrupt climatic shifts being documented the larger scale changes documented later in the record may be harder to explain. That said, *A. granulata* is not present in the period associated with the Last-Glacial-Maximum (see chapter 4) and could further support the idea of warm summer conditions. Interestingly, there is a clear shift in the sedimentology of the core over the period of GS-1 (Krainov *et al.*, 2017) (see figure 2.6) that is not being detected in the isotope record, and this could indicate these changes are predominantly occurring during the winter, and will be discussed further in chapter 7.

An additional problem in documenting if a GS-1 type signal can be found in Baunt, may also be due to the record starting during the period associated with the Younger Dryas, meaning there is no clear isotopic baseline of colder or warmer conditions prior to this event. If the record covered the earlier period of the late-glacial interstadial, it may have been easier to see a shift in conditions during the Younger Dryas, while extending the record into the LGM could provide more context as to whether this period is showing values that could be associated with conditions found during the Younger Dryas (GS-1). Alongside this issue, the chronology through this period is also problematic. Figure 3.17 highlights that this period is dated by two dates separated by 1 meter, however both values are close in age and, thus, these sediments could show similar values as they occur very close together in time, during a period of high sedimentation rates. This factor, alongside the dating uncertainties, make it difficult to identify exactly where a Younger Dryas response may be documented, and it may be that the chronological issues alongside the low sampling resolution may contribute to the muted responses documented in this section.

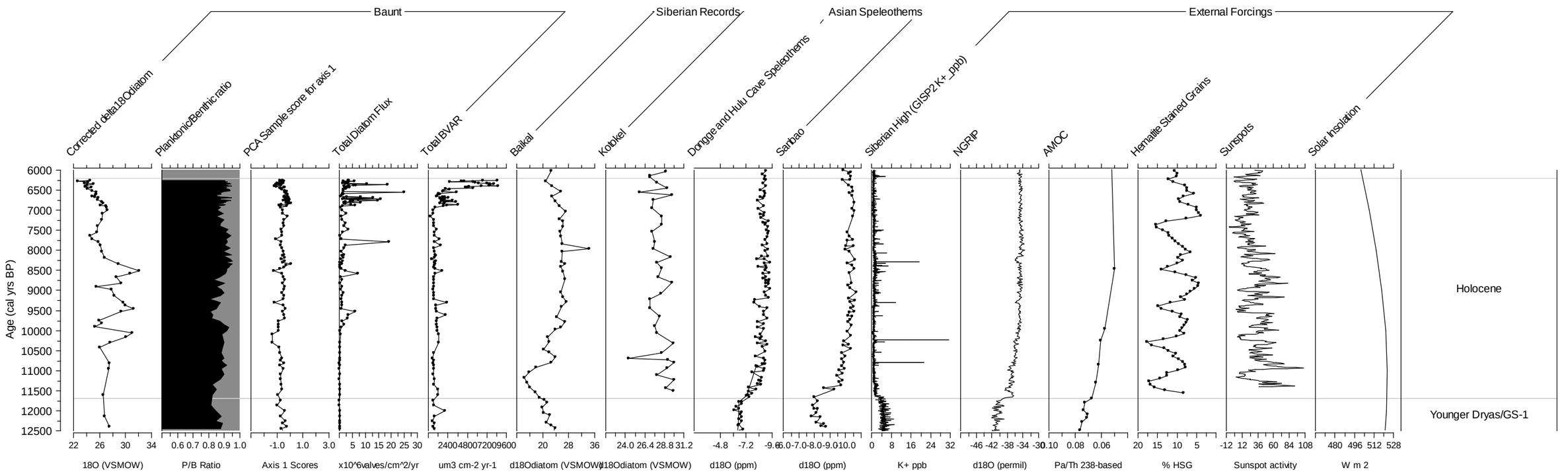

Figure 5.11: Lake Baunt $\delta^{18}O_{diatom}$ (VSMOW ppm) shown alongside P/B ratio, PCA axis 1 scores, Total diatom flux (x10^6valves/cm^2/yr) shown on a logged x-axis and biovolume accumulation rates (BVAR) (µm^{3}cm^{-2}yr^{-1}), alongside $\delta^{18}O_{diatom}$ records (VSMOW ppm) from Lake Baikal and Lake Kotokel and Asian speleothem records $\delta^{18}O$ signal (ppm) from Hulu (Wang *et al.*, 2001), Dongge (Dykosko *et al.*, 2005) and Sanbao (Dong *et al.,* 2010) caves. Also shown against proxies for external climate forcing's including GISP2 K+ signal (ppb) (Siberian High strength) (Mayewski *et al.*, 2004), NGRIP $\delta^{18}O$ signal (Greenland air temperature) (Rasmussen *et al.*, 2014), Pa/Th^{238} record (AMOC strength) (McManus *et al.*, 2004), Hematite Stained Grains (%) (IRD signal) (Bond *et al.*, 2001), GISP2 K+ signal (ppb) (Siberian High strength) (Mayewski *et al.*, 2004), Sunspots, and Solar Insolation from 60°N for June (W m^2)(Berger and Loutre, 1991).

5.4.4 Early Holocene (10.5-8.0 ka BP)

As discussed in section 5.3.2., this period of the Baunt record documents the largest magnitude and most frequent isotopic composition shifts. The large amplitude of these changes, with lows of ~24‰ and highs of ~30‰ are indicative of major hydrological variability. Several reasons may explain the occurrence of these larger shifts, particularly when compared with the previous discussion, and there is evidence from other sources, examined later in this section, to examine both intrinsic and extrinsic forcing.

One reason for the increased amplitude of these changes may be linked to their occurrence during the Early Holocene period, when insolation values reached their highest levels for the period that the $\delta^{18}O_{diatom}$ measurements cover (see figure 5.11). This increased insolation drove global scale climate changes and warming through the Early Holocene, with the Holocene Thermal Maximum being placed between 10-6 ka BP (Liu *et al.*, 2014b), with higher latitudes, particularly those away from large ice sheets, including Siberia, experiencing the earliest thermal maximum, placed between 10-8 ka BP (Jansen *et al.*, 2007; Renssen *et al.*, 2012). This solar insolation maxima resulted in warming in the Lake Baunt area at this time, however, temperature alone is unlikely to have driven the large magnitude of this rapid peak in the $\delta^{18}O_{diatom}$ record. This is because the Dansgaard temperature dependence relationship suggests that for every 1°C temperature increase the $\delta^{18}O_{precipitation}$ value only increases by 0.36‰ in Irkutsk (Seal and Shanks, 1998). Although this cannot be directly applied to the Baunt $\delta^{18}O_{diatom}$ record, it suggests that it could take a temperature shift of ~20°C within a couple of hundred years, which is far too large to be the only driver of the increased $\delta^{18}O$ values seen in the $\delta^{18}O_{diatom}$ record. Indeed, it has been suggested by Kostrova *et al.*, (2016) that precipitation derived from more southerly air mass sources were responsible for higher $\delta^{18}O_{diatom}$ values in the Earlier Holocene, compared to the later Holocene and present, where North Atlantic (westerly derived) sources were more dominant.

To consider the influence of varying precipitation sources for the Baunt record, isotope data for the wider Siberian region and southern regions of Mongolia

and China were considered. Data and models from the Global Network isotopes in Precipitation (GNIP) were utilised. Specifically, the Regionalized Cluster-Based Water Isotope Prediction (RCWIP) model was consulted (Terzer *et al.*, 2013). This integrates data from global network in precipitation stations and produces a gridded global model of seasonal and annual isotope data. Figure 5.12 shows the model's annual average output for $\delta^{18}O_{preciptation}$ in 2018, for Lake Baunt (55°11'15" N, 113°01'45" E), plotted against data for western central Siberian sites and Mongolian and Chinese sites. As a guide, these are plotted against transect of $\delta^{18}O_{preciptation}$ gridded data for 113° longitude (Lake Baunt), on a North-South latitudinal transect. This shows central and western Siberian sites have similar average $\delta^{18}O_{preciptation}$ values (12.62‰), while Lake Baunt's values are isotopically higher by approximately 4‰. It is possible that weakening of the Siberian High, as a result of solar insolation changes during the Early Holocene, could have increased the quantity and extended the season of summer westerly sourced precipitation, thus, increasing the influence of summer precipitation of the $\delta^{18}O_{lakewater}$ values, and subsequently on the $\delta^{18}O_{diatom}$ values. However, this may not be large enough to explain the elevated Baunt $\delta^{18}O_{diatom}$ values seen in the Early Holocene. In part, the increased insolation at this time, may also have signified increased temperatures, compared to modern values, coupled with increased seasonality and very warm summers and, therefore, higher $\delta^{18}O_{preciptation.}$ At the same time, it is also worth considering that, even today, a small proportion of summer winds in the Baunt area are derived from southern and eastern sources, meeting the prevailing westerly airflow. Figure 5.13 also shows average $\delta^{18}O_{preciptation}$ values for more southerly and easterly locations in Mongolia and China, and these have considerably lower (~8‰ difference) isotopic values than Lake Baunt, reflecting in part the influence of southerly and easterly winds. This may support the suggestion by Kostrova *et al.,* (2016), that more southerly sourced precipitation may be influencing the isotopic signal of the region. Although, by comparison to Lake Baikal, this may only be a small component (see section 5.5). The nature of the Early Holocene in Baunt, Baikal and Kotokel are discussed in more detail below.

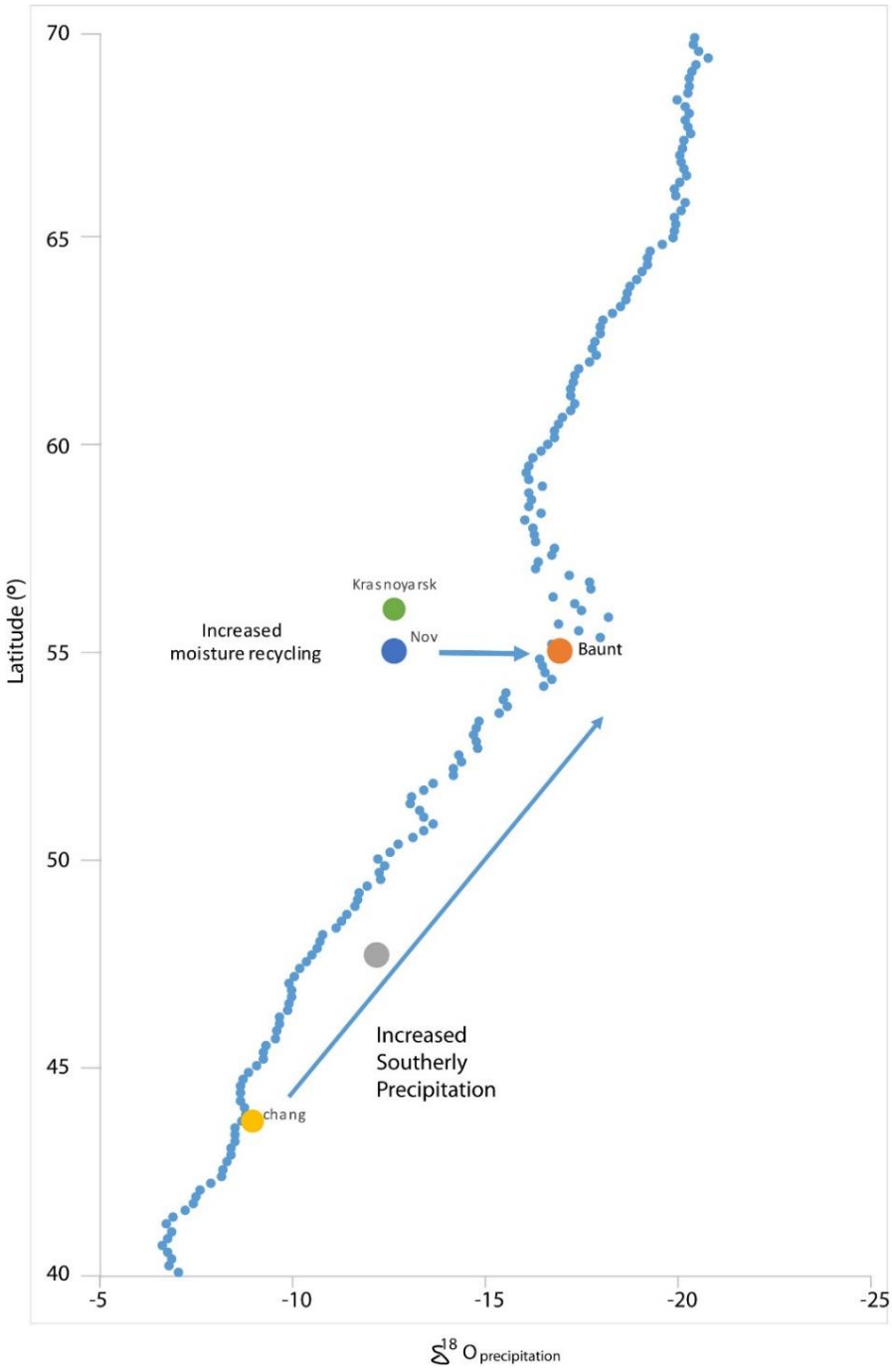

Figure 5.12: Regionalized Cluster-Based Water Isotope Prediction (RCWIP) model annual average output for $\delta^{18}O_{preciptation}$ in 2018 (Terzer *et al.*, 2013). Showing Lake Baunt (orange) (55°11'15" N, 113°01'45" E), plotted against data for western central Siberian sites (Blue (Novosibirsk) and Green(Krasnoyarsk) and Mongolian (Grey (Ulaanbaatar)) and Chinese site (Yellow (Chang Chun) plotted against a transect of $\delta^{18}O_{preciptation}$ gridded data for 113° longitude on a North-South latitudinal transect.

The events seen in this section may, therefore, be reflecting responses to climatic changes, causing alterations in the landscape. The early Holocene period is known for its unstable nature across the Northern Hemisphere, with several abrupt climatic events including the 10.3, 9.2 and 8.2 ka BP events being documented in many records (Heiri *et al.*, 2004; Hoek and Bos, 2007; Mayewski *et al.*, 2004; Wanner and Butikofer, 2008). As discussed previously, the drivers of these early Holocene events are often linked to freshwater pulses entering the North Atlantic during the deglacial period. Therefore, it is possible that the instability shown in the $\delta^{18}O_{diatom}$ record, may be a response to these North Atlantic events, which may affect continental Siberia though reorganisation of atmospheric circulation. Caution is, however, required here, as the shifts in the $\delta^{18}O_{diatom}$ record may be a response to changes in several factors, as discussed previously. There are also additional uncertainties, which make linkage to these abrupt events complicated and these are discussed below.

Chronological uncertainties make it difficult to assign the shifts seen in the $\delta^{18}O_{diatom}$ record to specific times, as the uncertainties from the BNT14 record at this time are in the region of ~±150 years and, thus, at some points the uncertainties are larger than the duration of climate variations (Heiri and Millet, 2005). This means that the Baunt record cannot be tied to specific abrupt climate events over this period. Despite the chronological uncertainties, it is possible to consider that these known climatic events may be triggering some of the changes documented, potentially through teleconnections between atmospheric systems. This has been considered by comparing the GISP2 potassium (K^+) record (Mayewski *et al.*, 2004) with the Baunt isotope record, and is shown in figures 5.11 and 5.13. This figure highlights that this period documents the largest variability in the GISP2 K^+ signal, which indicates that the Siberian High's strength is likely to have been unstable across this period. This, therefore, has potential to cause abrupt changes in the environment, which may explain the oscillations seen in the Lake Baunt record, however, again it is important to consider the chronological uncertainties with the Baunt record over this point, as these are large enough during this period to cause the age ranges for the main peaks and troughs to overlap (see figure 5.13),

where the uncertainties around the timing of peaks and troughs are shaded in red and blue respectively, showing that in many cases the shifts occur so close to each other that the ages for a peak often overlap with a trough in the record. This prevents any of the Baunt shifts across this period being tied to an individual shift in the K^+ record (see figure 5.13). Additionally, the large uncertainties and limited sampling resolution in the Baunt record make it difficult to determine the duration of the shifts. The K^+ signal documents extremely rapid fluctuations in the Siberian High, and it cannot be determined if the shifts recorded in Baunt are also this abrupt, due to the much lower resolution achievable in Lake Baunt, compared to shifts documented in the Greenland ice cores. Additionally, the responses documented by Lake Baunt are unlikely to have been linear, with for example, abrupt cooling potentially altering the $\delta^{18}O_{diatom}$ record by changing the $\delta^{18}O_{lakewater,}$ by reducing the input of glacial meltwater, or by changing the blocking position of the Siberian High and, consequently, altering precipitation sources. Therefore, although the K^+ record may indicate instability in the Siberian High strength at this time, potentially driving climatic instability in southern Siberia, the changes documented in the Lake Baunt system cannot yet, be directly linked to the north Atlantic events. The events in the $\delta^{18}O_{diatom}$ record may show some reflection of these events, through changes they may have caused on the $\delta^{18}O_{lakewater,}$ through variations in $\delta^{18}O_{precipitation,}$ which could be linked to source region changes, due to movement in the position of the Siberian High or because of fluctuations in the quantity of rainfall reaching Baunt. Changes could also be a result of the impact of temperature variations on the $\delta^{18}O_{lakewater}$. Either way, the responses documented in Lake Baunt are not a linear response to abrupt climate instability observed in the North Atlantic, and further work is required to understand how these events propagate and manifest themselves in southern Siberia.

Therefore, although in theory the shifts in the $\delta^{18}O_{diatom}$ record across this period could be climatically induced, potentially through Siberian High strength change as discussed above, this link can only be cautiously made at this time, and improvements in the resolution and chronological control would be required to assist with this.

The final shift in $\delta^{18}O_{diatom}$ values during this period occurs at ~8.1±3 ka, with age ranges allowing it to overlap with the widely documented 8.2 ka BP event in the Northern Hemisphere. A clear peak in Siberian High strength is documented for this period (figure 5.13), and this may indicate that the BNT14 record shows a response to this well documented 8.2 ka BP event. This may suggest that the Siberian High has temporally been increased in strength, potentially blocking moisture sources and increasing aridity. The limited rebound to higher values as documented in the earlier shifts, may be linked to the reductions in solar insolation (see figure 5.11), which occur at this point, meaning that after a climatic shift driven by Siberian High intensity changes, the region does not warm as rapidly. Despite the similar timing of the shift in Baunt, and of the well documented 8.2 ka BP event, caution is again required here, as the shift in the $\delta^{18}O_{diatom}$ record does not show an oscillation, but a general change in values, with no return to previous levels, potentially highlighting a more general change in the system, rather than a response to an abrupt event. The shift suggested for the Siberian High from the K^+ record is very abrupt (figure 5.11 and 5.13) and then returns to similar values to before the event, and the lack of a similar pattern in Lake Baunt is indicative of additional or alternative events causing the change in the $\delta^{18}O_{diatom}$ values. Therefore, the link to this event is cautious and more work is required to understand the changes in the system at this point. The potential link to this to the 8.2 ka BP event is considered in more detail in chapter 7.

5.4.5 Mid Holocene (~8.0-6.0 ka BP)

The reduction in the amplitude of changes after ~8 ka BP may be driven by a number of factors. This may be due to the declining solar insolation, which occurs across this period and is linked to global climatic shifts (Liu *et al.*, 2014b; Renssen *et al.*, 2012). Additionally, to this, figure 5.11 documents that this period shows a marked reduction in K+ fluctuations in the GSIP2 ice core and, therefore, the greater stability in the Siberian High may explain the greater stability in the $\delta^{18}O_{diatom}$ record. The increased stability in the Siberian High may be a response to more stable conditions in North Atlantic circulation. As discussed in section 5.4.1 and in chapter 1, the North Atlantic is considered a key driver of Northern Hemisphere climatic changes, due to changes in the

THC in response to salinity changes, driven by ice sheet melting. It is, therefore, likely that the greater atmospheric stability, and consequently, regional hydrological stability, is linked to greater THC stability in the North Atlantic post deglaciation.

The last section of the $\delta^{18}O_{diatom}$ record after 7 ka BP does show a decline in values, although this is considerably smaller than the earlier variations in the isotope record, but it does match a decrease in IRD, and a reduction in the Siberian High (figure 5.11). Nevertheless, the latter part of the record is more stable than the preceding part of the Holocene. It may mean that by this time any major loss of ice sheets has ended and, thus, there may be a rerouting of drainage patterns. It is unlikely the lack of abrupt shifts is linked to sampling resolution, as the number of samples at this point of the core is greater, due to higher concentrations of diatoms being preserved in this section of the core and, thus, preparation of appropriate weights of samples of analyses was more achievable. Despite the excellent sampling resolution at this point of the core, caution must also be applied when considering the upper section, due to chronological uncertainties (see chapter 4). Additional care is required in this section, as this is where levels of silt were highest within the samples, meaning they have undergone the largest corrections. The occurrence of high levels of silt in the upper samples (see figure 5.6), means this value particularly should be interpreted cautiously, and may represent a period of increased in-wash. Periods of high silt within the core could also suggest environmental changes, which may influence shifts within the $\delta^{18}O_{diatom}$ record, such as changes in the sources of material being deposited into Lake Baunt, which may indicate a change in the hydrological regime, potentially driving increasing in-washing of silt.

5.5 Regional Records

Oxygen isotope analyses on diatoms have become a frequently used proxy within Siberia, driven by their excellent preservation in lakes within the region. This means that, as more sites are analysed, it is possible to start to consider how this network can inform us about regional responses to palaeohydrological and palaeoclimatic changes. Lake Baikal and Lake Kotokel

are both located within the southern Siberian region, and their diatom oxygen isotope records provide an ideal opportunity to start this consideration for the LGIT and Holocene period. Figure 5.13 shows the three records together against age. The Baikal record's age model has been updated to use IntCal13 (by this author), as opposed to IntCal09, to allow all datasets to be calibrated using the same curve. As both IntCal curves are tree ring based at this point, there are not any significant changes to the Baikal chronology, although the first major isotope excursion has moved slightly older to ~ 11.0 ka BP. Considering these records together allows for a more detailed examination of the regional responses to palaeohydrological and palaeoclimatic events.

5.5.1 Regional and Hemispheric Expressions of the Younger Dryas/GS-1

The southern Siberian records (figures 5.13 and 5.11) all show similarities in their limited $\delta^{18}O_{diatom}$ responses to any form of Younger Dryas signal. In Lake Kotokel, $\delta^{18}O_{diatom}$ values through the Late-glacial period are very similar to the Holocene, while the Baikal signal is also muted during the Younger Dryas, although there is evidence for a Pre-Boreal Oscillation (see figure 5.13) (Mackay *et al.*, 2011). When combined it is possible to note that the records support the idea that there is no clear Younger Dryas signal in the $\delta^{18}O_{diatom}$ data. As discussed, there may be several reasons for this, however, similarity across sites lends support for the idea of continental regions still having warm summers through the Younger Dryas period, as discussed by Schenk *et al.*, (2018). This highlights the need to use multiple proxies from multiple sites, to build a regional understanding of palaeohydrological and palaeoclimatic changes, and this will be considered in more detail in chapter 7.

The Baunt record has also been compared to Asian speleothem records from Hulu (Wang *et al.*, 2001), Dongge (Yuan *et al.*, 2004) and Sanboa (Hai Cheng *et al.*, 2009) (see figure 5.11). These all show less negative $\delta^{18}O$ values during the period that the GSIP2 K+ record indicates a strong Siberian High. The speleothem records are considered to document the relative strength of the East Asian summer monsoon versus the winter monsoon, with the former bringing in Pacific precipitation, while the latter is controlled by cold Siberian winds (Wang *et al.*, 2001), although this has also been considered to relate

more to isotopic changes driven by the amount effect, that has been well documented for other speleothem isotope records (Lee and Swann, 2010). This, in turn has an impact on how far the coastal Asian speleothems can be used as a wider regional archive of precipitation. As discussed in chapter 1.4, the Siberian High and East Asian Monsoons have a modulating effect on the opposite system, with a strong Siberian High driving a stronger East Asian Winter Monsoon, as a result of the larger pressure gradient between the Siberian High and Aleutian Low (Tubi and Dayan, 2013). As discussed in section 5.4.1, Baunt's record is stable and does not appear to reflect the strengthened Siberian High and, therefore, this again suggests that the isotopes are not recording the cold arid conditions expected for this period. The NGRIP $\delta^{18}O$ record, also shown in figure 5.11 is thought to reflect air temperature (Steffensen *et al.*, 2008), and this documents colder conditions over Greenland across this period, which again highlights the difference with the responses recorded in the Siberian records, lending further support for the continental warm Younger Dryas summers hypothesis (Schenk *et al.*, 2018). However, there are a wider number of proxy records within this thesis, that record both summer and in some cases longer signals and, therefore, the expression of the Younger Dryas in Baunt, and the wider region, is discussed in chapter 7.

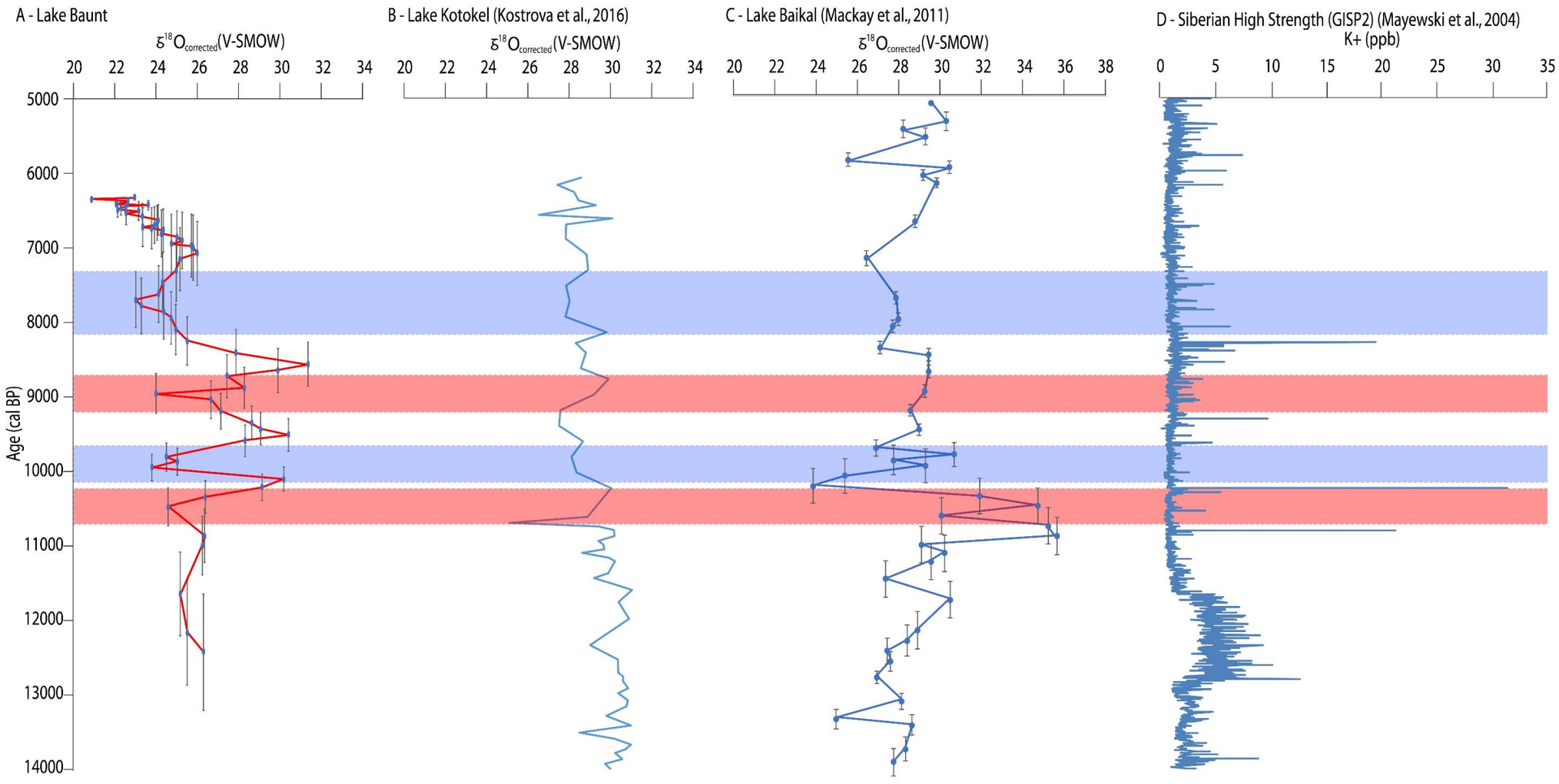

Figure 5.13: $\delta^{18}O_{diatom}$ records from: **(A)** Lake Baunt, **(B)** Lake Baikal and **(C)** Lake Kotokel shown alongside **(D)** the GSIP2 K^+ record of Siberian High Strength (Mayewski *et al.*, 2004). Red and blue bands highlight the chronological uncertainties associated with some of the peaks and troughs in the Lake Baunt record and how they compare to the other records.

5.5.2 Regional and Hemispheric Expressions of the Early-Mid Holocene

One of the most notable similarities between the Lake Baunt and Lake Baikal records shown in figure 5.13, are the large amplitude $\delta^{18}O_{diatom}$ shifts during the Early Holocene. Their occurrence between the two records are, however, slightly offset, with the onset of change in Baikal staring at ~11 ka BP, while Baunt's signal is suppressed until ~10.5ka BP. Due to the dating uncertainties on both records, it may be that these events start closer in time, but further dating work is required to confirm this. Nevertheless, based on current chronological controls, the initial peak in the Baikal record is almost ~1000 years earlier than in Baunt. Kotokel on the other hand documents only one oscillation during this period, centred around ~10.7ka BP. This shift in $\delta^{18}O_{diatom}$ values is the only event which appears in all three records (within dating errors). This may suggest a larger magnitude event, although, site-specific factors may also explain the variation between the regional records, particularly the evaporitic nature of the site.

In the case of Lake Baikal, the earlier onset of instability compared to Baunt could be produced by several factors. The most notable is the significant differences in catchment sizes between the two lakes. As discussed by Mackay *et al.*, (2011), the Baikal record shows a reflection of the proportion of input from southern versus northern sourced rivers, with the rapid warming suggesting a higher proportion from southern rivers and, thus, reduced Siberian High strength. It may be that the larger more southerly catchment from Baikal documents warming not detected further north. The isotopically higher values reported for the Early Holocene in Lake Baikal have been explained as being sourced through the influence of the southerly catchment form the Selenga River, contrasting with lower values through greater influence of rivers to the north, coincident with reduced AMOC and increased IRD fluxes in the North Atlantic. There is a ~7‰ ppm difference between these source waters, and this seems to explain the Baikal oxygen isotope record for the Early Holocene. The highest $\delta^{18}O_{diatom}$ values in Baunt are ~4‰ ppm lower than the highest value in Baikal, although the lowest values in both are similar.

This would make sense following the interpretation of Mackay *et al.*, (2011), indicating a major influence from the Selenga river, considering the much smaller catchment of Baunt, and, thus, much more of the summer precipitation being derived from rainfall. It is also worth noting, as mentioned elsewhere, that the lag in the shift to higher isotope values in Baunt, by comparison to Baikal (Figure 5.13), may reflect not only the southerly catchment influence on Baikal, but also the more northerly position of Lake Baunt.

Although a combination of early Holocene warming, seasonality, and a possible contribution of southerly winds, may explain the Lake Baunt increased $^{18}O_{diatom}$ values from ~10.5 ka BP, it does not explain the oscillations of higher and lower values that occur between ~10.5 and ~8 ka BP. Several other factors, therefore, need to be considered. The diatom flux record from BNT14 (see chapter 4) can assist in understanding these more rapid fluctuations, with rapid changes in flux occurring over this time (see figure 5.11). As discussed in chapter 4 this may be driven by changes in the lake conditions, and increased in-washing of nutrients, and this could indicate greater snowmelt or increased summer precipitation. Here it is worth considering the pattern of fluctuating isotope values seen in Baikal (Mackay *et al.*, 2011), where the shifts to lower values are interpreted as the influence of climatic cooling driven by weakened AMOC in the North Atlantic, and also seen in regional vegetation. Some of these lower isotope excursions are also seen in Baunt, particularly around 10.3-10 ka BP and at ~8.5-8 ka BP. The Baunt record seems to support the interpretation from Baikal of early Holocene cooling events. There is not, however, a perfect match and at ~7 ka BP and 9 ka BP isotope values in Baunt are sharply lowered, while in Baikal they are stable or rising, and this cannot be explained by dating uncertainties or sample resolution. It is possible, however to explain these differences by the melting of glaciers in the Baunt area, during the early Holocene being superimposed on the climatic signal interpreted for both lakes. In Baikal, as discussed later, carbon isotopes and CMAR data (chapter 6), suggest in-wash from melting glaciers in Baikal. It seems likely that, despite a delayed onset of warming, there would be a similar melting of local glaciers in the Baunt area, given the evidence for glaciation in the area during the Little Ice Age (Osipov and

Osipova 2014). $\delta^{18}O$ of meltwater will be isotopically lower than that of precipitation as $\delta^{18}O$ of snow is isotopically lower than rainwater, and this effect is magnified by altitudinal factors (He *et al.*, 2006). Thus, an influx of isotopically lower meltwater to the lake could explain the offset between the two records. In terms of climatology this seems sensible, as particularly at 9 ka BP, IRD is lower and Baikal is warm (Mackay *et al.*, 2011), and is also discussed with reference to CMAR and the carbon cycle in the next chapter.

5.6 Oxygen Isotope Summary

The Lake Baunt oxygen isotope record highlights several shifts between ~12.5-6 ka BP. These group into three sections, a stable early period between ~12.5-10.5 ka BP, a period with large magnitude abrupt shifts between ~10.5-8 ka BP and a more muted period between ~8-6 ka BP, but still with some variability. These appear to reflect changes in several factors, including the source, quantity and seasonality of precipitation as well as temperature. Some of the changes co-occur alongside known Northern Hemisphere climate events, including those at ~10.4, 9.3 and 8.2 ka BP, suggesting a climatic influence on these records, although dating uncertainties prevent confident correlations. Other well documented Northern Hemisphere climatic events are not identified, including the Younger Dryas. This is potentially caused by a summer season bias being introduced by the diatoms, and is potentially linked to theories based on the Younger Dryas having warm summers driven by a continental blocking high (Schenk *et al.*, 2018). Longer term solar insolation trends are also reflected. Other regional records show similarities and differences to Baunt, highlighting the importance of site-specific factors for understanding $\delta^{18}O_{diatom}$ records. Additional factors, including sampling resolution may have influenced the ability of some known climate events to be documented in the record, and this could be improved in the future.

6 The Lake Baunt Carbon Record

6.1 Introduction

Lakes are an important component of the global carbon cycle, acting as both a carbon source, as CO_2 is emitted from the lakewater to the atmosphere, contributing to global greenhouse gases, and recycled in the biosphere on contemporary timescales (Mendonça *et al.*, 2017), and a sink, as carbon is preserved within the sediments on geological timescales (Mendonça *et al.*, 2017). Sedimentation of organic carbon within lakes is much faster than observed in marine settings, due to higher sedimentation rates, increased proportions of terrestrial organic carbon and lower oxygen availability, meaning more organic carbon escapes mineralisation and is preserved (Mendonça *et al.*, 2017). Despite this, estimates of the organic carbon preserved within lake settings is poorly constrained, although it is estimated as 42 $Tg\dot{m}yr^{-1}$ (Dean and Gorham, 1998). When considered collectively with peatlands and reservoirs, these provide a carbon sink of 300 $Tg\dot{m}yr^{-1}$, despite only making up 2% of the earth's surface (Dean and Gorham, 1998), which reiterates their importance in the global carbon cycle.

Understanding carbon cycling is of particular importance in southern Siberia, due to its position at the boundary between continuous, discontinuous, and sporadic permafrost (Gordov and Vaganov, 2010). Permafrost is one of the largest pools of organic carbon (Schuur *et al.*, 2008), and changes to it, as a result of current warming, means that the organic carbon preserved in these settings is susceptible to remobilisation and mineralisation, creating a carbon source (Vonk *et al.*, 2012). These changes cause large alterations to lakes and their catchments, in these sensitive regions, increasing TOC in lakes as a result of thawing, which in turn causes vegetation change and increased erosion (Vonk *et al.*, 2012).

Despite the sensitivity of regions, including southern Siberia, to climate change induced alterations in the carbon cycle, carbon studies are relatively limited in this region. Considerations of the carbon content of lake sediments are, therefore, of great importance, with many techniques now allowing reconstruction of past climate and carbon dynamics over long timescales

(Meyers, 2003). As presented in chapter 2, Loss-On-Ignition (LOI) and Total Organic Carbon (TOC) can be used to estimate the bulk organic content that escapes remineralisation during deposition (Meyers and Lallier-Vergès, 1999) (see chapter 2). Alongside these, carbon mass accumulation rates (CMAR's) can be used to consider the accumulation of carbon, taking into account sedimentation rate shifts, although a fairly linear sedimentation rate is required (Meyers and Teranes, 2001). C/N ratios are also increasingly used, providing a method to consider the source of carbon (e.g. algal versus vascular plants) (Leng and Marshall, 2004; Meyers, 1994; Meyers and Lallier-Vergès, 1999). Finally, the $\delta^{13}C$ of sediments is also used to consider primary production and sources of organic matter preserved within sediments (Meyers, 2003). These will be explored in more detail below.

C3 phytoplankton preferentially use ^{12}C to produce organic matter, and this has a ~20‰ more enriched isotopic signature than the dissolved inorganic carbon source, and, therefore, as C3 phytoplankton are deposited in lake sediments, they remove ^{12}C from the surface water. During periods of high algal productivity this becomes depleted, increasing the $^{13}C/^{12}C$ ratio of the remaining inorganic carbon and, consequently, changing the $\delta^{13}C$ of organic matter produced in these depleted conditions (Meyers, 2003). Changes in sedimentary $\delta^{13}C$ can, therefore, inform about changes in primary productivity. However, algal produced organic matter is usually indistinguishable from organic matter produced by C3 Calvin pathway plants in the catchment, and this can make separating the contribution of these sources to $\delta^{13}C$ records complex (Meyers, 2003, 1994; Meyers and Lallier-Vergès, 1999). To overcome this, $\delta^{13}C$ is often studied alongside $C_{organic}/N_{total}$ ratios (C/N ratios), to allow the proportional importance of non-vascular algae compared to vascular plant to be considered (Meyers and Lallier-Vergès, 1999). These sources can be separated using C/N ratios due to the very low, if any, quantity of cellulose in lake algae, while vascular plants are cellulose rich (Meyers, 2003, 1994; Meyers and Lallier-Vergès, 1999).

These variables are also usually considered alongside organic carbon content, as this is an additional indicator of productivity in the environment. Total organic carbon content in lake sediments is the amount of organic carbon

sequestered that escapes remineralisation. However, the organic carbon content can be influenced by the sedimentation accumulation rates. In order to counter this, carbon content can be converted to carbon mass accumulation rates (CMAR) (Mackay *et al.*, 2017; Meyers and Teranes, 2001).

The growth of diatom isotope analyses (as discussed in chapter 5), alongside oxygen isotopes, includes nitrogen, silicon and carbon, which are occluded into diatom frustules. $\delta^{13}C_{diatom}$ analyses are increasingly used to provide palaeoenvironmental information into the carbon cycle (Hernández *et al.*, 2011). Many benefits exist for undertaking $\delta^{13}C_{diatom}$ analyses, particularly the increased precision offered by undertaking analyses on a single host organism, as opposed to bulk carbon samples (discussed above), where there is uncertainty linked to the wide range of potential sources of organic carbon to the sediments (Barker *et al.*, 2013; Hurrell *et al.*, 2011). The organic matter contained in the diatom frustule includes organic matter in the form of polysaccharides, proteins and long chain polyamines (Hernández *et al.*, 2011; Hurrell *et al.*, 2011). These are thought to be protected from decomposition in the water column and post-depositional diagenesis, unless the diatom is subject to dissolution (Abramson *et al.*, 2009; Webb *et al.*, 2016). This means the organic matter bound within the frustule, should provide a reliable proxy for the environmental conditions at the time it was laid down (Abramson *et al.*, 2009).

Currently the number of studies of $\delta^{13}C_{diatom}$ in lacustrine environments is small compared to marine settings (Hernández *et al.*, 2011), and this is linked to greater complexities in factors influencing $\delta^{13}C_{diatom}$ analyses in lakes (Hernández *et al.*, 2011). Despite this, the use of carbon isotopes has grown as methodological advances have progressed. In the marine realm, $\delta^{13}C_{diatom}$ values are generally considered to be influenced by primary productivity and the aquatic CO_2 concentration (Hernández *et al.*, 2011). In lacustrine settings $\delta^{13}C_{diatom}$ values are expected to reflect the balance between the nature and amount of carbon supplied to a lake, alongside the demand of the lake's aquatic ecosystem for carbon (Barker *et al.*, 2013). This is because the $\delta^{13}C_{diatom}$ value is determined by the carbon content of the lake-waters, which are taken up by the diatoms during cell formation, by photosynthesis. The

carbon that is taken up is in the form of dissolved inorganic carbon (DIC), with dissolved CO_2 being the preferred source. However, during periods of high demand diatoms can utilise bicarbonate (Giordano *et al.*, 2005; Webb *et al.*, 2016), which raises their $\delta^{13}C$. In some studies, it has been possible to utilise this relationship to make some inferences about the relationship between aridity/humidity and diatom carbon sourcing (Barker *et al.*, 2013). By examining the difference between $\delta^{13}C_{diatom}$ and measured $\delta^{13}C_{bulk}$, it was possible to determine that periods where the two were correlated occurred during dry periods, as diatoms depleted DIC. The relationship broke down as precipitation increased, as carbon was supplied from the catchment (Barker *et al.*, 2013). The Baunt record has $\delta^{13}C_{diatom}$, $\delta^{18}O_{diatom}$, and $\delta^{13}C_{bulk}$ data available on the same, or closely related, samples, and this can be used to explore some of the points raised in chapter 5 with regards to precipitation in the Early to Middle Holocene.

$\delta^{13}C_{diatom}$ measurements in lakes are affected by several of the factors discussed as influencing $\delta^{18}O_{diatom}$ (chapter 5), including species effects (Des Combes *et al.*, 2008), cell size, growth rate and metabolic pathways (Hernández *et al.*, 2011). Other important factors to consider when undertaking $\delta^{13}C_{diatom}$ studies include the influence of $^{13}C_{DIC}$ (dissolved inorganic carbon, DIC), as this will influence the $\delta^{13}C_{diatom}$ values and, therefore, careful consideration of carbon sources is essential. Changes in $^{13}C_{DIC}$ are influenced by alterations in dissolved organic carbon (DOC) and DIC entering the lake from thawing soils, and also by internal processes, such as autochthonous production and internal recycling (Webb *et al.*, 2016).

This section of the project aims to evaluate the effects of critical transitions, during the Early Holocene and end of the LGIT, on ecosystem functioning related to carbon cycling in lakes. It is anticipated that during increased periods of algal productivity, as discussed in chapter 4, $\delta^{13}C_{diatom}$ values will increase (enrich), while during less productive times, $\delta^{13}C_{diatom}$ values will decline (deplete). Increased catchment sourced $\delta^{13}C$, which can be differentiated from autochthonous carbon using C/N ratios, may provide the needed organics for diatoms, and this may result in a breakdown between $\delta^{13}C_{diatom}$ and $\delta^{13}C_{bulk}$

relationships (Barker *et al.*, 2013), and this will be considered by undertaking parallel $\delta^{13}C_{diatom}$ and $\delta^{13}C_{bulk}$ on some samples.

6.2 Methodology

6.2.1 $\delta^{13}C_{diatom}$ Methodology

47 samples were studied for $\delta^{13}C_{diatom}$ analyses. In many cases these analyses were undertaken on the same samples as $\delta^{18}O_{diatom}$ analyses. All samples underwent cleaning as detailed in chapter 5.1.2, following the method outlined by (Morley *et al.*, 2004). Particular care was taken for these samples, due to high concentrations of charcoal within the BNT14 core (Bezrukova pers. com.), which could significantly alter the results if left in the samples. To overcome this larger sample sizes were used and samples were sieved thoroughly at 10µm to remove charcoal. SEM imaging was undertaken at the Department of Earth Sciences, University College London, to visually check the samples prior to analyses.

After cleaning, analyses were undertaken at British Geological Survey, Keyworth, UK., on a Costech ECS4010 elemental analyser, which was interfaced with a VG dual inlet isotope ratio mass spectrometer (Hernández *et al.*, 2011). The samples were weighed into tin capsules and then dropped into a furnace at 1020°C under continuous flow of helium (Hurrell *et al.*, 2011). An oxygen gas pulse is used to promote an exothermal flash oxidation of the tin capsule, and the gases produced by the reaction are oxidised further in the lower part of the furnace. Excess oxygen and water are removed and the remaining N_2 and CO_2 are passed through a GC column and a thermal conductivity detector (Hurrell *et al.*, 2011). This produces an electrical signal that is proportional to N_2 and CO_2 concentrations in the helium stream, which the Costech software acquires and evaluates, producing the %N and %C data (Hurrell *et al.*, 2011). As %N data is very small in diatom samples it is not reported (Hurrell *et al.*, 2011). Following this, the helium stream carried the CO_2 through a -90°C trap, which removes any remaining water, before being held at the triple-trap at -196°C, where the CO_2 is frozen, and the N_2 and He is vented to the atmosphere. The Triple-Trap was evacuated, causing the CO_2 to expand into the inlet of the mass spectrometer. A second cryogenic trap,

positioned directly in from of the inlet, was then used to introduce the CO_2 closer to the source, which provides sufficient pressure of the CO_2, despite small volumes. Triple collectors on the mass spectrometer meant that CO_2 ion beams at m/z 44, 45 could be measured simultaneously, while a dual-inlet allowed rapid comparison of sample CO_2 with reference CO_2 (Hurrell *et al.*, 2011). The 44/45 m/z ratios were converted to $^{13}C/^{12}C$ ratios. Each run contained both between and within run replicates, alongside standard samples from BROC and SOILA and SOILC. All values were converted to the VPDB scale.

6.2.2 Bulk Sample Methodology

In total 142 bulk samples were studied from Lake Baunt, 100 of which were undertaken as part of a M.Sc dissertation project (Ledger, 2017), co-supervised in the laboratory by this author. Samples were initially placed in 5% HCl to remove any inorganic carbon, before undergoing 5 centrifuge rinses with deionised water. Samples were then freeze dried to remove remaining liquid, before being ground to a fine powder and stored in sealable test tubes. Analyses were also undertaken by combustion in a Costech ECS4010 elemental analyser and VG Optima mass spectrometer and were converted to the VPDB scale using within lab standards calibrated against NBS-22. Replicate samples were run to ensure precision. Bulk %C samples are reported as carbon mass accumulation rates (g C m^{-2} yr^{-1}).

6.3 Results

6.3.1 $\delta^{13}C_{diatom}$ Results

The results for the BNT14 $\delta^{13}C_{diatom}$ analyses are shown in figure 6.1. These document several variations in measurements across the core. Low (more negative) values are documented at the base of the record, between ~12.5-11.9 ka BP, although age uncertainties are large across this section (see figure 6.1). This period is followed by a stepped rise in values to a peak at ~9.4 ka BP where values reach –26.1‰. Values then fluctuate between ~–27‰ and –28.5‰ until ~8.6 ka BP, where values drop rapidly to a low of –32.3‰. This low value is only recorded in one sample, and is followed by a rapid rise to –26.9, at ~8.5 ka BP, and this may, therefore, represent a very rapid transition,

or may highlight a potential issue with this one sample. Analysis of additional samples in the future could help to resolve this. Following this period, the record falls more gradually to a low of –30.4‰ at ~7.85 ka BP, after which, it gradually increases.

6.3.2 Bulk Sample Results

Figure 6.2 documents the bulk isotope data from the Lake Baunt sediments. These cover the period between ~22.0 and 7.7 ka BP. Several shifts are seen in these records, with the bulk $\delta^{13}C$ (figure 6.2:A) starting with high values at ~22 ka BP, but declining rapidly to low values around –28‰ by ~21.7 ka BP. These lower values between –28‰ and –26‰ persist until ~20 ka BP, where values rise rapidly to 24.7‰ and then fluctuate between –25‰ to –24‰ until ~17.5 ka BP. Following this, values decline more gradually to a low of –28.6‰ at ~16.2 ka BP. After this, values rise again to a peak of –25.8‰ at ~14.6 ka BP, and then values fluctuate between –26‰ to –27.5‰ for the remainder of the record till ~7.7 ka BP.

The %C record (figure 6.2:B) is antiphase to the $\delta^{13}C_{bulk}$ record, with low values between ~20.5 to ~17.6 ka BP, and generally higher percentages for the remainder of the core, although lower troughs are documented at ~14.6 ka BP. After this, values fluctuate around 3%. CMAR (figure 6.2:C) fluctuate during the lower sections of the core, between 2.5-22 g C m^{-2} yr^{-1} until ~16.8 ka BP, where values become very low, under 5 g C m^{-2} yr^{-1}, until ~14.2 ka BP, although there is one reading at around 10 g C m^{-2} yr^{-1} at ~14.8 ka BP. From ~14 ka BP, CMAR rise rapidly to the largest peak in the record, which reaches 84 g C m^{-2} yr^{-1}, at ~13.7 ka BP, and this occurs as sedimentation rates increase rapidly, as seen in the MAR's in chapter 3 (figure 3.18). Values are high until ~13.4 ka BP, after which they return to levels under 20 g C m^{-2} yr^{-1}. By 12.3 ka BP values have fallen to under 10 g C m^{-2} yr^{-1}, where they remain until 10.2 ka BP, after which they rise slightly to fluctuate between 10-20 g C m^{-2} yr^{-1}, for the remainder of the record.

The C/N ratios (figure 6.2:D) show a different structure to the other records. Values start at 8.3 and rise to 14.2 by ~20.4 ka BP. This is followed by a rapid decline to a low of 8.5 by ~19.9 ka BP, which is followed by a gradual increase.

This increase is interrupted by a rapid peak to 19.1 at ~14.2 ka BP, however this shift is only seen in 1 sample and could be an anomaly, as after this, the samples return to their gradually increase over this period. The gradual rise plateaus from ~12.9 ka BP, after which, values fluctuate between 11-14 for the remainder of the record.

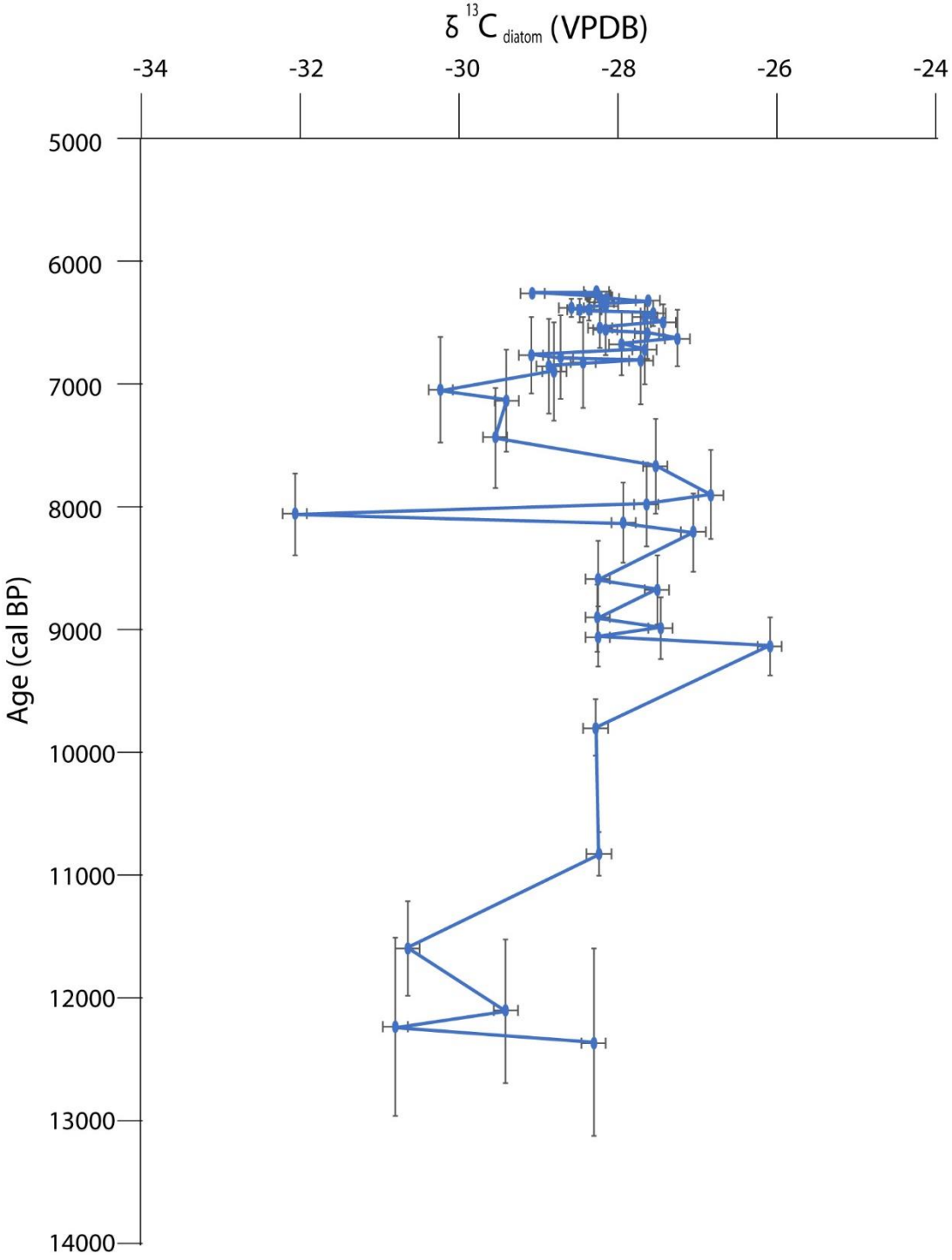

Figure 6.1: $\delta^{13}C_{diatom}$ record from Lake Baunt shown against age. Chronological uncertainty and isotopic errors are shown.

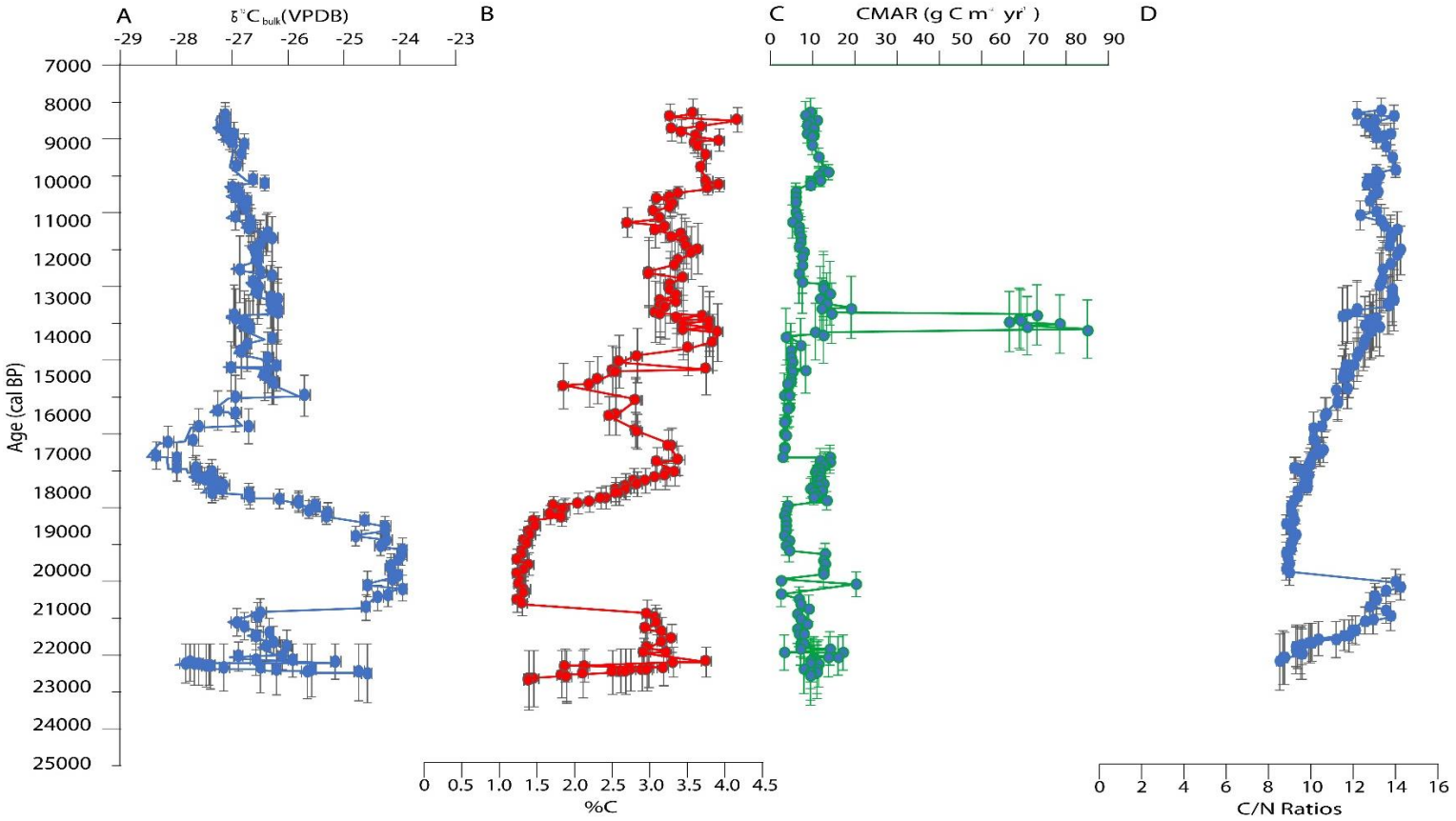

Figure 6.2: Lake Baunt bulk carbon isotope records shown against age with chronological uncertainty and analytical error. **(A)** $\delta^{13}C_{bulk}$ **(B)** %C **(C)** CMAR (g/per cm^{-2}/yr^{-1}) and **(D)** C/N Ratios.

6.4 Discussion

Throughout the record the values of the $\delta^{13}C_{bulk}$ samples all fall between ~–29‰ and –24‰, which highlights that they are dominated by C_3 plants as the main carbon source (Wang *et al.*, 2013). This is not unexpected at Lake Baunt, as there is no calcareous geology (see chapter 2) or C_4 plants present in the catchment (Brincat *et al.*, 2000; Mackay *et al.*, 2017), and, therefore, these will not influence the $\delta^{13}C_{DIC}$. However the $\delta^{13}C_{bulk}$ values cannot distinguish between algae and terrestrial C_3 plants (Wang *et al.*, 2013) and to overcome this issue, the C/N ratios can also be considered, as discussed in chapter 4. These can assist in determining between autochthonous or allochthonous organic matter sources (Meyers, 1994; Meyers and Lallier-Vergès, 1999), with algae having low C/N ratios of between 5-10 (Meyers and Lallier-Vergès, 1999). Aquatic vegetation has much higher ratios between 20-30, while terrestrial vegetation sits between 20-160 (Meyers and Lallier-Vergès, 1999).

6.4.1 The Late Pleniglacial and Heinrich 1

The bulk carbon samples start at ~22 ka BP, allowing consideration of changes to carbon cycling during the latter stages of the last glacial period, and particularly Heinrich 1 (figure 6.3). During this early part of the record the $\delta^{13}C_{bulk}$ are high and C/N ratios are low, highlighting the dominance of algae for sourcing organic matter, however, this shifts rapidly, as by ~22.4 ka BP, the $\delta^{13}C_{bulk}$ declines sharply as the C/N ratios rise, indicating increased content from other sources, potentially aquatic and terrestrial vegetation. The lowest values in the $\delta^{13}C_{bulk}$ and the highest in the %C are observed at the start of this shift, while the C/N peak is later at ~20.1 ka BP, suggesting that the changes documented by the C/N ratio may have a lagged response to the forcing that drives this change.

To consider this shift further the other proxies from Baunt are considered (see figure 6.3). This highlights that these occur alongside shifts in the diatom composition and biovolumes, and changes in the TOC and BSi. As discussed in chapter 4, this indicates major alterations within the lake and catchment at

this time, and the carbon data supports previous conclusions that. following the LGM, this site undergoes a period of increased productivity. This is further supported by the CMAR, which show an initial peak at the transition from the LGM and then have moderate values, suggestive of high organic matter production and sequestration. As in chapter 4, potential external drivers for this shift are unclear (figure 6.4), as Siberian High strength shows a slight decline, but solar insolation remains low. As discussed in chapter 4, this may indicate a time transgressive response to improved conditions following the LGM, potentially with slightly warmer temperatures and a shorter ice cover duration, allowing increased within lake and catchment productivity, driving the shifts documented in the C/N ratios and $\delta^{13}C_{bulk}$ record.

The specific changes in the lake conditions, which influence the dominance of the main diatom species *P. ocellata* and *A. granulata,* are also likely to influence the $\delta^{13}C_{bulk}$ record. Again following chapter 4, *A. granulata* requires warm summer temperatures and turbulence (Fedotov *et al.*, 2012; Kilham *et al.*, 1986) to dominate the assemblage, and this may affect the $\delta^{13}C_{bulk}$ values through the influence of the boundary layer. Boundary layers are caused by viscous water properties and thermal regime, and are composed of a film of water between 0.2 to > 1mm thick that sticks to the surface of a solid (e.g. plants and diatoms), and this does not participate in the general circulation of the water (Wang *et al.*, 2013). During turbulent conditions, this layer is usually thinner, leading to more depleted $\delta^{13}C_{bulk}$ values. Additionally turbulence can lead to depleted values as a result of atmospheric exchange (Wang *et al.*, 2013).

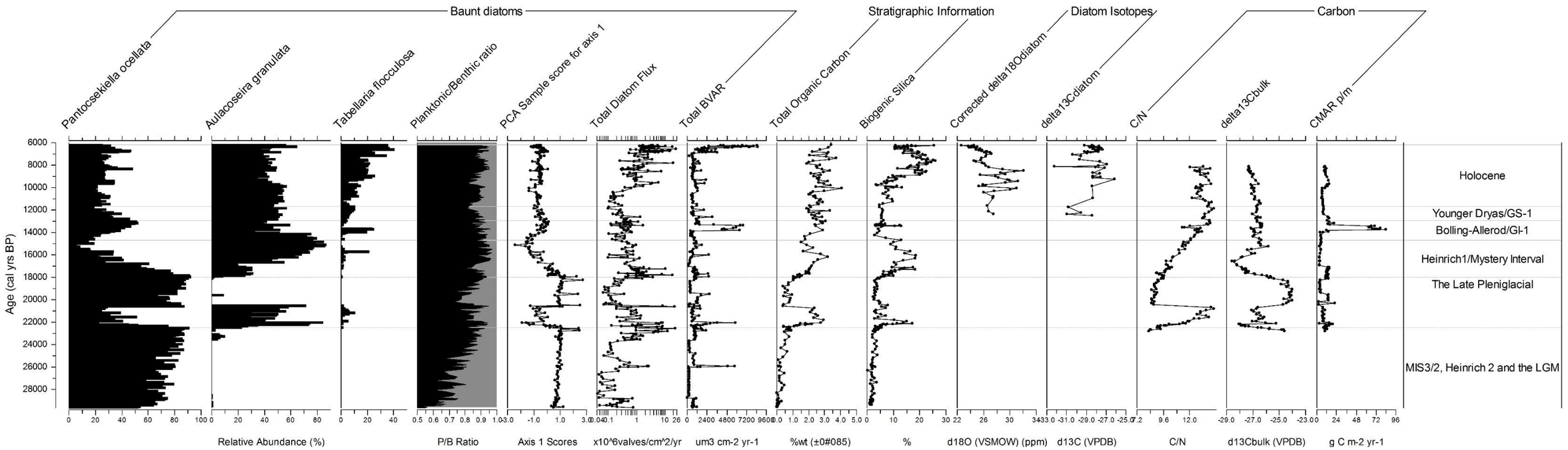

Figure 6.3: Lake Baunt carbon diatom summary (relative proportion (%) main species, P/B ratio, PCA scores, Diatom flux (x10^{6}valves/cm^2/yr) and BVAR (µm^3 cm^{-2} yr^{-1})) alongside TOC (% wt) and BSi (%), $\delta^{18}O_{diatom}$ (VSMOW) and $\delta^{13}C_{diatom}$ (VPDB) and bulk carbon measurements (C/N ratio, $\delta^{13}C_{bulk}$ (VPDB) and CMAR p/m (g C m^{-2} yr^{-1}) plotted against age (cal years BP).

Factors that can influence $\delta^{13}C_{bulk}$ values	Explanation
Water Turbulence	Turbulence causes thinning of the boundary layer, leading to more depleted $\delta^{13}C_{bulk}$ values (Des Combes *et al.*, 2008). Turbulence can also lead to depleted values, as a result of atmospheric exchange (Wang *et al.*, 2013).
Planktonic/Benthic Ratio	Proportional changes between benthic and planktonic species causes changes to $\delta^{13}C$ values, as benthic species have higher $\delta^{13}C$ (around –26±3‰) than planktonic species (–32±3‰) (France *et al.*, 1995), and, thus, a higher proportion of benthic species within the lake will increase $\delta^{13}C_{bulk}$ values.
Increased C from Methane Sources	CH_4 has significantly lowered $\delta^{13}C$ values of between –80 to –50 in methane gas sourced from themocarst Siberian lakes. It is possible these significantly depleted values might have an effect on postglacial $\delta^{13}C_{bulk}$ and $\delta^{13}C_{diatom}$ values if CH_4 became a significant source of dissolved carbonate (Webb *et al.*, 2016). As discussed elsewhere the similarity of $\delta^{13}C_{bulk}$ across the glacial and into the lateglacial and Holocene suggest this is not the case.
Soil Respiration	Soil respiration can influence $\delta^{13}C_{bulk}$ values. This is because as soils stabilise and mature, they increase soil respiration and supply $\delta^{13}C$ depleted dissolved carbon dioxide to lakes, which causes lowering of the $\delta^{13}C$ values preserved in sediments (Hammaklund, 1993; Mackay *et al.*, 2012)
Ice Cover	During periods with longer durations of ice cover, carbon exchange with the atmosphere is limited and, therefore, more ^{13}C has to be taken up,

	opposed to ^{12}C and consequently, values of $\delta^{13}C_{bulk}$ rise.
Increased C from diatom sources	As diatom primary productivity increases, diatoms preferentially removed ^{12}C from the DIC pool, and therefore this becomes depleted and their isotopic signature increases (Barker *et al.*, 2013).

Table 6.1: Factors which can influence $\delta^{13}C_{bulk}$ values.

From ~20.4 ka BP, transitions are seen in all the bulk carbon records, and these are also seen in the other Baunt proxies (diatoms, TOC, LOI), within dating errors. This shift highlights a return to autochthonous carbon sources, dominated by algae (see C/N ratios in figure 6.3). The $\delta^{13}C_{bulk}$ measurements are higher across this section, until ~17.8 ka BP, and this occurs as diatom flux and biovolumes, alongside TOC and BSi are low. CMAR values are initially high for this period, highlighting potential in-washing of sediment from the landscape, and then decline to very low values, due to limited organic matter production in Baunt's catchment. The higher $\delta^{13}C_{bulk}$ values may, therefore, be driven by this period of reduced productivity, with less algal demand for dissolved CO_2. The start of this period also has higher proportions of benthic algae, and these have more enriched $\delta^{13}C$ values than planktonic species (France *et al.*, 1995), and, thus, a higher proportion of these species within the lake may drive enriched $\delta^{13}C_{bulk}$ values. Additionally, this period may have extended durations of ice cover, causing limited carbon exchange with the atmosphere, and therefore more ^{13}C has to be up-taken, causing increased $\delta^{13}C_{bulk}$ values (see table 6.1)

As discussed in chapter 4, external drivers for the shift from a highly productive ecosystem between ~22.5 to ~20.5 ka BP, to a less productive ecosystem between ~20.5-18 ka BP are not that clear, although there is a slight increase in Siberian High strength, which could be driving this change. It is, therefore, assumed the main changes in the bulk carbon are linked to a slight strengthening in the Siberian High, which drives ecosystem changes within the landscape and may extend ice cover and reduce springtime overturning,

causing the shift in diatom species, which is reflected in the $\delta^{13}C_{bulk}$ and the C/N ratios. The increase in benthic species during this period of enriched $\delta^{13}C$ values may support this interpretation, as in cold conditions benthic diatom productivity is not as significantly affected as for planktonic species (Wang *et al.*, 2013).

From ~18 ka BP shifts are seen in many of the Baunt proxies, and these changes are also seen in the $\delta^{13}C_{bulk}$ record at ~17.8 ka BP. The gradual decline in $\delta^{13}C_{bulk}$ measurements coincides with gradually rising BSi, TOC and diatom biovolumes, again previously interpreted as a period of increased productivity (see chapter 4), or a period of increased soil erosion (see table 6.1). CMAR are elevated through this section, supporting increased productivity in the environment. The $\delta^{13}C_{bulk}$ decline may occur due to boundary changes, as *A. granulata* dominates alongside increased turbulence, and as a result of increasing input from vascular plants, which is shown by the gradually rising C/N ratios (Meyers and Lallier-Vergès, 1999), alongside a reduction in the benthic isotope species contribution to the $\delta^{13}C_{bulk}$ data.

The $\delta^{13}C_{bulk}$ depletion also occurs alongside declining AMOC strength and increased East Asian Winter Monsoon strength, associated with Heinrich 1. These climatic changes could drive the depletion, through increased lake turbidity, reducing nutrient in-wash (Meyers and Lallier-Vergès, 1999). High CMAR, which indicate that organic matter is being preserved in the Lake Baunt sediments and as the C/N ratios suggest a mixed source for organics at this time. Initially higher CMAR until 17.2 ka BP, could suggest instability in the landscape affecting sediment influx, with a reduction in vegetation promoting sediment influx in the catchment and allowing more carbon to the lake until ~17.2 ka BP. After this, low CMAR may be driven by increased aridity as a consequence of Heinrich 1. This is supported by the MARs data presented in chapter 3 (figure 3.18), which also suggests increased total sediment supply between 18-17.2 ka BP, after which time MARs are reduced.

As mentioned in chapter 4, this period of the Baunt record encompasses the aptly named mystery interval (Denton *et al.,* 2006), and these complexities are shown in the proxies from Baunt. The bulk carbon signal occurs alongside higher productivity, suggested by increased TOC, BSi and diatom biovolume, which require high nutrients and warm summer temperatures (figure 6.3) (Fedotov *et al.*, 2012; Kilham *et al.*, 1986). While increased turbulence could be a cause of the depletion in $\delta^{13}C_{bulk}$ values (as discussed above), climatic changes may be able to drive the increased productivity and increased aridity. While this period coincides with the Heinrich 1 event, it is possible that summer temperatures remain warm, however, increased summer wind strength, drove turbulence. Additionally, it is worth noting that this period sees higher insolation than earlier sections of the glacial part of the record and, thus, it is possible that a reduction in ice volume and permafrost in the region provides the nutrient input required for the higher productivity.

After the depleted $\delta^{13}C_{bulk}$ values, the $\delta^{13}C_{bulk}$ record undergoes gradual enrichment, starting at ~16.2 ka BP, which occur alongside increasing *A. granulata*. Again this suggests the $\delta^{13}C_{bulk}$ record is being influenced by changes within the algal community, although the continued rises in the C/N ratio are also indicative of a higher relative importance of carbon sourced from terrestrial vegetation (Wang *et al.*, 2013). This rise occurs as AMOC recovers and the EAWM declines in strength, suggesting a warmer more productive ecosystem, however, it is notable that the $\delta^{13}C_{bulk}$ values begin to increase to Lateglacial Interstadial/Holocene values before rises are seen in Asian speleothem records or the AMOC signal, which could be a function of sampling resolution and chronological controls (large uncertainties), although it could also reflect the less prolonged conditions imposed by Heinrich 1 in this region, and this may explain why other proxies (e.g. diatom biovolumes, TOC and BSi) don't show a clear Heinrich 1 imprint. This shift in the $\delta^{13}C_{bulk}$ values could, therefore, be linked to reduced aridity, increasing catchment vegetation. The stable CMAR during this period indicate that the landscape is more stable at this time.

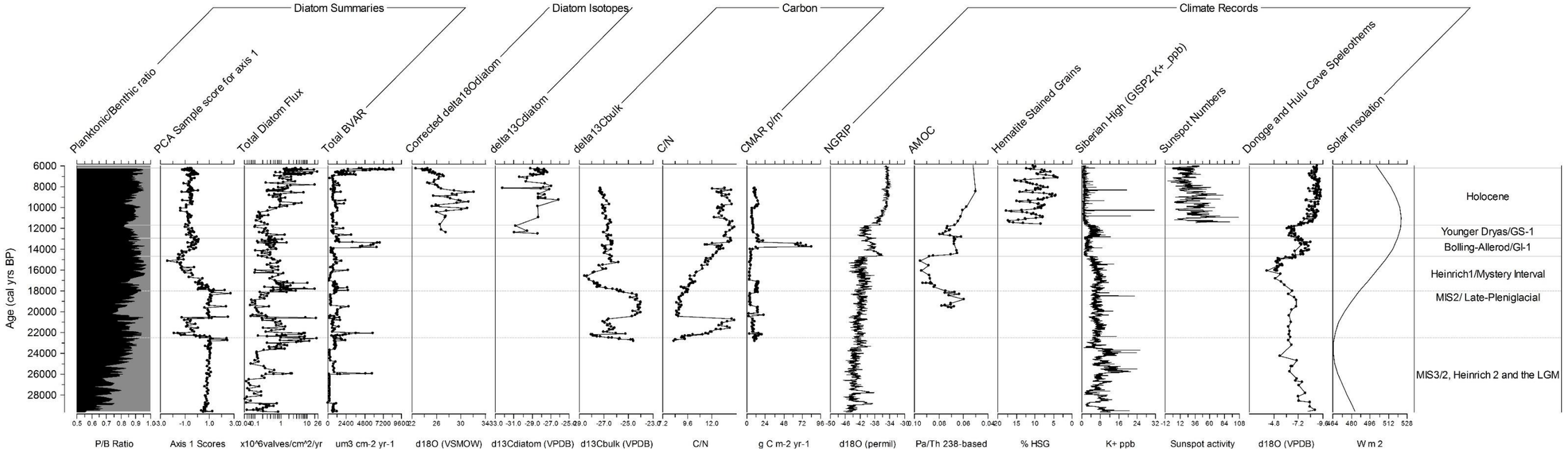

Figure 6.4: Lake Baunt carbon diatom summary (P/B ratio, PCA scores, Diatom flux (x10^{6}valves/cm^2/yr) and BVAR (µm^3 cm^{-2} yr^{-1})) alongside $\delta^{18}O_{diatom}$ (VSMOW) and $\delta^{13}C_{diatom}$ (VPDB) and bulk carbon measurements (C/N ratio, $\delta^{13}C_{bulk}$ (VPDB) and CMAR p/m (g C m^{-2} yr^{-1}) plotted against climate records for external forcing's, including NGRIP $\delta^{18}O$ signal (ppm)(Greenland air temperature) (Rasmussen *et al.*, 2014b), Pa/Th ^{238} record (AMOC strength) (McManus *et al.*, 2004), Hematite Stained Grains (IRD signal) (Bond *et al.*, 2001), GISP2 K+ signal (Siberian High strength) (Mayewski *et al.*, 2004), Sunspot numbers, Hulu (Wang *et al.*, 2001) and Dongge Caves $\delta^{18}O$ signal (ppm) and Solar Insolation at 60°N for July (W m^2)(Berger and Loutre, 1991).

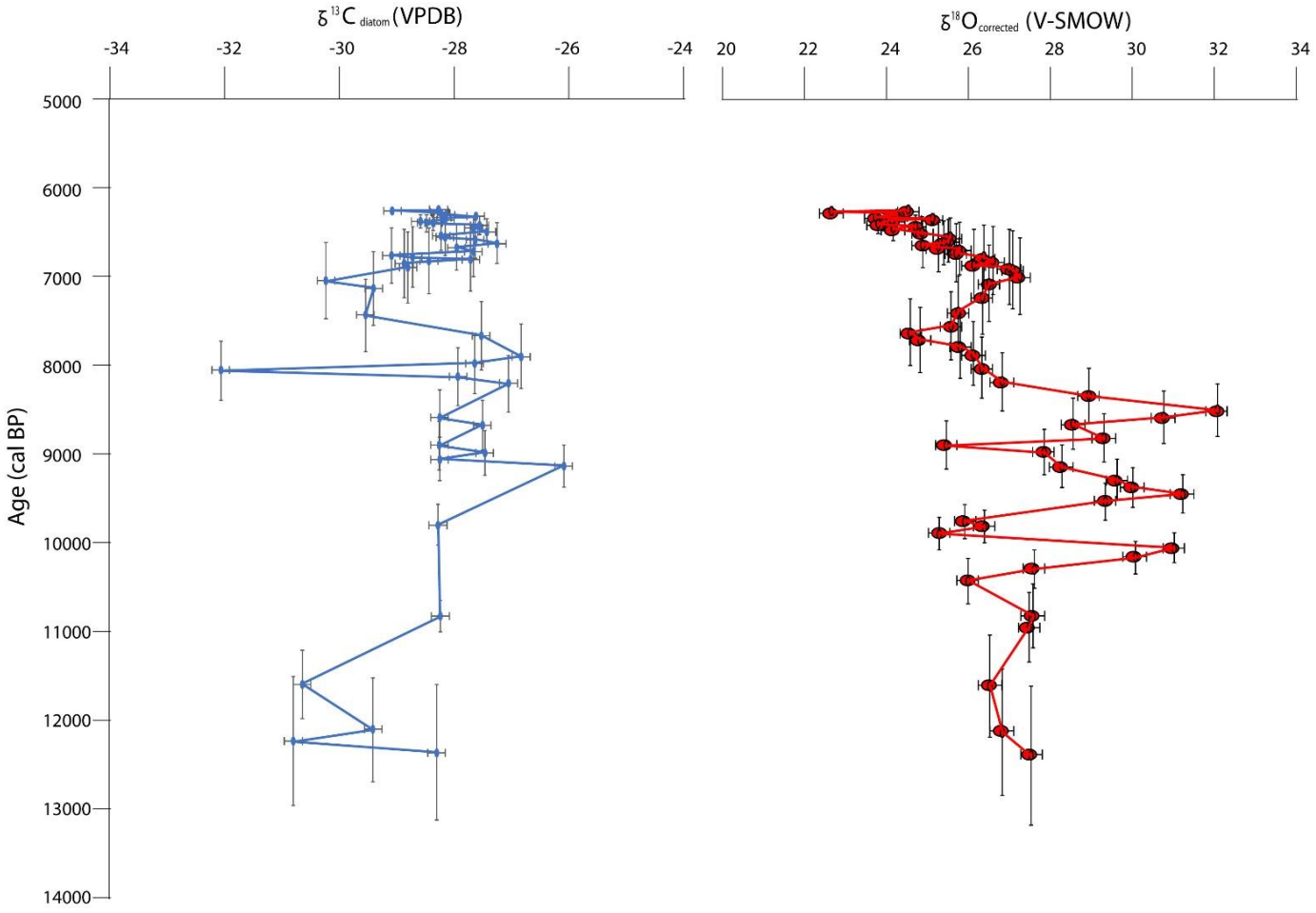

Figure 6.5: $\delta^{13}C_{diatom}$ record against $\delta^{18}O_{diatom}$ record from BNT14 against age (cal BP), both shown with age uncertainties and analytical errors.

6.4.2 The Last-Glacial-Interglacial-Transition

As discussed in chapter 4, the LGIT is a period known for abrupt climatic oscillations. Despite this, across the period associated with the Lateglacial-Interstadial (Bolling-Allerod/GI-1) and the Younger Dryas (GS-1), the bulk carbon records show fairly muted responses. The greater stability across this period may indicate stabilised landscape conditions, with more consistent carbon sources, which are also suggested by the more stable C/N ratio). A large shift is, however, seen in the CMAR, starting at ~13.7 ka BP until ~13.4 ka BP, although values remain relatively high until ~12.7 ka BP. This is likely to be driven by the interstadial conditions with melting glaciers in the Transbaikal region causing in-washing of sediments from the catchment. This is supported by the MAR data (see chapter 3; figure 3.18), which indicates increased sediment supply at this point.

The $\delta^{13}C_{bulk}$ values also show limited change across the period associated with the Younger Dryas, however, there is a slight decline in C/N ratios, which may indicate a relative increase in the proportion of organic matter from algal sources, potentially linked to reduced vegetation in the catchment. This is also seen in the CMAR, which reduces at this point, again suggesting reduced organic matter in the landscape, potentially due to greater aridity. A number of indicators suggest drier conditions and lower productivity, including biovolume accumulations rates, TOC, an initial shift in C/N ratios, and oxygen isotope values being much lower than values seen in the Early Holocene. These are interpreted to reflect more arid conditions, with a stronger Siberian High (see figure 6.4). From ~12.5 ka BP, samples are available from the $\delta^{13}C_{diatom}$ record (see figure 6.5), to allow greater consideration of the Younger Dryas period. The $\delta^{13}C_{diatom}$ values are broadly in range though the Lateglacial and Early Holocene, with the $\delta^{13}C_{bulk}$ samples (–30.9‰ to –26‰ for $\delta^{13}C_{diatom}$ and –27.2‰ to –25.8‰ for $\delta^{13}C_{bulk}$), suggesting a significant role for catchment carbon source on the $\delta^{13}C_{diatom}$, as demonstrated in geographically broad modern analogue studies (Webb *et al.*, 2016) . The earliest section of this record, during the Younger Dryas, shows depleted values between ~ –30‰ between ~12.3-11.7 ka BP (see figure 6.6) in the $\delta^{13}C_{diatom}$ values and

interestingly $\delta^{13}C_{bulk}$ values decline across this period. The higher $\delta^{13}C_{diatom}$ suggests lower productivity is limiting sourcing from bicarbonates, and there may be a link between aridity in the catchment and reduced carbon supply depleting DIC and, thus, $\delta^{13}C_{diatom}$ (Webb *et al.*, 2016).

6.4.3 The Holocene

The Holocene period reflects the most stable period in the Baunt bulk samples records, with much more muted fluctuations. C/N ratios stabilise around this time, and this may suggest a more stable landscape with sources remaining more consistent, although in both records there is some variability within a reduced range. The Baunt diatom P/B ratio is also more stable during this time period, and as discussed previously, benthic species often have more enriched $\delta^{13}C_{bulk}$ values than planktonic and, thus, stability in their relative proportions means greater stability in the $\delta^{13}C_{bulk}$ record (France *et al.*, 1995; Wang *et al.*, 2013)(see figure 6.4).

The stabilised conditions seen in the $\delta^{13}C_{bulk}$ record is not reflected in the $\delta^{13}C_{diatom}$ record (see figure 6.6), which shows several large amplitude shifts, during the Holocene period. The variability in the $\delta^{13}C_{diatom}$ is also partially reflected in the $\delta^{18}O_{diatom}$ record, which, as discussed in the previous chapter, are thought to relate to changes in precipitation amounts, warming temperatures and possibly precipitation source. The initial Holocene value increases in $\delta^{13}C_{diatom}$ are likely to be broadly linked to increased temperatures due to higher solar insolation, and increased precipitation due to a weakened Siberian High (figure 6.4). The sources of fluctuation in $\delta^{13}C_{diatom}$ in the early Holocene seem to relate to similar instability $\delta^{18}O_{diatom}$ although interpretation is difficult, as there are not identical sample numbers across the profile, due to small yields in samples. Taking that into account, it is apparent that there is a shift in both records to higher values after 11.5 ka BP, up to 11 ka BP, reflecting amelioration into the Holocene and for $\delta^{13}C_{diatom}$ this may be reflected in increased DIC and reduced sourcing from bicarbonates. Bulk carbon isotopes are also higher at this time and C/N ratios are also suggesting more vascular plants providing carbon to the lake. Between 11.2 ka BP and 9.7 ka BP there is a drop in C/N ratios and bulk carbon isotopes, that may suggest reduced

nutrient supply. This is at odds with the increase in the $\delta^{18}O_{diatom}$ values and could, in theory, support the idea that part of the increase in $\delta^{18}O_{diatom}$ relates to the precipitation source (see chapter 5). Unfortunately, $\delta^{13}C_{diatom}$ samples are not available at sufficient resolution to test this relationship through this early period.

One major change in the early Holocene record from Baunt does, however, have sufficient sampling resolution across several proxies to discuss these issues in more detail. Values recorded in the $\delta^{13}C_{diatom,}$ $\delta^{18}O_{diatom}$, $\delta^{13}C_{bulk}$, C/N ratios and CMAR records all rise, peaking ~9.3 ka BP in the $\delta^{18}O_{diatom}$ record. This is the clearest change across the range of proxies in (figure 6.6) in the Early Holocene. In chapter 5, it was suggested that high $\delta^{18}O_{diatom}$ values may reflect warming conditions due to their overlap with similar values in Lake Baikal (Mackay *et al.*, 2011), and it is possible that the changes seen across all of the records are a response to this warming. Very few combined $\delta^{13}C_{diatom}$ $\delta^{18}O_{diatom}$ and $\delta^{13}C_{bulk}$ records are available, but studies have shown a relationship between changes in $\delta^{18}O_{diatom}$ and carbon cycling, as derived from the relationship between $\delta^{13}C_{diatom}$ and $\delta^{13}C_{bulk,}$ (Barker *et al.*, 2013). While the context is very different, it is useful to examine the relationship between these three isotopic proxy data. In Baunt the rise in all three isotopes is unlike the Lake Challa example, perhaps unsurprisingly, given the different setting. What this rise suggests here, is that warmer conditions, as reflected in at least part of the $\delta^{18}O_{diatom}$ signal (chapter 5) coincides with a period of increased sediment influx and external carbon sources, as represented by C/N ratios and CMAR. The rise in both $\delta^{13}C_{diatom}$ and $\delta^{13}C_{bulk}$ suggest that the increased carbon supply is allowing increasing primary productivity, but DIC is sufficient to supply all of the carbon to the diatoms. In some of the early Holocene fluctuations, in between high and lower $\delta^{18}O_{diatom}$ values, there was a close correspondence to the Baikal record and this was suggested to relate to both Baikal and Baunt responding to intrinsic forcing. Thus, it could be argued that this shift to increased productivity in Baunt is being externally derived. Following this event, first $\delta^{18}O_{diatom,}$ and then $\delta^{13}C_{diatom}$ decline, while there is little change in the other records. On the basis of lowered $\delta^{18}O_{diatom}$ values that

would be expected from glacial meltwater than precipitation, it was argued that this shift may reflect increased glacial melt and input of glacial water to the lake. The decline in $\delta^{18}O_{diatom}$ and $\delta^{13}C_{diatom}$ could support this idea, with the possibility that the reduction in $\delta^{13}C_{diatom,}$ despite no change in $\delta^{13}C_{bulk,}$ may mean increased sourcing of bicarbonate from the influx of glacial material.

After this, values remain stable until a rapid shift at ~8.2 ka BP, where there is a short-lived decline in $\delta^{13}C_{diatom}$ and a more prolonged shift in $\delta^{18}O_{diatom}$. The latter coincides with changes seen in the Baikal and IRD records (chapter 5) and has been interpreted as a cooling event. There is limited information from some of the other proxies, but C/N ratios briefly drop and there is no change in $\delta^{13}C_{bulk}$. This scenario may be analogous in terms of carbon cycling to some of the effects seen in Lake Challa (Barker *et al.*, 2013), as the brief shift to carbon sourcing from algae and drop in temperature and possibly precipitation shown by $\delta^{18}O_{diatom,}$ coincides with a difference in the $\delta^{13}C_{diatom}$ and $\delta^{13}C_{bulk}$ values**,** potentially indicating a short lived shift drop in productivity in the diatom species. The 8.2 ka BP event is well documented through the Northern Hemisphere (H. Cheng *et al.*, 2009)(H. Cheng *et al.*, 2009), with strength increases seen in the Siberian High (see figure 6.4). These external drivers may, therefore, be causing an abrupt and short-lived period of climatic cooling, potentially with greater aridity, linked to stronger and prolonged blocking conditions induced by the Siberian High (Park *et al.*, 2014; Tubi and Dayan, 2013). This could be driving the abrupt shift reflected in the $\delta^{13}C_{diatom}$ record through reduced precipitation and supply of DIC. The differences between the $\delta^{13}C_{bulk}$ and $\delta^{13}C_{diatom}$ records may be linked to the wider sources reflected in the $\delta^{13}C_{bulk}$ records (Hurrell *et al.*, 2011), which may suggest the signal is more widespread.

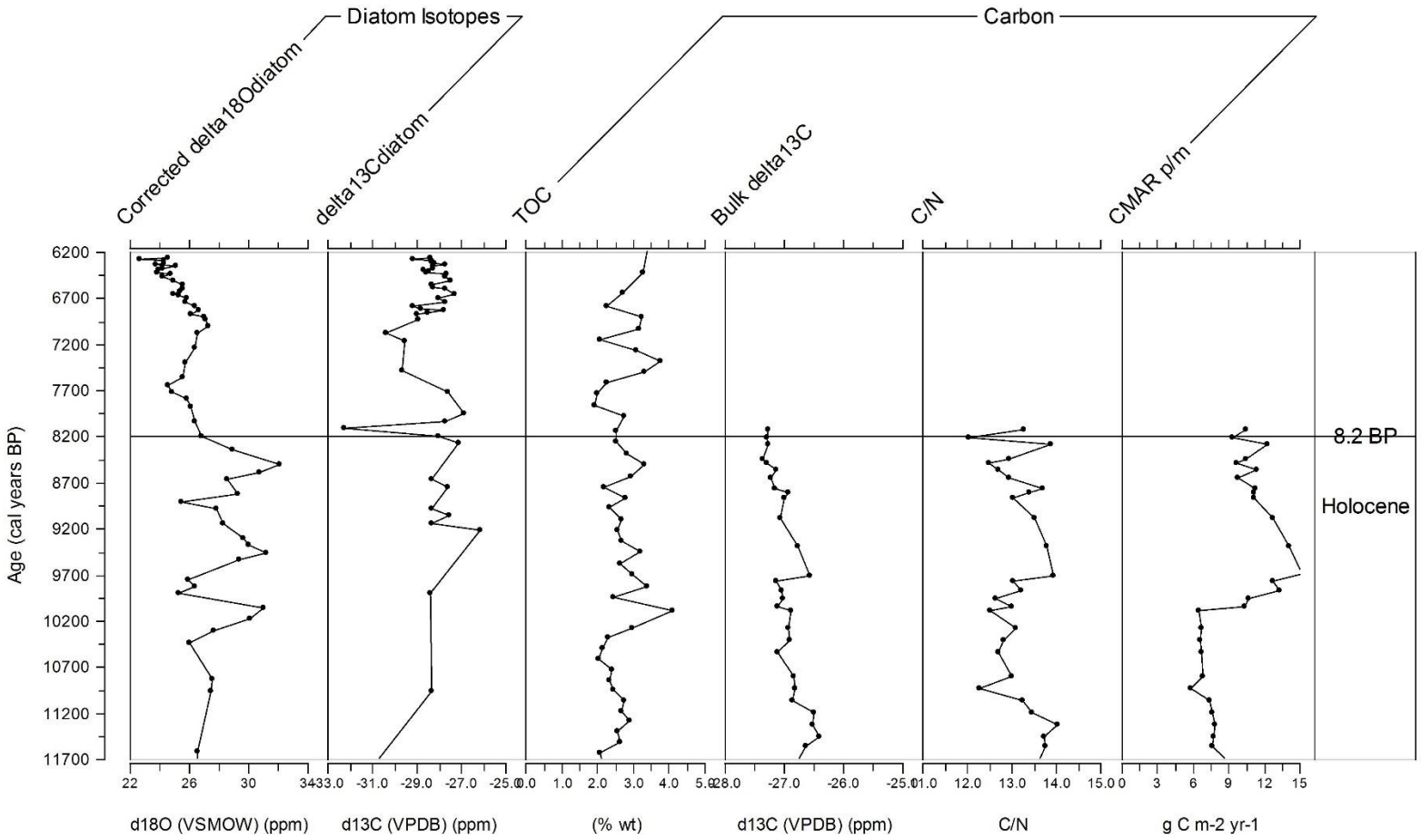

Figure 6.6: Diatom Isotope Records $\delta^{18}O_{diatom}$ and $\delta^{13}C_{diatom}$ against TOC, $\delta^{13}C_{bulk}$, C/N ratios and CMAR's.

6.5 Summary

In summary, several changes are seen in the bulk carbon and diatom carbon isotope records. These include the sources of organic matter across the BNT14 record, with some periods showing dominance of algal sources, while others have a more mixed signature. The $\delta^{13}C_{bulk}$ record responds to internal changes in the lake, such as through turbulence and diatom assemblage changes, while climatic influences are also apparent, driven through Siberian High strength changes, which influence the regions aridity. Greater stability is seen in the bulk carbon records during the Holocene period, however the $\delta^{13}C_{diatom}$ record shows greater complexity across this period, with shifts documented associated with the Younger Dryas and 8.2 BP events, driven by aridity changes, associated with strengthening of the Siberian High. The records show significant complexity, and this will be discussed further in the next chapter.

7 Lake Baunt, Siberia and the Northern Hemisphere

7.1 Introduction

The proxy records from Lake Baunt have highlighted major palaeoenvironmental changes occurring at the forest/steppe ecotone boundary in southern Siberia between ~29-6 ka BP. In this chapter individual records are brought together from Baunt, to consider the multiproxy story of ecological change. Multiproxy records from Baunt are then considered against wider Siberian studies, to place observed shifts into a regional context. Alongside this the records will be considered against important Northern Hemisphere climate archives, to consider changes across the hemisphere, allowing consideration of how climate changes propagate. Climate models will also be considered to discuss the current, albeit limited, attempts to incorporate continental Eurasian archives into understanding the drivers and their impacts on regional climate.

7.2 The Middle and Late Pleniglacial, the LGM and Heinrich 2 & 1

The Baunt record covers the last ~29 ka BP and, therefore, for the earlier part of this period it covers the LGM and a further intensified cooling around Heinrich 2 (~24-25 ka BP) (Bigg *et al.*, 2011; Cascalheira, 2013; Hemming, 2004), followed by a period of short-term warming (Rasmussen *et al.,* 2014). In the Greenland Ice core records this covers the end of GS-3 and through GI 2. In Baunt most of this time period is documented by low values for TOC, BSi, total diatom flux, and diatom biovolumes. Diatoms are dominated by *P*. ocellata, while benthic species occur in their highest relative proportion (see figure 7.1). These indicate that the LGM resulted in a fairly unproductive system in Lake Baunt, where arid conditions likely reduced the supply of nutrients and minerogenic material to the lake, resulting in thin snow cover, leading to high ice transparency, allowing *P. ocellata* to thrive as this species is able to survive under ice, assuming high light conditions (Malik and Saros, 2016), peaking around the time of Heinrich event 2.

This interpretation of a fairly unproductive system at this time fits well with results previously published in the wider Siberian literature. In Lake Kotokel,

conditions between 30-24 ka BP were considered to be at their driest, with no diatoms present, indicating an ecosystem collapse (Bezrukova *et al.*, 2010), although the period between 24-22 ka BP was considered to be more productive, potentially due to warmer conditions (Bezrukova *et al.*, 2010). Similarly, records from Lake Baikal have also been documented to have limited diatom preservation across this period, which has again been interpreted by some as a period of ecosystem collapse, as nutrients were limited, temperatures reduced and ice transparency was limited by clay particulates in the lake water (Karabanov *et al.*, 2004), although Mackay (2007) suggests that dissolution processes on already low diatom concentrations are a more parsimonious explanation.

The responses seen at Kotokel and Baikal, therefore, show some similarity to the Baunt record, with reduced algal productivity. However, unusually, diatoms are still preserved within the sediments of Baunt at this time, and this may be linked to site specific factors. Potentially, the geothermal activity close to Lake Baunt (Solotchin *et al.*, 2015) may be reducing the impact of continental cooling during the LGM, and this may have buffered the lake ecosystem, allowing algal productivity to be maintained. The period of amelioration recorded at Kotokel between 22-24 ka BP is also interesting, given the period of increased productivity documented at Baunt between 22.5-20.5 ka BP. This period is broadly in phase with a short lived return to interstadial conditions in the Greenland Ice cores, and also a period of increased EASM strength in the Hulu Cave (Wang *et al.,* 2001, Rasmussen, *et al.,* 2014).

It is worth noting in this discussion that diatom preservation needs to be considered. In the case of Lake Baikal, for example, the disappearance of diatom species during glacial phases has been the subject of significant debate. While it would be generally accepted that thermal regimes, turbidity, and thermodynamics within the lake during cold glacial conditions would have reduced diatom productivity, it has been suggested that variability in preservation is a better explanation of the absence of diatoms in glacial times (Colman *et al.,* 1995; Mackay 2007). Dissolution in modern samples from Baikal is a significant issue, and correction factors for this have been produced

to aid palaeoproductivity reconstructions (Battarbee *et al.*, 2005), however, they are not likely to be useful in glacial conditions. The reduced but continued productivity of algae in Baikal in glacial times has been supported by the identification of sterols associated with green algae, diatoms and zooplankton, that were present ~16-28 ka BP, although at admittedly lower levels than in the Lateglacial or Holocene (Mackay, 2007; Russell and Rosell-Melé, 2005). Taken together, these two lines of argument suggest that for Baikal the influence of LGM conditions can be seen to act on the diatom community, but the idea of complete ecosystem collapse is likely to be an oversimplification. Similarly, the general inferences regarding climatic downturn in Kotokel during the LGM are supported by indicators other than diatoms, such as pollen (Bezrukova *et al.*, 2010).

When considered against wider records (figure 7.2), it is clear that the records of the transition from MIS3 to MIS2, and the LGM, from Lake Baunt are consistent with conditions seen across the Northern Hemisphere. Greenland air temperatures are indicated to be low by the $\delta^{18}O$ record from NGRIP, and these closely correspond to strong Siberian High signals in GISP2, which are reflected in the limited productivity documented by Baunt. The GISP2 signal of Siberian High strength (Fig 7.3) also shows correspondence to the Asian speleothems, driven by the modulating influence these systems have on each other, due to pressure gradients (Park *et al.*, 2014; Tubi and Dayan, 2013). In Siberia the greater aridity and cooler temperatures are thought to be driven by the presence of large Northern Hemisphere ice sheets to the west, including the Fennoscandian ice sheet, which cause weakening of the flow of westerly winds (Katsuta *et al.*, 2018). This may cause changes to atmospheric systems, by obstructing their migration, and this can intensify and extend the duration of systems, including the Siberian high (Zhao *et al.*, 2017), and this in turn reduces productivity in these regions.

In summary, it appears that the general conditions from Baunt during the transition from MIS3 to MIS2 and the LGM, are dominated by arid cold conditions, with long periods of ice cover. Baunt, however, shows more resilience in its response, being able to sustain diatom productivity throughout

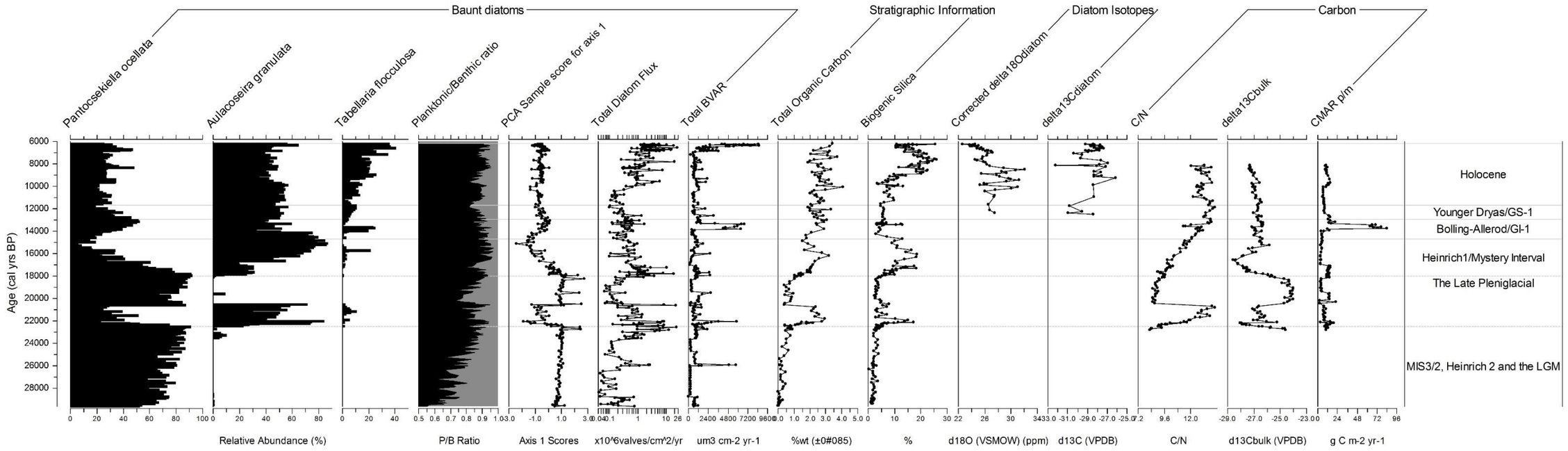

Figure 7.1: Summarised Lake Baunt diatom assemblage alongside Planktonic/Benthic ratio, total diatom flux (x10^{6}valves/cm^2/yr) shown on a logged x-axis, biovolume accumulation rates (BVAR) (µm^{3}cm^{-2}yr^{-1}), Total-Organic-Carbon (TOC) (%weight), Biogenic silica (BSi) (%), $\delta^{18}O_{diatom}$ (VSMOW ppm) and $\delta^{13}C_{diatom}$ (VPDB ppm) records alongside C/N ratios, $\delta^{13}C_{bulk}$ (VPDB ppm) and carbon mass accumulation rates (CMAR p/m) (g C m^{-2} yr^{-1}) plotted on the Baunt chronology.

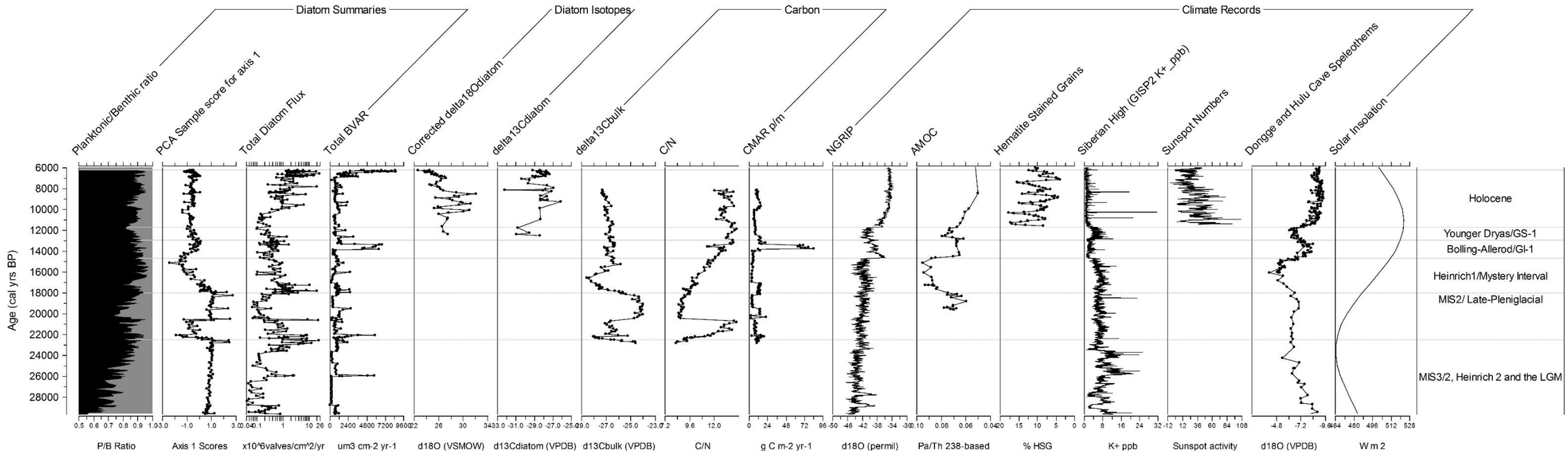

Figure 7.2: Lake Baunt P/B ratio, PCA axis 1 scores, Total diatom flux (x10^{6}valves/cm^2/yr) shown on a logged x-axis and biovolume accumulation rates (BVAR) (μm^{3}cm^{-2}yr^{-1}), $\delta^{18}O_{diatom}$ (VSMOW ppm) and $\delta^{13}C_{diatom}$ (VPDB ppm) records, alongside $\delta^{13}C_{bulk}$ (VPDB ppm), C/N ratios and carbon mass accumulation rates (CMAR p/m) (g C m^{-2} yr^{-1}). Shown against proxies for external climate forcing's including NGRIP $\delta^{18}O$ signal (Greenland air temperature) (Rasmussen *et al.*, 2014), Pa/Th^{238} record (AMOC strength) (McManus *et al.*, 2004), Hematite Stained Grains (%) (IRD signal) (Bond *et al.*, 2001), GISP2 K+ signal (ppb) (Siberian High strength) (Mayewski *et al.*, 2004), Sunspots, Hulu (Wang *et al.*, 2001) and Dongge Caves ($\delta^{18}O$ signal) (Dykosko *et al.*, 2005) and Solar Insolation from 60^{0}N for June (W m^2)(Berger and Loutre, 1991).

the period, which is rare. This may be linked to localised geothermal conditions.

Between 22.5-20.5 ka BP, the diatom record is dominated by *A. granulata*, while TOC rises, BSi shows a short-term peak at ~ 22.1 ka BP and diatom biovolume increases alongside diatom flux (see figure 7.1). Bulk carbon samples are also available for this time period, with low $\delta^{13}C_{bulk}$ values around ~–27‰, C/N ratio values start around 9 and reach 14, and CMAR are low (see figure 7.1). The transition from the previous period of a less productivity to this section is quite rapid in many of the records, particularly the diatoms, TOC, BSi and $\delta^{13}C_{bulk}$. The shift in the diatom species has been discussed as being linked to warmer summer conditions reaching a minimum of ~17°C (Fedotov *et al.*, 2012), with increased turbulence, to support the heavily silicified *A. granulata* (Kilham *et al.*, 1986; O'Farrell *et al.*, 2001). This species has been suggested to highlight increased nutrients, particularly silica and phosphorus (Kilham *et al.*, 1986; O'Farrell *et al.*, 2001), and the large shift in the C/N ratios, suggest these may be provided by increased organic matter from vascular plants (Meyers and Lallier-Vergès, 1999). The BSi peak early in this section is indicative of a rapid shift within the lake's algal community, as *P. ocellata* declines and *A. granulata* increases, and this is supported by the initial peak in total diatom flux, while the peak in biovolumes is higher across the zone due to the larger biovolume of *A. granulata,* compared to *P. ocellata.* The median biovolume of *A. granulata* is ~3 times greater than *P. ocellata*. The CMAR also peaks at the start of this period, and may be due to rapidly responding diatom communities. The slower increase in C/N ratios suggest increased contribution from vascular plants (Meyers, 1994), and does not match the BSi and CMAR, which may mean that there is an increase in productivity of aquatic plants in the littoral zone, and this is known to be influenced by ice cover (Duarte *et al.*, 1986). The decline in $\delta^{13}C_{bulk}$ values are also linked to changes within the lake system, with greater turbulence causing thinning of the boundary layers around the planktonic diatoms (Jørgensen and Revsbech, 1985), while reduced quantities of benthic species may also contribute to lower

values, as planktonic species have lower $\delta^{13}C$ ratio's compared to benthic species (France *et al.*, 1995; Wang *et al.*, 2013)

This section of the Baunt record has, therefore, been interpreted as a more productive period in the localised Baunt region, with a weaker Siberian High, potentially driving the increase in lake nutrients, through increased precipitation, while warmer summer temperatures are suggested by *A. granulata* (Fedotov *et al.*, 2012), supported by rising C/N ratios, indicating increased contribution from vascular plants, possibly macrophytes. A significant driver of these shifts is thought to be through changes in ice cover duration. Earlier ice free conditions, or later onset of ice in the autumn, could promote the changes in the diatom assemblage by increasing the period of time for overturning, providing the turbulence required for *A. granulata* (Winder and Hunter, 2008). Although it is also possible that increased winds during the summer season, potentially due to increased westerlies reaching the area after the semi-permanent Siberian High dissipates, could also drive this change.

When the changes through this period are considered against regional sites, there are several discrepancies. Lake Kotokel documents arid and cold conditions until ~17 ka BP, except for the period discussed in 7.1, where climatic amelioration is considered to occur between ~24-22 ka BP (Bezrukova *et al.*, 2010). This is based on the reappearance of diatoms at this time, but is slightly different to Baunt, where more productive and, therefore, potentially warmer and wetter conditions are considered to occur later than at Lake Kotokel, between ~22.5-20.5 ka BP. However, the dating uncertainties at the start of this event at Baunt are ±600 years (95% confidence), potentially meaning this event could overlap in time with the event documented in Kotokel, and this may suggest a regional period of potentially warmer and wetter conditions. It is also worth considering the Lake Kotokel chronology in more detail when comparing the sites. The radiocarbon ages used to constrain the Lake Kotokel chronology are based on bulk sediment samples, and are considered sound by the authors, however the $\delta^{13}C$ values are not reported and, therefore, caution is required. The authors note that there is no evidence

for inorganic carbonate in the lake and, thus, mineral carbon error has been excluded, although this is difficult to verify. The quoted uncertainties are also large for this record ranging from ± 180 to ± 460 years (95% confidence). Re-calibration of the Lake Kotokel dates with the more recent IntCal13 curve (Reimer *et al.*, 2013) has not changed the overall range of the dates (see table 7.1), suggesting there is some overlap between the evidence for climatic amelioration events recorded in the two lakes, once uncertainties are taken into account. One issue with comparing the two records is, however, the different approaches used to age modelling in this thesis, versus the age model in Bezrukova *et al.*,(2010), which may mean that it is not clear if these two event are potentially coeval . In order to address this issue the radiocarbon ages from Lake Kotokel were remodelled using the same *P_Sequence* age moddeling approach, with interpolation and deposition modelling, as was used to develop the Lake Baunt chronology. . This model is shown in figure 7.3, and demonstrates that the reappearnace of diatoms in Kotokel, between 810-880cm (Bezrukova *et al.*, 2010) dates from 25869-22675 ka BP to 23780-21498 ka BP. Within dating uncertainties, this overlaps comfortably with the Baunt ages for amelioration. However, it is worth noting that in both cases the uncertainties are large and, therefore, it is not possible to demonstrate absolutely that these represent the same event (see figure 7.4). Caution must also be applied here, as the reappearance of diatoms in Lake Kotokel may be linked to improved conditions for diatom preservation and reduced dissolution, rather than climatic changes. The latter parts of both records do, however, agree, with sustained periods of limited productivity occurring at both sites after the LGM. Drivers of the return to less productive conditions are tentatively linked to a slight increase in the Siberian High strength (see figure 7.2), which may have extended the period of its dominance to later in the spring, reducing the period available for overturning, preventing turbulence (Winder and Hunter, 2008) and, consequently, driving diatom assemblage changes as seen in Lake Baunt. A comparison to figure 7.2 suggests this period of increased productivity coincides, within dating uncertainty, with the warming in Greenland and changes to the EASM that follow Heinrich event 2. Although

this is a tentative correlation due to dating uncertainties, at this time, it seems to be the best correlation in Baunt and Kotokel to a well-known extrinsic event.

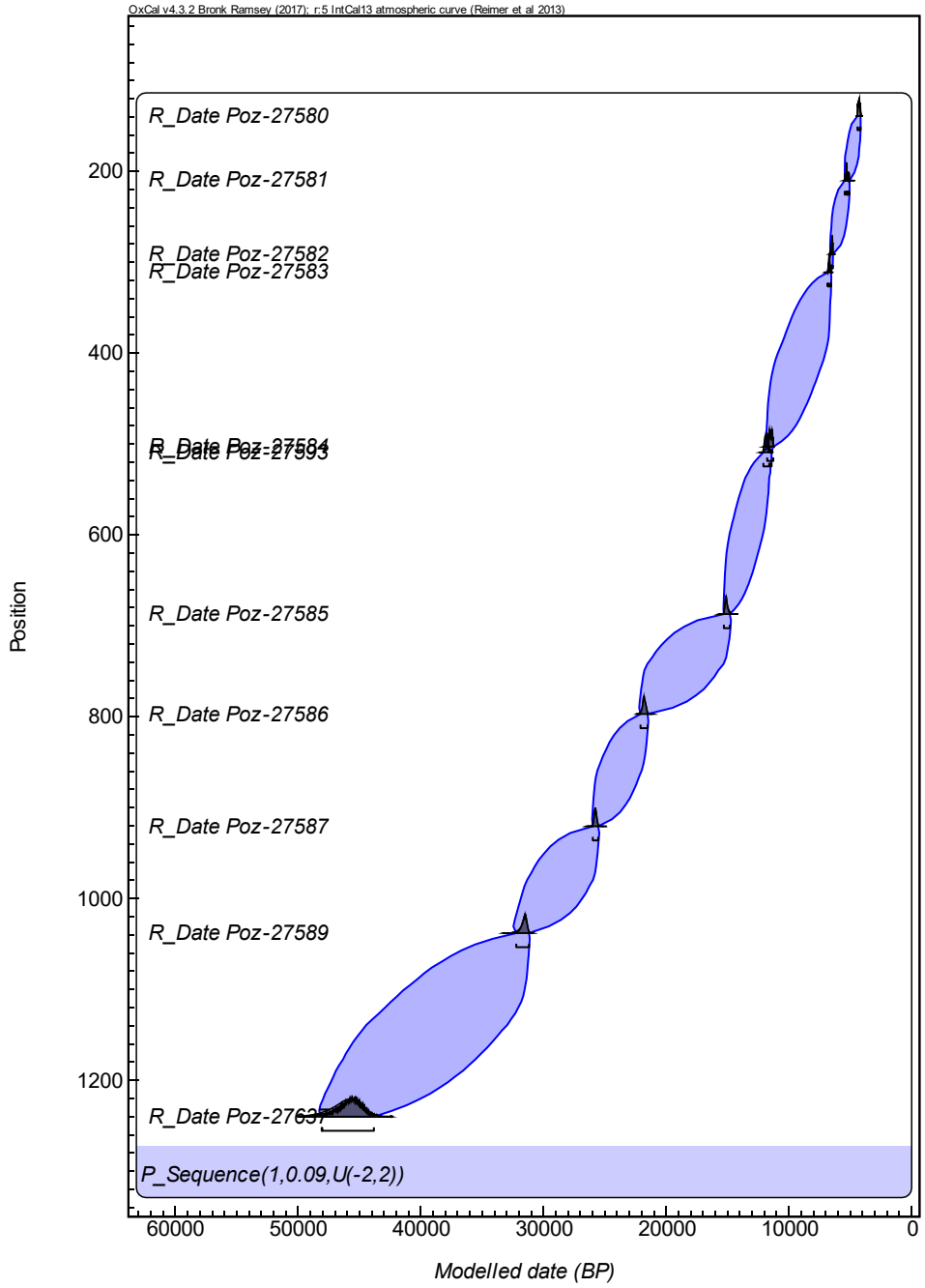

Figure 7.3: Lake Kotokel age model produced in OxCal 4.3 (Bronk Ramsey, 2008) using a *P_sequence* depositional model

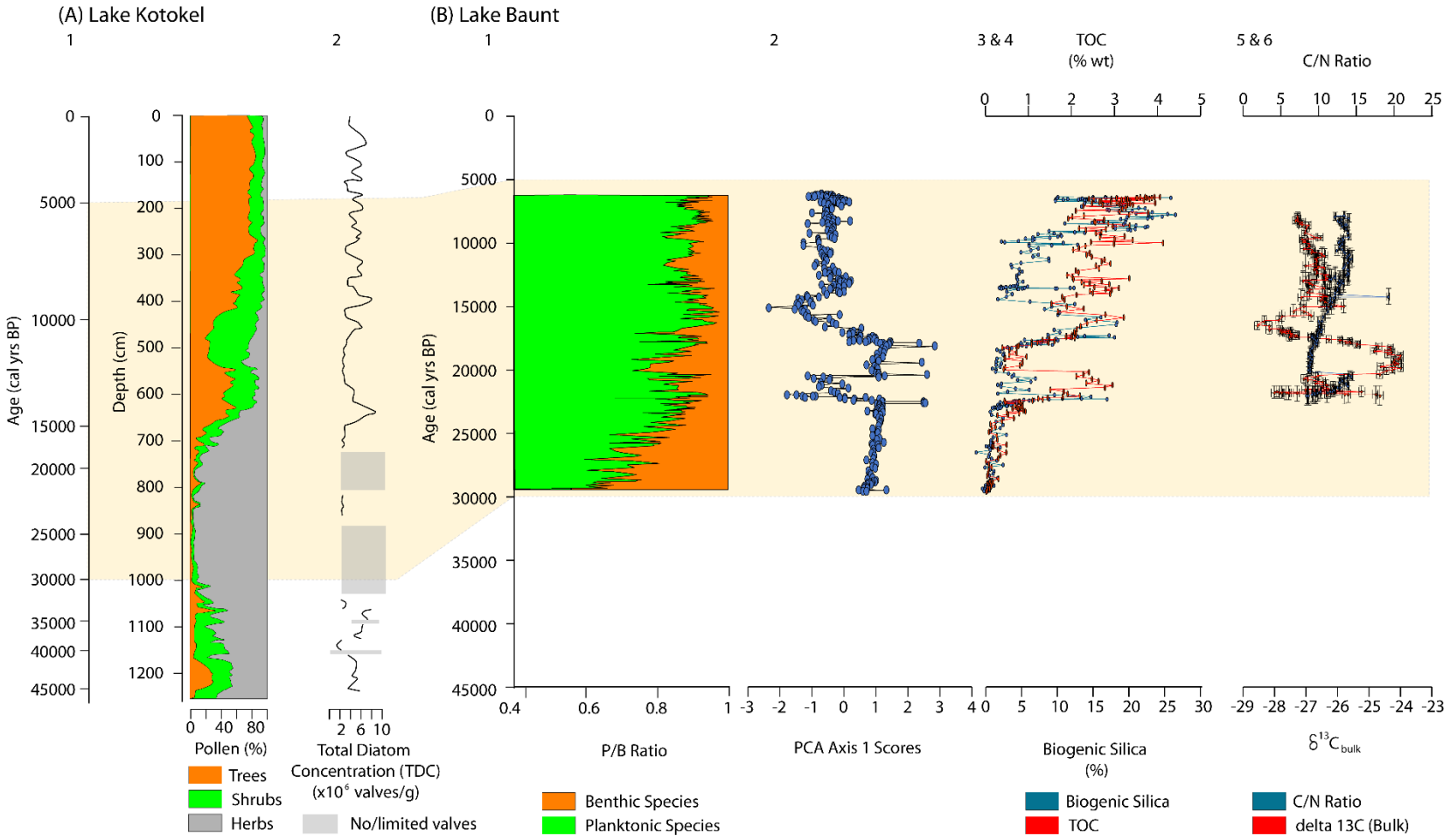

Figure 7.4: (A) Lake Kotokel records: (1) Pollen Summary, (2) Diatom Concentration from (Bezrukova *et al.*, 2010) plotted by depth shown with the new chronology (produced for this thesis) against **(B)** Lake Baunt records: (1) Planktonic/Benthic Ratio, (2) PCA Axis 1 scores, (3&4) Biogenic Silica and Total Organic Carbon and (5&6) C/N Ratios and $\delta^{13}C_{bulk}$ record. Banding shows the period of cross over between the two records.

Following the period between 22.5-20.5 ka BP the records from Baunt show a shift back to conditions similar to those seen in the LGM: *P. ocellata* dominates the diatom assemblage, diatom fluxes and biovolumes decline, and C/N ratios drop back to lower values around 8-9, while $\delta^{13}C_{bulk}$ values are higher (7.1), and TOC and BSi values are also low. As with the record during MIS3/MIS2 period and the LGM, this part of the record is suggested to be less productive within and around Lake Baunt.

The end of this glacial section also encompass the 'Mystery Interval' (18-14.7 ka BP) (Denton *et al.,* 2006) and covers some of the most complex transitions in the Baunt archive. This period starts with initially increasing values of *P. ocellata,* before they begin to decline around 17.5 ka BP*,* alongside proportionally increasing values of *A. granulata*. This occurs in combination with increased biovolumes, gradually rising C/N ratios and rising TOC and BSi values, while $\delta^{13}C_{bulk}$ values decline. These shifts are again suggested to highlight more productive conditions at Baunt, with warm summer temperatures allowing dominance of *A. granulata*, with increased nutrients and turbulence also allowing this species to thrive (Fedotov *et al.*, 2012; Kilham *et al.*, 1986; O'Farrell *et al.*, 2001). The changes in C/N ratios, suggest a greater proportion of organic matter is derived from vascular plants (Meyers and Lallier-Vergès, 1999), indicating that the landscape may be an important component for the changes in diatom assemblage in the lake. The changes in the $\delta^{13}C_{bulk}$ values are also driven by these changes, with increased turbulence and P/B ratio changes depleting the values (Des Combes *et al.*, 2008; Wang *et al.*, 2013).

The records within Lake Baunt, therefore, generally agree and suggest an initial decline in productivity, before the onset of more productive conditions, with overturning potentially creating the turbulence (Winder and Hunter, 2008). However, interpreting this becomes more complex when external sites are studied. This is because of the occurrence of Heinrich 1 (Chapter 1). Heinrich event 1 witnessed widespread deposition of IRD following extensive sea ice expansion and iceberg discharge from ice sheets in the Hudson straight (Hodell *et al.,* 2017), resulting in freshwater forcing impacting AMOC (Hostetler

et al., 1999; McManus *et al.*, 2004; Vidal *et al.*, 1997). The Heinrich stadial 1 period is documented to have contain widespread changes, including vegetation shifts (e.g. Penaud *et al.*, 2010) and monsoon strength alterations (Cai *et al.*, 2010; Stríkis *et al.*, 2015). Siberian High strengthening is thought to have caused southward retreat of the East Asian Summer Monsoon (Cai *et al.*, 2010) and, therefore, it would be anticipated that the ecosystem at Baunt would alter to reflect prolonged ice cover and aridity, as seen during the LGM. Figure 7.2 highlights that across this period Siberian High strength is higher than during the previous period, while co-occurring shifts are seen in corresponding systems, including the East Asian Monsoon. At Lake Baunt, the period coincides with rapidly changing diatom communities (as evidenced from changes in PCA1 scores (see Figure 7.1). However, the changes in diatoms and other proxy indicators unexpectedly suggest a period of warmer, more productive conditions. Given the dating uncertainties of ~±330 years in Baunt, and the significant difficulties in dating marine Heinrich layers (Hodell *et al.*, 2017), it is possible that the peak at ~18 ka BP in *P. ocellata*, a species that has been seen to thrive at Baunt during the LGM, could mark the start of this event, and this corresponds with the abrupt changes documented in the PCA. Significantly, It would also suggest that conditions in the later part of Heinrich 1 are much less severe.

The response in Baunt is complicated, but comparison with other sites may clarify if this is caused by intrinsic or extrinsic drivers. The Heinrich 1 time period in Lake Baikal is characterised by carbonate muds between 17.6-17.2 ka BP, and these are thought to be driven by dramatic runoff events in the Selenga river, as a result of changed precipitation during Heinrich 1 (Katsuta *et al.*, 2018). This indicates that hydrological changes may have occurred in the region. The complexities in phasing and dating of Heinrich 1 have been discussed elsewhere, in terms of the driving mechanisms of the IRD event and climatic signal seen in a number of records. The period, generally assigned to the Mystery Interval, begins with warming in the Greenland Ice cores, followed by a gradual weakening in AMOC, leading into Heinrich 1 (Figure 7.2) (McManus *et al.*, 2004). This may be the result of early melting of European

ice sheets weakening AMOC, before initiation of IRD from the Laurentide ice sheet after ~16.5 ka BP (Hodell *et al.*, 2017). This early phase of the Heinrich 1 stadial coincides with cooling in Greenland and changes to the East Asian Monsoon, with evidence for southward movement of the ITCZ, as the Northern Hemisphere cools. A detailed examination of Heinrich 1 IRD in the North Atlantic, from IODP-U1308 (Hodell *et al.*, 2017), suggest that there are two phases of IRD in the region, separated by a period of warming. The second IRD phase is also smaller and weaker than the initial event. Thus, there is evidence for a phased series of events making up Heinrich 1 and this may suggest that the hydrological changes in the Baikal region, and the complex transitions seen in Baunt, conform to a widespread global scale forcing event. The detail of how this may be directly expressed in Baunt are discussed below, with reference to climate modelling.

7.3 The Last-Glacial-Interglacial-Transition

The LGIT, from ~14.7 to 11.7 ka BP (Rasmussen *et al.*, 2014), encompasses some of the most well studied events from the Late Pleistocene. The earliest period of the LGIT covers the Bølling-Allerød (GI-1) interstadial. Across this period in Baunt changes are more muted than in earlier sections of the record (see figure 7.1). The diatoms through this period show increasing proportions of *P. ocellata,* while *A. granulata* has an initial decline and is then fairly stable, and *T. flocculosa* has a short-lived peak in the mid-point of the interstadial ~13.7 ka BP. This peak is also documented in the BSi record, which also has a rapid shift at this point, while TOC values rise across the interstadial period. C/N ratios continue their upward trend across this period, while the $\delta^{13}C_{bulk}$ is fairly stable, although several small fluctuations do occur. The CMAR show a substantial shift during this period, linked to the increased sedimentation rate (see chapter 3).

Collectively, the multiproxy changes documented at Lake Baunt, supports a warmer, wetter climate than the LGM and Heinrich 1. This is likely as warmer conditions would promote a longer ice free season, providing the overturning periods to support *A. granulata*, while periods of thermal stratification would

increasingly favour *P. ocellata* (Winder and Hunter, 2008). The rising C/N ratio alongside increased TOC, suggest increased organic matter in the landscape (Meyers and Lallier-Vergès, 1999), while the peak in CMAR may be due to sediment in washing as a result of glacier melt and potentially, permafrost thaw. Therefore, it appears that the Baunt proxies do show a response to the late-glacial-interstadial, however, this is more muted compared to some shifts documented earlier in the record.

Interstadial conditions are documented by several records in the Lake Baunt region, with Lake Kotokel highlighting its warmest and wettest period during the LGIT for the past ~47 ka BP (Bezrukova *et al.*, 2010), while others have inferred warmer temperatures for the region at the time, as shown by Katsuta *et al.,* (2018), where the BSi record has been used to infer temperature in Lake Baikal, suggesting peak interstadial warming at ~14.3 ka BP, accompanied by progressing moisture increases, which peak at ~13.8 ka BP (Katsuta *et al.*, 2018). In the wider Asian region, sites including Lake Balikun, Western China, show responses to this interstadial, with warmer conditions and increased glacier meltwaters (Zhao *et al.*, 2017), which again highlights a similar response to that seen in the Baunt CMAR's. Climatic forcing of the changes seen between ~14.7-12.9 ka BP are linked to the reduction in Siberian High strength, and this is linked to the rapid increase in AMOC, following Heinrich 1. The changes in the Siberian High, are mirrored in the increase in East Asian Summer monsoon strength, while increases in AMOC are also shown to be influencing air temperatures in Greenland (NGRIP). Therefore, it appears that the changes seen across this period in Baunt are linked to global patterns in climate.

Between 12.7-11.7 ka BP, across the Younger Dryas in the Baunt records, there is a low in total diatom flux and biovolume productivity, while $\delta^{13}C_{bulk}$ values show no major change. Changes in other values (TOC, BSi) are quite muted, although *P. ocellata* proportionally declines in the diatom record. In general $\delta^{18}O_{diatom}$ values for this period show a muted response, and this has been linked to the diatoms reflecting the summertime conditions, which, for the Younger Dryas, have been suggested to be warm in continental Europe

(Schenk *et al.*, 2018), but they are certainly lower than the later Holocene. The $\delta^{13}C_{diatom}$ are also lower than the subsequent Holocene and may reflect lower diatom productivity during this interstadial (see figure 7.2). It could be that the shift to low BSi values at the end of the interstadial, are also highlighting this change in diatom productivity. This highlights the complexities of these events being recorded, demonstrating the need for multiproxy studies.

7.4 The Holocene

From ~11.7 ka BP changes in many of the Lake Baunt data sets appear more muted, and this has been linked in many cases (e.g. chapters 4 and 6) (see figure 7.5), to greater stability during the Holocene. This stability is highlighted by stabilised C/N ratios, $\delta^{13}C_{bulk}$ and CMAR. TOC and BSi show gradually increasing levels, which could be linked to greater productivity in the lake and catchment, possibly suggesting a progressively warmer Holocene. Despite many of the records suggesting greater stability, this is not reflected in the diatom isotopes. The oxygen isotope record through the Holocene from Baunt, documents considerable variability. This is considered to be driven by a combination of factors, where higher values are thought to be linked to increased solar insolation and a higher proportion of precipitation, with a possible Pacific influence (see Chapter 5). This is alongside extrinsic forcing from AMOC variations, as seen through the similarity with Lake Baikal, and this is discussed below, in relation to climate models of both the general pattern of early Holocene climate and the ability to compare models and data.

The shifts seen in the $\delta^{13}C_{diatom}$ across this period also highlight changing conditions through the Early Holocene, however, the two records are substantially different. The peaks seen in the $\delta^{18}O_{diatom}$ record, may correspond to the most enriched period in the $\delta^{13}C_{diatom}$ record, with lower values associated with less turbulence, driven by thermal stratification (Wang *et al.*, 2013), resulting from reduced Siberian High strength, shorter ice durations and increased insolation, although both records may provide evidence for at least one episode of glacial melting. The notable decline in the $\delta^{13}C_{diatom}$ record at ~8.2 ka BP, is less clear in the $\delta^{18}O_{diatom,}$ although, it does occur during a period of low values in this record. The 8.2 ka BP event is well

known in the Northern Hemisphere (Heiri *et al.*, 2004; Hoek and Bos, 2007; Lowe *et al.*, 2008; Mayewski *et al.*, 2004), being linked to freshwater outbursts (Teller *et al.*, 2002), causing changes to ocean salinity and cooling around the north Atlantic. The appearance of a change in the Baunt $\delta^{13}C_{diatom}$ record at this time may, therefore, be driven by changes linked to this event. This is likely to be due to rapid, short lived increases in Siberian High strength, which are documented in the GISP2 K+ signal (Mayewski *et al.*, 2004) at this time (see figure 7.2), and could have caused climatic shifts at this point. These may have included increasing the ice duration, and reducing spring overturning, and this may indicate that the sight peak in *P. ocellata* could be driven by this event, potentially by reduced turbulence providing higher light conditions, which favour this species (Malik and Saros, 2016). The less clear response of this event, compared to earlier ones within the $\delta^{18}O_{diatom}$ record, may be due to reduced Northern Hemisphere ice sheets, which may mean that changes are not propagated as strongly from the North Atlantic to continental Siberia. Also, in Baikal, there is little evidence of impacts from the 8.2 ka BP event, apart from on the $\delta^{18}O_{diatom,}$ record, which suggests a period of increased aridity.

These early Holocene shifts show similarity to abrupt changes seen at Lake Baikal, during the early Holocene, highlighting that both sites may be responding to external climate forcings, however, as discussed in chapters 5 and 6, these shifts are not synchronous. The reasons for the variations in responses between Baikal and Baunt are due to several factors, particularly the large catchment size of Lake Baikal, which means its $\delta^{18}O_{diatom}$ values are strongly tied to proportional inputs from northern versus southern rivers, which is, in turn, linked to glacier melt. Across Baikal's catchment, there is a large ~7‰ $\delta^{18}O$ difference between source waters, which can drive the large magnitude shifts. The delayed start of the shifts in Baunt, compared to Baikal, may be due to the more northerly position of Baunt, particularly when compared against the Baikal catchment, which has a large proportion of the catchment to the south, due to the Selenga river. As discussed in chapter 6, several proxies show a synchronous shift at ~9.3 ka BP, and this, alongside the higher values in the $\delta^{18}O_{diatom}$ record, is thought to suggest warmer

conditions, with changes occurring in the Baunt record due to glacier melt. Therefore, it appears that the Baunt and Baikal records are showing responses to many of the same forcings, but their individual records are influenced by internal factors, such as local glacier melt.

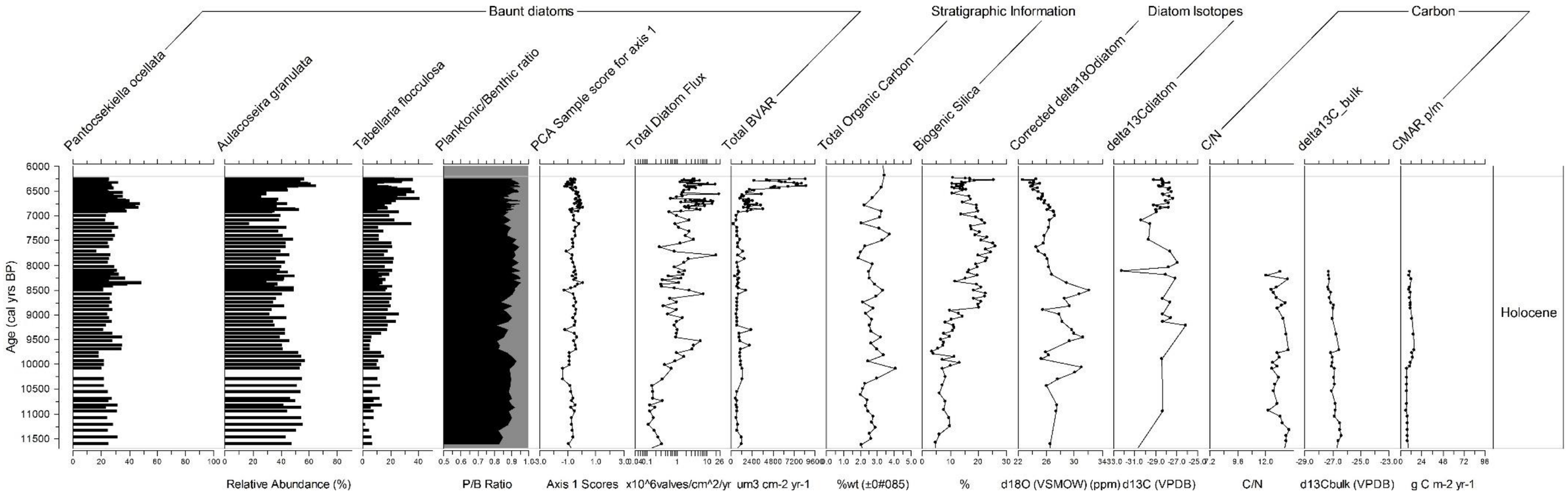

Figure 7.5: Summary of Lake Baunt change over the Holocene period, including dominant diatom assemblage alongside Planktonic/Benthic ratio, total diatom flux (x10^6valves/cm^2/yr) shown on a logged x-axis, biovolume accumulation rates (BVAR) (µ$m^3$$cm^{-2}$$yr^{-1}$), Total-Organic-Carbon (TOC) (%weight), Biogenic silica (BSi) (%), $\delta^{18}O_{diatom}$ (VSMOW ppm) and $\delta^{13}C_{diatom}$ (VPDB ppm) records alongside C/N ratios, $\delta^{13}C_{bulk}$ (VPDB ppm) and carbon mass accumulation rates (CMAR p/m) (g C m^{-2} yr^{-1}) plotted on the Baunt chronology.

7.5 Inferences from climate modelling

The main changes in the environmental record outlined above, have been discussed with reference to key hemispheric and regional climate archives. In order to consider the overall influence of climate variables in the past, it is useful, to some extent, to look at the attempts over recent years to generate and compare climate models for this region. Such an approach is not without problems, as there are only a relatively small number of model simulations that directly target the region and often these are largely focussed on understanding modern climatological phenomena, such as the relationship between the Siberian High and the Arctic oscillation (e.g. Zhang *et al.,* 2018). While such studies are potentially very interesting for understanding very abrupt seasonal to decadal scale changes in the region, there is not sufficient dating resolution to examine such changes in the LGIT. There are, however, a small number of studies that have developed model based simulations of Siberian climate, and are, therefore, relevant for discussion in relation to the Baunt environmental data. These comprise some studies that use large GCM models to evaluate a stable but important snapshot in time, such as the LGM (Crucifix, 2006; Gordon *et al.,* 2000). These types of models, such as the Hadley Centre coupled ocean atmosphere model, Had CM3, are used for climate prediction and are also used in IPCC assessments (Cane *et al.*, 1997). Such models are relatively well resolved spatially and have multiple layers for the ocean and atmosphere and, thus, are computationally expensive and rarely used for long transient simulations of past climate, although recent attempts to run such models over long time windows has added significant new insights into climate forcing. These highlight both the importance of the North Atlantic for driving abrupt climate change, along with insolation and CO_2, but also the complexities in understanding the expression of climate forcing away from regions close to the main zones overturning (e.g. Peltier and Vettoretti 2014, Vettoretti *et al.,* 2018).

It is more common, however, for individual models of intermediate complexity to be used, either to address specific questions relating to an aspect of the climate system, such as the East Asian Monsoon, or for there to be a large

scale comparison of different models and data to test the ability of models to predict particular scenarios (e.g. Crucifix *et al.,* 2012). While it is sometimes the case, that such exercises highlight systematic deficiencies in elements of the modelling, they also highlight regions where there is too little available past climate data for useful evaluation of the models, and also point to some counter-intuitive aspects of past climate (e.g. Zhang *et al.,* 2017b). Either way, such models are useful for consideration in the context of this thesis, where they highlight potential climatological forcing factors behind observations made from the Baunt study, or point to the need for more palaeodata in the region. Key aspects of the Baunt record, where models of past climate are relevan, include the different boundary conditions from full glacial to interglacial climates and the variability in dominant wind patterns and their influence on hydroclimate. These are discussed below, in terms of their potential influence on Lake Baunt, and Siberia as a whole.

7.5.1 Siberian Climate from the Last Glacial Maximum to the Last Termination

A key feature of the Lake Baunt record is the difference in the response of the proxy records from full glacial conditions during the glacial time periods, compared to the Lateglacial and Holocene. For example, there are important changes in the diatom species assemblage from ~15 ka BP, including the rise in importance of *T. flocculosa* and more subtle changes that are apparent in the PCA scores. Similarly, the variability of bulk carbon isotopes is much more muted in the record after 15 ka BP, and there is a major pulse of sediment at ~13.5 ka BP, coincident with the Lateglacial interstadial in Western Europe and GI-1 in the Greenland Ice cores. All of this points to very different prevailing conditions either side of a transition in the site that occurs somewhere between ~15-13 ka BP. One possible explanation for this is the reconfiguration of the global system after the Last Glacial maximum, and the move from a large to small ice sheet world (Dong *et al.,* 1998). There has been significant interest in ice sheet configuration and the dynamics of planetary waves through model/data comparison exercises such as the PMIP project. Of particular relevance here is the role of atmospheric circulation and patterns,

and precipitation and temperature variability in Siberia. Recent work, utilising the CAM 3 (GCM) atmospheric model, with prescribed ice sheet and a fixed ocean slab, has attempted to investigate the role of ice sheets during the LGM on atmospheric circulation (Löfverström *et al.*, 2014). The model utilises an integration of glacial, geological and model-based data for ice sheet dynamics (Kleman *et al.*, 2013), and is run in a set of simulations covering key points from the Last Interglacial to present. To elucidate the nature of the different patterns of climate over the last glacial to interglacial period, the model reconstructs full Interglacial conditions, mid interglacial cooling (Wohlfarth, 2013), and two periods of cooling in MIS 4 and the LGM. The model suggests that LGM conditions are very different in terms of ice sheet topography and the influence this has on atmospheric dynamics, compared to the Holocene, MIS5, or much of the Pleistocene. The atmospheric forcing over Siberia and Alaska at this time could explain the very different nature of proxy response in Baunt, and other records. It is suggested by the CAM 3 model that precipitation and air-mass patterns would be very different, with a dominant anticyclone over the region of Lake Baunt playing an important role in moderating the climate of the region.

One final interesting point from several studies, that is also very relevant here, is the influence of large LGM ice sheets on climate at this time that suggests a warmer and potentially drier Siberia. This has been suggested in modelling studies to mean that there is far less ice sheet development than might be expected (Löfverström *et al.*, 2014) in the region, especially when coupled with the impact of increased dust, reducing albedo (Krinner *et al.*, 2006). This is particularly relevant for the analyses of Lake Baunt in that it might explain the continued sedimentation into the lake through the LGM, without the need to invoke geothermal heating.

As discussed above, the expression of the Heinrich 1 event in Baunt is complicated and possibly has an initial cold phase with a peak in *P. ocellata* but this is then followed by evidence from both Baunt, and other sites in the region (e.g. Baikal), of a wetter phase in this stadial. There are relatively few studies of the H1 event specifically in Siberia, but there have been modelling

exercises on both the expression of Heinrich events and the impact in Siberia of earlier Heinrich events, that are relevant to this study. One issue with understanding these events has been the only very recent coupling of GCM and ice sheet models (Roberts *et al.*, 2014; Ziemen *et al.*, 2018), as opposed to more straightforward 'hosing experiments' (Roche *et al.*, 2014), using either GCM's or models of intermediate complexity. This is again partly due to the required computational time needed for more complex models to run a transient simulation. The coupling of the models is necessary to more reliably simulate an event that is thought to be driven by ocean ice interaction (Broecker *et al.*, 1992). Recently, an integrated GCM and glacial model study of Heinrich events has attempted to understand the nature of Heinrich events, through a coupled ice sheet model, PISM, and CMIP3 an atmosphere – ocean – vegetation enabled GCM (Ziemen *et al.*, 2018) and, as such, is the arguably the most detailed study available. There are several interesting features of the simulated Heinrich events in the model that are relevant to this discussion. As with other modelled meltwater pulse events (below), there are two stages to the Heinrich event, an initial phase where an unstable ice sheet surges into the ocean, and a post surge phase. In the former, the model suggests that the meltwater pulse signal dominates the climate system, while the configuration of the ice sheet is more important in the post-surge phase. The surge phase cooling in the Arctic ocean is also promoted by increased sea ice cover. The model also sees a significant atmospheric response, again, split into a surge and post-surge phase, driven most dominantly in the surge phase by the meltwater pulse and in the post-surge phase by the influence on atmospheric dynamics of the reduced ice sheet height. The surge phase sees cooling and an intensification of drying across Europe and into Siberia, but the post surge phase sees a recovery in precipitation in Europe, and for south-eastern Siberia, an increase in precipitation above pre-surge levels. While the model has some inconsistencies, not least the appearance of anomalous glaciers across Siberia in the initial spin up phases, the two-stage event may be reflected in the Baunt archive, with an initial cooling and drying, followed by evidence for wetter conditions. Models of intermediate complexity, focused on understanding the Asian monsoon during Heinrich events (Jin *et al.*, 2007),

also suggest a strengthening of the westerlies during the events, and this also may allow for the increased productivity seen in the Baunt record, in the second half of Heinrich 1.

7.5.2 The Lateglacial interstadial and the Younger Dryas

The Lateglacial comprises the warming coming out of Heinrich stadial 1, and a saw-tooth cooling leading into the Younger Dryas event. The former is now thought to be driven by ocean circulation, as part of the bipolar seesaw and, though not explicitly modelled, may be linked to the salt oscillator (Vettoretti *et al.*, 2018), suggested to drive D/O cycles. The expression of these is not yet clear for deep continental zones, with very spatially limited data model inter-comparisons, although regionally a warming trend would be expected (Clark *et al.*, 2012). The interpretation of the Baunt record at this time shows some evidence of interstadial conditions, with a peak in *T. flocculosa*, and a marked change in the overall diatom assemblage indicated in the PCA scores. There is also an influx of sediment into the lake during the Interstadial, that may instead relate to the loss of permafrost the area after the LGM (Tesi *et al.*, 2016; Velichko *et al.*, 2011), as the region becomes a major global supplier of CH_4 after the LGM.

After this time, there is a gradual decline in *P. ocellata* during the Younger Dryas. Models have now been developed for the global expression of the Younger Dryas. In particular, a recent global assessment of Younger Dryas hydroclimate, suggests it again has a two phase structure, and that the most significant response would be in the North Atlantic realm (Renssen *et al.*, 2018). This study also looked at specific regional responses to Younger Dryas forcing, based on an initial pulse of freshwater followed by a recovery phase. For Siberia, the model suggests only limited cooling of ~1˚C, but significantly reduced precipitation, which may explain some of the changes seen in the Baunt record, including the limited responses in the oxygen versus carbon diatom isotopes.

7.5.3 Early Holocene

The early and mid Holocene in the region has been the subject of some data/model inter-comparisons, but the very limited sources of proxy data that are suitable for these comparisons mean that any conclusions are, at best, uncertain. There is some evidence to support the inference in Baunt that the recovery into Holocene conditions out of the Younger Dryas is slow, with a thermal optimum ~11-9 ka BP (Zhang *et al.*, 2017b) and a gradual reduction across all models to the late Holocene. This is in broad agreement with the range of proxies across the Baunt archive. However, the multiple early Holocene oscillations in climate, seen in Baunt and other archives, are not yet the focus of many modelling studies with a wide geographic focus, although multiple climatic events at this time are reported for many regions (Hoek and Bos, 2007). There is evidence from one comparison between model output in the early Holocen that is relevant here, and that is the comparison between proxy data from Lake Baikal and a series of 20 year simulations from an atmospheric GCM, with fixed SST's and constant landscape (Bush, 2005; Mackay *et al.*, 2011). One climate oscillation, seen in Baunt, that has been the focus of a number of modelling studies, is the 8.2 ka BP event. The model suggests that the early Holocene sees significant seasonality and particularly cold winters, with this seasonality peaking around 9 ka BP, when obliquity is dominating and more effective humidity. Thus, there is some support from modelling for an unstable climate regime in the early part of the Holocene and a change to generally drier, warmer, and less seasonal conditions towards the end of the period covered by Baunt. This is interesting, as it overlaps with the period where there is reasonable agreement with at least part of the Baikal isotopic record, as well as for hydrological variability.

The forcing, geographic expression, and timing of this event has been the focus of much discussion (Renssen *et al.*, 2007). Recently, both climate model simulations and data/model comparison exercises suggest this is an event that, while short lived, has a global impact. For Siberia, model predictions of cooling in both summer and winter are suggested, along with reduced precipitation (Wiersma and Renssen, 2006). Recent modelling of multiple

ensembles suggests that, while this largely holds true, the impact in Siberia may be more muted (Wiersma *et al.*, 2011), and may feature time-transgressive warm and cold anomalies, with the latter being more prominent, after an initial short lived cooling event. One of the issues for understanding this event in the Baunt archive, is that it may also be superimposed on more gradual long term changes through the Holocene. The relatively muted nature of this event in a Siberian context is also supported by studies of the Holocene carbon dynamics in Lake Baikal, where a limited change in primary producers is limited (Mackay *et al.*, 2017).

8 Conclusions and Recommendations

8.1 Conclusions

This project aimed to reconstruct the lacustrine palaeoecology of Lake Baunt, over the past ~30 ka BP, to understand responses to environmental change and wider climate forcing in southern Siberia, and place this within the context of broader Northern Hemisphere changes. This was, in part, to add important context to the existing regional studies and to assess if records, such as Baunt, could help to provide new information relevant for the region's sensitivity to future climate change. This was based on an evaluation of the ecological, stratigraphic, chronological and stable isotope records developed for Baunt, through this research project. These data were integrated and evaluated to look for key periods of change within the Baunt archive and this was compared to regional records, notably Lakes Baikal and Kotokel. The results of this have been further considered against evidence of major changes in key climate archives from the Northern Hemisphere, to understand how this study fits within the framework of climate change, documented by important stratotypes, such as the Greenland Ice Cores. Finally, these analyses were considered against current prevailing theories of the major climate forcing factors, and formal model simulations, of how these may impact climate and environments in central Asia. The success of this project is now evaluated by a set of questions derived from these aims and objectives.

1. **Is the Lake Baunt record viable and coherent and does it show a series of changes across proxies?**

This project has undertaken 327 diatom analyses across the BNT14 core, providing a high resolution record of the diatom assemblage from Lake Baunt. This record is one of the best preserved assemblages of the past ~30 ka BP in the southern Siberian region, with low levels of dissolution across the whole core, and no periods of absent or very low concentrations of diatoms. Alongside the diatom assemblage, a range of organic and geochemical data were generated, including $\%C_{bulk}$, C/N ratios, $\delta^{13}C_{diatom}$ and $\delta^{18}O_{diatom}$ and some additional ^{14}C dates for the core, and additionally detailed Bayesian age

modelling was undertaken. Additional data was made available for comparison by Russian and UK colleagues, including stratigraphic logs, TOC, BSi, isotope geochemistry, additional ^{14}C ages, %TOC, C/N ratios and $^{13}C_{bulk}$ analyses). All of these data were evaluated and integrated, in this thesis, to assess environmental impacts.

The evaluation of these records suggested that this is a predominantly coherent archive, with fairly linear sedimentation rates, broad coherence between shifts seen in the different sedimentary and ecological proxies and no significant errors, or major turbidites observed. It is important to evaluate the integrity of the record, in a tectonically active region. However, the Baunt archive has presented some challenges, which have been addressed within this thesis. These include the two faults identified within the stratigraphy, at ~660cm and ~990cm. However, when these were compared to TOC, BSi, MAR's and a range of Bayesian depositional models, these faults do not seem to have had a detectable impact on the sediments and environmental record from Baunt. One reoccurring, issue has concerned the chronological controls from Lake Baunt. The final age model produced in this project is the best current representation of the age of the sediments in Baunt, and has been thoroughly evaluated through numerous iterations, and many different depositional scenarios. However, dating uncertainties in Baunt are variable, although they are predominantly centennial in scale. This variability can be problematic in places, because some of the changes known in key climate archives are extremely rapid, lasting decades to a few centuries, and, thus, caution has had to be applied when considering Baunt against wider records. However, the resolution of the Baunt chronology is not unusual for many records covering this period, when age models fully assess the inherent uncertainties. More precise models are available for Baunt, but as discussed during the evaluation in chapter 3, these are unlikely to be realistic and, therefore, have not been used.

The detailed age modelling study highlights a further issue with the BNT14 core, due to the lack of a set of radiocarbon dates in the upper 50cm of the record. It was found that there was an incompatibility between an assumed

present day age for the top of the core, and the radiocarbon dates, from 50cm down. The extrapolated trajectory up to the top of the core in any version of the age model based on the lower dates, suggests that the uppermost sediments were significantly older than present day. This finding was corroborated by the ^{210}Pb dating profile, undertaken in this project, and additional radiocarbon dating, coupled with multiple Bayesian age modelling experiments. All of these suggest that due to the difficulties in coring through ice, there have been problems with capturing the recent Holocene sediments for BNT14.

Further to these issues, the diatom assemblage from Lake Baunt, while well preserved, lacks a good modern analogue study, which would provide useful context for the palaeo assemblage. However, the study has been fortunate that shifts within the assemblage are notable, and species within the core are cosmopolitan, and, therefore, species ecologies were better understood than may have been the case had the assemblage contained many endemic species.

2. What are the main changes seen in Baunt?

Taken together, the Baunt record clearly documents a number of transitions across the record, often expressed in different ways, but in multiple proxies. These have been considered on the BNT14 final chronology, calibrated with IntCal13, and show:

- DAZ1 ~30-22.5 ka BP: limited productivity, dominated by *P. ocellata* suggested long ice cover durations, high light intensities with limited particulates and low BVAR, and unstable diatom flux, with a low period ~24 ka BP, coincident with low BVAR. This is interpreted as a cold and arid period at Baunt.
- DAZ2 ~22.5-20.5 ka BP: a shift in diatom dominance to *A. granulata,* alongside increased allochthonous organic matter, higher diatom fluxes and BVAR. Considered as a period of increased productivity within the lake and catchment, with greater spring and autumn overturning indicating shorter ice duration.

- DAZ3 ~20.5-18 ka BP: a return to less productive conditions dominated by *P. ocellata* with organics sourced from algal productivity. Higher $\delta^{13}C_{bulk}$ values due to reduced turbulence.
- DAZ4 ~ 18-15.1 ka BP: transition phase with shift from *P. ocellata,* which peaks at ~18 ka BP, to dominance of *A. granulata* by ~15.1 ka BP. A range of proxies indicate increased productivity within the lake (BSi, diatom flux) and a clear transition is shown in the PCA. CMAR are low throughout this zone.
- DAZ5 ~15.1-13.1 ka BP: Initial peak of *A. granulata* followed by a decline, and corresponding rise in *P. ocellata* which peaks at ~13.1 ka BP. There is a short peak in *T. flocculosa* at ~14-13.6 ka BP. And peaks occur in BVAR/CMAR and C/N ratios rise. Additionally, the first data is available for $\delta^{13}C_{diatom}$ and $\delta^{18}O_{diatom,}$ with $\delta^{13}C_{diatom}$ showing the lowest values seen in the record, while $\delta^{18}O_{diatom}$ has lower values than much of the latter record.
- DAZ6 ~13.1-6.2 ka BP: There are low levels of *T. flocculosa* at the start of the zone, which then rises throughout zone. Peak of *P. ocellata* at the start of the zone, followed by decline. Stable diatom flux at the start of the zone, with rising values from ~10 ka BP. $\delta^{13}C_{bulk}$ values are generally stable except a shift at ~9.3 ka BP, coinciding with rises in CMAR and C/N ratios, which are also relatively stable across this period, apart from this shift. $\delta^{13}C_{diatom}$ values rise until ~9.3 ka BP and $\delta^{18}O_{diatom}$ show a series of oscillations throughout the record, with greatest amplitude between ~11-8 ka BP. A shift is observed in both records (although most notably in the $\delta^{13}C_{diatom}$) at ~8.2 ka BP and a further paired oscillation is seen after this, through to ~6.5 ka BP.

3. Which changes across the Baunt proxies are reflected in data from other records and, thus, may be driven by extrinsic forcing?

Of the shifts outlined above, several of these correspond to changes seen in regional and wider records, at approximately the same time (within combined dating uncertainties). The period ~30-22.5ka BP corresponds with a time of

considerable Siberian High strength, and the periods of greatest strength coincide with the lowest diatom flux in this part of the Baunt data. The EASM is weak during this period, with its weakest point coinciding with the strongest Siberian High, and lowest BVAR and diatom flux in Baunt. This timing of this broadly encompasses the LGM and Heinrich stadial 2, highlighting that these events are recorded by Baunt. This is followed by increasing diatom flux, after which, the diatom assemblage shifts, as described above. These changes coincide with increased algal productivity in Lake Kotokel and weaker Siberian High strength. Further afield, warming is documented in Greenland (GI-2.2 and GI-2.1) and strengthening of the EASM. All of this, therefore, suggests that the switch between unproductive to productive conditions in Lake Baunt ~22.5 ka BP is broadly driven by climatic changes linked to the end of the LGM and HE2.

This period of increased productivity continues in Baunt until 20.5 ka BP, after which, a period of stability, defined by *P. ocellata* coincides with similarly stable conditions seen in GS2 in Greenland and in EASM strength and the Siberian High. Following this, dynamic changes are seen in a number of records, from both Siberia and the wider Northern Hemisphere. As described above, several transitions are observed in Baunt between ~18-15 ka BP, while over this time, changes are also seen in Lake Baikal and Kotokel. In Baikal, the period documents increased deposition of carbonate muds, associated with dramatic runoff events (Katsuta *et al.*, 2018), while Kotokel shows increased diatom productivity from ~17 ka BP (Bezrukova *et al.*, 2010). During this time, Siberian High strength is initially stable, with a slight weakening to the latter stages, while the EASM declines in strength, Greenland temperatures also decline and AMOC is very weak (McManus *et al.*, 2004; Wang *et al.*, 2001). This period encompasses the mystery interval and Heinrich event 1; potentially one of the most complex periods during the Late Quaternary. There are clear impacts on the climate regime, including precipitation changes, indicated by both Baikal and Baunt. Interestingly this fits in with climate models of a two stage Heinrich 1 event, with changes in hydroclimate over central Asia, and recent observations of a complex two stage Heinrich 1 event, in the North Atlantic.

The next transition seen in Baunt are in DAZ 5 (broadly ~15-13 ka BP) and coincide with shifts in Siberian records, including a suggested warmer and wetter period in Kotokel, which drives increased productivity, while Baikal documents warming and progressive increases in moisture. These changes occur during the lateglacial interstadial (Bølling-Allerød/GI-1), seen in Greenland and across Europe and the North Atlantic. It is strongly reflected as a period of high EASM and AMOC strength and reduced Siberian High strength. Following this episode, changes observed within Baunt appear to be driven by conditions associated with the Younger Dryas, which are documented by reduced AMOC and EASM strength and a very strong Siberian High. In Baunt, there is an indication of stronger forcings during the early stage, with peak *P. ocellata* at the start, and then declining throughout. In the later part of the Younger Dryas the signal is also clear in $\delta^{13}C_{diatom}$ record, while this is less so for the $\delta^{18}O_{diatom}$ data. This signal has also been noted in Baikal, where the later part of the Younger Dryas is associated with warmer conditions. These features of the Younger Dryas have been discovered in other palaeoclimatic records and have been suggested by transient model simulations. A two stage Younger Dryas has been recognised in Greenland, Europe, and East Asia, and is also a feature of several model simulations for this stadial. The lack of a clear signal in the $\delta^{18}O_{diatoms}$ record could tentatively be linked to the occurrence of warm Younger Dryas summers proposed by Schenk *et al.,* (2018), although the sampling resolution at Baunt is currently too small to make any firm conclusions.

The Early Holocene period in Baunt sees a number of features, which are potentially extrinsically forced, driving changes, predominantly in the diatom isotopes. Generally, there is good agreement between excursions seen in Lakes Baunt and Baikal. These are broadly in phase with changes in the Siberian High and AMOC strength, suggesting that the Early Holocene climate of Siberia was sensitive to changes in the North Atlantic region. There is, however, evidence for some of the shifts in the Baunt record to be driven by glacial meltwater input, and are, therefore, not recorded in other sites.

4. Has this study achieved the overall aim of the project?

From the above discussion, it is clear (despite some issues raised in the first section), that the Baunt record is recording some important responses to extrinsic climate forcing. This is important for two reasons. Firstly, some of these external climatic influences have been proposed to impact on the Lake Baikal record, however, because of its size and large catchment, this does not necessarily mean these changes are fully reflected elsewhere in southern Siberia, as Baikal is a very important, but unique archive. The fact that Baunt is recording similar events, albeit with its own expression, lends support to the idea that southern Siberia is very sensitive to climate forcing and that many events recorded in Baikal have an expression in Baunt. This is important because a key aim of this study was to test the influence of climate signals in an area remote from oceanic influences. Secondly, the sensitivity to both extrinsic and intrinsic factors recorded in the late last glacial and early to mid Holocene in Baunt, highlight the finely balanced nature of this ecosystem, which indicates its susceptibility to change as a result of current and future anthropogenic forcing. While within this project it has not possible to study the recent past, as initially anticipated, the fact that Baunt is so responsive to natural forcing is very important when considering future research (see below).

8.2 Recommendations for future work

Several recommendations can be made for future research, following completion of this project. As discussed above, issues exist within the Baunt archive, particularly concerning the chronological controls and lack of coverage over the mid to late Holocene. It is, therefore, recommended that further coring at Lake Baunt is undertaken, to capture the period between the record from the BNT13 short core (Bezrukova *et al.*, 2017) and the start of the record preserved in the BNT14 core. Additionally, it has been shown in this project that Baunt is sensitive to changes across MIS 1, 2, and late MIS3, however some of the most abrupt changes in the Late Quaternary period occur in early periods of MIS3 (~30-60 ka BP) and the period is increasingly being studied, beyond the ice core and marine records, with many new models being produced (Peltier and Vettoretti, 2014; Vettoretti *et al.*, 2018) to consider these

changes. MIS3 also includes critical periods for study of hominin distributions (Krause *et al.*, 2010, 2007). As the BNT14 core did not reach the base of sediments in Baunt, it is likely that sediments may be preserved from earlier MIS3, and it is recommended that a longer core is extracted from Baunt to allow studies of this period. This new core should have detailed sedimentological work undertaken, to ensure its suitability for further analyses.

Many of the conclusions made in this thesis have been limited due to chronological uncertainties, so future recommendations are made for additional radiocarbon dating to be undertaken BNT14 and any new cores. This is highly important in a tectonic region, as sedimentation may not have been linear, meaning dates are required at regular intervals. It is unlikely that there is a mineral carbon induced reservoir offset in Baunt, as there is no carbonate within the catchment, however, there is potential for an internal reservoir offset due to carbon storage within the lake. This means dating of modern samples is required to assess this. However, this is unlikely to be a major issue, as Baunt is a relatively shallow lake and even lake Baikal only has a ~500 modern reservoir effect.

Analyses within this study have highlighted the potential for tephrostratigraphy to be considered at Lake Baunt. Occasional shards have been documented in some sediments from Baunt, and a routine study of these would allow the potential for tephrostratigraphy for this region to be assessed. If successful, this may provide a way for improved site to site correlations and improvements of chronological controls, through the building of a tephra lattice.

The Baunt record has highlighted rapid shifts in many of its proxies, and this work could be furthered by undertaking higher resolution analyses, particularly during periods of abrupt shifts. Lengthening the $\delta^{18}O_{diatom}$ and $\delta^{13}C_{diatom}$ records back into the last glacial, would allow further consideration of changes in lake carbon cycling and hydrological changes through this period, further improving understanding of the lake's responses to abrupt changes, such as Heinrich 1. Alongside this, at the time of writing this thesis, analyses of some proxies from Lake Baunt (e.g. pollen), being considered by collaborators at the Institute of Archaeology and Ethnography, Russian Academy of Sciences,

Irkutsk, had not been completed and, therefore, upon completion of this additional work, it will be possible to integrate these records, with those currently available from Baunt, to further understand the ecosystem changes.

The diatom analyses and interpretation at Baunt, as discussed above, has been limited due to the lack of a modern analogue study and, therefore, further work at the site would benefit from considering this. Alongside such a study, it would be beneficial to analyse the seasonal or preferably monthly precipitation at Baunt, to provide a year-round context of variations in its characteristics, particularly in terms if isotopic changes.

Therefore, although this study has provided many new and novel insights into the impact of abrupt climate change in southern Siberia, like all exciting sites, they often throw up new and interesting questions from which to undertake work into the future.

Bibliography:

Abramson, L., Wirick, S., Lee, C., Jacobsen, C., Brandes, J.A., 2009. The use of soft X-ray spectromicroscopy to investigate the distribution and composition of organic matter in a diatom frustule and a biomimetic analog. *Deep Sea Research Part II: Topical Studies in Oceanography* 56, 1369–1380.

Adams, J.K., Peng, Y., Rose, N.L., Shchetnikov, A.A., Mackay, A.., 2018. Diatom community responses to long-term multiple stressors at Lake Gusinoye , Siberia pre-print.

Adkins, J.F., 2013. The role of deep ocean circulation in setting glacial climates. *Paleoceanography* 28, 539–561.

Aitchison, J., 1986. The Statistical Analysis of Compositional Data. *Journal of the Royal Statistical Society. Series B (Methodological)* 44, 139–177.

Allen, B.D., Anderson, R.Y., 2000. A continuous, high-resolution record of late Pleistocene climate variability from the Estancia basin, New Mexico. *Geological Society of America Bulletin* 112, 1444–1458.

Alley, R.B., 2004. Abrupt climate change. *Scientific American* 291, 62–69.

Alley, R.B., 2007. Wally Was Right: Predictive Ability of the North Atlantic “Conveyor Belt” Hypothesis for Abrupt Climate Change. *Annual Review of Earth and Planetary Sciences* 35, 241–272.

Alley, R.B., Andrews, J.T., Brigham-Grette, J., Clarke, G.K.C., Cuffey, K.M., Fitzpatrick, J.J., Funder, S., Marshall, S.J., Miller, G.H., Mitrovica, J.X., Muhs, D.R., Otto-Bliesner, B.L., Polyak, L., White, J.W.C., 2010. History of the Greenland Ice Sheet: paleoclimatic insights. *Quaternary Science Reviews* 29, 1728–1756.

Alley, R.B., Marotzke, J., Nordhaus, W.D., Overpeck, J.T., Peteet, D.M., Pielke, R.A., Pierrehumbert, R.T., Rhines, P.B., Stocker, T.F., Talley, L.D., Wallace, J.M., 2003. Abrupt climate change. *Science* 299, 2005–2010.

Alvarez-Solas, J., Ramstein, G., 2011. On the triggering mechanism of Heinrich events. *Proceedings of the National Academy of Sciences* 108, E1359–E1360.

Anchukaitis, K.J., Buckley, B.M., Cook, E.R., Cook, B.I., D’Arrigo, R.D., Ammann, C.M., 2010. Influence of volcanic eruptions on the climate of the Asian monsoon region. *Geophysical Research Letters* 37, L22703.

Anderson, D.E., 1997. Younger Dryas research and its implications for understanding abrupt climatic change. *Progress in Physical Geography* 21, 230–249.

Anderson, N.J., 1994. Comparative planktonic diatom biomass responses to lake and catchment disturbance. *Journal of Plankton Research* 16, 133–150.

Anderson, N.J., D'Andrea, W., Fritz, S.C., 2009. Holocene carbon burial by lakes in SW Greenland. *Global Change Biology* 15, 2590–2598.

Andersson, C., Risebrobakken, B., Jansen, E., Dahl, S.O., 2003. Late Holocene surface ocean conditions of the Norwegian Sea (Vøring Plateau). *Paleoceanography* 18, 1044.

Appleby, P.G., 2002. Chronostratigraphic Techniques in Recent Sediments. In: Tracking Environmental Change Using Lake Sediments. Kluwer Academic Publishers, Dordrecht, pp. 171–203.

Appleby, P.G., Nolan, P.J., Gifford, D.W., Godfrey, M.J., Oldfield, F., Anderson, N.J., Battarbee, R.W., 1986. 210Pb dating by low background gamma counting. *Hydrobiologia* 143, 21–27.

Appleby, P.G., Oldfieldz, F., 1983. The assessment of 210Pb data from sites with varying sediment accumulation rates. *Hydrobiologia* 103, 29–35.

Atkinson, T.C., Briffa, K.R., Coope, G.R., 1987. Seasonal temperatures in Britain during the past 22,000 years, reconstructed using beetle remains. *Nature* 325, 587–592.

Avery, R.S., Xuan, C., Kemp, A.E.S., Bull, J.M., Cotterill, C.J., Fielding, J.J., Pearce, R.B., Croudace, I.W., 2017. A new Holocene record of geomagnetic secular variation from Windermere, UK. *Earth and Planetary Science Letters* 477, 108–122.

B-Béres, V., Lukács, Á., Török, P., Kókai, Z., Novák, Z., T-Krasznai, E., Tóthmérész, B., Bácsi, I., 2016. Combined eco-morphological functional groups are reliable indicators of colonisation processes of benthic diatom assemblages in a lowland stream. *Ecological Indicators* 64, 31–38.

B-Béres, V., Török, P., Kókai, Z., Lukács, Á., T-Krasznai, E., Tóthmérész, B., Bácsi, I., 2017. Ecological background of diatom functional groups: Comparability of classification systems. *Ecological Indicators* 82, 183–188.

Bakke, J., Lie, Ø., Heegaard, E., Dokken, T., Haug, G.H., Birks, H.H.,

Dulski, P., Nilsen, T., 2009. Rapid oceanic and atmospheric changes during the Younger Dryas cold period. *Nature Geoscience* 2, 202–205.

Barber, D.C., Dyke, A., Hillaire-Marcel, C., Jennings, A.E., Andrews, J.T., Kerwin, M.W., Bilodeau, G., McNeely, R., Southon, J., Morehead, M.D., Gagnon, J.-M., 1999. Forcing of the cold event of 8,200 years ago by catastrophic drainage of Laurentide lakes 400, 344–348.

Barber, H.G., Haworth, E.Y., 1981. A guide to the morphology of the diatom frustule : with a key to the British freshwater genera. *Freshwater Biological Association*.

Barker, P., Fontes, J.-C., Gasse, F.F., Druart, J.-C., 1994. Experimental dissolution of diatom silica in concentrated salt solutions and implications for paleoenvironmental reconstruction. *Limnology and Oceanography* 39, 99–110.

Barker, P.A., Hurrell, E.R., Leng, M.J., Plessen, B., Wolff, C., Conley, D.J., Keppens, E., Milne, I., Cumming, B.F., Laird, K.R., Kendrick, C.P., Wynn, P.M., Verschuren, D., 2013. Carbon cycling within an East African lake revealed by the carbon isotope composition of diatom silica: a 25-ka record from Lake Challa, Mt. Kilimanjaro. *Quaternary Science Reviews* 66, 55–63.

Barker, P.A., Leng, M.J., Gasse, F., Huang, Y., 2007. Century-to-millennial scale climatic variability in Lake Malawi revealed by isotope records. *Earth and Planetary Science Letters* 261, 93–103.

Baskaran, M., Nix, J., Kuyper, C., Karunakara, N., 2014. Problems with the dating of sediment core using excess (210)Pb in a freshwater system impacted by large scale watershed changes. *Journal of environmental radioactivity* 138, 355–63.

Battarbee, R., Juggins, S., Gasse, F., Anderson, N., Bennion, H., Cameron, N., Ryves, D., Pailles, C., Chalie, F., Telford, R., 2001. An Information System for Palaeoenvironmental Reconstruction. *EDDI* 81, 1–94.

Battarbee, R.W., Jones, V.J., Flower, R.J., Cameron, N.G., Bennion, H., Carvalho, L., Juggins, S., 2002. Diatoms. In: Tracking Environmental Change Using Lake Sediments. Kluwer Academic Publishers, Dordrecht, pp. 155–202.

Battarbee, R.W., Kneen, M.J., 1982. The use of electronically counted microspheres in absolute diatom analysis. *Limnology and Oceanography* 27, 184–188.

Battarbee, R.W., Mackay, A.W., Jewson, D.H., Ryves, D.B., Sturm, M., 2005. Differential dissolution of Lake Baikal diatoms: correction factors

and implications for palaeoclimatic reconstruction. *Global and Planetary Change* 46, 75–86.

Bemis, B.E., Spero, H.J., Bijma, J., Lea, D.W., 1998. Reevaluation of the oxygen isotopic composition of planktonic foraminifera: Experimental results and revised paleotemperature equations. *Paleoceanography* 13, 150–160.

Benson, L., Liddicoat, J., Smoot, J., Sarna-Wojcicki, A., Negrini, R., Lund, S., 2003. Age of the Mono Lake excursion and associated tephra. *Quaternary Science Reviews* 22, 135–140.

Berger, A., Li, X.S., Loutre, M.F., 1999. Modelling northern hemisphere ice volume over the last 3Ma. *Quaternary Science Reviews* 18, 1–11.

Berger, A., Loutre, M.F., 1991. Insolation values for the climate of the last 10 million years. *Quaternary Science Reviews* 10, 297–317.

Bezrukova, E., 2012. Last glacial–interglacial vegetation and environments in southern Siberia: Chronology, forcing and feedbacks. *Quaternary International* 279–280, 50–50.

Bezrukova, E. V., Amosova, A.A., Chubarov, V.M., Finkelshtein, A.L., Kulagina, N. V., 2017. Environmental changes in the northeast of the Buryat Republic during the Holocene post-Optimum: First results. *Contemporary Problems of Ecology* 10, 431–440.

Bezrukova, E. V., Belov, A. V., Orlova, L.A., 2011. Holocene vegetation and climate variability in North Pre-Baikal region, East Siberia, Russia. *Quaternary International* 237, 74–82.

Bezrukova, E. V., Tarasov, P.E., Solovieva, N., Krivonogov, S.K., Riedel, F., 2010. Last glacial-interglacial vegetation and environmental dynamics in southern Siberia: Chronology, forcing and feedbacks. *Palaeogeography, Palaeoclimatology, Palaeoecology* 296, 185–198.

Bidle, K.D., Brzezinski, M.A., Long, R.A., Jones, J.L., Azam, F., 2003. Diminished efficiency in the oceanic silica pump caused by bacteria-mediated silica dissolution. *Limnology and Oceanography* 48, 1855–1868.

Bigg, G.R., Levine, R.C., Green, C.L., 2011. Modelling abrupt glacial North Atlantic freshening: Rates of change and their implications for Heinrich events. *Global and Planetary Change* 79, 176–192.

Biskaborn, B.K., Herzschuh, U., Bolshiyanov, D., Savelieva, L., Diekmann, B., 2012. Environmental variability in northeastern Siberia during the last ~13,300yr inferred from lake diatoms and sediment–geochemical parameters. *Palaeogeography, Palaeoclimatology,*

Palaeoecology 329–330, 22–36.

Björck, S., Rundgren, M., Ingólfsson, Ó., Funder, S., 1997. The Preboreal oscillation around the Nordic Seas: terrestrial and lacustrine responses. *Journal of Quaternary Science* 12, 455–465.

Blockley, S., Candy, I., Matthews, I., Langdon, P., Langdon, C., Palmer, A., Lincoln, P., Abrook, A., Taylor, B., Conneller, C., Bayliss, A., MacLeod, A., Deeprose, L., Darvill, C., Kearney, R., Beavan, N., Staff, R., Bamforth, M., Taylor, M., *et al.*, 2018. The resilience of postglacial hunter-gatherers to abrupt climate change. *Nature Ecology and Evolution* 2, 810–818.

Blockley, S.P.E., Blaauw, M., Bronk Ramsey, C., van der Plicht, J., 2007. Building and testing age models for radiocarbon dates in Lateglacial and Early Holocene sediments. *Quaternary Science Reviews* 26, 1915–1926.

Blockley, S.P.E., Bourne, A.J., Brauer, A., Davies, S.M., Hardiman, M., Harding, P.R., Lane, C.S., MacLeod, A., Matthews, I.P., Pyne-O'Donnell, S.D.F., Rasmussen, S.O., Wulf, S., Zanchetta, G., 2014. Tephrochronology and the extended intimate (integration of ice-core, marine and terrestrial records) event stratigraphy 8–128 ka b2k. *Quaternary Science Reviews* 106, 88–100.

Blockley, S.P.E., Housley, R. a., 2009. Calibration commentary 51, 287–290.

Blockley, S.P.E., Lane, C.S., Hardiman, M., Rasmussen, S.O., Seierstad, I.K., Steffensen, J.P., Svensson, A., Lotter, A.F., Turney, C.S.M.M., Bronk Ramsey, C., 2012. Synchronisation of palaeoenvironmental records over the last 60,000 years, and an extended INTIMATE 1 event stratigraphy to 48,000 b2k. *Quaternary Science Reviews* 36, 2–10.

Blockley, S.P.E., Lowe, J.J., Walker, M.J.C., Asioli, A., Trincardi, F., Coope, G.R., Donahue, R.E., Pollard, A.M., 2004. Bayesian analysis of radiocarbon chronologies: examples from the European Late-glacial. *Journal of Quaternary Science* 19, 159–175.

Blockley, S.P.E., Pyne-O'Donnell, S.D.F., Lowe, J.J., Matthews, I.P., Stone, A., Pollard, A.M., Turney, C.S.M., Molyneux, E.G., 2005. A new and less destructive laboratory procedure for the physical separation of distal glass tephra shards from sediments. *Quaternary Science Reviews* 24, 1952–1960.

Bloom, A.A., Palmer, P.I., Fraser, A., Reay, D.S., Frankenberg, C., 2010. Large-scale controls of methanogenesis inferred from methane and gravity spaceborne data. *Science* 327, 322–325.

Blyakharchuk, T., Eirikh, A., Mitrofanova, E., Kang, S.-C., 2017. High resolution palaeoecological records for climatic and environmental changes during the last 1350 years from Manzherok Lake, western foothills of the Altai Mountains, Russia. *Quaternary International* 447, 59–74.

Bol'shakov, V.A., 2017. On the use of geomagnetic excursions for establishing the chronostratigraphic scale of the Brunhes orthozone and correlation of pleistocene geological sequences: Problems remain. *Izvestiya, Physics of the Solid Earth* 53, 885–897.

Bond, G., 1997. A Pervasive Millennial-Scale Cycle in North Atlantic Holocene and Glacial Climates. *Science* 278, 1257–1266.

Bond, G., Broecker, W., Johnsen, S., McManus, J., Labeyrie, L., Jouzel, J., Bonani, G., 1993. Correlations between climate records from North Atlantic sediments and Greenland ice. *Nature* 365, 143–147.

Bond, G., Kromer, B., Beer, J., Muscheler, R., Evans, M.N., Showers, W., Hoffmann, S., Lotti-Bond, R., Hajdas, I., Bonani, G., 2001. Persistent solar influence on North Atlantic climate during the Holocene. *Science* 294, 2130–2136.

Bonhommet, N. Babkine, J., 1969. Sur la présence d'aimantations inversées dans la Chaîne des Puys. *c.r. acad. sci. paris* 264, 92–94.

Bowman, S., 1990. Radiocarbon dating. University of California Press.

Braak, C.J.F., Smilauer, P., 2012. Canoco reference manual and user's guide: software for ordination, version 5.0.

Brandriss, M.E., O'Neil, J.R., Edlund, M.B., Stoermer, E.F., 1998. Oxygen isotope fractionation between diatomaceous silica and water. *Geochimica et Cosmochimica Acta* 62, 1119–1125.

Brauer, A., Hajdas, I., Blockley, S.P.E., Bronk Ramsey, C., Christl, M., Ivy-Ochs, S., Moseley, G.E., Nowaczyk, N.N., Rasmussen, S.O., Roberts, H.M., Spötl, C., Staff, R.A., Svensson, A., Bronk Ramsey, Christopher Christl, M., Ivy-Ochs, S., Moseley, G.E., Nowaczyk, N.N., Rasmussen, S.O., Roberts, H.M., *et al.*, 2014. The importance of independent chronology in integrating records of past climate change for the 60-8 ka INTIMATE time interval. *Quaternary Science Reviews* 106, 47–66.

Brauer, A., Haug, G.H., Dulski, P., Sigman, D.M., Negendank, J.F.W., 2008. An abrupt wind shift in western Europe at the onset of the Younger Dryas cold period. *Nature Geoscience* 1, 520–523.

Brewer, T.S., Leng, M.J., Mackay, A.W., Lamb, A.L., Tyler, J.J., Marsh, N.G., 2008. Unravelling contamination signals in biogenic silica oxygen isotope composition: the role of major and trace element geochemistry. *Journal of Quaternary Science* 23, 321–330.

Brincat, D., Yamada, K., Ishiwatari, R., Uemura, H., Naraoka, H., 2000. Molecular-isotopic stratigraphy of long-chain n-alkanes in Lake Baikal Holocene and glacial age sediments. *Organic Geochemistry* 31, 287–294.

Broecker, W., Bond, G., Klas, M., Clark, E., McManus, J., 1992. Origin of the northern Atlantic's Heinrich events. *Climate Dynamics* 6, 265–273.

Broecker, W.S., 1994. Massive iceberg discharges as triggers for global climate change. *Nature* 372, 421–424.

Broecker, W.S., Stocker, T.F., 2006. The Holocene CO 2 rise: Anthropogenic or natural? *Eos, Transactions American Geophysical Union* 87, 27–27.

Broecker, W.S., van Donk, J., 1970. Insolation changes, ice volumes, and the O 18 record in deep-sea cores. *Reviews of Geophysics* 8, 169–198.

Bronk Ramsey, C., 2001. Development of the Radiocarbon Calibration Program. *Radiocarbon* 43, 355–363.

Bronk Ramsey, C., 2008. Deposition models for chronological records. *Quaternary Science Reviews* 27, 42–60.

Bronk Ramsey, C., 2009. Bayesian Analysis of Radiocarbon Dates. *Radiocarbon* 51, 337–360.

Bronk Ramsey, C., 2009. Dealing with outliers and offsets in radiocarbon dating. *Radiocarbon* 51, 1023–1045.

Bronk Ramsey, C., Dee, M., Lee, S., Nakagawa, T., Staff, R.A., 2010. Developments in the Calibration and Modeling of Radiocarbon Dates. *Radiocarbon* 52, 953–961.

Bronk Ramsey, C., Lee, S., 2013. Recent and Planned Developments of the Program OxCal. *Radiocarbon* 55, 720–730.

Brooks, S.J., Matthews, I.P., Birks, H.H., Birks, H.J.B., 2012. High resolution Lateglacial and early-Holocene summer air temperature records from Scotland inferred from chironomid assemblages. *Quaternary Science Reviews* 41, 67–82.

Browman, D.L., 1993. Radiocarbon After Four Decades: An

Interdisciplinary Perspective, edited by Royal E. Taylor, Austin Long, and Renee S. Kra, Springer-Verlag, New York. *Bulletin of the History of Archaeology* 3, 14.

Brown, S., Higham, T., Slon, V., Pääbo, S., Meyer, M., Douka, K., Brock, F., Comeskey, D., Procopio, N., Shunkov, M., Derevianko, A., Buckley, M., 2016. Identification of a new hominin bone from Denisova Cave, Siberia using collagen fingerprinting and mitochondrial DNA analysis. *Scientific reports* 6, 23559.

Buizert, C., Adrian, B., Ahn, J., Albert, M., Alley, R.B., Baggenstos, D., Bauska, T.K., Bay, R.C., Bencivengo, B.B., Bentley, C.R., Brook, E.J., Chellman, N.J., Clow, G.D., Cole-Dai, J., Conway, H., Cravens, E., Cuffey, K.M., Dunbar, N.W., Edwards, J.S., *et al.*, 2015. Precise interpolar phasing of abrupt climate change during the last ice age. *Nature* 520, 661–5.

Bush, A.B.G., 2005. CO 2 /H 2 O and orbitally driven climate variability over central Asia through the Holocene. *Quaternary International* 136, 15–23.

Buvit, I., Terry, K., 2011. The twilight of Paleolithic Siberia: Humans and their environments east of Lake Baikal at the late-glacial/Holocene transition. *Quaternary International* 242, 379–400.

Cai, Y., Tan, L., Cheng, H., An, Z., Edwards, R.L., Kelly, M.J., Kong, X., Wang, X., 2010. The variation of summer monsoon precipitation in central China since the last deglaciation. *Earth and Planetary Science Letters* 291, 21–31.

Camuera, J., Jiménez-Moreno, G., Ramos-Román, M.J., García-Alix, A., Toney, J.L., Anderson, R.S., Jiménez-Espejo, F., Bright, J., Webster, C., Yanes, Y., Carrión, J.S., 2019. Vegetation and climate changes during the last two glacial-interglacial cycles in the western Mediterranean: A new long pollen record from Padul (southern Iberian Peninsula). *Quaternary Science Reviews* 205, 86–105.

Cane, M.A., Clement, A.C., Kaplan, A., Kushnir, Y., Pozdnyakov, D., Seager, R., Zebiak, S.E., Murtugudde, R., 1997. Twentieth-Century Sea Surface Temperature Trends. *Science* 275, 957–960.

Cascalheira, J., 2013. Hunter–gatherer ecodynamics and the impact of the Heinrich event 2 in Central and Southern Portugal. *Quaternary International* 318, 117–127.

Channell, J.E.T., 2006. Late Brunhes polarity excursions (Mono Lake, Laschamp, Iceland Basin and Pringle Falls) recorded at ODP Site 919 (Irminger Basin). *Earth and Planetary Science Letters* 244, 378–393.

Chapligin, B., Meyer, H., Bryan, A., Snyder, J., Kemnitz, H., 2012a. Assessment of purification and contamination correction methods for analysing the oxygen isotope composition from biogenic silica. *Chemical Geology* 300–301, 185–199.

Chapligin, B., Meyer, H., Swann, G.E.A., Meyer-Jacob, C., Hubberten, H.W., 2012b. A 250 ka oxygen isotope record from diatoms at Lake El'gygytgyn, far east Russian Arctic. *Climate of the Past* 8, 1621–1636.

Chen, X., Yang, X., Dong, X., Liu, E., 2012. Influence of environmental and spatial factors on the distribution of surface sediment diatoms in Chaohu Lake, southeast China. *Acta Bot. Croat* 71, 299–310.

Cheng, H., Edwards, R.L., Broecker, W.S., Denton, G.H., Kong, X., Wang, Y., Zhang, R., Wang, X., 2009. Ice age terminations. *Science* 326, 248–252.

Cheng, H., Edwards, R.L., Sinha, A., Spötl, C., Yi, L., Chen, S., Kelly, M., Kathayat, G., Wang, X., Li, X., Kong, X., Wang, Y., Ning, Y., Zhang, H., 2016. The Asian monsoon over the past 640,000 years and ice age terminations. *Nature* 534, 640–646.

Cheng, H., Fleitmann, D., Edwards, R.L., Wang, X., Cruz, F.W., Auler, A.S., Mangini, A., Wang, Y., Kong, X., Burns, S.J., Matter, A., 2009. Timing and structure of the 8.2 kyr B.P. event inferred from 18O records of stalagmites from China, Oman, and Brazil. *Geology* 37, 1007–1010.

Cherepanova, M. V., Usol'tseva, M. V., Pushkar, V.S., Dubrovina, Y.F., 2010. Morphogenesis in Cyclotella ocellata — complex from Lake El'gygytgyn (Chukchi Peninsula) during the Pleistocene-Holocene. *Paleontological Journal* 44, 1252–1261.

Chizhova, J.N., Vasilchuk, J.Y., Yoshikawa, K., Budantseva, N.A., Golovanov, D.L., Sorokina, O.I., Stanilovskaya, J.V., Vasil'chuk, Y.K., 2015. Isotope composition of snow cover in the Lake Baikal area. *Лёд и Снег* 55, 55–66.

Churakova (Sidorova), O. V., Bryukhanova, M. V., Saurer, M., Boettger, T., Naurzbaev, M.M., Myglan, V.S., Vaganov, E.A., Hughes, M.K., Siegwolf, R.T.W., 2014. A cluster of stratospheric volcanic eruptions in the AD 530s recorded in Siberian tree rings. *Global and Planetary Change* 122, 140–150.

Chytrý, M., Danihelka, J., Kubešová, S., Lustyk, P., Ermakov, N., Hájek, M., Hájková, P., Kočí, M., Otýpková, Z., Roleček, J., Řezníčková, M., Šmarda, P., Valachovič, M., Popov, D., Pišút, I., 2007. Diversity of forest vegetation across a strong gradient of climatic continentality: Western Sayan Mountains, southern Siberia. *Plant Ecology* 196, 61–83.

Clark, P.U., Archer, D., Pollard, D., Blum, J.D., Rial, J.A., Brovkin, V., Mix, A.C., Pisias, N.G., Roy, M., 2006. The middle Pleistocene transition: characteristics, mechanisms, and implications for long-term changes in atmospheric pCO2. *Quaternary Science Reviews* 25, 3150–3184.

Clark, P.U., Dyke, A.S., Shakun, J.D., Carlson, A.E., Clark, J., Wohlfarth, B., Mitrovica, J.X., Hostetler, S.W., McCabe, A.M., 2009. The Last Glacial Maximum. *Science* 325, 710–714.

Clark, P.U., Mix, A.C., 2002. Ice sheets and sea level of the Last Glacial Maximum. *Quaternary Science Reviews* 21, 1–7.

Clark, P.U., Pollard, D., 1998. Origin of the Middle Pleistocene Transition by ice sheet erosion of regolith. *Paleoceanography* 13, 1–9.

Clark, P.U., Shakun, J.D., Baker, P.A., Bartlein, P.P.J., Brewer, S., Brook, E., Carlson, A.E., Cheng, H., Kaufman, D.S., Liu, Z., Marchitto, T.M., Mix, A.C., Morrill, C., Otto-Bliesner, B.L., Pahnke, K., Russell, J.J.M.J., Whitlock, C., Adkins, J.F., Blois, J.L.J., *et al.*, 2012. Global climate evolution during the last deglaciation. *Proceedings of the National Academy of Sciences* 109, 1134–1142.

Cohen, A.S., 2003. Paleolimnology : the history and evolution of lake systems. Oxford University Press, Oxford, New York.

Cole-Dai, J., Ferris, D.G., Lanciki, A.L., Savarino, J., Thiemens, M.H., McConnell, J.R., 2013. Two likely stratospheric volcanic eruptions in the 1450s C.E. found in a bipolar, subannually dated 800 year ice core record. *Journal of Geophysical Research: Atmospheres* 118, 7459–7466.

Colman, S.M., Peck, J.A., Karabanov, E.B., Carter, S.J., Bradbury, J.P., King, J.W., Williams, D.F., 1995. Continental climate response to orbital forcing from biogenic silica records in Lake Baikal. *Nature* 378, 769–771.

Colman, S.M.M., Jones, G.A. a., Rubin, M., King, J.W.W., Peck, J.A. a., Orem, W.H.H., 1996. AMS radiocarbon analyses from Lake Baikal, Siberia: Challenges of dating sediments from a large, oligotrophic lake. *Quaternary Science Reviews* 15, 669–684.

Conley, D.J., 1988. Biogenic silica as an estimate of siliceous microfossil abundance in Great Lakes sediments. *Biogeochemistry* 6, 161–179.

Coope, G.R., Lemdahl, G., Lowe, J.J., Walkling, A., 1998. Temperature gradients in northern Europe during the last glacial–Holocene transition (14-9 14C kyr BP) interpreted from coleopteran assemblages. *Journal of Quaternary Science* 13, 419–433.

Cornish, R., 2017. The gravel fans of upper Glen Roy, Lochaber, Scotland: their importance for understanding glacial, proglacial and glaciolacustrine dynamics during the Younger Dryas cold period in an Atlantic margin setting. *Proceedings of the Geologists' Association* 128, 83–109.

Cremer, H., Wagner, B., 2003. The diatom flora in the ultra-oligotrophic Lake El'gygytgyn, Chukotka. *Polar Biology* 26, 105–114.

Crucifix, M., 2006. Does the Last Glacial Maximum constrain climate sensitivity? *Geophysical Research Letters* 33, L18701.

Crucifix, M., Harrison, S., Brierley, C., 2012. Recent and deep pasts in paleoclimate model intercomparison project. *Eos, Transactions American Geophysical Union* 93, 539–539.

Crucifix, M., Loutre, M.F., Berger, A., 2005. Commentary on "the anthropogenic greenhouse era began thousands of years ago." *Climatic Change* 69, 419–426.

Cubasch, U., Wuebbles, D., Chen, D., Facchini, M.C., Frame, D., Mahowald, N., Winther, J.-G., 2013. Introduction in Climate Change 2013. *Intergovernmental Panel on Climate Change 2013: The Physical Science Basis. Contribution of Working Group I to the Fifth Assessment Report of the Intergovernmental Panel on Climate Change* 119–158.

Cumming, B.F., Willson, S.E., Hall, R.I., Smol, J.P., 1995. Diatoms from British Columbia (Canada) lakes and their relationship to salinity, nutrients and other limnological variables. J. Cramer in der Gebrüder Borntraeger Verlagsbuchhandlung.

Cvijanovic, I., Langen, P.L., Kaas, E., Ditlevsen, P.D., 2013. Southward Intertropical Convergence Zone Shifts and Implications for an Atmospheric Bipolar Seesaw. *Journal of Climate* 26, 4121–4137.

Dansgaard, W., Clausen, H.B., Gundestrup, N., Hammer, C.U., Johnsen, S.F., Kristinsdottir, P.M., Reeh, N., 1982. A New Greenland Deep Ice Core. *Science* 218, 1273–1277.

Dansgaard, W., Johnsen, S.J., Clausen, H.B., Dahl-Jensen, D., Gundestrup, N.S., Hammer, C.U., Hvidberg, C.S., Steffensen, J.P., Sveinbjörnsdottir, a. E., Jouzel, J., Bond, G., 1993. Evidence for general instability of past climate from a 250-kyr ice-core record. *Nature* 364, 218–220.

de Menocal, P.B., 2001. Cultural Responses to Climate Change During the Late Holocene. *Science* 292, 667–673.

De Vivo, B., Rolandi, G., Gans, P.B., Calvert, A., Bohrson, W.A., Spera,

F.J., Belkin, H.E., 2001. New constraints on the pyroclastic eruptive history of the Campanian volcanic Plain (Italy). *Mineralogy and Petrology* 73, 47–65.

De Vos, B., Vandecasteele, B., Deckers, J., Muys, B., 2005. Capability of Loss-on-Ignition as a Predictor of Total Organic Carbon in Non-Calcareous Forest Soils. *Communications in Soil Science and Plant Analysis* 36, 2899–2921.

Dean, J.R., Leng, M.J., Mackay, A.W., 2014. Is there an isotopic signature of the Anthropocene? *The Anthropocene Review* 1, 276–287.

Dean, W.E., 1974. Determination of Carbonate and Organic Matter in Calcareous Sediments and Sedimentary Rocks by Loss on Ignition: Comparison With Other Methods. *SEPM Journal of Sedimentary Research* Vol. 44, 242–248.

Dean, W.E., Gorham, E., 1998. Magnitude and significance of carbon burial in lakes, reservoirs, and peatlands. *Geology* 26, 535.

deMenocal, P., Bond, G., 1997. Holocene climate less stable than previously thought. *Eos, Transactions American Geophysical Union* 78, 447–454.

Demske, D., Heumann, G., Granoszewski, W., Nita, M., Mamakowa, K., Tarasov, P.E., Oberhänsli, H., 2005. Late glacial and Holocene vegetation and regional climate variability evidenced in high-resolution pollen records from Lake Baikal. *Global and Planetary Change* 46, 255–279.

Denham, C.R., Cox, A., 1971. Evidence that the Laschamp polarity event did not occur 13 300–30 400 years ago. *Earth and Planetary Science Letters* 13, 181–190.

Denton, G. H., Broecker, W. S., Alley, R.B., 2006. The mystery interval 17.5 to 14.5 kyrs ago. *PAGES News* 14, 14–16.

Dergachev, V.A., Raspopov, O.M., Van Geel, B., Zaitseva, G.I., 2004. The “Sterno-Etrussia” geomagnetic excursion around 2700 BP and changes of solar activity, cosmic ray intensity, and climate. *Radiocarbon* 46, 661–681.

Des Combes, H.J., Esper, O., De La Rocha, C.L., Abelmann, A., Gersonde, R., Yam, R., Shemesh, A., 2008. Diatom δ13C, δ15N, and C/N since the last glacial maximum in the southern ocean: potential impact of species composition. *Paleoceanography* 23, 1–12.

Dietze, E., Maussion, F., Ahlborn, M., Diekmann, B., Hartmann, K., Henkel, K., Kasper, T., Lockot, G., Opitz, S., Haberzettl, T., 2014.

Sediment transport processes across the Tibetan Plateau inferred from robust grain-size end members in lake sediments. *Climate of the Past* 10, 91–106.

Dong, B., Valdes, P.J., 1998. Simulations of the Last Glacial Maximum climates using a general circulation model: prescribed versus computed sea surface temperatures. *Climate Dynamics* 14, 571–591.

Douka, K., Slon, V., Jacobs, Z., Ramsey, C.B., Shunkov, M. V., Derevianko, A.P., Mafessoni, F., Kozlikin, M.B., Li, B., Grün, R., Comeskey, D., Devièse, T., Brown, S., Viola, B., Kinsley, L., Buckley, M., Meyer, M., Roberts, R.G., Pääbo, S., *et al.*, 2019. Age estimates for hominin fossils and the onset of the Upper Palaeolithic at Denisova Cave. *Nature* 565, 640–644.

Duarte, C.M., Kalff, J., Peters, R.H., 1986. Patterns in Biomass and Cover of Aquatic Macrophytes in Lakes. *Canadian Journal of Fisheries and Aquatic Sciences* 43, 1900–1908.

Duleba, M., Kiss, K.T., Földi, A., Kovács, J., Borojević, K.K., Molnár, L.F., Plenković-Moraj, A., Pohner, Z., Solak, C.N., Tóth, B., Ács, É., 2015. Morphological and genetic variability of assemblages of *Cyclotella ocellata* Pantocsek/ *C. comensis* Grunow complex (Bacillariophyta, Thalassiosirales). *Diatom Research* 30, 283–306.

Dykosko, C., Edwards, R., Cheng, H., Yuan, D., Cai, Y., Zhang, M., Lin, Y., Qing, J., An, Z., Revenaugh, J., 2005. A high-resolution, absolute-dated Holocene and deglacial Asian monsoon record from Dongge Cave, China. *Earth and Planetary Science Letters* 233, 71–86.

Earle, C.J., Brubaker, L.B., Anderson, P.M., 1996. Charcoal in northcentral Alaskan lake sediments: relationships to fire and late-Quaternary vegetation history. *Review of Palaeobotany and Palynology* 92, 83–95.

Edlund, M.B., Willlams, R.M., Soninkhishig, N., 2003. The planktonic diatom diversity of ancient Lake Hovsgol, Mongolia. *Phycologia* 42, 232–260.

Eicher, U., Siegenthaler, U., 1976. Palynological and oxygen isotope investigations on Late-Glacial sediment cores from Swiss lakes. *Boreas* 5, 109–117.

Engels, S., van Geel, B., 2012. The effects of changing solar activity on climate: contributions from palaeoclimatological studies. *Journal of Space Weather and Space Climate* 2, A09.

EPICA, C.M., 2004. Eight glacial cycles from an Antarctic ice core. *Nature* 429, 623–628.

Fedotov, A.P., Vorobyeva, S.S., Vershinin, K.E., Nurgaliev, D.K., Enushchenko, I. V., Krapivina, S.M., Tarakanova, K. V., Ziborova, G.A., Yassonov, P.G., Borissov, A.S., 2012. Climate changes in East Siberia (Russia) in the Holocene based on diatom, chironomid and pollen records from the sediments of Lake Kotokel. *Journal of Paleolimnology* 47, 617–630.

Fernandes, R., Millard, A.R., Brabec, M., Nadeau, M.-J., Grootes, P., 2014. Food Reconstruction Using Isotopic Transferred Signals (FRUITS): A Bayesian Model for Diet Reconstruction. *PLoS ONE* 9, e87436.

Ferronsky, V.I., Polyakov, V.A., Kuprin, P.N., Vlasova, L.S., 2014. Hydrotroilite as a bioindicator of paleohydrological and paleoclimatic processes in the Caspian basin. *Water Resources* 41, 473–487.

Finkelstein, S.A., Gajewski, K., 2008. Responses of Fragilarioid-dominated diatom assemblages in a small Arctic lake to Holocene climatic changes, Russell Island, Nunavut, Canada. *Journal of Paleolimnology* 40, 1079–1095.

Fisher, R.E., Sriskantharajah, S., Lowry, D., Lanoisellé, M., Fowler, C.M.R., James, R.H., Hermansen, O., Lund Myhre, C., Stohl, A., Greinert, J., Nisbet-Jones, P.B.R., Mienert, J., Nisbet, E.G., 2011. Arctic methane sources: Isotopic evidence for atmospheric inputs. *Geophysical Research Letters* 38, L21803.

Flower, R., Ryves, D., 2009. Diatom preservation: differential preservation of sedimentary diatoms in two saline lakes. *Acta Botanica Croatia* 68, 381–399.

France, R.L., Ecol, M., Ser, P., 1995. Carbon-13 enrichment in benthic compared to planktonic algae: foodweb implications. *Marine Ecology Progress Series* 124, 307–312.

Ganopolski, A., Winkelmann, R., Schellnhuber, H.J., 2016. Critical insolation–CO2 relation for diagnosing past and future glacial inception. *Nature* 529, 200–203.

Garnett, Mark H. Hardie, S. L. Murray, C., Reimer, P J., Reimer, R.W., 2011. Radiocarbon. *Radiocarbon* 43, 461–463.

Genkal, S.I., Popovskaya, G.I., 2008. Morphological variability of Cyclotella ocellata from Lake Khubsugul (Mongolia). *Diatom Research* 23, 75–91.

Gibbard, P.L., Head, M.J., 2009. IUGS ratification of the Quaternary System/Period and the Pleistocene Series/Epoch with a base at 2.58

MA. *Quaternaire* 20, 411–412.

Gibbons, A., 2015. Human Evolution. Cave was lasting home to Denisovans. *Science* 349, 1270–1271.

Giordano, M., Beardall, J., Raven, J.A., 2005. CO2 Concentrating Mechanisms in Algae: Mechanisms, Environmental Modulation, and Evolution. *Annual Review of Plant Biology* 56, 99–131.

Godwin, H., 1962. Half-life of Radiocarbon. *Nature* 195, 984–984.

Goosse, H., Arzel, O., Luterbacher, J., Mann, M.E., Renssen, H., Riedwyl, N., Timmermann, A., Xoplaki, E., Wanner, H., 2006. The origin of the European “Medieval Warm Period.” *Climate of the Past* 2, 99–113.

Gordon, C., Cooper, C., Senior, C.A., Banks, H., Gregory, J.M., Johns, T.C., Mitchell, J.F.B., Wood, R.A., 2000. The simulation of SST, sea ice extents and ocean heat transports in a version of the Hadley Centre coupled model without flux adjustments. *Climate Dynamics* 16, 147–168.

Gordov, E.P., Vaganov, E.A., 2010. Siberia Integrated Regional Study: multidisciplinary investigations of the dynamic relationship between the Siberian environment and global climate change. *Environmental Research Letters* 5, 015007.

Gray, L.J., Beer, J., Geller, M., Haigh, J.D., Lockwood, M., Matthes, K., Cubasch, U., Fleitmann, D., Harrison, G., Hood, L., Luterbacher, J., Meehl, G.A., Shindell, D., van Geel, B., White, W., 2010. Solar Influences on Climate. *Reviews of Geophysics* 48, RG4001.

Guillevic, M., Bazin, L., Landais, A., Stowasser, C., Masson-Delmotte, V., Blunier, T., Eynaud, F., Falourd, S., Michel, E., Minster, B., Popp, T., Prié, F., Vinther, B.M., 2014. Evidence for a three-phase sequence during Heinrich Stadial 4 using a multiproxy approach based on Greenland ice core records. *Climate of the Past* 10, 2115–2133.

Guiry, M.D., Guiry, G.M., 2018. AlgaeBase. World-wide electronic publication [WWW Document]. URL http://www.algaebase.org (accessed 9.8.18).

Gus’kova, E.G., Raspopov, O.M., Dergachev, V.A., Iosifidi, A.G., Sinitsyna, G. V., 2012a. Manifestation of the gothenburg geomagnetic field excursion in sediments on the northwestern Central Russian Upland. *Geomagnetism and Aeronomy* 52, 675–683.

Gus’kova, E.G., Raspopov, O.M., Dergachev, V.A., Iosifidi, A.G., Sinitsyna, G. V., 2012b. The Gothenburg geomagnetic excursion as a

chronological marker for the Allerød interstadial in the Central Russian Upland. *Izvestiya, Atmospheric and Oceanic Physics* 48, 823–831.

Guskova, E.G., Raspopov, O.M., Piskarev, A.L., Dergachev, V.A., 2007. Manifestation of the Gothenburg geomagnetic field excursion in the Barents Sea bottom sediments. *Geomagnetism and Aeronomy* 47, 781–786.

Hall, I.R., Bianchi, G.G., Evans, J.R., 2004. Centennial to millennial scale Holocene climate-deep water linkage in the North Atlantic. *Quaternary Science Reviews* 23, 1529–1536.

Hammaklund, D., 1993. A distinct δ13C decline in organic lake sediments at the Pleistocene-Holocene transition in southern Sweden. *Boreas* 22, 236–243.

Hammer, Ø., Harper, D.A.. D.A., Ryan, D.D., Hammer, O., Harper, D.A.. D.A., Ryan, P.., 2001. PAST: Paleontological statistics software package for education and data analysis. *Palaeontologia Electronica 178kb. T. Harper. Geological Museum*.

Hampton, S.E., Gray, D.K., Izmest'eva, L.R., Moore, M. V, Ozersky, T., 2014. The rise and fall of plankton: long-term changes in the vertical distribution of algae and grazers in Lake Baikal, Siberia. *PloS one* 9, e88920.

Hanna, E., Huybrechts, P., Steffen, K., Cappelen, J., Huff, R., Shuman, C., Irvine-Fynn, T., Wise, S., Griffiths, M., Hanna, E., Huybrechts, P., Steffen, K., Cappelen, J., Huff, R., Shuman, C., Irvine-Fynn, T., Wise, S., Griffiths, M., 2008. Increased Runoff from Melt from the Greenland Ice Sheet: A Response to Global Warming. *Journal of Climate* 21, 331–341.

Hansson, S. V., Kaste, J.M., Olid, C., Bindler, R., 2014. Incorporation of radiometric tracers in peat and implications for estimating accumulation rates. *Science of the Total Environment* 493, 170–177.

Hausmann, S., Pienitz, R., 2009. Seasonal water chemistry and diatom changes in six boreal lakes of the Laurentian Mountains (Québec, Canada): Impacts of climate and timber harvesting. *Hydrobiologia* 635, 1–14.

Hays, J.D., Imbrie, J., Shackleton, N.J., 1976. Variations in the Earth's Orbit: Pacemaker of the Ice Ages. *Science* 194, 1121–1132.

He, Y., Pang, H., Theakstone, W.H.H., Zhang, D., Lu, A., Song, B., Yuan, L., Ning, B., 2006. Spatial and temporal variations of oxygen isotopes in snowpacks and glacial runoff in different types of glacial area in western China. *Annals of Glaciology* 43, 269–274.

Hegewald, E., Hindáková, A., 1997. Variabilität von einer natürlichen Population und von Klonen des Cyclotella ocellata-Komplexes (Bacillariophyceae) aus dem Gallbergweiher, Nordwestdeutschland. *Algological Studies/Archiv für Hydrobiologie, Supplement Volumes* 86, 17–37.

Heinrich, H., 1988. Origin and consequences of cyclic ice rafting in the Northeast Atlantic Ocean during the past 130,000 years. *Quaternary Research* 29, 142–152.

Heiri, O., Lotter, A.F., Lemcke, G., 2001. Loss on ignition as a method for estimating organic and carbonate content in sediments: reproducibility and comparability of results. *Journal of Paleolimnology* 25, 101–110.

Heiri, O., Millet, L., 2005. Reconstruction of Late Glacial summer temperatures from chironomid assemblages in Lac Lautrey (Jura, France). *Journal of Quaternary Science* 20, 33–44.

Heiri, O., Tinner, W., Lotter, A.F., 2004. Evidence for cooler European summers during periods of changing meltwater flux to the North Atlantic. *Proceedings of the National Academy of Sciences of the United States of America* 101, 15285–15288.

Hemming, S.R., 2004. Heinrich events: Massive late Pleistocene detritus layers of the North Atlantic and their global climate imprint. *Reviews of Geophysics* 42, RG1005.

Henderson, G., Slowey, N., 2000. Evidence from U-Th dating against Northern Hemisphere forcing of the penultimate deglaciation. *Nature* 404, 61–66.

Hernández, A., Bao, R., Giralt, S., Barker, P.A., Leng, M.J., Sloane, H.J., Sáez, A., 2011. Biogeochemical processes controlling oxygen and carbon isotopes of diatom silica in Late Glacial to Holocene lacustrine rhythmites. *Palaeogeography, Palaeoclimatology, Palaeoecology* 299, 413–425.

Hesse, R., Khodabakhsh, S., 2016. Anatomy of Labrador Sea Heinrich layers. *Marine Geology* 380, 44–66.

Hicock, S.R., Lian, O.B., Mathewes, R.W., 1999. 'Bond cycles' recorded in terrestrial Pleistocene sediments of southwestern British Columbia, Canada. *Journal of Quaternary Science* 14, 443–449.

Hildebrandt, S., Müller, S., Kalugin, I.A., Dar'in, A. V., Wagner, M., Rogozin, D.Y., Tarasov, P.E., 2015. Tracing the North Atlantic decadal-scale climate variability in a late Holocene pollen record from southern

Siberia. *Palaeogeography, Palaeoclimatology, Palaeoecology* 426, 75–84.

Hillebrand, H., Dürselen, C.D., Kirschtel, D., Pollingher, U., Zohary, T., 1999. Biovolume calculation for pelagic and benthic microalgae. *Journal of Phycology* 35, 403–424.

Hodell, D.A., Nicholl, J.A., Bontognali, T.R.R., Danino, S., Dorador, J., Dowdeswell, J.A., Einsle, J., Kuhlmann, H., Martrat, B., Mleneck-Vautravers, M.J., Rodríguez-Tovar, F.J., Röhl, U., 2017. Anatomy of Heinrich Layer 1 and its role in the last deglaciation. *Paleoceanography* 32, 284–303.

Hoek, W.Z., Bos, J.A.A., 2007. Early Holocene climate oscillations—causes and consequences. *Quaternary Science Reviews* 26, 1901–1906.

Horiuchi, K., Minoura, K., Hoshino, K., Oda, T., Nakamura, T., Kawai, T., 2000. Palaeoenvironmental history of Lake Baikal during the last 23000 years. *Palaeogeography, Palaeoclimatology, Palaeoecology* 157, 95–108.

Horne, A.J., Goldman, C.R., 1994. Lake Ecology Overview: Chapter 1. In: Limnology. McGraw-Hill Co., New York, USA, p. 576.

Hostetler, S.W., Clark, P.U., Bartlein, P.J., Mix, A.C., Pisias, N.J., 1999. Atmospheric transmission of North Atlantic Heinrich events. *Journal of Geophysical Research* 104, 3947–3952.

Howarth, R.W., 2008. Coastal nitrogen pollution: A review of sources and trends globally and regionally. *Harmful Algae* 8, 14–20.

Huhne, C., Slingo, J. (eds), 2011. Climate: Observations, projections and impacts - Russia, Met Office Publication.

Hulbe, C., 2010. Extreme iceberg generation exposed. *Nature Geoscience* 3, 80–81.

Hulbe, C.L., 1997. An ice shelf mechanism for Heinrich layer production. *Paleoceanography* 12, 711–717.

Hulbe, C.L., MacAyeal, D.R., Denton, G.H., Kleman, J., Lowell, T. V., 2004. Catastrophic ice shelf breakup as the source of Heinrich event icebergs. *Paleoceanography* 19, PA1004.

Hurrell, E.R., Barker, P.A., Leng, M.J., Vane, C.H., Wynn, P., Kendrick, C.P., Verschuren, D., Alayne Street-Perrott, F., 2011. Developing a methodology for carbon isotope analysis of lacustrine diatoms. *Rapid Communications in Mass Spectrometry* 25, 1567–1574.

Huybers, P., 2006. Early Pleistocene glacial cycles and the integrated summer insolation forcing. *Science* 313, 508–11.

Ilyashuk, B., Gobet, E., Heiri, O., Lotter, A.F., van Leeuwen, J.F.N., van der Knaap, W.O., Ilyashuk, E., Oberli, F., Ammann, B., 2009. Lateglacial environmental and climatic changes at the Maloja Pass, Central Swiss Alps, as recorded by chironomids and pollen. *Quaternary Science Reviews* 28, 1340–1353.

Imbrie, J., Berger, A., Boyle, E. a., Clemens, S.C., Duffy, A., Howard, W.R., Kukla, G., Kutzbach, J., Martinson, D.G., McIntyre, A., Mix, a. C., Molfino, B., Morley, J.J., Peterson, L.C., Pisias, N.G., Prell, W.L., Raymo, M.E., Shackleton, N.J., Toggweiler, J.R., 1993. On the structure and origin of major glaciation cycles 2. The 100,000-year cycle. *Paleoceanography* 8, 699–735.

IPCC, 2013. Summary for Policymakers. In: Stocker, T.F., D. Qin, G.-K. Plattner, M. Tignor, S. K. Allen (Ed.), Limate Change 2013: The Physical Science Basis. Contribution of Working Group I to the Fifth Assessment Report of the Intergovernmental Panel on Climate Change. Cambridge University Press, Cambridge UK, New York USA, pp. 1–35.

Izmest'eva, L.R., Moore, M. V., Hampton, S.E., Ferwerda, C.J., Gray, D.K., Woo, K.H., Pislegina, H. V., Krashchuk, L.S., Shimaraeva, S. V., Silow, E.A., 2016. Lake-wide physical and biological trends associated with warming in Lake Baikal. *Journal of Great Lakes Research* 42, 6–17.

Jansen, E., Overpeck, J., Briffa, K.R., Duplessy, J.-C., Joos, F., Masson-Delmotte, V., Olago, D., Otto-Bliesner, B., Richard Peltier, W., Rahmstorf, S., Ramesh, R., Raynaud, D., Rind, D., Solomina, O., Villalba, R., Zhang, D., 2007. Palaeoclimate: 6.5.1 Climate Forcing and Response During the Current Interglacial. In: Solomon, S., Qin, D., Manning. M., Chen. Z., Marquis. M., Averyt. K.B., Tignor, M., Miller, H.L. (Ed.), Climate Change 2007: The Physical Science Basis. Contribution of Working Group I to the Fourth Assessment Report of the Intergovernmental Panel on Climate Change. Cambridge University Press, Cambridge, UK and New York, NY, USA, pp. 459–462.

Jeong, J.-H., Ou, T., Linderholm, H.W., Kim, B.-M., Kim, S.-J., Kug, J.-S., Chen, D., 2011. Recent recovery of the Siberian High intensity. *Journal of Geophysical Research: Atmospheres* 116, D23102.

Jewson, D.H., 1992. Size reduction, reproductive strategy and the life cycle of a centric diatom. *Philosophical Transactions - Royal Society of London, B* 336, 191–213.

Jin, L., Chen, F., Ganopolski, A., Claussen, M., 2007. Response of East Asian climate to Dansgaard/Oeschger and Heinrich events in a coupled

model of intermediate complexity. *Journal of Geophysical Research* 112, D06117.

Jinguo Dong, Yongjin Wang, Hai Cheng, Hardt, B., Edwards, R.L., Xinggong Kong, Jiangying Wu, Shitao Chen, Dianbing Liu, Xiuyang Jiang, Kan Zhao, 2010. A high-resolution stalagmite record of the Holocene East Asian monsoon from Mt Shennongjia, central China. *The Holocene* 20, 257–264.

Johnson, R.G., Lauritzen, S.-E., 1995. Hudson Bay-Hudson Strait jökulhlaups and Heinrich events: a hypothesis. *Palaeogeography, Palaeoclimatology, Palaeoecology* 117, 123–137.

Jones, P.D., Mann, M.E., 2004. Climate over past millennia. *Reviews of Geophysics* 42, 1–42.

Jones, V.J., 2013. Diatom Introduction. In: Encyclopedia of Quaternary Science: Second Edition. Elsevier, pp. 471–480.

Jørgensen, B.B., Revsbech, N.P., 1985. Diffusive boundary layers and the oxygen uptake of sediments and detritus1. *Limnology and Oceanography* 30, 111–122.

Kaczmarska, I., Poulíčková, A., Sato, S., Edlund, M.B., Idei, M., Watanabe, T., Mann, D.G., 2013. Proposals for a terminology for diatom sexual reproduction, auxospores and resting stages. *Diatom Research* 28, 263–294.

Kalmychkov, G. V., Kuz'min, M.I., Pokrovskii, B.G., Kostrova, S.S., 2007. Oxygen isotopic composition in diatom algae frustules from Lake Baikal sediments: Annual mean temperature variations during the last 40 Ka. *Doklady Earth Sciences* 413, 206–209.

Kamatani, A., 1982. Dissolution rates of silica from diatoms decomposing at various temperatures. *Marine Biology* 68, 91–96.

Karabanov, E., Williams, D., Kuzmin, M., Sideleva, V., Khursevich, G., Prokopenko, A., Solotchina, E., Tkachenko, L., Fedenya, S., Kerber, E., Gvozdkov, A., Khlustov, O., Bezrukova, E., Letunova, P., Krapivina, S., 2004. Ecological collapse of Lake Baikal and Lake Hovsgol ecosystems during the Last Glacial and consequences for aquatic species diversity. *Palaeogeography, Palaeoclimatology, Palaeoecology* 209, 227–243.

Kaspi, Y., Sayag, R., Tziperman, E., 2004. A "triple sea-ice state" mechanism for the abrupt warming and synchronous ice sheet collapses during Heinrich events. *Paleoceanography* 19, 1–12.

Katsuta, N., Ikeda, H., Shibata, K., Saito-Kokubu, Y., Murakami, T., Tani, Y., Takano, M., Nakamura, T., Tanaka, A., Naito, S., Ochiai, S.,

Shichi, K., Kawakami, S. ichi, Kawai, T., 2018. Hydrological and climate changes in southeast Siberia over the last 33 kyr. *Global and Planetary Change* 164, 11–26.

Kawamura, K., Parrenin, F., Lisiecki, L., Uemura, R., Vimeux, F., Severinghaus, J.P., Hutterli, M.A., Nakazawa, T., Aoki, S., Jouzel, J., Raymo, M.E., Matsumoto, K., Nakata, H., Motoyama, H., Fujita, S., Goto-Azuma, K., Fujii, Y., Watanabe, O., 2007. Northern Hemisphere forcing of climatic cycles in Antarctica over the past 360,000 years. *Nature* 448, 912–916.

Keigwin, L.D., Lehman, S.J., 1994. Deep Circulation Change Linked to Heinrich Event-1 and Younger Dryas in a Middepth North-Atlantic Core. *Paleoceanography* 9, 185–194.

Kent, D.V., Hemming, S.R., Turrin, B.D., 2002. Laschamp Excursion at Mono Lake? *Earth and Planetary Science Letters* 197, 151–164.

Kharuk, V.I., Ranson, K.J., Oskorbin, P.A., Im, S.T., Dvinskaya, M.L., 2013. Climate induced birch mortality in Trans-Baikal lake region, Siberia. *Forest Ecology and Management* 289, 385–392.

Khursevich, G.K., Karabanov, E.B., Prokopenko, A.A., Williams, D.F., Kuzmin, M.I., Fedenya, S.A., Gvozdkov, A.A., 2001. Insolation regime in Siberia as a major factor controlling diatom production in Lake Baikal during the past 800,000 years. *Quaternary International* 80–81, 47–58.

Kilham, P., Kilham, S.S., Hecky, R.E., 1986. Hypothesized resource relationships among African planktonic diatoms. *Limnology and Oceanography* 31, 1169–1181.

Kilham, S.S., Kilham, P., 1975. *Melosira granulata* (Ehr.) Ralfs: morphology and ecology of a cosmopolitan freshwater diatom. *SIL Proceedings, 1922-2010* 19, 2716–2721.

Kilham, S.S., Theriot, E.C., Fritz, S.C., Fritz, C., 1996. in the large lakes of the Linking planktonic diatoms and climate change Yellowstone ecosystem using resource theory. *Limnology and Oceanography* 41, 1052–1062.

Kingston, J.D., 2005. Orbital controls on seasonality. In: Brockman, D.K., van Schaik, C.P. (Eds.), Seasonality in Primates: Studies of Living and Extinct Human and Non-Human Primates. Cambridge University Press, Cambridge, pp. 520–541.

Kissel, C., Guillou, H., Laj, C., Carracedo, J.C., Nomade, S., Perez-Torrado, F., Wandres, C., 2011. The Mono Lake excursion recorded in phonolitic lavas from Tenerife (Canary Islands): Paleomagnetic analyses and coupled K/Ar and Ar/Ar dating. *Physics of the Earth and Planetary*

Interiors 187, 232–244.

Klaar, M.J., Kidd, C., Malone, E., Bartlett, R., Pinay, G., Chapin, F.S., Milner, A., 2015. Vegetation succession in deglaciated landscapes: implications for sediment and landscape stability. *Earth Surface Processes and Landforms* 40, 1088–1100.

Kleman, J., Fastook, J., Ebert, K., Nilsson, J., Caballero, R., 2013. Pre-LGM Northern Hemisphere ice sheet topography. *Climate of the Past* 9, 2365–2378.

Knie, M., Hübener, T., 2007. Morphological variability of the Cyclotella ocellata-krammeri-rossii complex in field samples and cultures. In: Kusber, W.-H., Jahn, R. (Eds.), Proceedings of the 1st Central European Diatom Meeting. Freie Universität Berlin, Berlin, pp. 83–86.

Knudson, B.M., Kipling, T.H., 1957. Ecology of the Epiphytic Diatom Tabellaria Flocculosa (Roth) Kutz. Var. Flocculosa in Three. *Journal of Ecology* 45, 93–112.

Koivo, L., Seppälä, M., 1994. Diatoms from an ice-wedge furrow, Ungava Peninsula, Quebec, Canada. *Polar Research* 13, 237–241.

Konen, M. E., Jacobs, P. M., Lee, B. C., Talaga, B. J., Mason, J.A., 2002. Equations for predicting soil organic carbon using loss-on-ignition for north central U.S. soils - ProQuest. *Soil Science Society of America* 66, 1878–1881.

Kopp, G., Krivova, N., Wu, C.J., Lean, J., 2016. The Impact of the Revised Sunspot Record on Solar Irradiance Reconstructions. *Solar Physics* 291, 2951–2965.

Koppen, J.D., 1975. A Morphological and taxonomic consideration of Tabellaria (Bacillariophyceae) from the Northcentral United States. *Journal of Phycology* 11, 236–244.

Koppen, J.D., 1978. Distribution and Aspects of the Ecology of the Genus Tabellaria Ehr. (Bacillariophyceae) in the Northcentral United States. *American Midland Naturalist* 99, 383.

Kossler, A., Tarasov, P., Schlolaut, G., Nakagawa, T., Marshall, M., Brauer, A., Staff, R., Ramsey, C.B., Bryant, C., Lamb, H., Demske, D., Gotanda, K., Haraguchi, T., Yokoyama, Y., Yonenobu, H., Tada, R., 2011. Onset and termination of the late-glacial climate reversal in the high-resolution diatom and sedimentary records from the annually laminated SG06 core from Lake Suigetsu, Japan. *Palaeogeography, Palaeoclimatology, Palaeoecology* 306, 103–115.

Kostrova, S.S., Meyer, H., Chapligin, B., Kossler, A., Bezrukova, E. V.,

Tarasov, P.E., 2013. Holocene oxygen isotope record of diatoms from Lake Kotokel (southern Siberia, Russia) and its palaeoclimatic implications. *Quaternary International* 290–291, 21–34.

Kostrova, S.S., Meyer, H., Chapligin, B., Tarasov, P.E., Bezrukova, E. V., 2014. The last glacial maximum and late glacial environmental and climate dynamics in the Baikal region inferred from an oxygen isotope record of lacustrine diatom silica. *Quaternary International* 348, 25–36.

Kostrova, S.S., Meyer, H., Tarasov, P.E., Bezrukova, E. V., Chapligin, B., Kossler, A., Pavlova, L.A., Kuzmin, M.I., 2016. Oxygen isotope composition of diatoms from sediments of Lake Kotokel (Buryatia). *Russian Geology and Geophysics* 57, 1239–1247.

Kozhov, M.M., 1950. Fresh water of Eastern Siberia. OGIZ Press, Irkutsk.

Krainov, M.A., Bezrukova, E. V., Shchetnikov, A.A., Kerber, E. V., 2018. First Data on the Gothenburg and Mono Lake Excursions in Paleomagnetic Records from Bottom Sediments of Lakes of Transbaikalia (Exemplified by Baunt Lake). *Doklady Earth Sciences* 481, 980–983.

Krainov, M.A., Bezrukova, E. V, Kerber, E. V, Levina, O. V, Ivanov, E. V, Shchetnikov, A.A., Filinov, I.A., 2017. First results of study of Lake Baunt bottom sediments (northern Transbaikalia). *Russian Geology and Geophysics* 58, 1401–1411.

Krammer, K. and Lange-Bertalot, H., 1986. Bacillariophyceae. 1: Teil: Naviculaceae., Süßwasserf. ed. Gustav Fischer Verlag, Stuttgart, New York.

Krammer, K. and Lange-Bertalot, H., 1988. Bacillariophyceae. 2: Teil: Bacillariaceae, Epithmiaceae, Surirellaceae., Süßwasserf. ed. Gustav Fischer Verlag, Stuttgart, New York.

Krammer, K. and Lange-Bertalot, H., 1991a. Bacillariophyceae. 3: Teil: Centrales, Fragilariaceae, Eunotiaceae., Süßwasserf. ed. Gustav Fischer Verlag, Stuttgart, Jena.

Krammer, K. and Lange-Bertalot, H., 1991b. Bacillariophyceae. 4: Teil: Achnanthaceae., Süßwasserf. ed. Gustav Fischer Verlag, Stuttgart, Jena.

Krammer, K., 2002. Diatoms of Europe. Diatoms of the European Inland Waters and Comparable Habitats. Volume 3: Cymbella. Germany.

Krause, J., Fu, Q., Good, J.M., Viola, B., Shunkov, M. V, Derevianko, A.P., Pääbo, S., 2010. The complete mitochondrial DNA genome of an

unknown hominin from southern Siberia. *Nature* 464, 894–897.

Krause, J., Orlando, L., Serre, D., Viola, B., Prüfer, K., Richards, M.P., Hublin, J.-J., Hänni, C., Derevianko, A.P., Pääbo, S., 2007. Neanderthals in central Asia and Siberia. *Nature* 449, 902–904.

Kravitz, B., Robock, A., 2011. Climate effects of high-latitude volcanic eruptions: Role of the time of year. *Journal of Geophysical Research* 116, D01105.

Krinner, G., Boucher, O., Balkanski, Y., 2006. Ice-free glacial northern Asia due to dust deposition on snow. *Climate Dynamics* 27, 613–625.

Krivonogov, S.K., Yamamuro, M., Takahara, H., Kazansky, A.Y., Klimin, M.A., Bobrov, V.A., Safonova, I.Y., Phedorin, M.A., Bortnikova, S.B., 2012. An abrupt ecosystem change in Lake Beloye, southern Western Siberia: Palaeoclimate versus local environment. *Palaeogeography, Palaeoclimatology, Palaeoecology* 331–332, 194–206.

Kumke, T., Kienel, U., Weckström, J., Korhola, A., Hubberten, H.-W., 2004. Inferred Holocene paleotemperatures from diatoms at Lake Lama, Central Siberia. *Arctic antarctic and alpine research* 36, 624–634.

Laj, C., Guillou, H., Kissel, C., 2014. Dynamics of the earth magnetic field in the 10–75 kyr period comprising the Laschamp and Mono Lake excursions: New results from the French Chaîne des Puys in a global perspective. *Earth and Planetary Science Letters* 387, 184–197.

Lamb, A.L., Leng, M.J., Sloane, H.J., Telford, R.J., 2005. A comparison of the palaeoclimate signals from diatom oxygen isotope ratios and carbonate oxygen isotope ratios from a low latitude crater lake. *Palaeogeography, Palaeoclimatology, Palaeoecology* 223, 290–302.

Lane, C.S., Blockley, S.P.E., Bronk Ramsey, C., Lotter, a. F., 2011. Tephrochronology and absolute centennial scale synchronisation of European and Greenland records for the last glacial to interglacial transition: A case study of Soppensee and NGRIP. *Quaternary International* 246, 145–156.

Lane, C.S., Blockley, S.P.E., Mangerud, J., Smith, V.C., Lohne, S., Tomlinson, E.L., Matthews, I.P., Lotter, A.F., 2012. Was the 12.1ka Icelandic Vedde Ash one of a kind? *Quaternary Science Reviews* 33, 87–99.

Lane, C.S., Brauer, A., Blockley, S.P.E., Dulski, P., 2013. Volcanic ash reveals time-transgressive abrupt climate change during the Younger Dryas. *Geology* 41, 1251–1254.

Lange-Bertalot, H., 2001. Diatoms of Europe: Diatoms of the Europe

inland waters and comparable habitats. Volume 2: Navicula sensu stricto, 10 Genera separated from Navicula sensu lato, Frustulia. ed. Germany.

Langereis, C.G., van Hoof, A.A.M., Rochette, P., 1992. Longitudinal confinement of geomagnetic reversal paths as a possible sedimentary artefact. *Nature* 358, 226–230.

Ledger, M., 2017. Abrupt climate change impacts on lacustrine carbon dynamics in Southern Siberia: an investigation into Lake Baunt. (No. Unpublished MSc Thesis).

Lee, J.-E., Swann, A.L., 2010. Evaluation of the "amount effect" at speleothem sites in the Asian monsoon region. *IOP Conference Series: Earth and Environmental Science* 9, 012023.

Leng, M.J., Barker, P.A., 2006. A review of the oxygen isotope composition of lacustrine diatom silica for palaeoclimate reconstruction. *Earth-Science Reviews* 75, 5–27.

Leng, M.J., Marshall, J.D., 2004. Palaeoclimate interpretation of stable isotope data from lake sediment archives. *Quaternary Science Reviews* 23, 811–831.

Leng, M.J., Sloane, H.J., 2008. Combined oxygen and silicon isotope analysis of biogenic silica. *Journal of Quaternary Science* 23, 313–319.

Leng, M.J., Swann, G.E.A., 2010. Stable Isotopes from Diatom Silica. In: Smol, J.P.; Stoermer, E.F. (Ed.), The Diatoms : Applications for the Environmental and Earth Sciences. Cambridge University Press, Cambridge, pp. 127–143.

Leps, J., Smilauer, P., 2003. Multivariate Analysis of Ecological Data using CANOCO. Cambridge University Press, Cambridge.

Lewis, S.L., Maslin, M.A., 2015. Defining the Anthropocene. *Nature* 519, 171–180.

Libby, W.F., 1955. Radiocarbon Dating., 2nd ed. University of Chicago Press, Chicago.

Libby, W.F., Anderson, E.C., Arnold, J.R., 1949. Age Determination by Radiocarbon Content: World-Wide Assay of Natural Radiocarbon. *Science (New York, N.Y.)* 109, 227–8.

Lisiecki, L.E., Raymo, M.E., 2005. A Pliocene-Pleistocene stack of 57 globally distributed benthic δ 18 O records. *Paleoceanography* 20, PA1003 (1-17).

Lister, A.M., Stuart, A.J., 2008. The impact of climate change on large mammal distribution and extinction: Evidence from the last glacial/interglacial transition. *Comptes Rendus Geoscience* 340, 615–620.

Litt, T., Pickarski, N., Heumann, G., Stockhecke, M., Tzedakis, P.C., 2014. A 600,000 year long continental pollen record from Lake Van, eastern Anatolia (Turkey). *Quaternary Science Reviews* 104, 30–41.

Liu, F., Feng, Z., 2012. A dramatic climatic transition at 4000 cal. yr BP and its cultural responses in Chinese cultural domains. *The Holocene* 22, 1181–1197.

Liu, Z., Wen, X., Brady, E.C., Otto-Bliesner, B., Yu, G., Lu, H., Cheng, H., Wang, Y., Zheng, W., Ding, Y., Edwards, R.L., Cheng, J., Liu, W., Yang, H., 2014a. Chinese cave records and the East Asia Summer Monsoon. *Quaternary Science Reviews* 83, 115–128.

Liu, Z., Zhu, J., Rosenthal, Y., Zhang, X., Otto-Bliesner, B.L., Timmermann, A., Smith, R.S., Lohmann, G., Zheng, W., Elison Timm, O., 2014b. The Holocene temperature conundrum. *Proceedings of the National Academy of Sciences of the United States of America* 111, E3501-5.

Lockwood, M., Harrison, R.G., Woollings, T., Solanki, S.K., 2010. Are cold winters in Europe associated with low solar activity? *Environmental Research Letters* 5, 024001.

Löfverström, M., Caballero, R., Nilsson, J., Kleman, J., 2014. Evolution of the large-scale atmospheric circulation in response to changing ice sheets over the last glacial cycle. *Climate of the Past* 10, 1453–1471.

Lowe, D.J., 2011. Tephrochronology and its application: A review. *Quaternary Geochronology* 6, 107–153.

Lowe, J., Hoek, W.Z., 2001. Inter-regional correlation of palaeoclimatic records for the Last Glacial–Interglacial Transition: a protocol for improved precision recommended by the INTIMATE project group. *Quaternary Science Reviews* 20, 1175–1187.

Lowe, J.J., Blockley, S., Trincardi, F., Asioli, A., Cattaneo, A., Matthews, I.P., Pollard, M., Wulf, S., 2007. Age modelling of late Quaternary marine sequences in the Adriatic: Towards improved precision and accuracy using volcanic event stratigraphy. *Continental Shelf Research* 27, 560–582.

Lowe, J.J., Ramsey, C.B., Lane, C.S., 2015. The RESET project: constructing a European tephra lattice for refined synchronisation of environmental and archaeological events during the last c. 100 ka.

Quaternary Science Reviews 118, 1–17.

Lowe, J.J., Rasmussen, S.O., Björck, S., Hoek, W.Z., Steffensen, J.P., Walker, M.J.C., Yu, Z.C., 2008. Synchronisation of palaeoenvironmental events in the North Atlantic region during the Last Termination: a revised protocol recommended by the INTIMATE group. *Quaternary Science Reviews* 27, 6–17.

Lowe, J.J., Walker, M.J.C., 2000. Radiocarbon Dating the Last Glacial-Interglacial Transition (Ca. 14–9 14C Ka Bp) in Terrestrial and Marine Records: The Need for New Quality Assurance Protocols. *Radiocarbon* 42, 53–68.

Lowe, J.J., Walker, M.J.C., 2015. Reconstructing Quaternary Environments, 3rd ed. Routledge, London and New York.

Lund, S., Benson, L., Negrini, R., Liddicoat, J., Mensing, S., 2017. A full-vector paleomagnetic secular variation record (PSV) from Pyramid Lake (Nevada) from 47–17 ka: Evidence for the successive Mono Lake and Laschamp Excursions. *Earth and Planetary Science Letters* 458, 120–129.

Lund, S.P., Platzman, E., Thouveny, N., Camoin, G., 2007. Evidence for Two New Paleomagnetic Field Excursions ~2,500 and ~12,500 Years Ago from the South Pacific Ocean Region (Tahiti). *American Geophysical Union, Fall Meeting 2007, abstract id. GP42A-05*.

Lund, S.P., Schwartz, M., Keigwin, L., Johnson, T., 2005. Deep-sea sediment records of the Laschamp geomagnetic field excursion (~41,000 calendar years before present). *Journal of Geophysical Research: Solid Earth* 110.

MacAyeal, D.R., 1993. Binge/purge oscillations of the Laurentide Ice Sheet as a cause of the North Atlantic's Heinrich events. *Paleoceanography* 8, 775–784.

Mackay, A., Ryves, D., Morley, D., Jewson, D., Rioual, P., 2006. Assessing the vulnerability of endemic diatom species in Lake Baikal to predicted future climate change: a multivariate approach. *Global Change Biology* 12, 2297–2315.

Mackay, A.W., 2007. The paleoclimatology of Lake Baikal: A diatom synthesis and prospectus. *Earth-Science Reviews* 82, 181–215.

Mackay, A.W., Bezrukova, E. V., Boyle, J.F., Holmes, J.A., Panizzo, V.N., Piotrowska, N., Shchetnikov, A., Shilland, E.M., Tarasov, P., White, D., 2013a. Multiproxy evidence for abrupt climate change impacts on terrestrial and freshwater ecosystems in the Ol'khon region of Lake Baikal, central Asia. *Quaternary International* 290–291, 46–56.

Mackay, A.W., Bezrukova, E. V., Leng, M.J., Meaney, M., Nunes, A., Piotrowska, N., Self, A., Shchetnikov, A., Shilland, E., Tarasov, P., Wang, L., White, D., 2012. Aquatic ecosystem responses to Holocene climate change and biome development in boreal, central Asia. *Quaternary Science Reviews* 41, 119–131.

Mackay, A.W., Karabanov, E., Leng, M.J., Sloane, H.J., Morley, D.W., Panizzo, V.N., Khursevich, G., Williams, D., 2008. Reconstructing hydrological variability in Lake Baikal during MIS 11: an application of oxygen isotope analysis of diatom silica. *Journal of Quaternary Science* 23, 365–374.

Mackay, A.W., Ryves, D.B., Battarbee, R.W., Flower, R.J., Jewson, D., Rioual, P., Sturm, M., 2005. 1000 years of climate variability in central Asia: assessing the evidence using Lake Baikal (Russia) diatom assemblages and the application of a diatom-inferred model of snow cover on the lake. *Global and Planetary Change* 46, 281–297.

Mackay, A.W., Seddon, A.W.R., Leng, M.J., Heumann, G., Morley, D.W., Piotrowska, N., Rioual, P., Roberts, S., Swann, G.E.A., 2017. Holocene carbon dynamics at the forest–steppe ecotone of southern Siberia. *Global Change Biology* 23, 1942–1960.

Mackay, A.W., Swann, G.E. a., Fagel, N., Fietz, S., Morley, D., Rioual, P., Tarasov, P., Leng, M.J., 2013b. Hydrological instability during the Last Interglacial in central Asia: a new diatom oxygen isotope record from Lake Baikal. *Quaternary Science Reviews* 66, 45–54.

Mackay, A.W., Swann, G.E.A., Brewer, T.S., Leng, M.J., Morley, D.W., Piotrowska, N., Rioual, P., White, D., 2011. A reassessment of late glacial - Holocene diatom oxygen isotope record from Lake Baikal using a geochemical mass-balance approach. *Journal of Quaternary Science* 26, 627–634.

MacKenzie, A.B., Hardie, S.M.L., Farmer, J.G., Eades, L.J., Pulford, I.D., 2011. Analytical and sampling constraints in ^{210}Pb dating. *The Science of the total environment* 409, 1298–304.

MacLeod, A., Palmer, A., Rose, J., Bryant, C., Merritt, J., 2011. Timing of glacier response to Younger Dryas climatic cooling in Scotland. *Global and Planetary Change* 79, 264–274.

Maier, D.B., Gälman, V., Renberg, I., Bigler, C., Béatrice, D., Veronika, M., Ingemar, G., Christian Bigler, R., Maier, D.B., Gälman, V., Renberg, I., Bigler, C., 2018. Using a decadal diatom sediment trap record to unravel seasonal processes important for the formation of the sedimentary diatom signal. *Journal of Paleolimnology* 60, 133–152.

Malik, H.I., Saros, J.E., 2016. Effects of temperature, light and nutrients on five Cyclotella sensu lato taxa assessed with in situ experiments in arctic lakes. *Journal of Plankton Research* 38, 431–442.

Malik, H.I., Warner, K.A., Saros, J.E., 2018. Diatom Research Comparison of seasonal distribution patterns of Discostella stelligera and Lindavia bodanica in a boreal lake during two years with differing ice-off timing Comparison of seasonal distribution patterns of Discostella stelligera and Lindavia bodanica in a boreal lake during two years with differing ice-off timing. *Diatom Research* 33, 1–11.

Mangerud, J., Bolstad, M., Elgersma, A., Helliksen, D., Landvik, J.Y., Lycke, A.K., Lønne, I., Salvigsen, O., Sandahl, T., Sejrup, H.P., 1987. The Late Weichselian glacial maximum in western Svalbard. *Polar Research* 5, 275–278.

Mangerud, J., Gulliksen, S., Larsen, E., 2010. 14 C-dated fluctuations of the western flank of the Scandinavian Ice Sheet 45-25 kyr BP compared with Bølling-Younger Dryas fluctuations and Dansgaard-Oeschger events in Greenland. *Boreas* 39, 328–342.

Mangerud, J., Svend, A., Berglund, B.E., Donner, J.J., 1974. Quaternary stratigraphy of Norden, a proposal for terminology and classification. *Boreas* 3, 109–126.

Mann, M.E., Zhang, Z., Rutherford, S., Bradley, R.S., Hughes, M.K., Shindell, D., Ammann, C., Faluvegi, G., Ni, F., 2009. Global signatures and dynamical origins of the Little Ice Age and Medieval Climate Anomaly. *Science* 326, 1256–1260.

Marcott, S.A., Clark, P.U., Padman, L., Klinkhammer, G.P., Springer, S.R., Liu, Z., Otto-Bliesner, B.L., Carlson, A.E., Ungerer, A., Padman, J., He, F., Cheng, J., Schmittner, A., 2011. Ice-shelf collapse from subsurface warming as a trigger for Heinrich events. *Proceedings of the National Academy of Sciences of the United States of America* 108, 13415–13419.

Marcott, S.A., Shakun, J.D., Clark, P.U., Mix, A.C., 2013. A reconstruction of regional and global temperature for the past 11,300 years. *Science* 339, 1198–1201.

Marston, R.A., 2010. Geomorphology and vegetation on hillslopes: Interactions, dependencies, and feedback loops. *Geomorphology* 116, 206–217.

Martin-Puertas, C., Matthes, K., Brauer, A., Muscheler, R., Hansen, F., Petrick, C., Aldahan, A., Possnert, G., van Geel, B., 2012. Regional atmospheric circulation shifts induced by a grand solar minimum. *Nature Geoscience* 5, 397–401.

Martinson, D.G., Pisias, N.G., Hays, J.D., Imbrie, J.D., Moore, T.C., Shackleton, N.J., 1987. Age dating and isotopic analyses of sediment core RC11-120: Supplement to: Age Dating and the orbital theory of the ice ages: development of a high-resolution 0 to 300,000-year chronostratigraphy. *Quaternary Research* 27, 1–29.

Maslin, M., Seidov, D., Lowe, J., Maslin, M, Seidov D, L.J., Maslin, M., Seidov, D., Lowe, J., 2001. Synthesis of the Nature and Causes of Rapid Climate Transitions During the Quaternary. *The Oceans and Rapid Climate Change* 126, 9–52.

Mayewski, P.A., Rohling, E.E., Curt Stager, J., Karlén, W., Maasch, K.A., David Meeker, L., Meyerson, E.A., Gasse, F., van Kreveld, S., Holmgren, K., Lee-Thorp, J., Rosqvist, G., Rack, F., Staubwasser, M., Schneider, R.R., Steig, E.J., 2004. Holocene climate variability. *Quaternary Research* 62, 243–255.

McCabe, A.M., Clark, P.U., Clark, J., Dunlop, P., 2007. Radiocarbon constraints on readvances of the British-Irish Ice Sheet in the northern Irish Sea Basin during the last deglaciation. *Quaternary Science Reviews* 26, 1204–1211.

McGowan, S., Gunn, H. V., Whiteford, E.J., John Anderson, N., Jones, V.J., Law, A.C., 2018. Functional attributes of epilithic diatoms for palaeoenvironmental interpretations in South-West Greenland lakes. *Journal of Paleolimnology* 60, 273–298.

McManus, J.F., Francois, R., Gherardi, J.-M., Keigwin, L.D., Brown-Leger, S., 2004. Collapse and rapid resumption of Atlantic meridional circulation linked to deglacial climate changes. *Nature* 428, 834–837.

Medina-Elizalde, M., Burns, S.J., Polanco-Martinez, J., Lases-Hernández, F., Bradley, R., Wang, H.-C., Shen, C.-C., 2017. Synchronous precipitation reduction in the American Tropics associated with Heinrich 2. *Scientific reports* 7, 11216.

Meese, D.A., Gow, A.J., Grootes, P., Stuiver, M., Mayewski, P.A., Zielinski, G.A., Ram, M., Taylor, K.C., Waddington, E.D., 1994. The Accumulation Record from the GISP2 Core as an Indicator of Climate Change Throughout the Holocene. *Science* 266, 1680–1682.

Members, B., 2005. A new Quaternary record of regional tectonic, sedimentation and paleoclimate changes from drill core BDP-99 at Posolskaya Bank, Lake Baikal. *Quaternary International* 136, 105–121.

Mendonça, R., Müller, R.A., Clow, D., Verpoorter, C., Raymond, P., Tranvik, L.J., Sobek, S., 2017. Organic carbon burial in global lakes and reservoirs. *Nature Communications* 8, 1694.

Merlis, T.M., Schneider, T., Bordoni, S., Eisenman, I., Merlis, T.M., Schneider, T., Bordoni, S., Eisenman, I., 2013. The Tropical Precipitation Response to Orbital Precession. *Journal of Climate* 26, 2010–2021.

Meyers, P.A., 1994. Preservation of elemental and isotopic source identification of sedimentary organic matter. *Chemical Geology* 114, 289–302.

Meyers, P.A., 2003. Applications of organic geochemistry to paleolimnological reconstructions: A summary of examples from the Laurentian Great Lakes. In: Organic Geochemistry. Pergamon, pp. 261–289.

Meyers, P.A., Lallier-Vergès, E., 1999. Lacustrine sedimentary organic matter records of Late Quaternary paleoclimates. *Journal of Paleolimnology* 21, 345–372.

Meyers, P.A., Teranes, J.L., 2001. Sediment Organic Matter. In: Tracking Environmental Change Using Lake Sediments. Kluwer Academic Publishers, Dordrecht, pp. 239–269.

Morley, D.W., Leng, M.J., Mackay, A.W., Sloane, H.J., 2005. Late glacial and Holocene environmental change in the Lake Baikal region documented by oxygen isotopes from diatom silica. *Global and Planetary Change* 46, 221–233.

Morley, D.W., Leng, M.J., Mackay, A.W., Sloane, H.J., Rioual, P., Battarbee, R.W., 2004. Cleaning of lake sediment samples for diatom oxygen isotope analysis. *Journal of Paleolimnology* 31, 391–401.

Mörner, N.-A., 1977. The Gothenburg Magnetic Excursion. *Quaternary Research* 7, 413–427.

Mortlock, R.A., Froelich, P.N., 1989. A simple method for the rapid determination of biogenic opal in pelagic marine sediments. *Deep Sea Research Part A. Oceanographic Research Papers* 36, 1415–1426.

Müller, S., Tarasov, P.E., Hoelzmann, P., Bezrukova, E. V., Kossler, A., Krivonogov, S.K., 2014. Stable vegetation and environmental conditions during the Last Glacial Maximum: New results from Lake Kotokel (Lake Baikal region, southern Siberia, Russia). *Quaternary International* 348, 14–24.

Müller, U.C., Fletcher, W.J., Milner, A.M., Scheiter, S., 2013. Interhemispheric anti-phasing of orbitally driven monsoon intensity: Implications for ice-volume forcing in the high latitudes. *Earth and Planetary Science Letters* 377–378, 34–42.

Müller, U.C., Pross, J., Tzedakis, P.C., Gamble, C., Kotthoff, U., Schmiedl, G., Wulf, S., Christanis, K., 2011. The role of climate in the spread of modern humans into Europe. *Quaternary Science Reviews* 30, 273–279.

Murakami, T., Takamatsu, T., Katsuta, N., Takano, M., Yamamoto, K., Takahashi, Y., Nakamura, T., Kawai, T., 2012. Centennial- to millennial-scale climate shifts in continental interior Asia repeated between warm–dry and cool–wet conditions during the last three interglacial states: evidence from uranium and biogenic silica in the sediment of Lake Baikal, southeast Si. *Quaternary Science Reviews* 52, 49–59.

Mursula, K., Usoskin, I.G., Kovaltsov, G.A., 2001. Persistent 22-year cycle in sunspot activity: Evidence for a relic solar magnetic field. *Solar Physics* 198, 51–56.

Nami, H.G., de la Peña, P., Vásquez, C.A., Feathers, J., de la Peña, P., 2016. Palaeomagnetic results and new dates of sedimentary deposits from Klasies River Cave 1, South Africa. *South African Journal of Science* Volume 112.

NASA Earth Observatory, 2015. Fire and Smoke Around Lake Baikal : Natural Hazards.

Nenakhov, V.M., Nikitin, A. V., 2007. Structure, magmatism, and Paleozoic tectonic evolution of the Uakit Zone in the context of the formation of the Angara-Vitim batholith in the western Transbaikal region. *Geotectonics* 41, 114–129.

Nöel, M., Tarling, D.H., 1975. The Laschamp geomagnetic 'event.' *Nature* 253, 705–707.

Nomokonova, T., Losey, R.J., Goriunova, O.I., Weber, A.W., Goriunova, ga I., Weber, A.W., 2013. A freshwater old carbon offset in Lake Baikal, Siberia and problems with the radiocarbon dating of archaeological sediments: Evidence from the Sagan-Zaba II site. *Quaternary International* 290–291, 110–125.

Novello, V.F., Cruz, F.W., Vuille, M., Stríkis, N.M., Edwards, R.L., Cheng, H., Emerick, S., De Paula, M.S., Li, X., Barreto, E.D.S., Karmann, I., Santos, R. V, 2017. A high-resolution history of the South American Monsoon from Last Glacial Maximum to the Holocene. *Scientific Reports* 7, 44267.

Nowaczyk, N.R., Arz, H.W., Frank, U., Kind, J., Plessen, B., 2012. Dynamics of the Laschamp geomagnetic excursion from Black Sea sediments. *Earth and Planetary Science Letters* 351–352, 54–69.

O'Farrell, I., Tell, G., Podlejski, A., 2001. Morphological variability of Aulacoseira granulata (Ehr.) Simonsen (Bacillariophyceae) in the Lower Parana River (Argentina). *Limnology* 2, 65–71.

O'Reilly, C.M., Sharma, S., Gray, D.K., Hampton, S.E., Read, J.S., Rowley, R.J., Schneider, P., Lenters, J.D., McIntyre, P.B., Kraemer, B.M., Weyhenmeyer, G.A., Straile, D., Dong, B., Adrian, R., Allan, M.G., Anneville, O., Arvola, L., Austin, J., Bailey, J.L., *et al.*, 2015. Rapid and highly variable warming of lake surface waters around the globe. *Geophysical Research Letters* 42, 10773–10781.

Oberhansli, H., Mackay, A., 2005. Introduction to "Progress towards reconstructing past climate in Central Eurasia, with special emphasis on Lake Baikal." *Global Planet Change* 46, 1–7.

Ogurtsov, M.G., 2005. On the Possibility of Forecasting the Sun's Activity Using Radiocarbon Solar Proxy. *Solar Physics* 231, 167–176.

Oldfield, F., Richardson, N., Appleby, P.G., 1995. Radiometric dating (210Pb, 137Cs, 241Am) of recent ombrotrophic peat accumulation and evidence for changes in mass balance. *The Holocene* 5, 141–148.

Osipov, E.Y., Osipova, O.P., 2014. Mountain glaciers of southeast Siberia: current state and changes since the Little Ice Age. *Annals of Glaciology* 55, 167–176.

Pan, Y., Stevenson, R.J., Hill, B.H., Herlihy, A.T., Collins, G.B., 1996. Using Diatoms as Indicators of Ecological Conditions in Lotic Systems: A Regional Assessment. *Journal of the North American Benthological Society* 15, 481–495.

Park, T.-W., Jeong, J.-H., Deng, Y., Zhou, R., Cai, M., 2014. Quantitative decomposition of radiative and non-radiative contributions to temperature anomalies related to siberian high variability. *Climate Dynamics* 45, 1207–1217.

Passy, S.I., 2007a. Community analysis in stream biomonitoring: what we measure and what we don't. *Environmental Monitoring and Assessment* 127, 409–417.

Passy, S.I., 2007b. Diatom ecological guilds display distinct and predictable behavior along nutrient and disturbance gradients in running waters. *Aquatic Botany* 86, 171–178.

Past Interglacials working group of PAGES, Berger, B., Crucifix, M., Hodell, D.A., Mangili, C., McManus, J.F., Otto-Bliesner, B., Pol, K., Raynaud, D., Skinner, L.C., Tzedakis, P.C., Wolff, E.W., Yin, Q.Z., Abe-Ouchi, A., Barbante, C., Brovkin, V., Cacho, I., Capron, E., Ferretti, P., *et al.*, 2016. Interglacials of the last 800,000 years. *Reviews of*

Geophysics 54, 162–219.

Paulsen, D.E., Li, H.C., Ku, T.L., 2003. Climate variability in central China over the last 1270 years revealed by high-resolution stalagmite records. *Quaternary Science Reviews* 22, 691–701.

Peck, V.L., Hall, I.R., Zahn, R., Grousset, F., Hemming, S.R., Scourse, J.D., 2007. The relationship of Heinrich events and their European precursors over the past 60 ka BP: a multi-proxy ice-rafted debris provenance study in the North East Atlantic. *Quaternary Science Reviews* 26, 862–875.

Peltier, W.R., Vettoretti, G., 2014. Dansgaard-Oeschger oscillations predicted in a comprehensive model of glacial climate: A “kicked” salt oscillator in the Atlantic. *Geophysical Research Letters* 41, 7306–7313.

Penaud, A., Eynaud, F., Turon, J.L., Blamart, D., Rossignol, L., Marret, F., Lopez-Martinez, C., Grimalt, J.O., Malaizé, B., Charlier, K., 2010. Contrasting paleoceanographic conditions off Morocco during Heinrich events (1 and 2) and the Last Glacial Maximum. *Quaternary Science Reviews* 29, 1923–1939.

Pérez-Mejías, C., Moreno, A., Sancho, C., Bartolomé, M., Stoll, H., Cacho, I., Cheng, H., Edwards, R.L., 2017. Abrupt climate changes during Termination III in Southern Europe. *Proceedings of the National Academy of Sciences of the United States of America* 114, 10047–10052.

Pérez-Martínez, C., Cruz-Pizarro, L., Sánchez-Castillo, P., 1992. Auxosporulation in Cyclotella ocellata (Bacillariophyceae) under natural and experimental conditions. *Journal of Phycology* 28, 608–615.

Petersen, S. V., Schrag, D.P., Clark, P.U., 2013. A new mechanism for Dansgaard-Oeschger cycles. *Paleoceanography* 28, 24–30.

Petit, J.R., Basile, I., Leruyuet, A., Raynaud, D., Lorius, C., Jouzel, J., Stievenard, M., Lipenkov, V.Y., Barkov, N.I., Kudryashov, B.B., Davis, M., Saltzman, E., Kotlyakov, V., 1997. Four climate cycles in Vostok ice core. *Nature* 387, 359–360.

Petit, J.R., Jouzel, J., Raynaud, D., Barkov, N.I., Barnola, J.-M., Basile, I., Bender, M., Chappellaz, J., Davis, M., Delaygue, G., Delmotte, M., Kotlyakov, V.M., Legrand, M., Lipenkov, V.Y., Lorius, C., PEpin, L., Ritz, C., Saltzman, E., Stievenard, M., 1999. Climate and atmospheric history of the past 420,000 years from the Vostok ice core, Antarctica 399, 429–436.

Petrova, G.N., Pospelova, G.A., 1990. Excursions of the magnetic field during the Brunhes chron. *Physics of the Earth and Planetary Interiors*

63, 135–143.

Pfister, C., Brázdil, R., 2006. Social vulnerability to climate in the “Little Ice Age”?: an example from Central Europe in the early 1770s. *Climate of the Past Discussions* 2, 123–155.

Piotrowska, N., Bluszcz, A., Demske, D., Granoszewski, W., Heumann, G., 2007. Extraction and AMS radiocarbon dating of pollen from Lake Baikal sediments. *Radiocarbon* 46, 181–187.

Piotrowska, N., Oberhänsli, 2009. Radiocarbon dating of Lake Baikal sediments: A comparison between pollen and TOC ages. *EGU General Assembly 2009, held 19-24 April, 2009 in Vienna, Austria http://meetings.copernicus.org/egu2009, p.3796* 11, 3796.

Prokopenko, A., 2001. Continental response to Heinrich events and Bond cycles in sedimentary record of Lake Baikal, Siberia. *Global and Planetary Change* 28, 217–226.

Prokopenko, A.A., Karabanov, E.B., Williams, D.F., Kuzmin, M.I., Shackleton, N.J., Crowhurst, S.J., Peck, J.A., Gvozdkov, A.N., King, J.W., 2001. Biogenic Silica Record of the Lake Baikal Response to Climatic Forcing during the Brunhes. *Quaternary Research* 55, 123–132.

Prokopenko, A.A., Khursevich, G.K., Bezrukova, E. V., Kuzmin, M.I., Boes, X., Williams, D.F., Fedenya, S.A., Kulagina, N. V., Letunova, P.P., Abzaeva, A.A., 2007. Paleoenvironmental proxy records from Lake Hovsgol, Mongolia, and a synthesis of Holocene climate change in the Lake Baikal watershed. *Quaternary Research* 68, 2–17.

Prokopenko, A.A., Williams, D.F., 2004. Deglacial methane emission signals in the carbon isotopic record of Lake Baikal. *Earth and Planetary Science Letters* 218, 135–147.

Prokopenko, A.A., Williams, D.F., Karabanov, E.B., Khursevich, G.K., 1999. Response of Lake Baikal ecosystem to climate forcing and pCO2 change over the last glacial/interglacial transition. *Earth and Planetary Science Letters* 172, 239–253.

Prokopenko, A.A., Williams, D.F., Kuzmin, M.I., Karabanov, E.B., Khursevich, G.K., Peck, J.A., 2002. Muted climate variations in continental Siberia during the mid-Pleistocene epoch. *Nature* 418, 65–68.

Pross, J., Koutsodendris, A., Christanis, K., Fischer, T., Fletcher, W.J., Hardiman, M., Kalaitzidis, S., Knipping, M., Kotthoff, U., Milner, A.M., Müller, U.C., Schmiedl, G., Siavalas, G., Tzedakis, P.C., Wulf, S., 2015. The 1.35-Ma-long terrestrial climate archive of Tenaghi Philippon, northeastern Greece: Evolution, exploration, and perspectives for future

research. *Newsletters on Stratigraphy* 48, 253–276.

Rach, O., Brauer, A., Wilkes, H., Sachse, D., 2014. Delayed hydrological response to Greenland cooling at the onset of the Younger Dryas in western Europe. *Nature Geoscience* 7, 109–112.

Raisbeck, G.M., Cauquoin, A., Jouzel, J., Landais, A., Petit, J.R., Lipenkov, V.Y., Beer, J., Synal, H.A., Oerter, H., Johnsen, S.J., Steffensen, J.P., Svensson, A., Yiou, F., 2017. An improved north-south synchronization of ice core records around the 41 kyr 10Be peak. *Climate of the Past* 13, 217–229.

Ramsey, C.B., Scott, E.M., van der Plicht, J., 2013. Calibration for Archaeological and Environmental Terrestrial Samples in the Time Range 26–50 ka cal BP. *Radiocarbon* 55, 2021–2027.

Ransom, C.J., 1973. Magnetism and Archaeology. *Nature* 242, 518–519.

Rasmussen, S.O., Andersen, K.K., Svensson, A.M., Steffensen, J.P., Vinther, B.M., Clausen, H.B., Siggaard-Andersen, M.-L., Johnsen, S.J., Larsen, L.B., Dahl-Jensen, D., Bigler, M., Röthlisberger, R., Fischer, H., Goto-Azuma, K., Hansson, M.E., Ruth, U., 2006. A new Greenland ice core chronology for the last glacial termination. *Journal of Geophysical Research* 111, D06102.

Rasmussen, S.O., Bigler, M., Blunier, T., Buchardt, S.L., Clausen, H.B.H.B., Cvijanovic, I., Johnsen, S.J., Fischer, H., Gkinis, V., Guillevic, M., Hoek, W.Z., Lowe, J.J., Pedro, J.B., Popp, T., Seierstad, I.K., Steffensen, J.P., Svensson, A.M., Vallelonga, P., Vinther, B.M.B.M.B.M., *et al.*, 2014a. A stratigraphic framework for robust naming and correlation of abupt climatic changes during the last glacial period based on three synchronized Greenland ice core records. *Quaternary Science Reviews* 106, 14–28.

Rasmussen, S.O., Birks, H.H., Blockley, S.P.E., Brauer, A., Hajdas, I., Hoek, W.Z., Lowe, J.J., Moreno, A., Renssen, H., Roche, D.M., Svensson, A.M., Valdes, P., Walker, M.J.C., 2014b. Dating, synthesis, and interpretation of palaeoclimatic records of the Last Glacial cycle and model-data integration: advances by the INTIMATE (INTegration of Ice-core, MArine and TErrestrial records) COST Action ES0907. *Quaternary Science Reviews* 106, 1–13.

Rasmussen, S.O., Vinther, B.M., Clausen, H.B., Andersen, K.K., 2007. Early Holocene climate oscillations recorded in three Greenland ice cores. *Quaternary Science Reviews* 26, 1907–1914.

Rasmussen, T.L., van Weering, T.C.E., Labeyrie, L., 1997. Climatic instability, ice sheets and ocean dynamics at high northern latitudes

during the last glacial period (58-10 KA BP). *Quaternary Science Reviews* 16, 71–80.

Raymo, M.E., 1997. The timing of major climate terminations. *Paleoceanography* 12, 577–585.

Reich, D., Green, R.E., Kircher, M., Krause, J., Patterson, N., Durand, E.Y., Viola, B., Briggs, A.W., Stenzel, U., Johnson, P.L.F., Maricic, T., Good, J.M., Marques-Bonet, T., Alkan, C., Fu, Q., Mallick, S., Li, H., Meyer, M., Eichler, E.E., *et al.*, 2010. Genetic history of an archaic hominin group from Denisova Cave in Siberia. *Nature* 468, 1053–1060.

Reich, D., Patterson, N., Kircher, M., Delfin, F., Nandineni, M.R., Pugach, I., Ko, A.M.-S., Ko, Y.-C., Jinam, T.A., Phipps, M.E., Saitou, N., Wollstein, A., Kayser, M., Pääbo, S., Stoneking, M., 2011. Denisova admixture and the first modern human dispersals into Southeast Asia and Oceania. *American journal of human genetics* 89, 516–528.

Reid, G.C., 1997. Solar forcing of global climate change since the mid-17th century. *Climatic Change* 37, 391–405.

Reimer, P., Baillie, M., Bard, E., 2009. IntCal09 and Marine09 radiocarbon age calibration curves, 0-50,000 yeats cal BP. *Radiocarbon* 51, 1111–1150.

Reimer, P., Bard, E., Bayliss, A., Beck, J.W., Blackwell, P.G., Bronk Ramsey, C., Buck, C.E., Cheng, H., Edwards, R.L., Friedrich, M., Grootes, P.M., Guilderson, T.P., Haflidason, H., Hajdas, I., Hatté, C., Heaton, T.J., Hoffmann, D.L., Hogg, A.G., Hughen, K.A., *et al.*, 2013. IntCal13 and Marine13 Radiocarbon Age Calibration Curves 0–50,000 Years cal BP. *Radiocarbon* 55, 1869–1887.

Reimer, P.J., Reimer, R.W., 2001. A Marine Reservoir Correction Database and On-Line Interface. *Radiocarbon* 43, 461–463.

Renssen, H., Goosse, H., Fichefet, T., 2007. Simulation of Holocene cooling events in a coupled climate model. *Quaternary Science Reviews* 26, 2019–2029.

Renssen, H., Goosse, H., Roche, D.M., Seppä, H., 2018. The global hydroclimate response during the Younger Dryas event. *Quaternary Science Reviews* 193, 84–97.

Renssen, H., Seppä, H., Crosta, X., Goosse, H., Roche, D.M., 2012. Global characterization of the Holocene Thermal Maximum. *Quaternary Science Reviews* 48, 7–19.

Reshetova, S.A., Bezrukova, E. V., Panizzo, V., Henderson, A., Ptitsyn, A.B., Daryin, A. V., Kalugin, I.A., 2013. Vegetation of Central

Transbaikalia in the Late Glacial period and Holocene. *Geography and Natural Resources* 34, 172–178.

Reynolds, B.C., Aggarwal, J., Brzezinski, M.A., Cardinal, D., Engström, E., Georg, R.B., Land, M., Leng, M., Opfergelt, S., Vroon, P.Z., 2006. An inter-laboratory calibration of Si isotope reference materials. *Geochimica et Cosmochimica Acta* 70, A529.

Riato, L., Della Bella, V., Leira, M., Taylor, J.C., Oberholster, P.J., 2017. A diatom functional-based approach to assess changing environmental conditions in temporary depressional wetlands. *Ecological Indicators* 78, 205–213.

Rignot, E., Casassa, G., Gogineni, P., Krabill, W., Rivera, A., Thomas, R., 2004. Accelerated ice discharge from the Antarctic Peninsula following the collapse of Larsen B ice shelf. *Geophysical Research Letters* 31, L18401.

Rimet, F., Bouchez, A., 2011. Use of diatom life-forms and ecological guilds to assess pesticide contamination in rivers: Lotic mesocosm approaches. *Ecological Indicators* 11, 489–499.

Rioual, P., Andrieu-Ponel, V., de Beaulieu, J.-L.L., Reille, M., Svobodova, H., Battarbee, R.W., 2007. Diatom responses to limnological and climatic changes at Ribains Maar (French Massif Central) during the Eemian and Early Würm. *Quaternary Science Reviews* 26, 1557–1609.

Rioual, P., Andrieu-Ponel, V., Rietti-Shati, M., Battarbee, R.W., De Beaulieu, J.L., Cheddadi, R., Reille, M., Svobodova, H., Shemesh, A., 2001. High-resolution record of climate stability in France during the last interglacial period. *Nature* 413, 293–296.

Rioual, P., Mackay, A.W., 2005. A diatom record of centennial resolution for the Kazantsevo Interglacial stage in Lake Baikal (Siberia). *Global and Planetary Change* 46, 199–219.

Roberts, W.H.G., Valdes, P.J., Payne, A.J., 2014. Topography's crucial role in Heinrich Events. *Proceedings of the National Academy of Sciences of the United States of America* 111, 16688–16693.

Robock, A., Mao, J., 1992. Winter warming from large volcanic eruptions. *Geophysical Research Letters* 19, 2405–2408.

Roche, D.M., Paillard, D., Caley, T., Waelbroeck, C., 2014. LGM hosing approach to Heinrich Event 1: results and perspectives from data–model integration using water isotopes. *Quaternary Science Reviews* 106, 247–261.

Rohling, E.J., Pälike, H., 2005. Centennial-scale climate cooling with a sudden cold event around 8,200 years ago. *Nature* 434, 975–979.

Round, F.E., Crawford, R.M., Mann, D.G., 1990. The Diatoms. Biology and Morphology of the Genera. Cambridge University Press, Cambridge.

Rudaya, N., Tarasov, P., Dorofeyuk, N., Solovieva, N., Kalugin, I., Andreev, A., Daryin, A., Diekmann, B., Riedel, F., Tserendash, N., Wagner, M., 2009. Holocene environments and climate in the Mongolian Altai reconstructed from the Hoton-Nur pollen and diatom records: a step towards better understanding climate dynamics in Central Asia. *Quaternary Science Reviews* 28, 540–554.

Ruddiman, W., 2017. Geographic evidence of the early anthropogenic hypothesis. *Anthropocene* 20, 4–14.

Ruddiman, W.F., 2005. The Early Anthropogenic Hypothesis a year later. An editorial reply. *Climate Change* 69, 427–434.

Ruddiman, W.F., 2006a. Orbital changes and climate. *Quaternary Science Reviews* 25, 3092–3112.

Ruddiman, W.F., 2006b. Ice-driven CO 2 feedback on ice volume. *Clim. Past* 2, 43–55.

Rühland, K.M., Paterson, A.M., Smol, J.P., 2015. Lake diatom responses to warming: reviewing the evidence. *Journal of Paleolimnology*.

Russell, M., Rosell-Melé, A., 2005. Preliminary study of fluxes of major lipid biomarker classes in the water column and sediments of Lake Baikal, Russia. *Global and Planetary Change* 46, 45–56.

Rytsk, E.Y., Kovach, V.P., Kovalenko, V.I., Yarmolyuk, V. V., 2007. Structure and evolution of the continental crust in the Baikal Fold Region. *Geotectonics* 41, 440–464.

Ryves, D.., Juggins, S., Fritz, S.., Battarbee, R.., 2001. Experimental diatom dissolution and the quantification of microfossil preservation in sediments. *Palaeogeography, Palaeoclimatology, Palaeoecology* 172, 99–113.

Ryves, D.B., Battarbee, R.W., Fritz, S.C., 2009. The dilemma of disappearing diatoms: Incorporating diatom dissolution data into palaeoenvironmental modelling and reconstruction. *Quaternary Science Reviews* 28, 120–136.

Ryves, D.B., Battarbee, R.W., Juggins, S., Fritz, S.C., Anderson, N.J.,

2006. Physical and chemical predictors of diatom dissolution in freshwater and saline lake sediments in North America and West Greenland. *Limnology and Oceanography* 51, 1355–1368.

Ryves, D.B., Jewson, D.H., Sturm, M., Battarbee, R.W., Flower, R.J., Mackay, A.W., Granin, N.G., 2003. Quantitative and qualitative relationships between planktonic diatom communities and diatom assemblages in sedimenting material and surface sediments in Lake Baikal, Siberia. *Limnology and Oceanography* 48, 1643–1661.

Samartin, S., Heiri, O., Lotter, A.F., Tinner, W., 2012. Climate warming and vegetation response after Heinrich event 1 (16 700-16 000 cal yr BP) in Europe south of the Alps. *Climate of the Past* 8, 1913–1927.

Sanchez-Cabeza, J.A., Ruiz-Fernández, A.C., 2012. 210Pb sediment radiochronology: An integrated formulation and classification of dating models. *Geochimica et Cosmochimica Acta* 82, 183–200.

Sarnthein, M., Stattegger, K., Dreger, D., Erlenkeuser, H., Grootes, P., Haupt, B.J., Jung, S., Kiefer, T., Kuhnt, W., Pflaumann, U., Schäfer-Neth, C., Schulz, H., Schulz, M., Seidov, D., Simstich, J., Kreveld, S. van, Vogelsang, E., Völker, A., Weinelt, M., 2001. Fundamental Modes and Abrupt Changes in North Atlantic Circulation and Climate over the last 60 ky — Concepts, Reconstruction and Numerical Modeling. In: chäfer P., Ritzrau W., Schlüter M., T.J. (Ed.), The Northern North Atlantic: A Changing Environment. Springer Berlin Heidelberg, pp. 365–410.

Schelske, C.L., Peplow, A., Brenner, M., Spencer, C.N., 1994. Low-background gamma counting: applications for 210Pb dating of sediments. *Journal of Paleolimnology* 10, 115–128.

Schenk, F., Väliranta, M., Muschitiello, F., Tarasov, L., Heikkilä, M., Björck, S., Brandefelt, J., Johansson, A. V., Näslund, J.-O., Wohlfarth, B., 2018. Warm summers during the Younger Dryas cold reversal. *Nature Communications* 9, 1634.

Schiff, C.J., Kaufman, D.S., Wolfe, A.P., Dodd, J., Sharp, Z., 2009. Late Holocene storm-trajectory changes inferred from the oxygen isotope composition of lake diatoms, south Alaska. *Journal of Paleolimnology* 41, 189–208.

Schlolaut, G., Brauer, A., Nakagawa, T., Lamb, H.F., Tyler, J.J., Staff, R.A., Marshall, M.H., Bronk Ramsey, C., Bryant, C.L., Tarasov, P.E., 2017. Evidence for a bi-partition of the Younger Dryas Stadial in East Asia associated with inversed climate characteristics compared to Europe. *Scientific Reports* 7, 44983.

Schmidt, A., Thordarson, T., Oman, L.D., Robock, A., Self, S., 2012.

Climatic impact of the long-lasting 1783 Laki eruption: Inapplicability of mass-independent sulfur isotopic composition measurements. *Journal of Geophysical Research: Atmospheres* 117, D23116.

Schmidt, I., Bradtmöller, M., Kehl, M., Pastoors, A., Tafelmaier, Y., Weninger, B., Weniger, G.-C., 2012. Rapid climate change and variability of settlement patterns in Iberia during the Late Pleistocene. *Quaternary International* 274, 179–204.

Schmidt, M., Botz, R., Rickert, D., Bohrmann, G., Hall, S.R., Mann, S., 2001. Oxygen isotopes of marine diatoms and relations to opal-A maturation. *Geochimica et Cosmochimica Acta* 65, 201–211.

Schmidt, R., Kamenik, C., Lange-Bertalot, H., Klee, R., 2004. Fragilaria and Staurosira (Bacillariophyceae) from sediment surfaces of 40 lakes in the Austrian Alps in relation to environmental variables, and their potential for palaeoclimatology. *Journal of Limnology* 63, 171–189.

Schmidt, R., Psenner, R., Müller, J., Indinger, P., Kamenik, C., 2002. Impact of late glacial climate variations on stratification and trophic state of the meromictic lake Längsee (Austria): Validation of a conceptual model by multi proxy studies. *Journal of Limnology* 61, 49–60.

Schuur, E.A.G., Bockheim, J., Canadell, J.G., Euskirchen, E., Field, C.B., Goryachkin, S. V., Hagemann, S., Kuhry, P., Lafleur, P.M., Lee, H., Mazhitova, G., Nelson, F.E., Rinke, A., Romanovsky, V.E., Shiklomanov, N., Tarnocai, C., Venevsky, S., Vogel, J.G., Zimov, S.A., 2008. Vulnerability of Permafrost Carbon to Climate Change: Implications for the Global Carbon Cycle. *BioScience* 58, 701–714.

Seal, R.R., Shanks, W.C., 1998. Oxygen and hydrogen isotope systematics of Lake Baikal, Siberia: Implications for paleoclimate studies. *Limnology and Oceanography* 43, 1251–1261.

Seierstad, I.K., Abbott, P.M., Bigler, M., Blunier, T., Bourne, A.J., Brook, E., Buchardt, S.L., Buizert, C., Clausen, H.B., Cook, E., Dahl-Jensen, D., Davies, S.M., Guillevic, M., Johnsen, S.J., Pedersen, D.S., Popp, T.J., Rasmussen, S.O., Severinghaus, J.P., Svensson, A., *et al.*, 2014. Consistently dated records from the Greenland GRIP, GISP2 and NGRIP ice cores for the past 104 ka reveal regional millennial-scale δ18O gradients with possible Heinrich event imprint. *Quaternary Science Reviews* 106, 29–46.

Sha, L., Jiang, H., Seidenkrantz, M.-S., Muscheler, R., Zhang, X., Knudsen, M.F., Olsen, J., Knudsen, K.L., Zhang, W., 2016. Solar forcing as an important trigger for West Greenland sea-ice variability over the last millennium. *Quaternary Science Reviews* 131, 148–156.

Shackleton, N.J., Imbrie, J., Hall, M.A., 1983. Oxygen and carbon

isotope record of East Pacific core V19-30: implications for the formation of deep water in the late Pleistocene North Atlantic. *Earth and Planetary Science Letters* 65, 233–244.

Shackleton, N.J., Opdyke, N.D., 1973. Oxygen Isotope and Palaeomagnetic Stratigraphy of Equatorial Pacific Core V28-238: Oxygen Isotope Temperatures and Ice Volumes on a 105 Year and 106 Year Scale. *Quaternary Research* 3, 39–55.

Shatsillo, A.V., Fedyukin, I.V., Powerman, V.I., 2014. Paleomagnetism of the Late Paleozoic granites of the Angara-Vitim batholith and the host rocks of the Baikal-Patom folded area: Tectonic implications. *Russian Geology and Geophysics* 55, 864–880.

Shchetnikov, A.A., 2007. Morphotectonics of lacustrine basins: The Baikal rift zone as an example. *Russian Journal of Pacific Geology* 1, 120–129.

Shichi, K., Takahara, H., Hase, Y., Watanabe, T., Nara, F.W., Nakamura, T., Tani, Y., Kawai, T., 2013. Vegetation response in the southern Lake Baikal region to abrupt climate events over the past 33calkyr. *Palaeogeography, Palaeoclimatology, Palaeoecology* 375, 70–82.

Sigl, M., Winstrup, M., McConnell, J.R., Welten, K.C., Plunkett, G., Ludlow, F., Büntgen, U., Caffee, M., Chellman, N., Dahl-Jensen, D., Fischer, H., Kipfstuhl, S., Kostick, C., Maselli, O.J., Mekhaldi, F., Mulvaney, R., Muscheler, R., Pasteris, D.R., Pilcher, J.R., *et al.*, 2015. Timing and climate forcing of volcanic eruptions for the past 2,500 years. *Nature* 523, 543–549.

Slon, V., Mafessoni, F., Vernot, B., de Filippo, C., Grote, S., Viola, B., Hajdinjak, M., Peyrégne, S., Nagel, S., Brown, S., Douka, K., Higham, T., Kozlikin, M.B., Shunkov, M. V., Derevianko, A.P., Kelso, J., Meyer, M., Prüfer, K., Pääbo, S., 2018. The genome of the offspring of a Neanderthal mother and a Denisovan father. *Nature* 561, 113–116.

Smith, A.C., Leng, M.J., Swann, G.E.A., Barker, P.A., Mackay, A.W., Ryves, D.B., Sloane, H.J., Chenery, S.R.N., Hems, M., 2016. An experiment to assess the effects of diatom dissolution on oxygen isotope ratios. *Rapid Communications in Mass Spectrometry* 30, 293–300.

Snoeijs, P.J.M., 1990. Effects of temperature on spring bloom dynamics of epilithic diatom communities in the Gulf of Bothnia. *Journal of Vegetation Science* 1, 599–608.

Sobek, S., Durisch-Kaiser, E., Zurbrügg, R., Wongfun, N., Wessels, M., Pasche, N., Wehrli, B., 2009. Organic carbon burial efficiency in lake sediments controlled by oxygen exposure time and sediment source.

Limnology and Oceanography 54, 2243–2254.

Soja, A.J., Tchebakova, N.M., French, N.H.F., Flannigan, M.D., Shugart, H.H., Stocks, B.J., Sukhinin, A.I., Parfenova, E.I., Chapin, F.S., Stackhouse, P.W., 2007. Climate-induced boreal forest change: Predictions versus current observations. *Global and Planetary Change* 56, 274–296.

Solotchin, P.A., Sklyarov, E. V., Solotchina, E.P., Zamana, L. V., Sklyarova, O.A., Solotchin, P. A., Sklyarov, E. V., Solotchina, E. P., Zamana, L. V., Sklyarova, O.A., 2015. A New Find of Kogarkoite Na3SO4F in Transbaikalia. *Doklady Earth Sciences* 462, 643–647.

Steffensen, J.P., Andersen, K.K., Bigler, M., Clausen, H.B., Dahl-Jensen, D., Fischer, H., Goto-Azuma, K., Hansson, M., Johnsen, S.J., Jouzel, J., Masson-Delmotte, V., Popp, T., Rasmussen, S.O., Röthlisberger, R., Ruth, U., Stauffer, B., Siggaard-Andersen, M.-L., Sveinbjörnsdóttir, Á.E., Svensson, A., *et al.*, 2008. High-resolution Greenland ice core data show abrupt climate change happens in few years. *Science* 321, 680–684.

Stenger-Kovács, C., Lengyel, E., Crossetti, L.O., Üveges, V., Padisák, J., 2013. Diatom ecological guilds as indicators of temporally changing stressors and disturbances in the small Torna-stream, Hungary. *Ecological Indicators* 24, 138–147.

Stine, S., 1994. Extreme and persistent drought in California and Patagonia during mediaeval time. *Nature* 369, 546–549.

Stocker, T.F., Johnsen, S.J., 2003. A minimum thermodynamic model for the bipolar seesaw. *Paleoceanography* 18, 1087.

Street-Perrott, F.A., Barker, P.A., 2008. Biogenic silica: a neglected component of the coupled global continental biogeochemical cycles of carbon and silicon. *Earth Surface Processes and Landforms* 33, 1436–1457.

Stríkis, N.M., Chiessi, C.M., Cruz, F.W., Vuille, M., Cheng, H., De Souza Barreto, E.A., Mollenhauer, G., Kasten, S., Karmann, I., Edwards, R.L., Bernal, J.P., Sales, H. dos R., 2015. Timing and structure of Mega-SACZ events during Heinrich Stadial 1. *Geophysical Research Letters* 42, 5477–5484.

Stuart, A.J., Kosintsev, P.A., Higham, T.F.G., Lister, A.M., 2004. Pleistocene to Holocene extinction dynamics in giant deer and woolly mammoth. *Nature* 431, 684–689.

Stuiver M. and R.S. Kra, 1986. Calibration issue, Proceedings of the 12th International 14C conference. *Radiocarbon* 28, 805–1030.

Svensson, A., Andersen, K.K., Bigler, M., Clausen, H.B., Dahl-Jensen, D., Davies, S.M., Johnsen, S.J., Muscheler, R., Parrenin, F., Rasmussen, S.O., Röthlisberger, R., Seierstad, I., Steffensen, J.P., Vinther, B.M., 2008. A 60 000 year Greenland stratigraphic ice core chronology. *Climate of the Past* 4, 47–57.

Swann, G.E.A., Leng, M.J., 2009. A review of diatom δ18O in palaeoceanography. *Quaternary Science Reviews* 28, 384–398.

Swann, G.E.A., Leng, M.J., Juschus, O., Melles, M., Brigham-Grette, J., Sloane, H.J., 2010. A combined oxygen and silicon diatom isotope record of Late Quaternary change in Lake El'gygytgyn, North East Siberia. *Quaternary Science Reviews* 29, 774–786.

Swann, G.E.A., Leng, M.J., Sloane, H.J., Maslin, M.A., Onodera, J., 2007. Diatom oxygen isotopes: Evidence of a species effect in the sediment record. *Geochemistry, Geophysics, Geosystems* 8, Q06012.

Swann, G.E.A., Mackay, A.W., 2006. Potential limitations of biogenic silica as an indicator of abrupt climate change in Lake Baikal, Russia. *Journal of Paleolimnology* 36, 81–89.

Swann, G.E.A., Mackay, A.W., Leng, M.J., Demory, F., 2005. Climatic change in Central Asia during MIS 3/2: a case study using biological responses from Lake Baikal. *Global and Planetary Change* 46, 235–253.

Swann, G.E.A., Mackay, A.W., Vologina, E., Jones, M.D., Panizzo, V.N., Leng, M.J., Sloane, H.J., Snelling, A.M., Sturm, M., 2018. Lake Baikal isotope records of Holocene Central Asian precipitation. *Quaternary Science Reviews* 189, 210–222.

Swann, G.E.A., Patwardhan, S. V, 2011. Application of Fourier Transform Infrared Spectroscopy (FTIR) for assessing biogenic silica sample purity in geochemical analyses and palaeoenvironmental research. *Clim. Past* 7, 65–74.

Tapolczai, K., Bouchez, A., Stenger-Kovács, C., Padisák, J., Rimet, F., 2016. Trait-based ecological classifications for benthic algae: review and perspectives. *Hydrobiologia* 776, 1–17.

Tarasov, P., Bezrukova, E., Karabanov, E., Nakagawa, T., Wagner, M., Kulagina, N., Letunova, P., Abzaeva, A., Granoszewski, W., Riedel, F., 2007. Vegetation and climate dynamics during the Holocene and Eemian interglacials derived from Lake Baikal pollen records. *Palaeogeography, Palaeoclimatology, Palaeoecology* 252, 440–457.

Tarasov, P.E., Bezrukova, E. V., Krivonogov, S.K., 2009. Late Glacial and Holocene changes in vegetation cover and climate in southern

Siberia derived from a 15 kyr long pollen record from Lake Kotokel. *Climate of the Past Discussions* 5, 127–151.

Tchebakova, N.M., Parfenova, E., Soja, A.J., 2009. The effects of climate, permafrost and fire on vegetation change in Siberia in a changing climate. *Environmental Research Letters* 4, 045013.

Tchebakova, N.M., Parfenova, E.I., Korets, M.A., Conard, S.G., 2016. Potential change in forest types and stand heights in central Siberia in a warming climate. *Environmental Research Letters* 11, 035016.

Teller, J.T., Leverington, D.W., Mann, J.D., 2002. Freshwater outbursts to the oceans from glacial Lake Agassiz and their role in climate change during the last deglaciation. *Quaternary Science Reviews* 21, 879–887.

Terzer, S., Wassenaar, L.I., Araguás-Araguás, L.J., Aggarwal, P.K., 2013. Global isoscapes for delta18O and delta2H in precipitation: improved prediction using regionalized climatic regression models. *Hydrology and Earth System Sciences Discussions* 10, 7351–7393.

Tesi, T., Muschitiello, F., Smittenberg, R.H., Jakobsson, M., Vonk, J.E., Hill, P., Andersson, A., Kirchner, N., Noormets, R., Dudarev, O., Semiletov, I., Gustafsson, Ö., 2016. Massive remobilization of permafrost carbon during post-glacial warming. *Nature Communications* 7, 13653.

Thompson, W.G., Goldstein, S.L., 2006. A radiometric calibration of the SPECMAP timescale. *Quaternary Science Reviews* 25, 3207–3215.

Tingley, M.P., Huybers, P., 2013. Recent temperature extremes at high northern latitudes unprecedented in the past 600 years. *Nature* 496, 201–205.

Todd, M.C., Mackay, A.W., 2003. Large-Scale Climatic Controls on Lake Baikal Ice Cover. *Journal of Climate* 16, 3186–3199.

Törnqvist, R., Jarsjö, J., Pietroń, J., Bring, A., Rogberg, P., Asokan, S.M., Destouni, G., 2014. Evolution of the hydro-climate system in the Lake Baikal basin. *Journal of Hydrology* 519, 1953–1962.

Trouet, V., Van Oldenborgh, G.J., 2013. KNMI Climate Explorer: A Web-Based Research Tool for High-Resolution Paleoclimatology. *Tree-Ring Research* 69, 3–13.

Tsybzhitov, T.K., Gonchikov, B.-M.N., Tsybikdorzhiev, T.T., Khubrakova, B.T., Tsybzhitov, A.T., 2006. The soil cover pattern in Western Transbaikal region as displayed on a 1: 500 000 scale map. *Eurasian Soil Science* 39, 29–34.

Tsygankov, A.A., Matukov, D.I., Berezhnaya, N.G., Larionov, A.N., Posokhov, V.F., Tsyrenov, B.T., Khromov, A.A., Sergeev, S.A., 2007. Late Paleozoic granitoids of western Transbaikalia: magma sources and stages of formation. *Russian Geology and Geophysics* 48, 120–140.

Tubi, A., Dayan, U., 2013. The Siberian High: teleconnections, extremes and association with the Icelandic Low. *International Journal of Climatology* 33, 1357–1366.

Tzedakis, P.C., 1993. Long-term tree populations in northwest Greece through multiple Quaternary climatic cycles. *Nature* 364, 437–440.

Tzedakis, P.C., Crucifix, M., Mitsui, T., Wolff, E.W., 2017. A simple rule to determine which insolation cycles lead to interglacials. *Nature* 542, 427–432.

Tzedakis, P.C., Emerson, B.C., Hewitt, G.M., 2013. Cryptic or mystic? Glacial tree refugia in northern Europe. *Trends in Ecology & Evolution* 28, 696–704.

Tzedakis, P.C., Hooghiemstra, H., Pälike, H., 2006. The last 1.35 million years at Tenaghi Philippon: revised chronostratigraphy and long-term vegetation trends. *Quaternary Science Reviews* 25, 3416–3430.

Tzedakis, P.C., Pälike, H., Roucoux, K.H., de Abreu, L., 2009. Atmospheric methane, southern European vegetation and low-mid latitude links on orbital and millennial timescales. *Earth and Planetary Science Letters* 277, 307–317.

Tziperman, E., Gildor, H., 2003. On the mid-Pleistocene transition to 100-kyr glacial cycles and the asymmetry between glaciation and deglaciation times. *Paleoceanography* 18, 1–8.

Udovič, G.M., Aleksandra, Petar, C., Utinic´., Z.˘, Bosak, S.I., Stankovic´., S., Stankovic´., I.S., Mršic, G., Mršic´., M., Kralj, K., Borojevic´, B., Anamarija, B., And, C. ´ U., Plenkovic´-, ¯elka, Moraj, P.-, 2017. Defining centric diatoms of most relevant phytoplankton functional groups in deep karst lakes. *Hydrobiologia* 788, 161–191.

Ufimtsev, G.F., Shchetnikov, A.A., Filinov, I.A., 2009. Neotectonic inversions in the Baikal Rift System. *Russian Geology and Geophysics* 50, 618–627.

van der Plicht, J., van Geel, B., Bohncke, S.J.P., Bos, J.A.A., Blaauw, M., Speranza, A.O.M., Muscheler, R., Björck, S., 2004. The Preboreal climate reversal and a subsequent solar-forced climate shift. *Journal of Quaternary Science* 19, 263–269.

van Donk, E., Kilham, S.S., 1990. Temperature effects on silicon and

phosphorus-limited growth and competitive interactions among three diatoms. *Journal of Phycology* 26, 40–50.

van Geel, B., Bokovenko, N.A., Burova, N.D., Chugunov, K.V., Dergachev, V.A., Dirksen, V.G., Kulkova, M., Nagler, A., Parzinger, H., van der Plicht, J., Vasiliev, S.S., Zaitseva, G.I., 2004. Climate change and the expansion of the Scythian culture after 850 BC: a hypothesis. *Journal of Archaeological Science* 31, 1735–1742.

van Geel, B., Buurman, J., Waterbolk, H.T., 1996. Archaeological and palaeoecological indications of an abrupt climate change in The Netherlands, and evidence for climatological teleconnections around 2650 BP. *Journal of Quaternary Science* 11, 451–460.

van Geel, B., Raspopov, O.M., Renssen, H., van der Plicht, J., Dergachev, V.A., Meijer, H.A.J., 1999. The role of solar forcing upon climate change. *Quaternary Science Reviews* 18, 331–338.

van Hardenbroek, M., Chakraborty, A., Davies, K.L., Harding, P., Heiri, O., Henderson, A.C.G., Holmes, J.A., Lasher, G.E., Leng, M.J., Panizzo, V.N., Roberts, L., Schilder, J., Trueman, C.N., Wooller, M.J., 2018. The stable isotope composition of organic and inorganic fossils in lake sediment records: Current understanding, challenges, and future directions. *Quaternary Science Reviews* 196, 154–176.

van Raden, U.J., Colombaroli, D., Gilli, A., Schwander, J., Bernasconi, S.M., van Leeuwen, J., Leuenberger, M., Eicher, U., 2013. High-resolution late-glacial chronology for the Gerzensee lake record (Switzerland): δ18O correlation between a Gerzensee-stack and NGRIP. *Palaeogeography, Palaeoclimatology, Palaeoecology* 391 (B), 13–24.

Vasil'ev, S.A., 2011. Old traditions, new tendencies: Final Paleolithic cultural development in southern Siberia. *Quaternary International* 242, 371–378.

Vaughan, D.G., Comiso, J.C., Allison, I., Carrasco, J., Kaser, G., Kwok, R., Mote, P., Murray, T., Paul, F., Ren, J., Rignot, E., Solomina, O., Steffen, K., Zhang, T., Stocker, T.F., Qin, D., Plattner, G.-K., Tignor, M., Allen, S.K., *et al.*, 2013. IPCC Observations: Cryosphere. In: Climate Change 2013: The Physical Science Basis. Contribution of Working Group I to the Fifth Assessment Report of the Intergovernmental Panel on Climate Change. In: Stocker, T.F., Qin, D., Plattner, G.-V., Tignor, M., Allen, S.K., Boschung, J., Nauels, A., Xia, Y., Bex, V., Midgley, P.M. (Eds.), Climate Change 2013: The Physical Sci- Ence Basis. Contribution of Working Group I to the Fifth Assessment Report of the Intergovernmental Panel on Climate Change. Cambridge University Press, Cambridge UK, New York USA, pp. 317–382.

Velichko, A.A., Timireva, S.N., Kremenetski, K. V, MacDonald, G.M., Smith, L.C., 2011. West Siberian Plain as a late glacial desert. *Quaternary International* 237, 45–53.

Verosub, K.L., Banerjee, S.K., 1977. Geomagnetic excursions and their paleomagnetic record. *Reviews of Geophysics* 15, 145.

Vettoretti, G., Peltier, W.R., Vettoretti, G., Peltier, W.R., 2018. Fast Physics and Slow Physics in the Nonlinear Dansgaard–Oeschger Relaxation Oscillation. *Journal of Climate* 31, 3423–3449.

Vidal, L., Labeyrie, L., Cortijo, E., Arnold, M., Duplessy, J.C., Michel, E., Becqué, S., van Weering, T.C.E., 1997. Evidence for changes in the North Atlantic Deep Water linked to meltwater surges during the Heinrich events. *Earth and Planetary Science Letters* 146, 13–27.

von Grafenstein, U., Erlenkeuser, Brauer, Jouzel, Johnsen, 1999. A mid-european decadal isotope-climate record from 15,500 to 5000 years B.P. *Science* 284, 1654–1657.

Vonk, J.E., Sánchez-García, L., van Dongen, B.E., Alling, V., Kosmach, D., Charkin, A., Semiletov, I.P., Dudarev, O. V, Shakhova, N., Roos, P., Eglinton, T.I., Andersson, A., Gustafsson, O., 2012. Activation of old carbon by erosion of coastal and subsea permafrost in Arctic Siberia. *Nature* 489, 137–140.

Wagner, F., Aaby, B., Visscher, H., 2002. Rapid atmospheric CO2 changes associated with the 8,200-years-B.P. cooling event. *Proceedings of the National Academy of Sciences of the United States of America* 99, 12011–12014.

Wagner, G., Beer, J., Laj, C., Kissel, C., Masarik, J., Muscheler, R., Synal, H.-A., 2000. Chlorine-36 evidence for the Mono Lake event in the Summit GRIP ice core. *Earth and Planetary Science Letters* 181, 1–6.

WAIS Divide Project Members, W., Buizert, C., Cuffey, K.M., Severinghaus, J.P., Baggenstos, D., Fudge, T.J., Steig, E.J., Markle, B.R., Winstrup, M., Rhodes, R.H., Brook, E.J., Sowers, T.A., Clow, G.D., Cheng, H., Edwards, R.L., Sigl, M., McConnell, J.R., Taylor, K.C., 2015. The WAIS Divide deep ice core WD2014 chronology - Part 1: Methane synchronization (68-31 ka BP) and the gas age-ice age difference. *Climate of the Past* 11, 153–173.

Walker, B.D., McCarthy, M.D., Fisher, A.T., Guilderson, T.P., 2008. Dissolved inorganic carbon isotopic composition of low-temperature axial and ridge-flank hydrothermal fluids of the Juan de Fuca Ridge. *Marine Chemistry* 108, 123–136.

Walker, M., Johnsen, S., Rasmussen, S.O., Popp, T., Steffensen, J.-P.,

Gibbard, P., Hoek, W., Lowe, J., Andrews, J., Björck, S., Cwynar, L.C., Hughen, K., Kershaw, P., Kromer, B., Litt, T., Lowe, D.J., Nakagawa, T., Newnham, R., Schwander, J., 2009. Formal definition and dating of the GSSP (Global Stratotype Section and Point) for the base of the Holocene using the Greenland NGRIP ice core, and selected auxiliary records. *Journal of Quaternary Science* 24, 3–17.

Walker, M.J.C., Berkelhammer, M., Björck, S., Cwynar, L.C., Fisher, D.A., Long, A.J., Lowe, J.J., Newnham, R.M., Rasmussen, S.O., Weiss, H., 2012. Formal subdivision of the Holocene Series/Epoch: a Discussion Paper by a Working Group of INTIMATE (Integration of ice-core, marine and terrestrial records) and the Subcommission on Quaternary Stratigraphy (International Commission on Stratigraphy). *Journal of Quaternary Science* 27, 649–659.

Walker, M.J.C., Björck, S., Lowe, J.J., 2001. Integration of ice core, marine and terrestrial records (INTIMATE) from around the North Atlantic region: An introduction. *Quaternary Science Reviews* 20, 1169–1174.

Walker, M.J.C., Coope, G.R., Sheldrick, C., Turney, C.S.M., Lowe, J.J., Blockley, S.P.E., Harkness, D.D., 2003. Devensian Lateglacial environmental changes in Britain: a multi-proxy environmental record from Llanilid, South Wales, UK. *Quaternary Science Reviews* 22, 475–520.

Walter, K.M., Zimov, S.A., Chanton, J.P., Verbyla, D., Chapin, F.S., 2006. Methane bubbling from Siberian thaw lakes as a positive feedback to climate warming. *Nature* 443, 71–75.

Wang, L., Mackay, A.W., Leng, M.J., Rioual, P., Panizzo, V.N., Lu, H., Gu, Z., Chu, G., Han, J., Kendrick, C.P., 2013. Influence of the ratio of planktonic to benthic diatoms on lacustrine organic matter δ13C from Erlongwan maar lake, northeast China. *Organic Geochemistry* 54, 62–68.

Wang, Y.J., Cheng, H., Edwards, R.L., An, Z.S., Wu, J.Y., Shen, C.C., Dorale, J.A., 2001. A high-resolution absolute-dated late Pleistocene Monsoon record from Hulu Cave, China. *Science* 294, 2345–2348.

Wanner, H., Butikofer, J., 2008. Holocene Bond Cycles: Real or Imaginary? *Geografie - Sbornik Ceske Geograficke Spolecnsti* 113, 338–350.

Wanner, H., Mercolli, L., Grosjean, M., Ritz, S.P., 2014. Holocene climate variability and change; a data-based review. *Journal of the Geological Society* 172, 254–263.

Wanner, H., Solomina, O., Grosjean, M., Ritz, S.P., Jetel, M., 2011.

Structure and origin of Holocene cold events. *Quaternary Science Reviews* 30, 3109–3123.

Webb, M., Barker, P.A., Wynn, P.M., Heiri, O., van Hardenbroek, M., Pick, F., Russell, J.M., Stott, A.W., Leng, M.J., 2016. Interpretation and application of carbon isotope ratios in freshwater diatom silica. *Journal of Quaternary Science* 31, 300–309.

Wenxiang, W., Tungsheng, L., 2004. Possible role of the “Holocene Event 3” on the collapse of Neolithic Cultures around the Central Plain of China. *Quaternary International* 117, 153–166.

Westover, K.S., Fritz, S.C., Blyakharchuk, T.A., Wright, H.E., 2006. Diatom paleolimnological record of Holocene climatic and environmental change in the Altai Mountains, Siberia. *Journal of Paleolimnology* 35, 519–541.

Wiersma, A.P., Renssen, H., 2006. Model–data comparison for the 8.2 ka BP event: confirmation of a forcing mechanism by catastrophic drainage of Laurentide Lakes. *Quaternary Science Reviews* 25, 63–88.

Wiersma, A.P., Roche, D.M., Renssen, H., 2011. Fingerprinting the 8.2 ka event climate response in a coupled climate model. *Journal of Quaternary Science* 26, 118–127.

Wildfires sweep through Siberia | World news | The Guardian [WWW Document], n.d. URL http://www.theguardian.com/world/2015/apr/13/siberian-wildfires-people-killed-and-hundreds-injured (accessed 4.27.16).

Willeit, M., Ganopolski, A., Calov, R., Brovkin, V., 2019. Mid-Pleistocene transition in glacial cycles explained by declining CO_2 and regolith removal. *Science Advances* 5, eaav7337.

Williams, C., Flower, B.P., Hastings, D.W., 2012. Seasonal Laurentide Ice Sheet melting during the “Mystery Interval” (17.5-14.5 ka). *Geology* 40, 955–958.

Williams, D.F., Peck, J., Karabanov, E.B., Prokopenko, A.A., Kravchinsky, V., King, J., Kuzmin, M.I., 1997. Lake Baikal Record of Continental Climate Response to Orbital Insolation During the Past 5 Million Years. *Science* 278, 1114–1117.

Williams, J.W., Blois, J.L., Shuman, B.N., 2011. Extrinsic and intrinsic forcing of abrupt ecological change: case studies from the late Quaternary. *Journal of Ecology* 99, 664–677.

Wilson, K.E., Leng, M.J., Mackay, A.W., 2014. The use of multivariate statistics to resolve multiple contamination signals in the oxygen isotope

analysis of biogenic silica. *Journal of Quaternary Science* 29, 641–649.

Winder, M., Hunter, D.A., 2008. Temporal organization of phytoplankton communities linked to physical forcing. *Oecologia* 156, 179–192.

Winder, M., Reuter, J.E., Schladow, S.G., 2009. Lake warming favours small-sized planktonic diatom species. *Proceedings. Biological sciences* 276, 427–35.

Wohlfarth, B., 2013. A review of Early Weichselian climate (MIS 5d-a) in Europe. *SKB Technical Report* 13-03, 1–79.

World, V. of the, n.d. VolcanoDiscovery: volcanoes worldwide - news, info, photos, and tours to volcanoes and volcanic areas, earthquake information / VolcanoDiscovery [WWW Document]. URL https://www.volcanodiscovery.com/home.html (accessed 9.19.18).

Wu, B., Wang, J., 2002. Winter Arctic Oscillation, Siberian High and East Asian Winter Monsoon. *Geophysical Research Letters* 29, 3-1-3–4.

Wunsam, S., Schmidt, R., Klee, R., 1995. Cyclotella-taxa (Bacillariophyceae) in lakes of the Alpine region and their relationship to environmental variables. *Aquatic Sciences* 57, 360–386.

Wunsch, C., 2003. Greenland—Antarctic phase relations and millennial time-scale climate fluctuations in the Greenland ice-cores. *Quaternary Science Reviews* 22, 1631–1646.

Xia, J., Ito, E., Engstrom, D.R., 1997. Geochemistry of ostracode calcite: Part 1. An experimental determination of oxygen isotope fractionation. *Geochimica et Cosmochimica Acta* 61, 377–382.

Xu, H., Chang, F., Luo, Y., Sun, X., 2009. Palaeoenvironmental changes from pollen record in deep sea core PC-1 from northern Okinawa Trough, East China Sea during the past 24 ka. *Chinese Science Bulletin* 54, 3739–3748.

Yakhnenko, V.M., Mamontov, A.M., Luczynski, M., 2008. East-Siberian coregonid fishes: their occurrence, evolution and present status. *Environmental Biotechnology* 4, 41–53.

Yang, H., Turner, S., 2013. Radiometric dating for recent lake sediments on the Tibetan Plateau. *Hydrobiologia* 713, 73–86.

Yuan, D., Cheng, H., Edwards, R.L., Dykoski, C.A., Kelly, M.J., Zhang, M., Qing, J., Lin, Y., Wang, Y., Wu, J., Dorale, J.A., An, Z., Cai, Y., 2004. Timing, duration, and transitions of the last interglacial Asian monsoon. *Science* 304, 575–578.

Yuan, Y., Wang, B., Tang, X., Liu, Z., 1991. Paleomagnetic Results of Core NS-76 in Nansha Sea Area. In: Distributions of Marine Environmental Research in Nansha Islands and in Its Neighboring Sea Area (1). Hubei Sci. Technol. Press, pp. 301–308.

Zalasiewicz, J., Williams, M., Gibbard, P., Hounslow, M.W., Kerr, A.C., Pearson, P., Marshall, J., 2008. Are we now living in the Anthropocene. *GSA Today* 18, 1–8.

Zalasiewicz, J., Williams, M., Haywood, A., Ellis, M., 2011. The Anthropocene: a new epoch of geological time? *Philosophical transactions. Series A, Mathematical, physical, and engineering sciences* 369, 835–841.

Zalat, A., Vildary, S.S., 2007. Environmental change in Northern Egyptian Delta lakes during the late Holocene, based on diatom analysis. *Journal of Paleolimnology* 37, 273–299.

Zhang, Y., Renssen, H., Seppä, H., Valdes, P.J., 2017a. Holocene temperature trends in the extratropical Northern Hemisphere based on inter-model comparisons. *Journal of Quaternary Science* 33, 464–476.

Zhang, Y., Renssen, H., Seppä, H., Valdes, P.J., 2017b. Holocene temperature evolution in the Northern Hemisphere high latitudes – Model-data comparisons. *Quaternary Science Reviews* 173, 101–113.

Zhao, J., An, C.-B., Huang, Y., Morrill, C., Chen, F.-H., 2017. Contrasting early Holocene temperature variations between monsoonal East Asia and westerly dominated Central Asia. *Quaternary Science Reviews* 178, 14–23.

Zhu, R., Zhang, R., Deng, C., Pan, Y., Liu, Q., Sun, Y., 2007. Are Chinese loess deposits essentially continuous? *Geophysical Research Letters* 34, L17306.

Ziemen, F.A., Kapsch, M.-L., Klockmann, M., Mikolajewicz, U., 2018. Heinrich events show two-stage climate response in transient glacial simulations. *Climate of the Past Discussions* 1–22.

Zorzi, C., Sanchez Goñi, M.F., Anupama, K., Prasad, S., Hanquiez, V., Johnson, J., Giosan, L., 2015. Indian monsoon variations during three contrasting climatic periods: The Holocene, Heinrich Stadial 2 and the last interglacial–glacial transition. *Quaternary Science Reviews* 125, 50–60.

Zurzolo, C., Bowler, C., 2001. Exploring Bioinorganic Pattern Formation in Diatoms . A Story of Polarized Trafficking. *Plant Physiology* 127, 1339–1345.